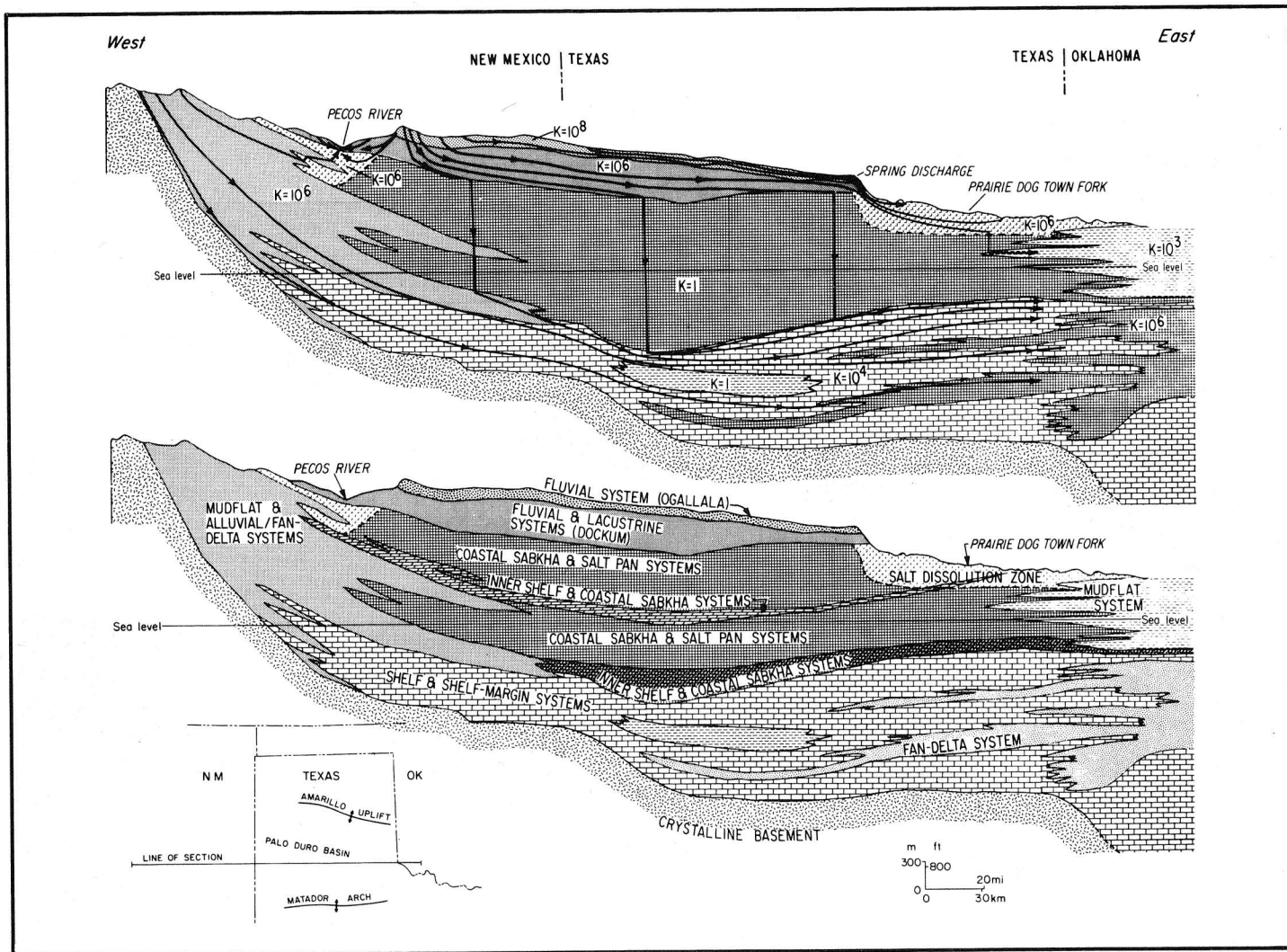# Geology and Geohydrology of the Palo Duro Basin, Texas Panhandle

## A Report on the Progress of Nuclear Waste Isolation Feasibility Studies (1980)



T. C. Gustavson, R. L. Bassett, R. J. Finley, A. G. Goldstein, C. R. Handford, J. H. McGowen, M. W. Presley, R. W. Baumgardner, Jr., M. E. Bentley, S. P. Dutton, J. A. Griffin, A. D. Hoadley, R. C. Howard, D. A. McGookey, K. A. McGillis, D. P. Palmer, P. J. Ramondetta, E. Roedder, W. W. Simpkins, and W. D. Wiggins

Geological Circular 81-3

# GEOLOGY AND GEOHYDROLOGY OF THE
# PALO DURO BASIN, TEXAS PANHANDLE

A Report on the Progress of Nuclear
Waste Isolation Feasibility Studies (1980)

Annual Report

for period October 1, 1979 - September 30, 1980

by

T. C. Gustavson, R. L. Bassett, R. J. Finley, A. G. Goldstein,
C. R. Handford, J. H. McGowen, M. W. Presley, R. W. Baumgardner, Jr.,
M. E. Bentley, S. P. Dutton, J. A. Griffin, A. D. Hoadley, R. C. Howard, D. A. McGookey,
K. A. McGillis, D. P. Palmer, P. J. Ramondetta, E. Roedder, W. W. Simpkins, and W. D. Wiggins

# CONTENTS

## FIGURES

## TABLES

## PLATE

## PURPOSE AND SCOPE

### Research Staff

*Integrated study of the basin structure, tectonic history, physical stratigraphy, hydrogeology, geochemistry, geomorphology, natural resources, and rock physics of the Palo Duro and Dalhart Basins in the Texas Panhandle is part of a national evaluation of ancient salt basins as potential sites for isolation and management of nuclear wastes.*

Since early 1977, the Bureau of Economic Geology has been evaluating several salt-bearing basins within the State of Texas as part of the national nuclear repository program. The Bureau, a research unit of The University of Texas and the State of Texas, is conducting a long-term program to gather and interpret all geologic and hydrologic information necessary for description, delineation, and evaluation of salt-bearing and related strata in the Palo Duro and Dalhart Basins of the Texas Panhandle.

The program in FY80 was divided into five broad research tasks, which were addressed by a surficial analysis and shallow stratigraphy group, a hydrology and geochemistry group, a basin analysis group, a host-rock analysis group, and a seismicity and tectonic environment group (fig. 1). The surficial analysis and shallow stratigraphy group has collected remotely sensed, surface and subsurface data to describe land resources, surface processes, and rates and styles of geomorphic development. The hydrology and geochemistry group has continued analysis of shallow and deep fluid circulation within the basins and has initiated studies of rock and fluid geochemistry within the salt-bearing units. The basin analysis group has characterized the major salt-bearing stratigraphic units within the basins and has assessed the potential for generating and trapping hydrocarbons within the basins. Concurrently, the host-rock analysis group has continued a study of cores from two drilling sites for analysis of salt and other lithologic units within the cores. The newly formed seismicity and tectonic environment group has initiated studies of deep-basement structure and tectonic development of the basin and has made an analysis of surface fracture systems.

This paper, a summary of progress during FY80, presents principal conclusions and reviews methods used and types of data and maps generated. Topical reports, discussing various geological aspects of the Palo Duro and Dalhart Basins in detail, are being published as phases of the study are completed. This research was supported by the Department of Energy and its predecessor the Energy Research and Development Administration under contracts numbered EY-77-S-05-5466 (FY78), DE-AC97-79ET44614 (FY79), and DE-AC97-ET46615 (FY80).
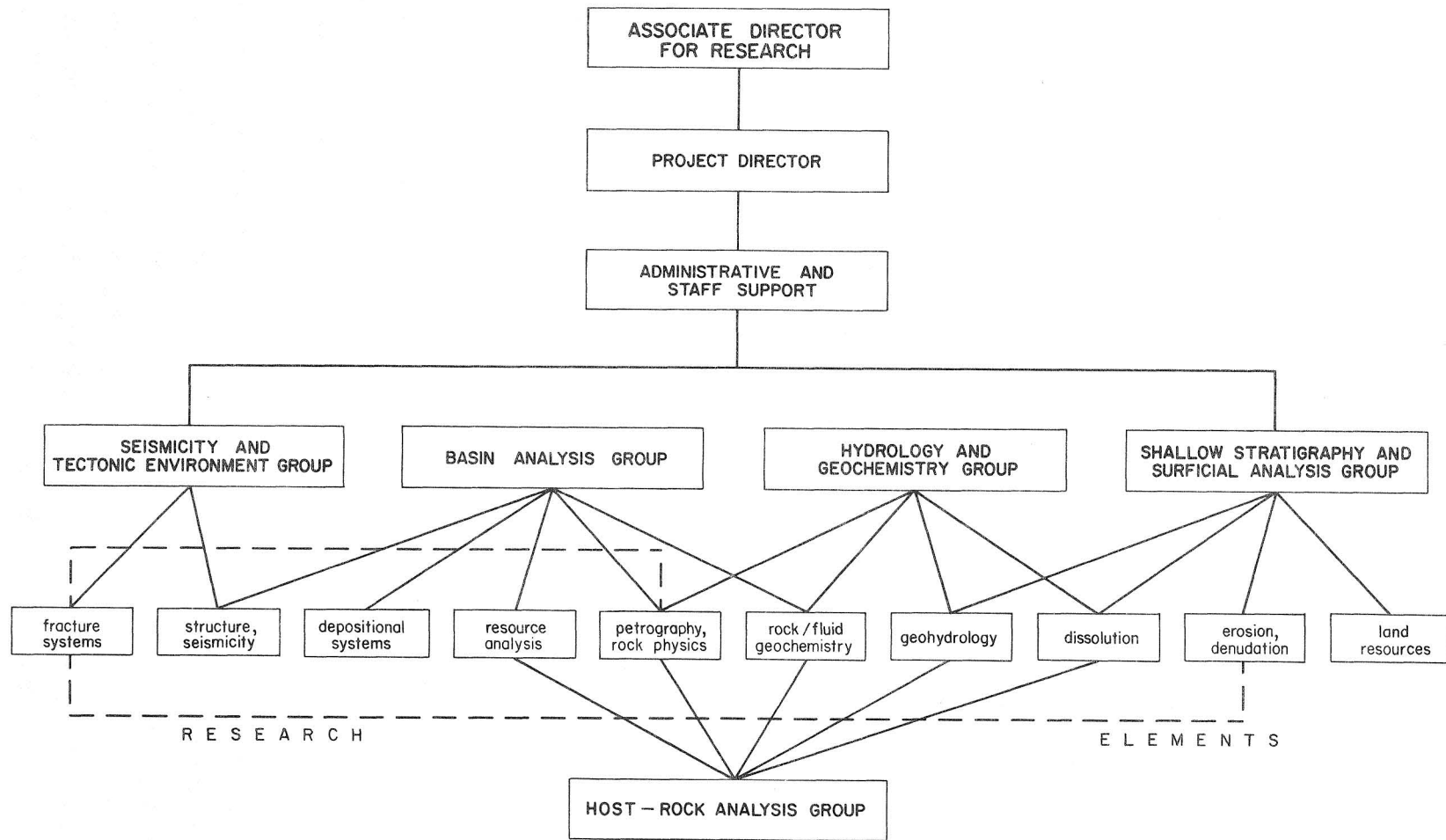
Figure 1. Organizational structure of the West Texas Waste Isolation Program (FY 1981).

## PALO DURO AND DALHART BASIN STUDIES--A SUMMARY OF THIRD-YEAR RESEARCH ACTIVITIES

*Research Staff*

*The third year of analysis was highlighted by initiation of regional basement structural analysis, quantification of geophysical log parameters, analyses of water content of basin salts, continuation of petroleum source-rock analysis, hydrogeologic mapping, characterization of cores, genetic stratigraphic facies mapping, climatic-geomorphic monitoring of the Texas Panhandle, and continued investigations of the processes, timing, and rates of salt dissolution. Each study provides a basis for detailed data interpretation and future integration of research elements.*

The Palo Duro Basin is a moderately small subbasin of the Permian Basin of southwest Texas and southeastern New Mexico. The Permian Basin is a region where the crust was depressed, allowing thick accumulations of sediments beginning early in the Pennsylvanian Period and continuing through the Permian Period. Within this depressed region, small blocks of the crust were displaced along deep-seated faults, creating a system of subbasins separated by basement uplifts. The uplifts were apparently formed by motion along high-angle reverse faults. The Palo Duro Basin is bounded on the north by the Amarillo Uplift, upthrust toward the north-northeast, and on the south by the Matador Arch, upthrust toward the south. Thus, the basin is underlain by an uplifted block of crust that probably experienced north-northeast extensional deformation during its formation.

Upper Permian salt-bearing rocks in the Palo Duro and Dalhart Basins have been subdivided into four lithogenetic units: (1) the combined lower Clear Fork and Tubb Formations, (2) the combined upper Clear Fork and Glorieta Formations, (3) the San Andres Formation, and (4) the post-San Andres (Guadalupian and Ochoan) strata. Each of these units contains bedded salt at depths between 300 and 900 m (960 and 2,880 ft), and net salt thicknesses exceed 100 m (320 ft). These salt-bearing units are composed of an upward succession of carbonates overlain by evaporites and red beds. This succession is a record of deposition in marine shelf and coastal evaporite environments; the environments shifted gradually seaward through time.

Clay mineral assemblages within Permian evaporites in the Palo Duro Basin have been identified by chemical analyses and by X-ray diffraction. They consist of (1) combinations of the mixed-layer clays, chlorite-swelling chlorite, chlorite vermiculite, and chlorite smectite, and (2) discrete phases of illite and chlorite. The in situ water content of bedded salt and the nature of its occurrence are being determined by optical evaluation of water content, titration by Karl-Fischer method,

and heat treatment. Values obtained in the preliminary investigation range from 0.15 to 2.44 percent free water, which does not include hydroxyl water.

A conceptual model has been developed for regional ground-water flow in the Texas Panhandle and eastern New Mexico. Flow is governed by the regional topography and the heterogeneous distribution of permeability associated with the multiple genetic depositional systems and facies. In the Palo Duro Basin, local topographic influences have little effect on deep ground waters because of the intervening thick, low-permeability evaporite section. Hydraulic head relationships indicate that fluid could move downward through the evaporites. A steady eastward decline of heads in the deep brine systems suggests that regional hydraulic connection permits flow between outcropping recharge areas in east-central New Mexico and discharge areas in North-Central Texas and in western Oklahoma.

Pennsylvanian and Wolfcampian (Lower Permian) basinal shales contain up to 2.4 percent organic carbon and are fair to very good hydrocarbon source rocks. Physical characteristics of the organic matter indicate maximum paleotemperatures. Pennsylvanian and Wolfcampian kerogen is yellow orange to orange; vitrinite reflectance averages 0.5 percent, an indication that temperatures were probably high enough to begin generation of hydrocarbons from lipid-rich organic material.

The Little Red River heads along the eastern Caprock Escarpment of the Southern High Plains. Field studies within the basin have revealed that recent erosion was considerable. Exported suspended-sediment load for the 1979 water year was over 340,000 metric tons (309,000 t). Rates of basin development and denudation were estimated using hypsometric analysis. The 40-km-long (24-mi-long) Little Red River basin is 380,000 years old, as calculated from an estimated average retreat rate from its original easternmost extent of 110 mm (4.3 inches) per yr (over 320 km; 200 mi) for the 3-million-year-old Ogallala Formation. The long-term denudation rate is 0.47 mm (0.02 inches) per yr, a rate somewhat less than the modern denudation rate.

In eastern Briscoe and Hall Counties, Texas, at least 400 sinkholes and collapse depressions were noted. In a smaller test area that covers approximately 13 percent of the counties, 36 sinkholes and 2 depressions have formed since 1940.

A zone of salt dissolution, noted on geophysical logs, structural cross sections, and salt thickness maps, borders the Palo Duro Basin on the west, north, and east and parallels the escarpment of the Southern High Plains. Recently formed sinkholes, collapse depressions, or open fractures have been noted in each of the New Mexico and Texas counties within the salt dissolution zone, an indication that surface collapse over the entire zone of salt dissolution is an active regional process.

# BASEMENT STRUCTURE AND TECTONIC DEVELOPMENT OF THE PALO DURO BASIN

Arthur G. Goldstein

*Basement structure of the Palo Duro Basin is being studied as an aid in understanding current seismicity and fracture development in cover rocks. Preliminary conclusions suggest that the basin is bounded by high-angle reverse faults and is developed on a block of crust that was not depressed as greatly as the surrounding blocks.*

Although a bedded salt repository in the Palo Duro Basin would be situated in rocks deposited in a structurally quiescent region, the basin was formed through crustal deformation. There are several factors affecting repository siting that call for a study of the crustal structure of the Palo Duro Basin. Current seismicity is localized along the Amarillo Uplift (Coffman and Von Hake, 1973), which bounds the Palo Duro Basin on the north (fig. 2). Any attempt to correlate seismicity with existing faults requires a detailed understanding of the structure of that area. Because most of these earthquakes have had foci within the basement, that part of the crust is of most interest for a study.

Linear drainage patterns on the surface of the High Plains suggest fracture control (Finley and Gustavson, in press). A commonly cited origin for linear surface features, particularly in geologically young materials, is upward propagation of basement faults and fracture zones (Babcock, 1973; Cook and Johnson, 1970; Hodgson, 1965; Gilbert, 1882). Clearly, before this mechanism can be ascribed to the Palo Duro Basin, we must determine the nature of any faults within its basement. Fracture zones, inferred from linear surface features, are most likely to be areas of greater ground-water movement and thus zones of potential evaporite dissolution, which could represent severe loss of integrity to a waste repository.

Basement structure is being studied from several approaches. All available data from wells penetrating basement rocks are being compiled. Much of this compilation has been completed (Dutton and others, 1979), and current work focuses on augmenting and reinterpreting the data. Special attention is being directed to the Amarillo Uplift since it is the dominant structural feature of the region and the locus of seismic energy release. Regional gravity of the Texas Panhandle is being analyzed by two-dimensional modeling to provide a quantitative test of proposed structural models.

The Palo Duro Basin and its bounding uplifts can be compared to adjacent basins and uplifts (fig. 2) that formed at the same time, some of which have been highly studied and are well understood. Possibly the best understood of these structural

elements are the Wichita Uplift and the Anadarko Basin in Oklahoma (fig. 2). The Wichita Uplift is the southeast extension of the Amarillo Uplift. It is bounded on the north by a major fault system (Harlton, 1963) composed of high-angle reverse faults (Ham and others, 1964) (fig. 3). The compressional nature of this fault system is well displayed by tightly folded adjacent sedimentary rocks in the Anadarko Basin (Harlton, 1963). It was previously proposed that Pennsylvanian basement uplifts and basins were formed through crustal extension and are bounded by normal faults. According to current data, this does not appear to be possible since crustal thinning and volcanism, which usually occur with extension, are absent in this region.

If this compressional concept of basement faults is applied to the Palo Duro Basin, several observed phenomena can be explained. Figure 4 is a schematic southwest-northeast cross section through the basin. The Amarillo Uplift and the Matador Arch are bounded by high-angle reverse faults that steepen with depth. This interpretation indicates that the Palo Duro Basin is a block of crust that was uplifted with respect to surrounding regions. This may explain the limited petroleum maturation in the basin despite its favorable source-rock potential (Gustavson and others, 1980c) since the basin would not have been buried to depths sufficient for thermal maturity. Because this basement block probably underwent northeast-southwest extension, northwest-striking extensional structural trends may have been propagated upward and might account for the strong coincident lineament development (Finley and Gustavson, in press).

Although conclusions on the development of the Palo Duro Basin and adjacent uplifts are preliminary, these areas resemble basement uplifts and basins of the middle Rocky Mountains, which formed in association with cratonward thrusting. The Palo Duro Basin and associated features apparently formed in association with cratonward thrusting in the Ouachita-Marathon foldbelt and thrustbelt.

In conclusion, studies of the basement structure of the Palo Duro Basin will aid in research on seismicity of the region and in establishing structural/tectonic models for development of the area. These models should provide a framework for interpreting both remote sensing data and bedrock fracture data, which will, in turn, be related to ongoing studies of salt dissolution.
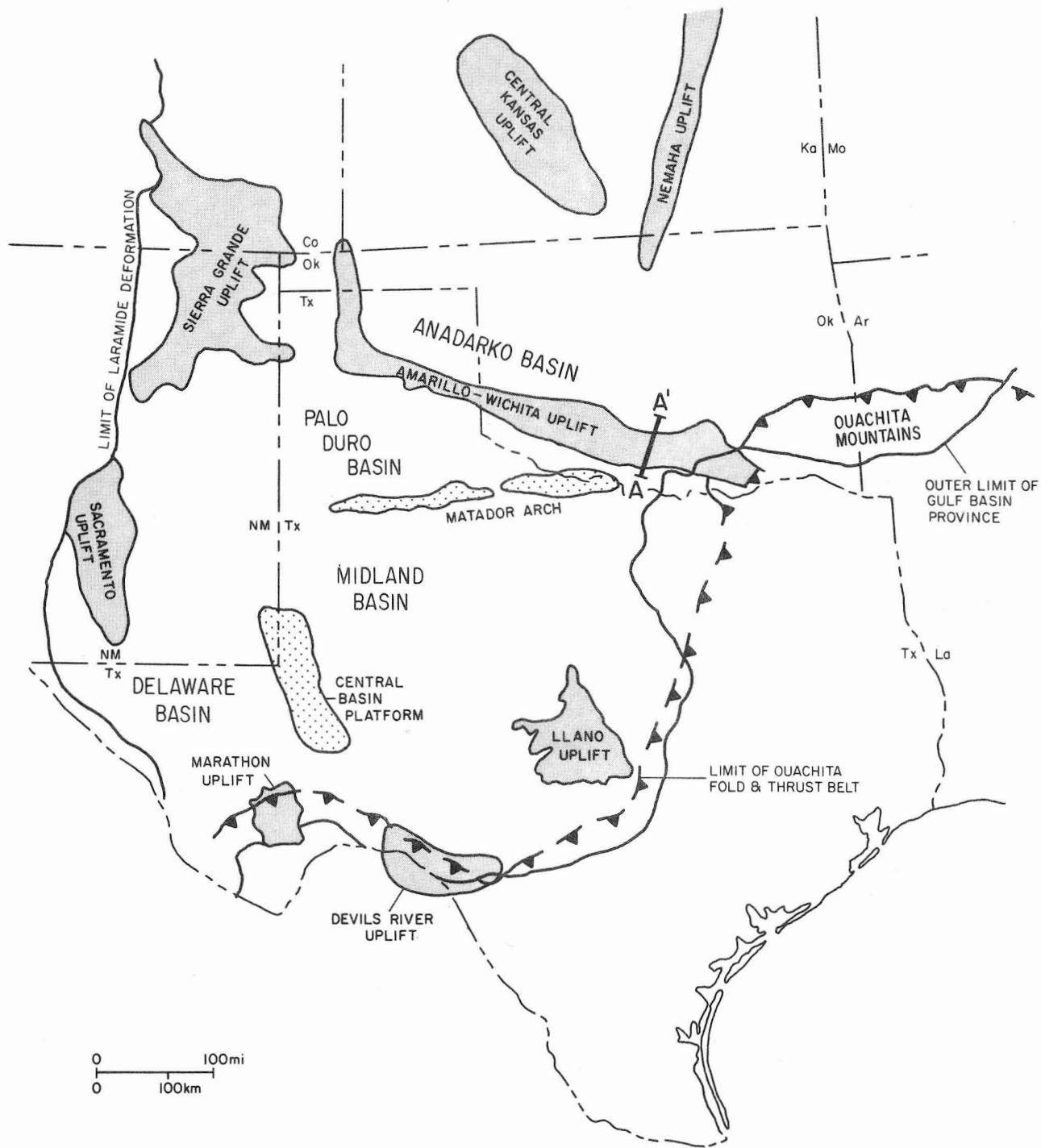
Figure 2. Generalized structure map of Texas and vicinity showing the locations of basement uplifts and intervening basins. Also included is the eastward limit of Laramide (Cenozoic) deformation, which masks the earlier structures and the limit of the Ouachita foldbelt and thrustbelt that formed synchronously with most of the uplifts.

7
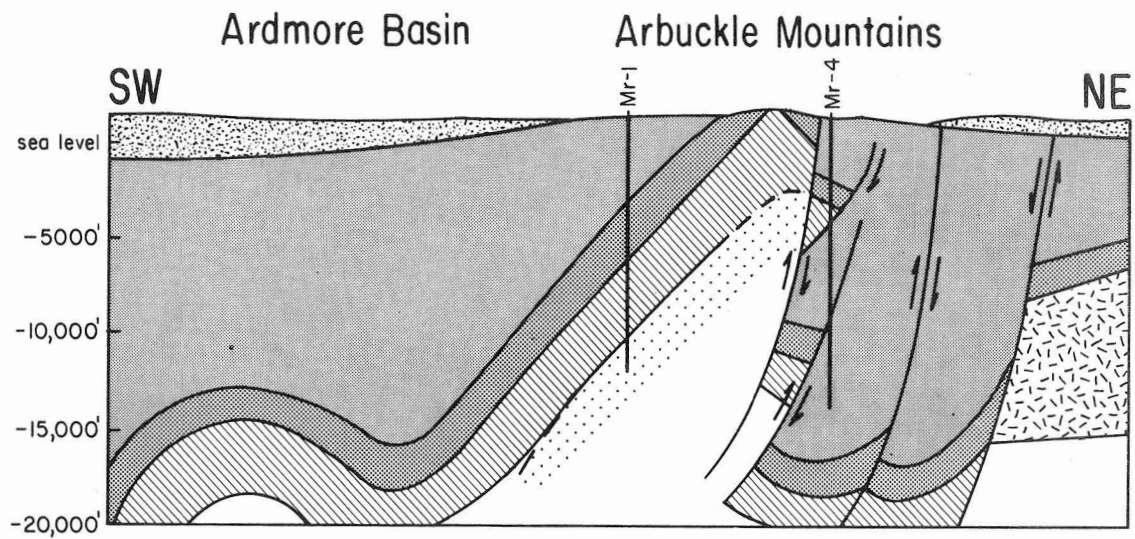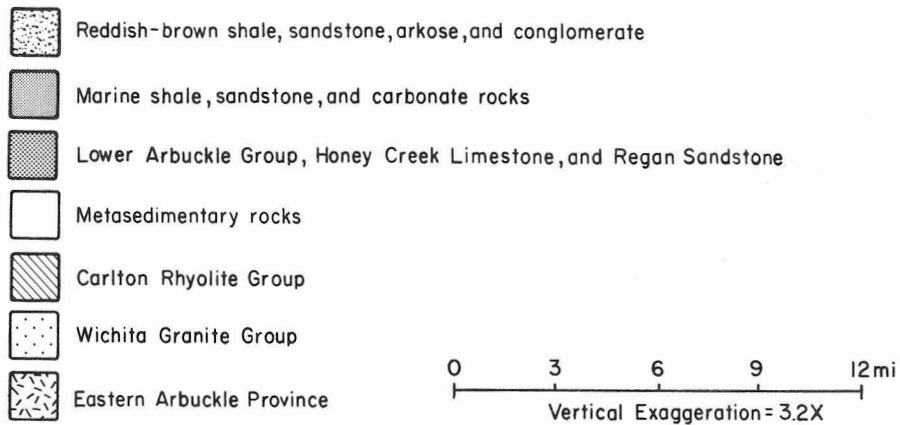
Figure 3. Northwest-southeast cross section through the Arbuckle (Wichita) Uplift and the Ardmore Basin (after Ham and others, 1964). Cross section A-A' is located on figure 2.

8
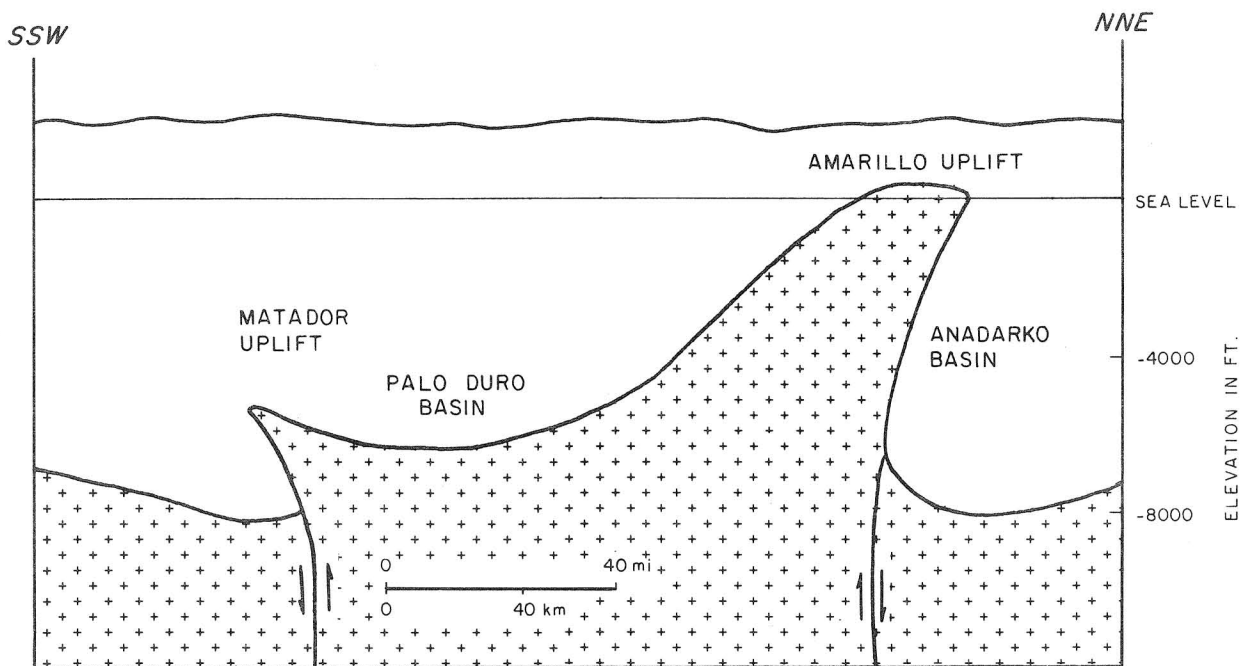
Figure 4. Interpretive schematic cross section through the Palo Duro Basin showing the high-angle reverse faults. Although the vertical dimension is exaggerated, the basin can be viewed as being isolated on an uplifted block of crust surrounded by deeper basins.

# PERMEABLE SHEET SANDSTONES OF THE GLORIETA FORMATION INTERTONGUE WITH SALT-BEARING ROCKS IN THE NORTHWESTERN TEXAS PANHANDLE

Mark W. Presley

*The Glorieta Sandstone in the northwestern Texas Panhandle was deposited in eolian environments landward of mud-rich tidal flats and coastal evaporites. Local porosity exhibited by this unit may enhance salt dissolution processes. However, the sandstone is limited in occurrence to marginal areas of the Palo Duro Basin.*

The Glorieta Sandstone in the Dalhart Basin and the northwestern Palo Duro Basin is commonly intercalated with salt (figs. 5 and 6). Sandstone beds are generally porous and permeable. Study of the nature and distribution of Glorieta sandstone facies is important because water can be transported through such permeable beds to produce subsurface salt dissolution. Investigation of the Glorieta Sandstone also provides a basis for evaluating potential for copper deposits, uranium deposits, and carbon dioxide gas.

Glorieta Sandstone is thickest along a northeast-southwest linear trend. Net sandstone along this trend is as much as 90 m (300 ft) thick (fig. 5). Glorieta Sandstone beds are tabular and laterally persistent. Cores of Glorieta sandstones in the area indicate that deposition was primarily within continental eolian environments (figs. 7 and 8). Glorieta eolian sandstones are well sorted, cross-stratified, and commonly exhibit a bimodal grain-size distribution (fig. 8). This bimodality is typically expressed as alternations of laminae composed of fine to medium sand with laminae composed of coarse silt to very fine sand. Laminae commonly dip at angles up to 34 degrees and are inferred to compose relatively large eolian cross-stratification sets. Within the Glorieta Sandstone, grain-size bimodality decreases upward and finer grain sizes become predominant. In cores, eolian sandstone units interbedded with salt are halite cemented and have low porosity. Drill cuttings of Glorieta eolian sandstones in the northwestern Panhandle typically consist of free sand grains of relatively uniform size. Although textural analysis of such samples is impossible, the surface morphology of individual sand grains resembles grain-surface morphologies described from modern eolian sands (Krinsley and Doornkamp, 1973; Folk, 1978). As observed by scanning electron microscope, Glorieta sand grains show overall grain smoothness, upturned quartz cleavage plates, impact depressions with smooth margins, and "turtle skin" silica coats. Rare cuttings of indurated, non-friable sandstone show a high maturity and a probable multicyclic history for individual grains.

In the Dalhart and northern Palo Duro Basins, mudflat and salt flat facies that are equivalent to the Glorieta sandstone are predominantly interlaminated mudstone and siltstone and chaotic mudstone-salt mixtures. These were deposited in mud-rich evaporitic tidal flats (fig. 7). Mudflat to eolian-flat transitions typically coarsen upward and are considered broadly regressive (figs. 9 and 10). In the western Palo Duro Basin, Glorieta eolian environments graded to the east into evaporitic mudflats during early Glorieta time, and into supratidal salt brine pans and shallow-water marine environments in late Glorieta time (fig. 7).

Studies are continuing on applications of Glorieta facies concepts to problems in salt dissolution and porosity development. For example, salt beds in the eastern Dalhart Basin commonly pinch out to the northwest in areas where Glorieta sandstone facies are present (fig. 10). McGookey (this volume) shows that this loss of salt to the northwest may be due to a combination of salt dissolution and salt pinch-out into terrestrial deposits. The Glorieta Sandstone is an aquifer along the western (eastern New Mexico) and northern (Amarillo Uplift and Oldham Nose) margins of the Palo Duro Basin. The sandstone is confined to the landward margin of the Glorieta depositional basin. Currently, salt dissolution is occurring along these basin margin areas and possibly is locally enhanced by water movements within the Glorieta aquifer. However, any salt dissolution resulting from fluids within the sandstone will be limited to basin margin areas.
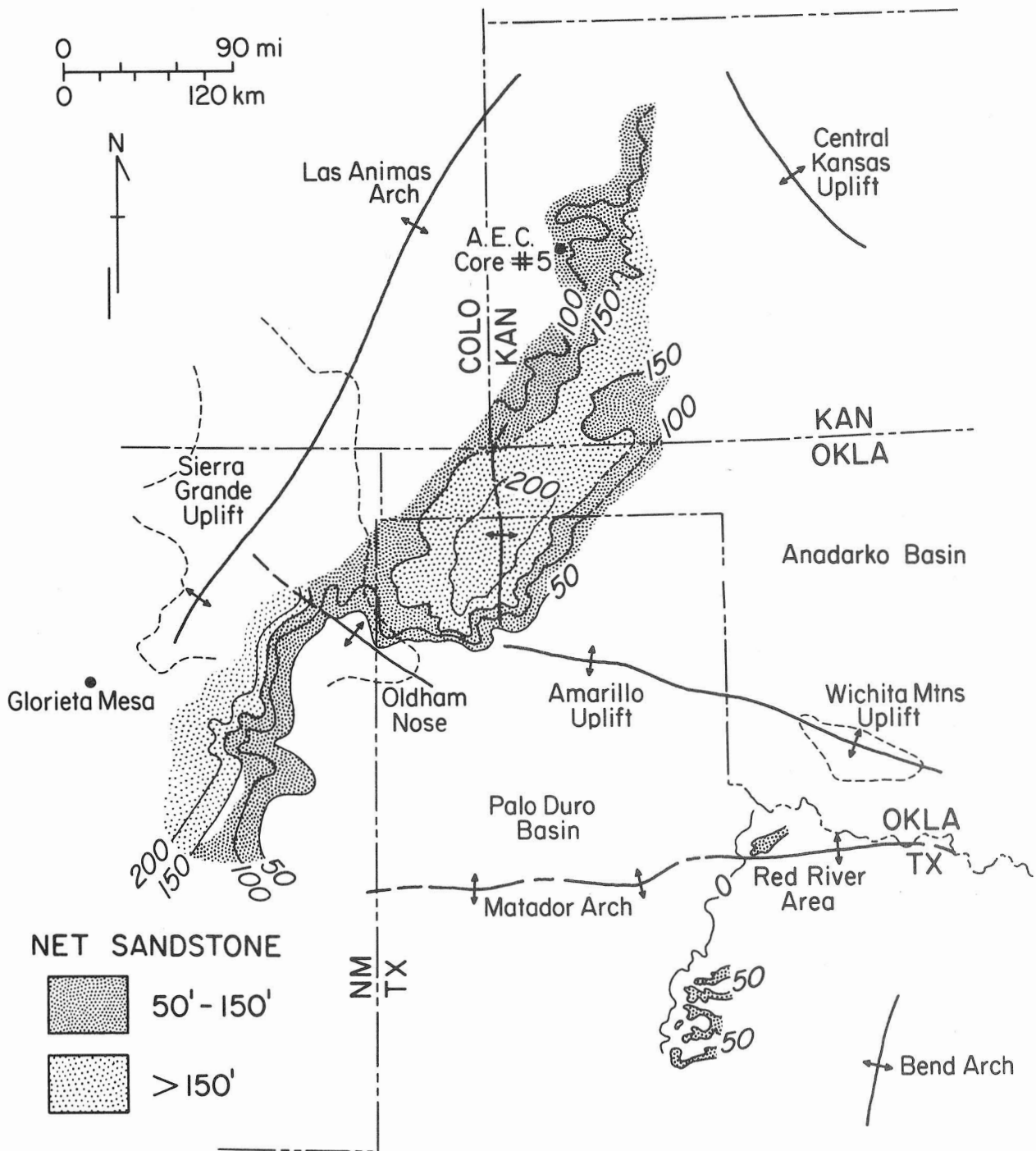
Figure 5. Location map of study area. Thickest net Glorieta Sandstone occurs in a southwest-northeast linear trend from eastern New Mexico to western Kansas. Net sandstone values in western Kansas are from Holdoway (1978). Net sandstone values in the southeastern Texas Panhandle are from Smith (1974), who mapped the San Angelo Formation, a time equivalent of the Glorieta. Glorieta Sandstone has been studied in central New Mexico by Milner (1978).
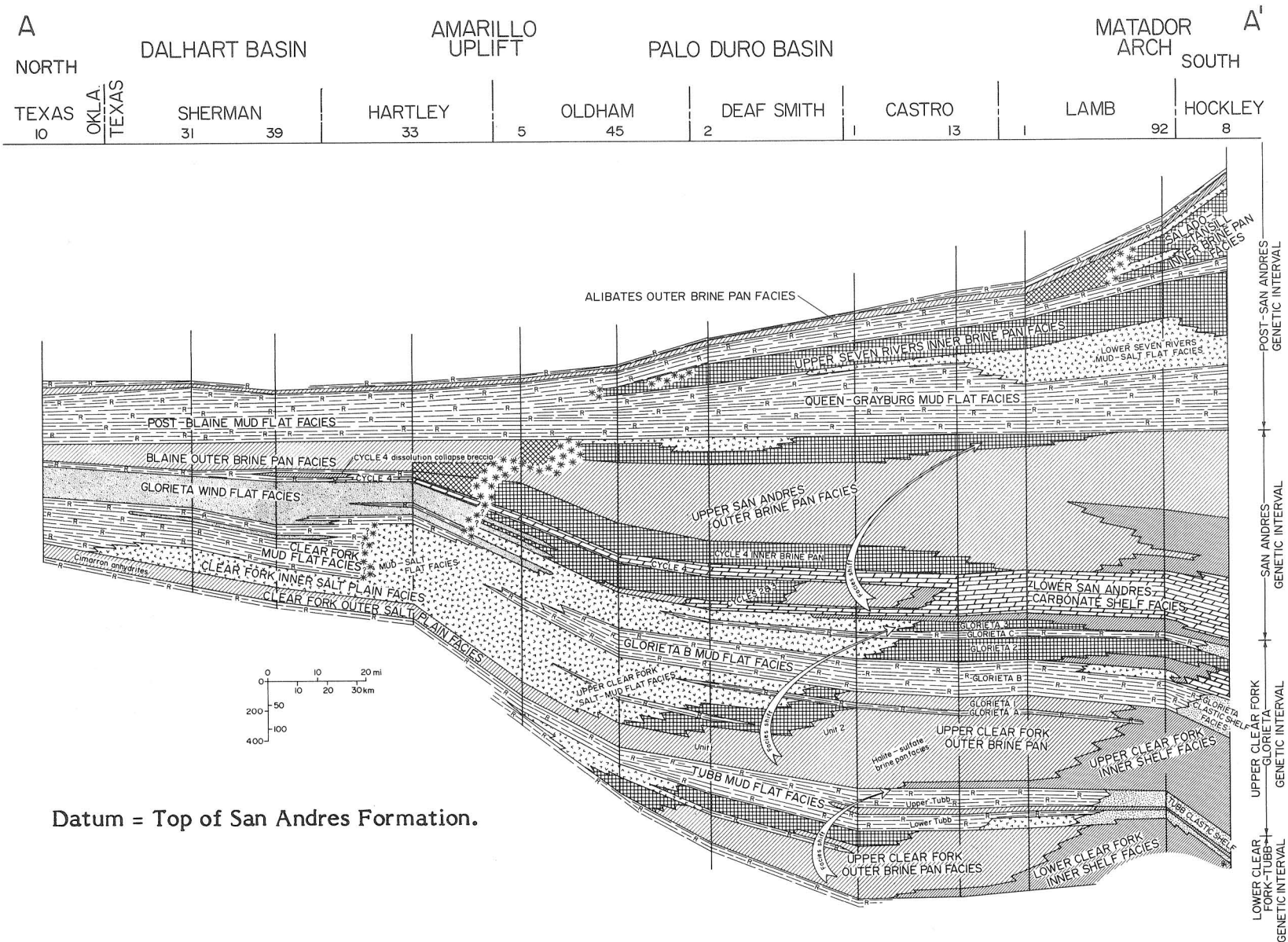
Figure 6. Regional north-south facies cross section of salt-bearing rocks in the Texas Panhandle. Eolian (wind-flat) facies of the Glorieta Sandstone compose tabular beds in the northern part of the cross section. Glorieta mudflat facies in the Palo Duro Basin are composed of interbedded mudstone-siltstone and evaporites. Glorieta clastic shelf facies south of the Matador Arch are sandy dolomites. For line of section and legend, see page 14.

# EXPLANATION
## FACIES INTERPRETATIONS
### EVAPORITE-CARBONATE SYSTEMS

←—LANDWARD                 SEAWARD—→

| | INNER SALT PLAIN | INNER BRINE PAN | 1.OUTER BRINE PAN or 2.OUTER SALT PLAIN | INNER SHELF | CARBONATE SHELF |
|---|---|---|---|---|---|
| DEPOSITIONAL SYSTEM → | INNER SALT PLAIN | INNER BRINE PAN | 1.OUTER BRINE PAN or 2.OUTER SALT PLAIN | INNER SHELF | CARBONATE SHELF |
| Alternate terminology | Salt-mud flat, mud-salt flat, salt flat | Halite brine pan | 1.Halite-sulfate brine pan, sulfate brine pan | | |
| Description → | Chaotic salt-mudstone mixtures, mudstone | Relatively mud-free salt, commonly banded; mudstone | 1.Relatively mud-free salt interbedded with bedded anhydrite (gypsum) 2.Chaotic salt-mudstone mixtures interbedded with mudstone-anhydrite | Dolomite, finely crystal-line, commonly anhydritic | Dolomite, finely crystal-line, commonly fossili-ferous; limestone |

### SILICICLASTIC SYSTEMS

←—LANDWARD                SEAWARD—→

| | WIND FLAT | RED BED | CLASTIC SHORELINE |
|---|---|---|---|
| DEPOSITIONAL SYSTEM → | WIND FLAT | RED BED | CLASTIC SHORELINE |
| Alternate terminology and facies | Eolian systems | Mudflat, mud-wind flat facies, alluvial plain | |
| Description → | Sandstone, well-sorted, frosted grains, typically cross-stratified, facies position updip from mud flats/brine pan | Mudstone and siltstone, typically interlaminated; sandstone | Sandstone, typically inter-bedded with dolomite, facies position seaward of red beds |

indicator that facies re-cord may be altered by subsurface dissolution of salt. Facies interpre-tations updip from indi-cator are unclear.

Salt dissolution. Loss of salt beds is due to modern or ancient dissolution pro-cesses. Question marks in-dicate uncertainty, typical-ly where loss of salt beds may be facies controlled

0  20  40  60  80 mi
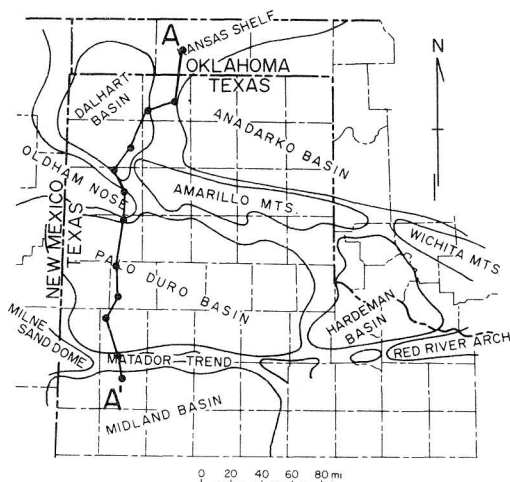
**Figure 6 (continued).**

## LOCATION MAP

14
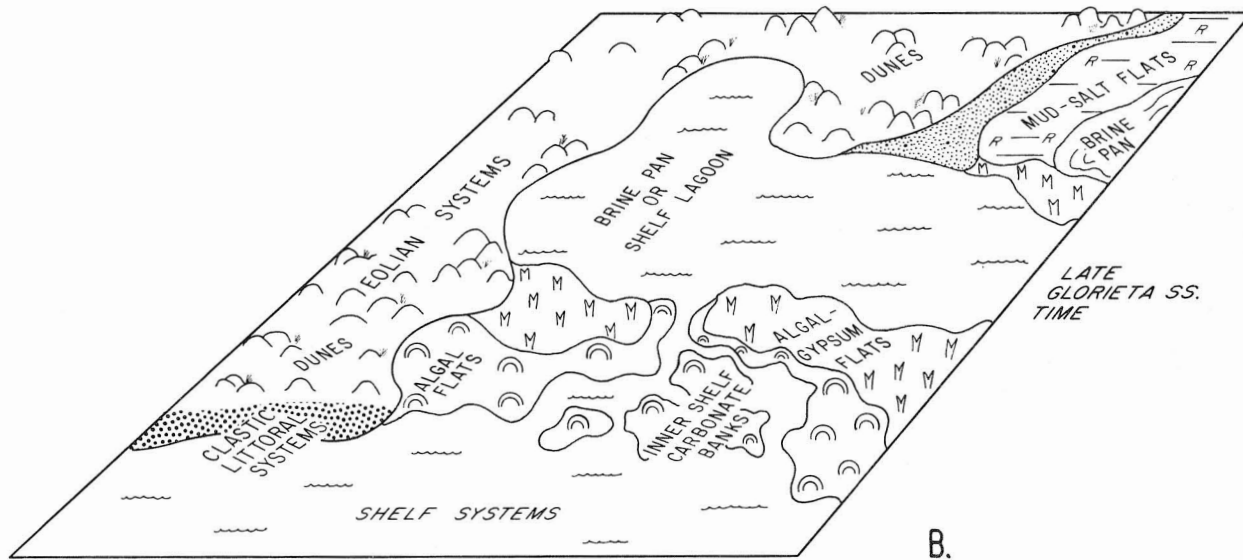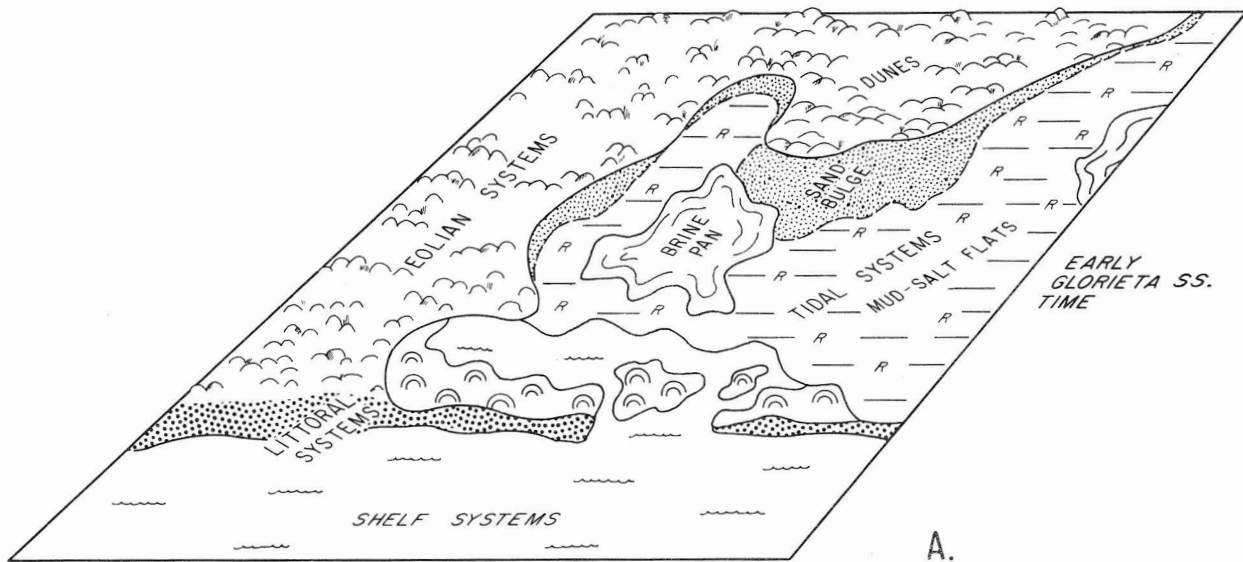
Figure 7. Paleogeography during Glorieta time. (A) During early Glorieta time, eolian flats graded progressively southward into mudflats and then into shallow marine shelf environments. (B) During late Glorieta time (early San Andres time) there was a landward shift in environments, and eolian systems formed the shoreline of broad evaporitic brine pans and lagoons.

15
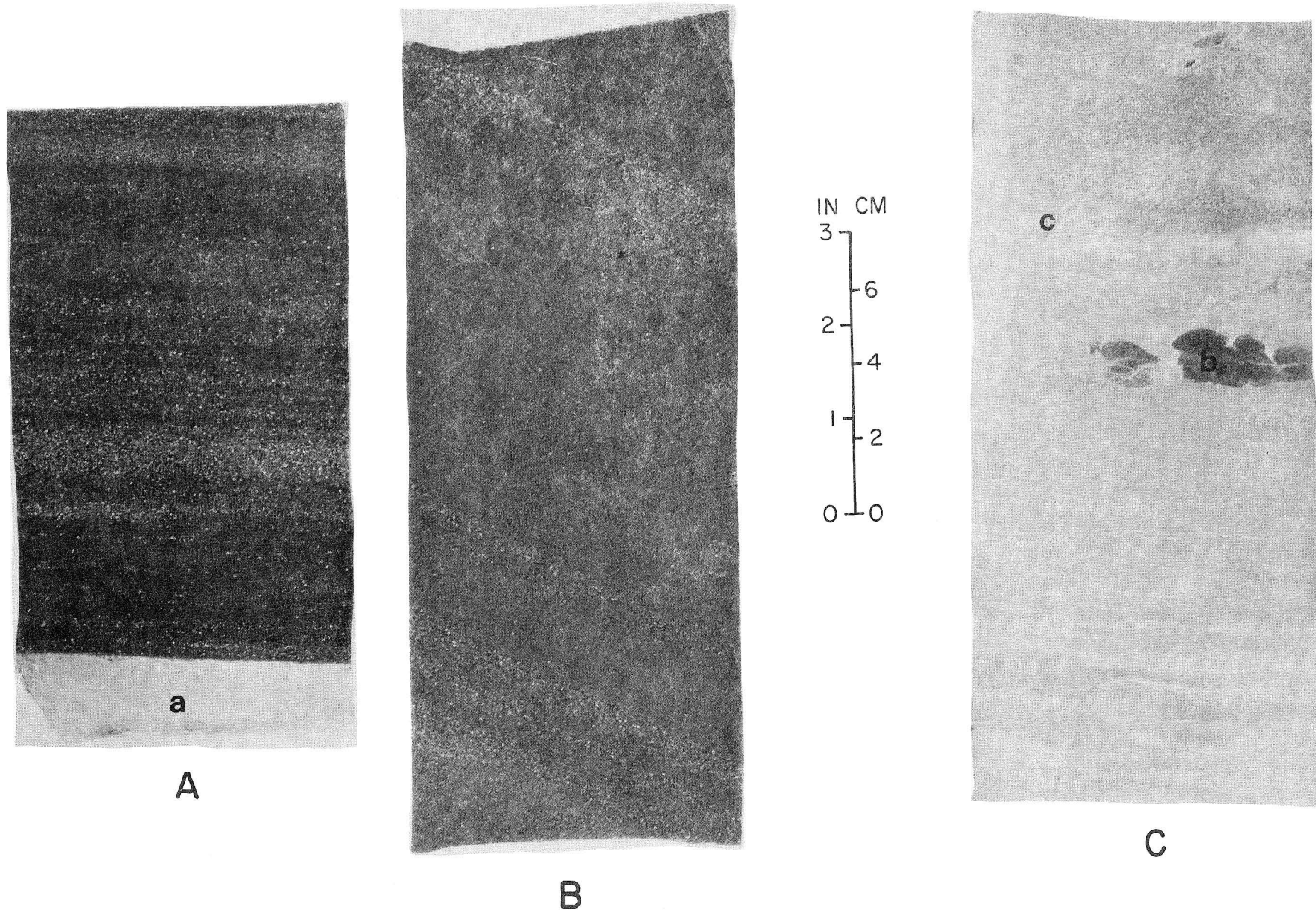
Figure 8. Eolian sandstone facies of Cedar Hills (Glorieta) Sandstone, western Kansas, in U.S. Atomic Energy Commission core number 5. (A) Bimodal smooth-laminated sandstone exhibits interlaminae of differing grain sizes and is halite cemented. Fracture-filling halite is at bottom of sample (a). Depth of sample 2,032 ft (619.6 m). (B) Such bimodal sandstones typically exhibit high-angle cross-stratification. Depth of sample 2,017 ft (614.8 m). (C) Laminated siltstone contains nodular anhydrite (b) and is overlain by sandstone. Flowage structures at contact (c) suggest soft-sediment loading by sand. Depth of sample 2,039 ft (621.5 m).
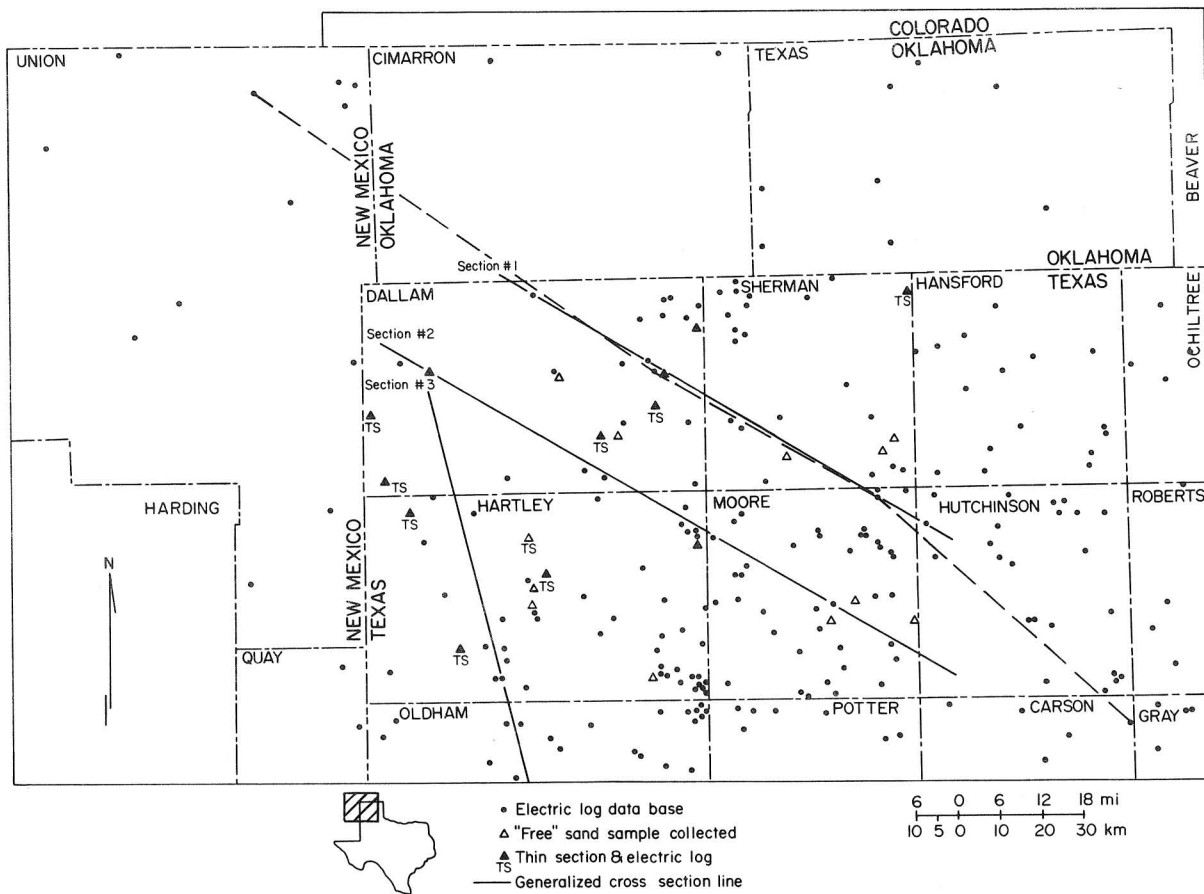
Figure 9. Dalhart Basin study area. Symbols show types of well data and lines of section (on file at the Bureau of Economic Geology) used to make interpretations. Dashed line is cross section shown in figure 10.

17
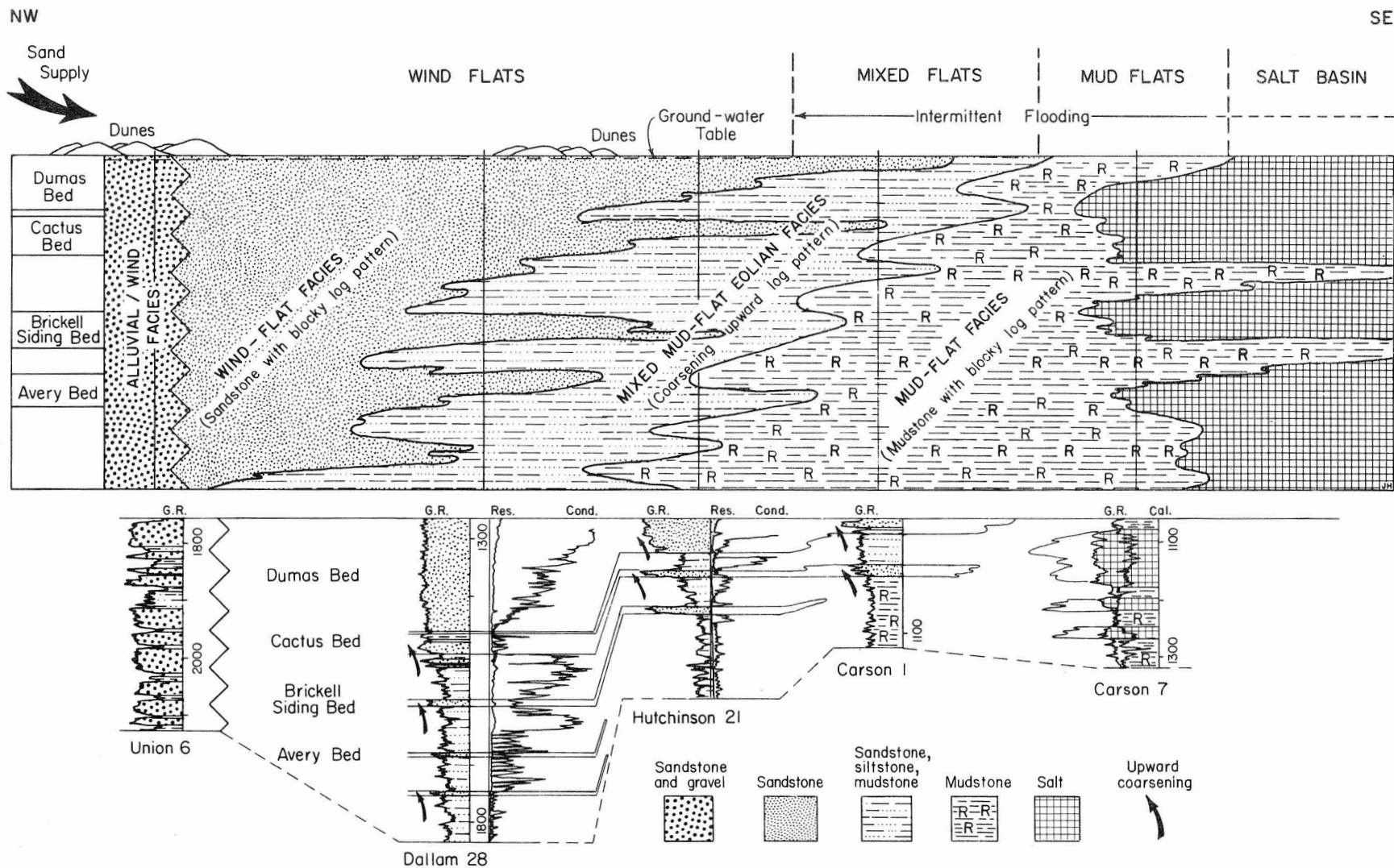
Figure 10. Facies cross section of Glorieta Sandstone model in the Dalhart Basin, where sandstone facies intertongue to southeast with mudstone and salt. Location shown is in figure 9. Section is a typical northwest to southeast transect across the Dalhart Basin into the Anadarko Basin. Alluvial plain/wind-flat facies grade progressively basinward (to the southeast) into coastal wind-flat facies deposited where eolian processes were predominant, then into transitional facies, and finally into mudflat and salt basin facies. Upward coarsening at the base of sandstone beds of the Glorieta Formation is a record of repetitive, gradual basinward shifts of these environments.

# STATISTICAL ANALYSIS OF LITHOLOGIC INTERPRETATIONS FROM WELL LOGS

*Mark W. Presley*

*Analysis of geophysical well log parameters from the Randall and Swisher Counties test wells provides statistical justification for interpreting lithofacies from logs. Such analysis is considered important in extending observations from cores to regional analysis of salt beds where data are limited to well logs.*

Many rock types noted in cores of salt-bearing formations in the Palo Duro Basin can be identified by use of geophysical well logs. Subjective interpretations of various types of salt, anhydrite, dolomite, and siliciclastics have been described previously (Presley, 1979a; McGillis, 1980). The goal of this continuing study has been the mathematical justification for these lithic interpretations and the development of statistically justified interpretive techniques.

To calibrate lithic interpretations by use of geophysical well logs, wire-line logs from test wells drilled by the Department of Energy were computer digitized. Cores from these wells penetrate all salt-bearing stratigraphic units and are presently under study at the Bureau of Economic Geology. Available geophysical well log curves from these core holes include measurements of natural gamma radiation (gamma ray), various sonic parameters (sonic travel time, sonic amplitude, and variable density), borehole diameter (caliper), and electrical resistivity, as well as derived measurements of porosity and density (bulk density, density porosity, and neutron porosity). Statistical analysis was adapted to Statistical Package for Social Sciences (SPSS) computer software; frequency (univariant), scattergram (bivariant), and discriminant (univariant to multivariant) programs have been used.

As an example of preliminary analyses, comparisons of neutron porosity and density porosity values taken from the test wells at depth intervals of 1 ft can be used for discriminating a wide variety of lithic types (fig. 11). Various rock types exhibit distinctive combinations of neutron and density porosity values, which plot in widely separated groups.

Sonic logs with gamma ray curves are available from many oil and gas wells in the Palo Duro Basin. Criteria for interpreting lithologies from sonic logs in the Randall and Swisher Counties test wells can be extended to sonic logs from other parts of the basin. A plot of gamma ray values versus sonic travel time taken at 1-ft intervals down the borehole shows lithologic groupings (fig. 12). An expanded-scale plot of these parameters for salt lithologies was compared to core descriptions of the

Glorieta Formation from the test wells (figs. 13 and 14). Massive salt as illustrated in figure 14 typically exhibits gamma ray values less than 15 API units and sonic travel times of 67 to 70 microseconds. Values for both log parameters increase with increasing mudstone content.

Precise statistical analysis of criteria for interpreting lithology from well logs is continuing. For applications of log interpretation criteria developed from the Randall and Swisher Counties test wells, sources of error and non-lithologic controls on wire-line logs such as borehole diameter, drilling mud density, and mathematical assumptions in derivation of log curves are being considered. Statistical analysis of lithologic interpretations from logs is considered important in regional analysis of salt beds since core is available from only a few selected sites, and wire-line logs are available from over all the study area.
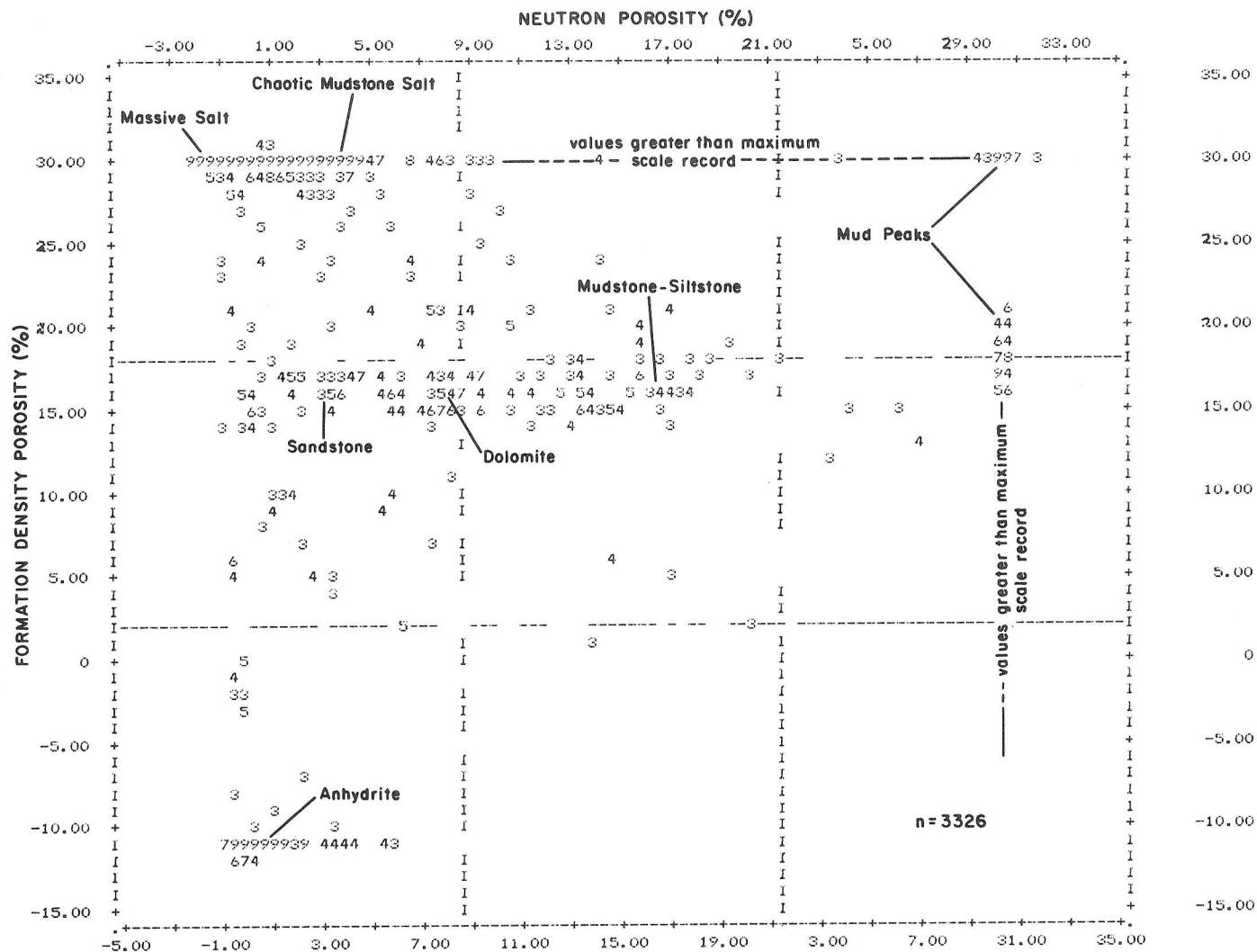
Figure 11. Plot of density porosity versus neutron porosity values in Permian salt-bearing units in the Swisher County test well. Sampling of log values was at 1-ft intervals down the borehole. Discriminations of rock types as illustrated in this example are related directly to lithic descriptions of cores. Numbers plotted indicate frequency of occurrence for one pair of neutron and density porosity values. Frequencies of occurrence of only one or two at a particular plotting position are not shown; frequencies of occurrence of nine or greater are represented by the number 9. Points defining salt at density porosity values of 30 percent result from off-scale readings in intervals where the borehole has been enlarged by salt solution during drilling.

GAMMA RAY (API units)

```
          7.50      22.50      37.50      52.50      67.50      82.50      97.50     112.50     127.50     142.50
        .+----+----+----+----+----+----+----+----+----+----+----+----+----+----+----+----+----+----+----+----+----+.
140.00  +                                        I                                     I                          +    140.00
        I                                        I                                     I                          I
        I                                        I                                     I                          I
        I                                        I                                     I                          I
130.00  +                                        I                                     I                          +    130.00
        I                                        I                                     I                          I
        I                                        I                                     I                          I
        I                                        I                                     I                          I
120.00  +                                        I                                     I                          +    120.00
        I                                        I                                     I                          I
        I                                        I                                     I                          I
        I                                        I                                     I                          I
        I                                        I                                     I                          I
110.00  +                                        I                                     I                          +    110.00
        I                                        I                                     I                          I
        I------------------------------------------------------------------------------------------------------I
        I                                        3                                     I                          I
        I                                        I                                     I                          I
100.00  +                                                   3                          I                          +    100.00
        I                                                        3                     I                          I
        I                                                   3                          I                          I
        I                                       3    534                               I                          I
        I                              4    I      3   3                               I                          I
90.00   +  Chaotic                           53   4434  3                              I                          +    90.00
        I  Mudstone-Salt                          33448    3                           I                          I
        I                                    3       3  3 55  534                       I                          I
        I                                          3  3 387  38                         I                          I
        I                       3            5   3 33 444735443                         I                          I
80.00   + Massive     4   5   73 3           6364   3 3569  544      Mudstone-Siltstone  I                         +    80.00
        I  Salt            5      3433 5537 3355 6668554 43                              I                          I
        I            343534965 56 5 46 4 7 333 5 67475 43                               I                          I
        I----356459989979957339 33534334698698355------------------------------------I
        I    495999999959668867347 46 4644357933                                       I
70.00   +  69999999987899677 4 4433 6574456 6533                                        I                         +    70.00
        I 39999999998999 7 3865 6535  35 497 3                                          I                          I
        I 59999975 45 454 3   346  3   3   6    4                                       I                          I
        I  465  5 3 44 34      4  3 36   4 433 3 3                                       I                          I
        I   7 437  54 4        34 4   5  5 I                                             I                          I
60.00   +  6 3  3 333  37366  3  3  4      3       Sandstone                             I                         +    60.00
        I 37967 4 545    634  3                    3                                     I                          I
        I 998   957586965 5  6533           I                                            I                          I
        I 499848999 4653 4  54              I                                            I                          I
        I 59998 697  7                      I                                            I                          I
50.00   +4799993 4          Dolomite        I                                            I    n = 3335            +    50.00
        I   53  3  Anhydrite                I                                            I                          I
        I                                   I                                            I                          I
        I                                   I                                            I                          I
        I                                   I                                            I                          I
40.00   +                                   I                                            I                          +    40.00
        .+----+----+----+----+----+----+----+----+----+----+----+----+----+----+----+----+----+----+----+----+----+.
          0      15.00      30.00      45.00      60.00      75.00      90.00     105.00     120.00     135.00     150.00
```

INTERNAL TRANSIT TIME (microseconds/ft)

22

Figure 12. Plot of sonic travel time versus level of natural gamma radiation in salt-bearing units in the Swisher County test well. Sampling of log values was at 1-ft intervals down the borehole. Statistical analysis of gamma ray and sonic values is important since these logs are available from many oil and gas wells in the Palo Duro Basin. Frequencies of one and two are filtered from display. Drill bit size was 8.5 inches (21.6 cm); maximum borehole enlargement was generally less than 13 inches (33 cm), and mud density at the time of logging was 10.2 lbs/gal (1.2 g/cm$^3$).
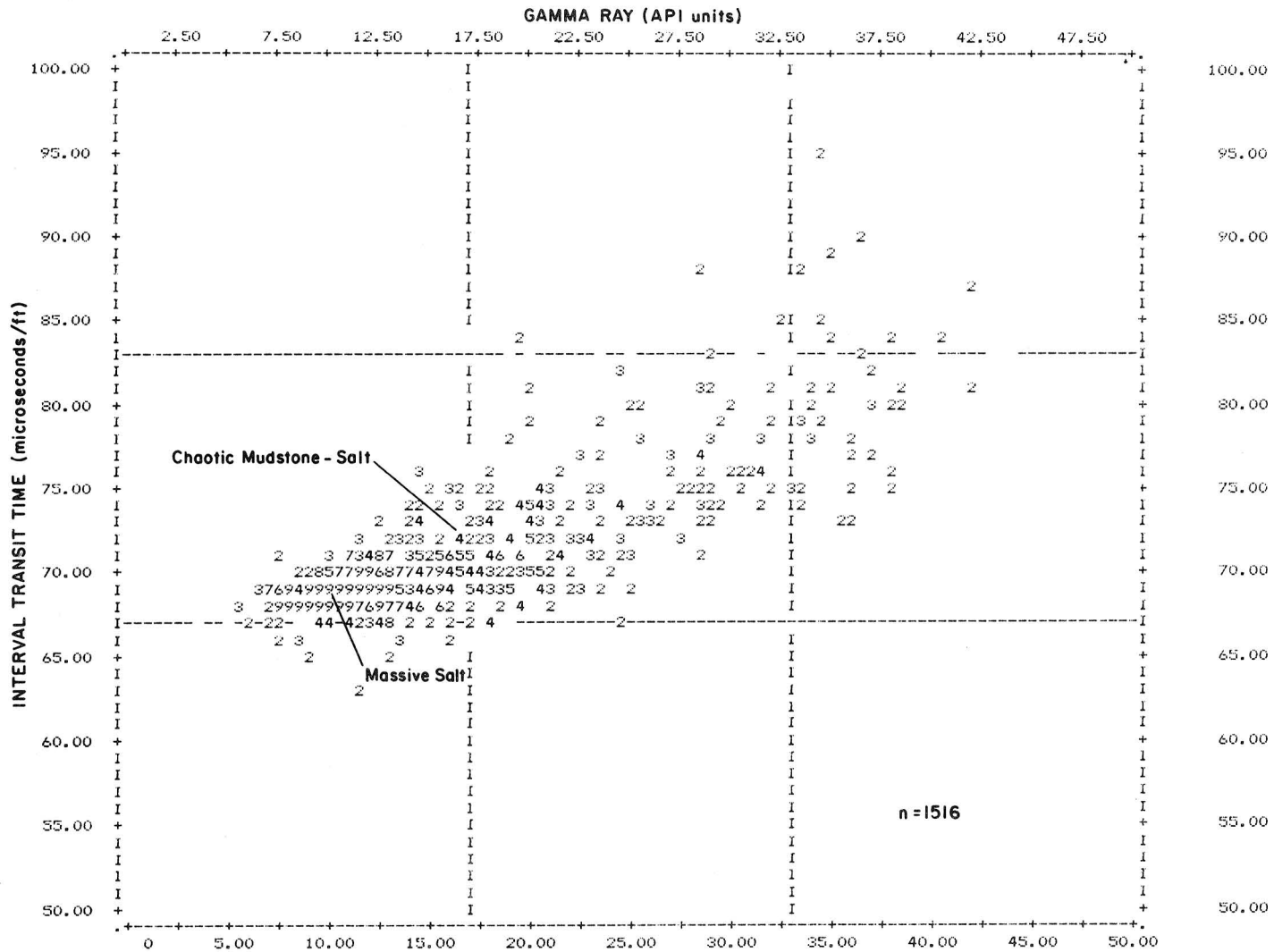
Figure 13. Plot of sonic travel time versus level of natural gamma radiation for salt lithologies in the Randall County test well. This plot of gamma ray versus sonic values can be compared to core descriptions of the Glorieta Formation (fig. 14). Massive salt typically exhibits gamma ray values less than 15 API units, and sonic travel times of 67 to 70 microseconds. Values for both log parameters increase with increasing mudstone content. Drill bit size was 8.5 inches (21.6 cm); maximum borehole enlargement owing to solution of salt was generally 11 to 14 inches (28 to 36 cm), and mud density at the time of logging was 10.6 lbs/gal (1.3 g/cm$^3$). Frequencies of one are filtered from display.
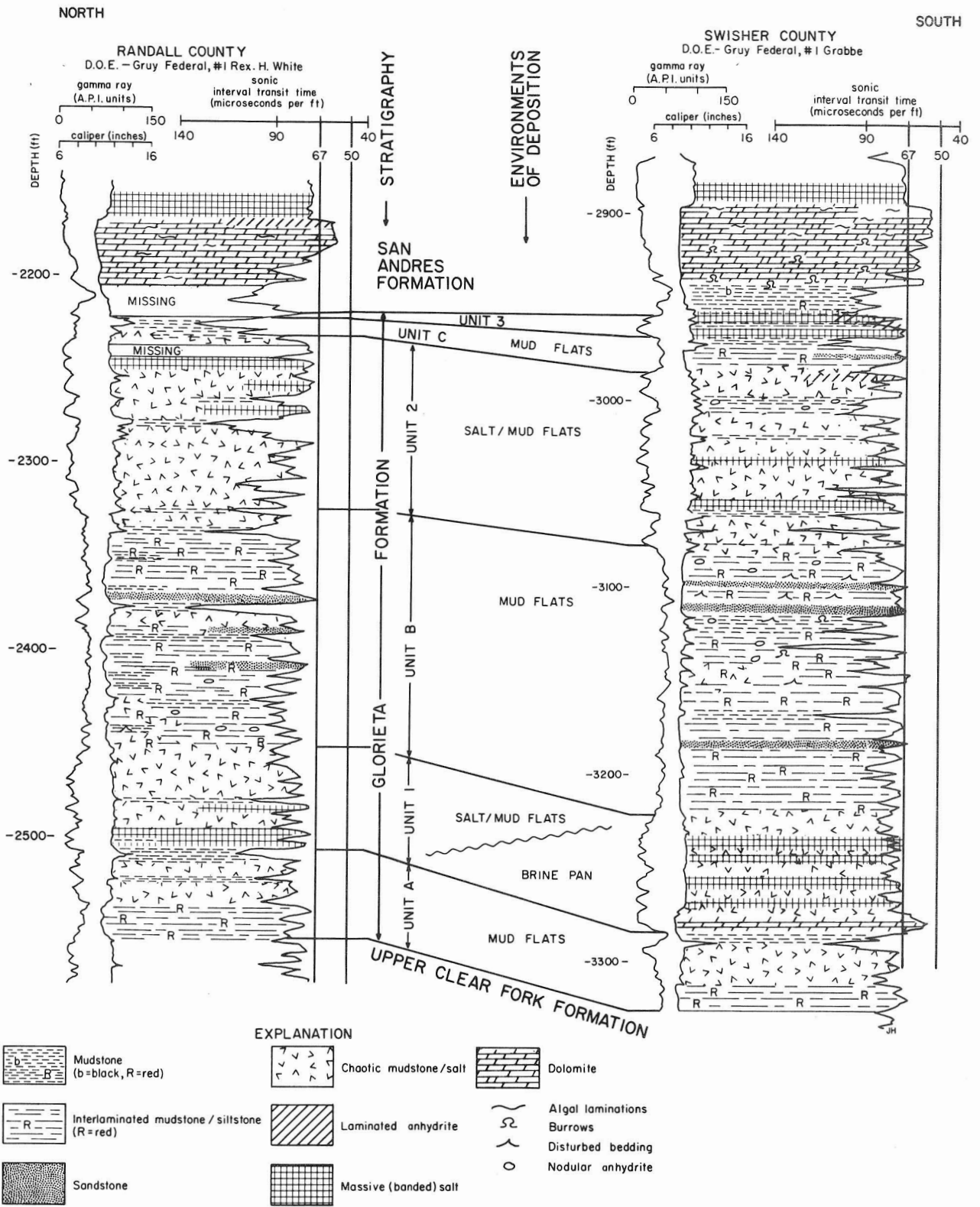
Figure 14. Lithic descriptions of core compared to well logs of the Glorieta Formation and the lower part of the San Andres Formation, Randall and Swisher Counties test wells. Location shown in figure 15. Sonic and gamma ray values of salt descriptions are consistent with lithic groupings on plots of sonic and gamma ray values in figures 12 and 13.

24

# UPPER CLEAR FORK AND GLORIETA SALT STRATIGRAPHY AND SALT PURITY

Mark W. Presley and Kathy A. McGillis

*The upper Clear Fork and Glorieta Formations contain interbedded massive salt, chaotic mudstone-salt, and mudstone. Upper Clear Fork massive salt beds occur in the Dalhart Basin and in the northern Palo Duro Basin. Massive salt in the Glorieta Formation is most common in the western Palo Duro Basin.*

The upper Clear Fork and Glorieta Formations constitute a single lithogenetic unit in the Palo Duro and Dalhart Basins and are composed of interbedded red beds, evaporites, and carbonates. This investigation is one of several studies aimed at understanding the stratigraphy and facies distribution within each Permian salt-bearing sequence in the Palo Duro and Dalhart Basins.

Thickest net salt in the lower part of the upper Clear Fork Formation is in the Dalhart Basin, whereas thickest net salt in the upper part of this formation is in the central and northern Palo Duro Basin (figs. 15 and 16). Upper Clear Fork salt beds intertongue to the south with nonporous carbonates and bedded anhydrite and to the north with red beds (fig. 16). Glorieta net salt is thickest in the western Palo Duro Basin (fig. 17). Glorieta salt beds occur in units between thick beds of red mudstone and siltstone (fig. 18).

Salt beds in the upper Clear Fork and Glorieta Formations occur from depths of 300 to 1,500 m (1,000 to 5,000 ft) within the study area. Subsurface dissolution of Glorieta salt has occurred along the Amarillo Uplift. McGookey (this volume) has investigated the problem of distinguishing effects of salt dissolution from salt facies changes in this area and provides guidelines for interpretation.

Seaward facies in upper Clear Fork and Glorieta Formations are predominantly dolomitic mudstones that contain nodular anhydrite and exhibit upward-shoaling successions of facies similar to those observed in modern coastal carbonate sabkhas. Landward of the shoaling carbonates was a vast salt plain, or sabkha, in which evaporites were deposited in supratidal brine pans and salt flats (fig. 6). Brine pan environments on the seaward parts of the salt plain were intermittently flooded from periodic tides or ground-water seepage. Deposits of gypsum and relatively massive salt formed in the ponded waters. Salt flat environments landward of brine pans were relatively exposed; deposition of evaporites on salt flats was as salt crusts and by interstitial precipitation in previously deposited clastic, evaporite, and carbonate host sediments. Periodically, particularly in Glorieta time, evaporite sedimentation was

terminated by the development of broad mud-rich tidal flats that extended across the entire salt plain.

Evaporites in upper Clear Fork-Glorieta strata are arranged in cycles of marine shelf, brine pan, and salt flat facies. Detailed facies mapping of upper Clear Fork cycle 2A provides an example of the stages of development of one of these cycles (figs. 19 and 20). In the central Palo Duro Basin, a typical succession of facies in unit 2A is (1) algal-laminated dolomite, grading upward into (2) laminated anhydrite interbedded with massive salt, and capped by (3) chaotic mudstone-salt. In the southern Palo Duro Basin, these facies grade into dolomite; to the north they grade into chaotic mudstone-salt. This succession is considered a record of relatively rapid transgression at the beginning of unit 2A time, followed by a gradual basinward shift in brine pan and salt flat environments during the continued deposition of the unit.

The upper Clear Fork and Glorieta Formations together exhibit a broad cycle of southerly regression (fig. 6). Upper Clear Fork facies in the central Texas Panhandle record the dominance of carbonate and evaporite deposition in inner shelf, brine pan, and salt flat environments (fig. 19). During Glorieta time, as southerly regression reached a maximum, mudflat and salt flat environments were predominant in the central Texas Panhandle (fig. 14). In the western Palo Duro Basin, in what was presumably an area of greater subsidence, there was periodic development of brine pans and deposition of some relatively massive salt.

Application of these facies concepts to upper Clear Fork and Glorieta rocks allows predictions of lateral and vertical changes in salt quality and purity on a regional scale as well as locally in the vicinity of a potential repository bed. Capability to make such interpretations will be vital in area and site characterization.
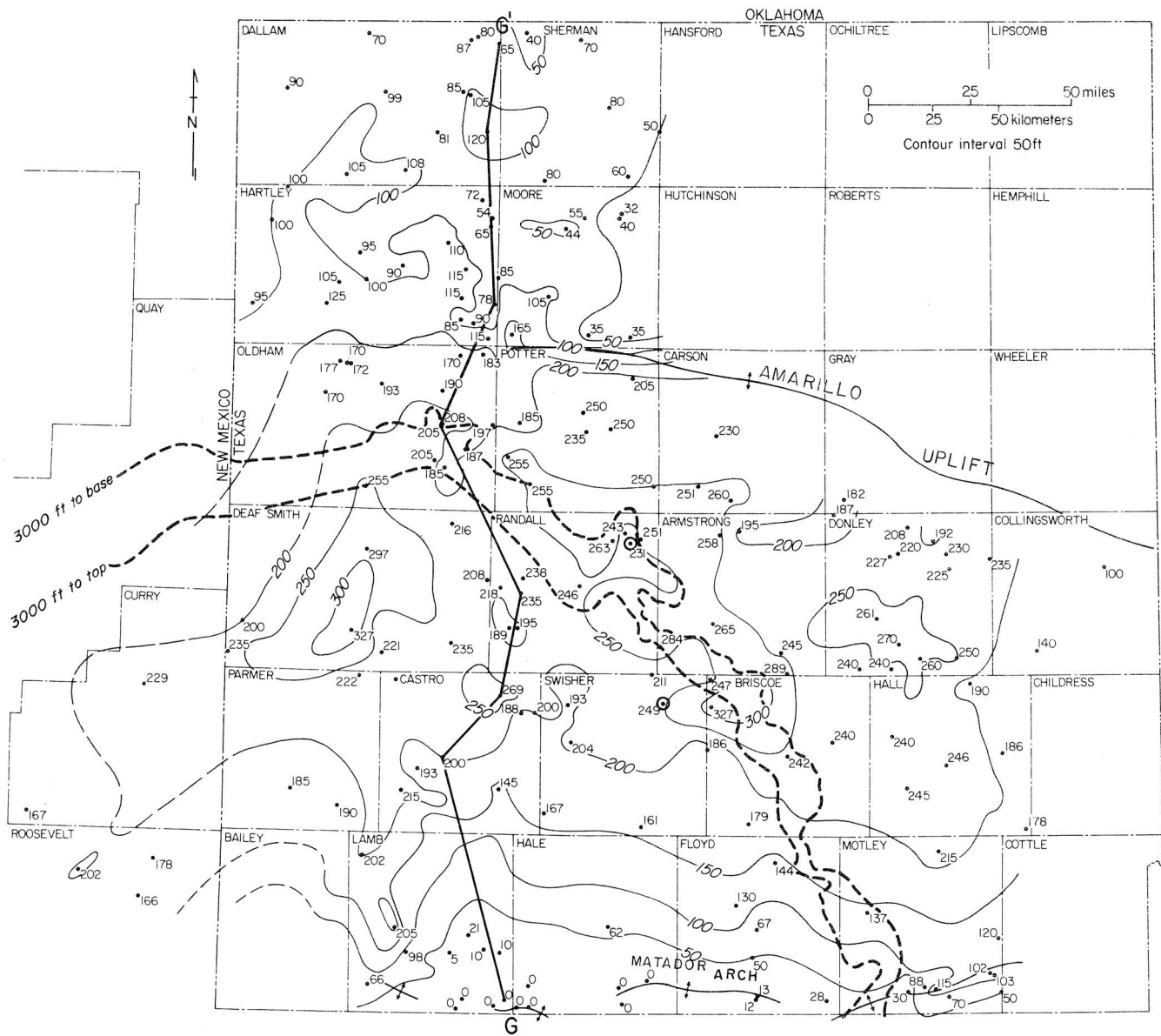
Figure 15. Net salt map of upper Clear Fork Formation. Depths of 3,000 ft (914 m) to the top and base of the unit are shown by dashed line; upper Clear Fork salt beds are at shallower depths to the north. Cores used in this study are circled data points.
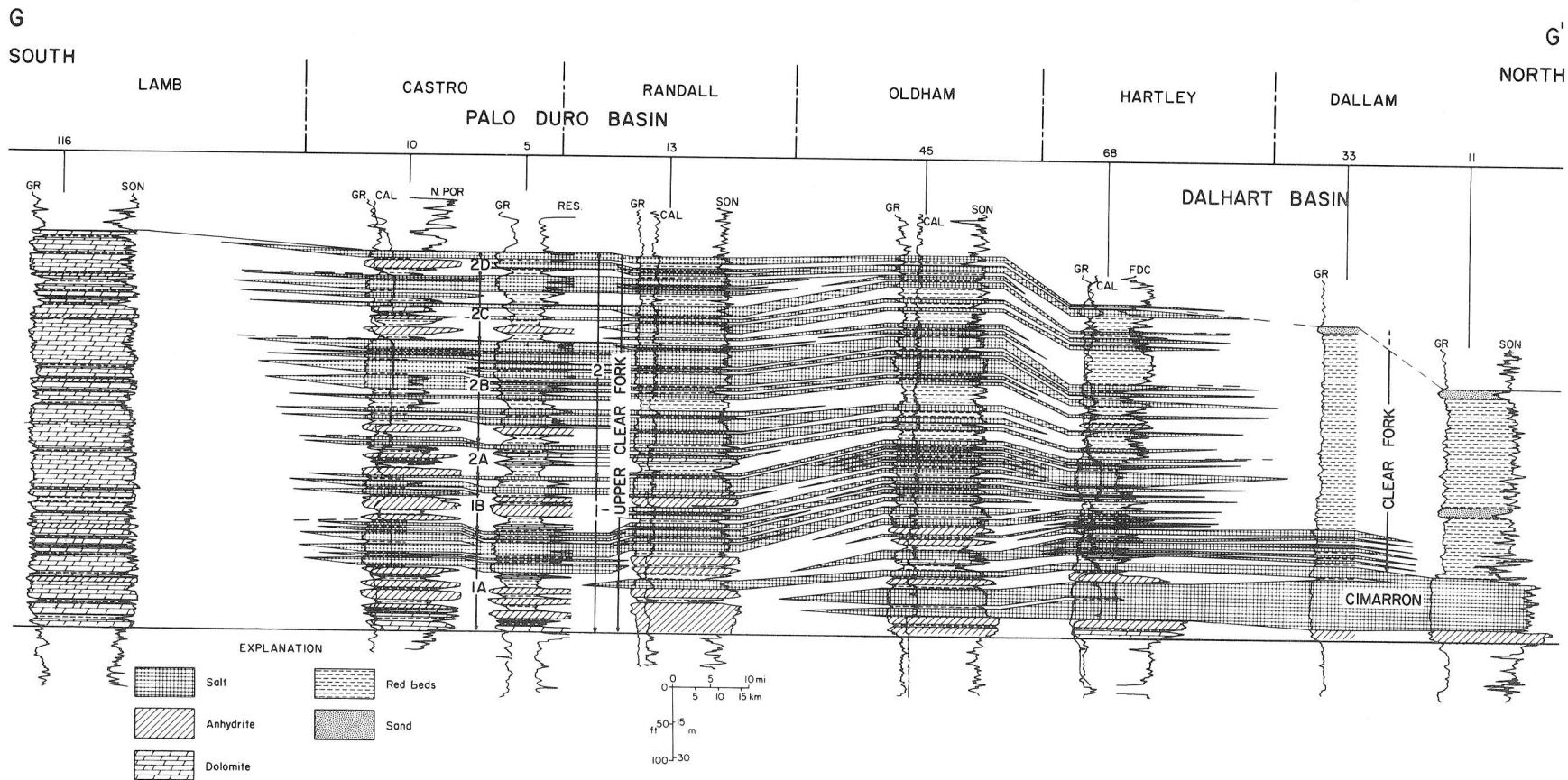
Figure 16.   Regional north-south cross section G-G' of upper Clear Fork Formation shows generalized lithologic interpretations. For location, see figure 15.
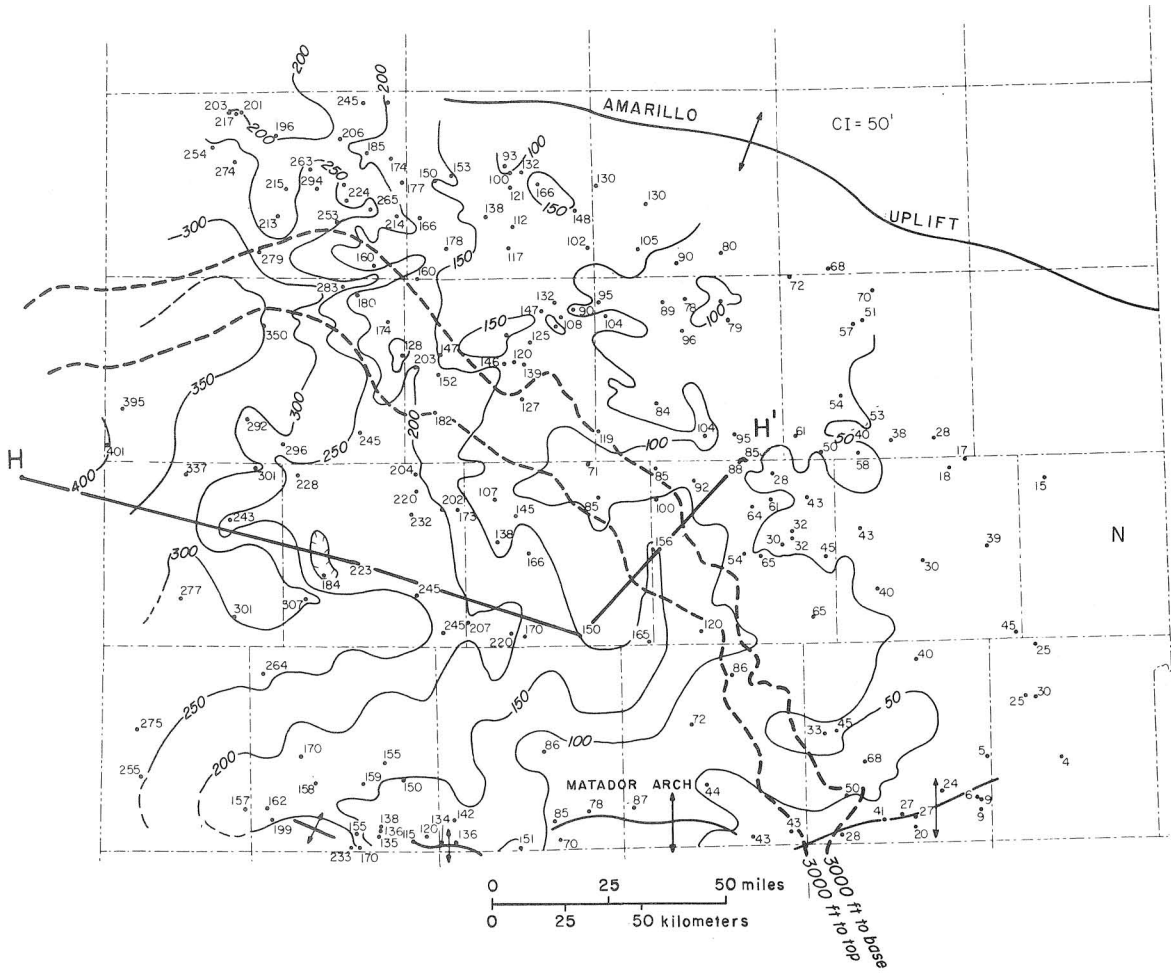
Figure 17. Net salt map of the Glorieta Formation. Depths of 3,000 ft (914 m) to the top and base of the unit are shown by dashed line; Glorieta salt beds are at shallower depths to the north.
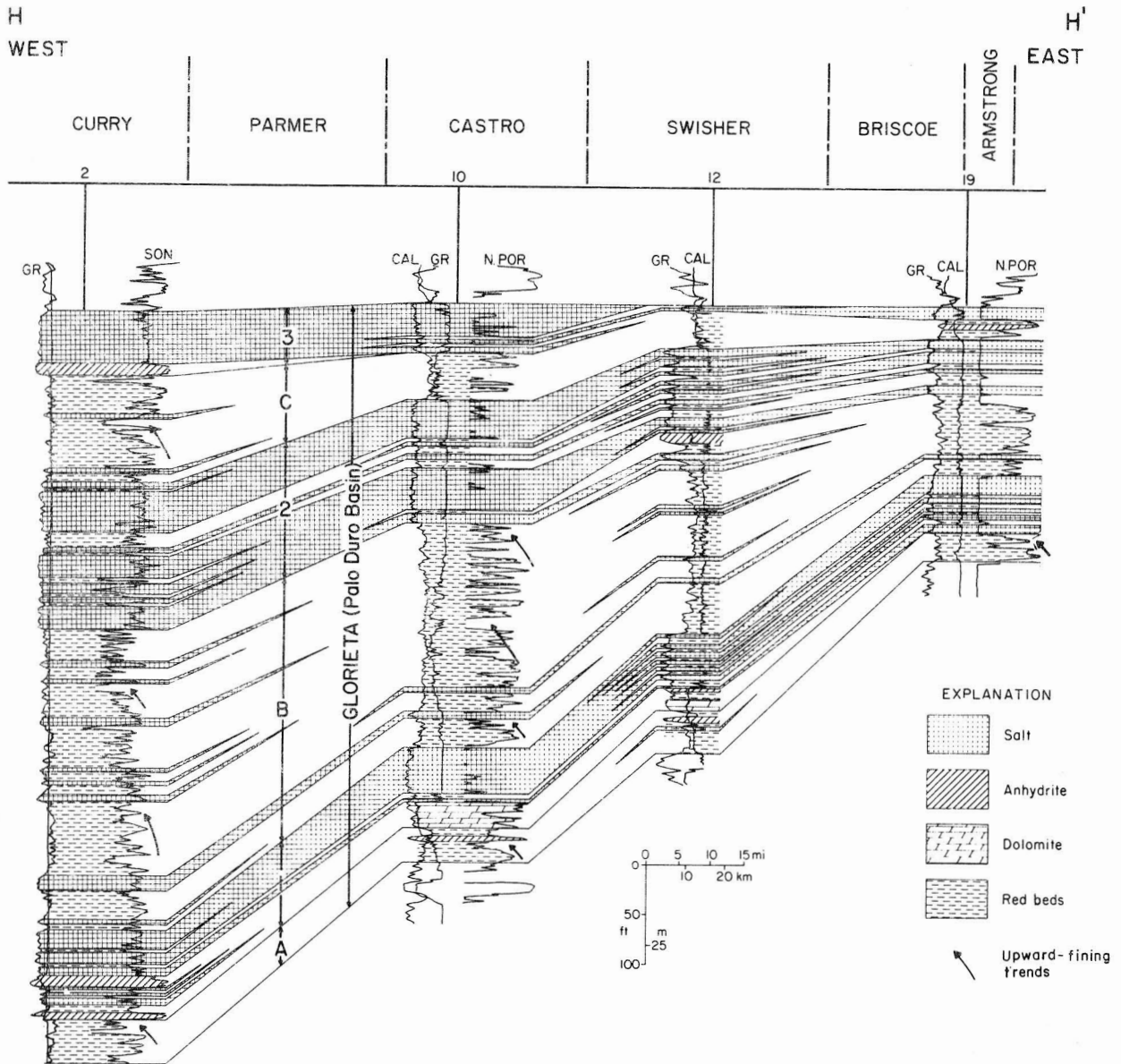
Figure 18. Regional east-west cross section H-H' of Glorieta Formation shows generalized lithologic interpretations. For location, see figure 17.
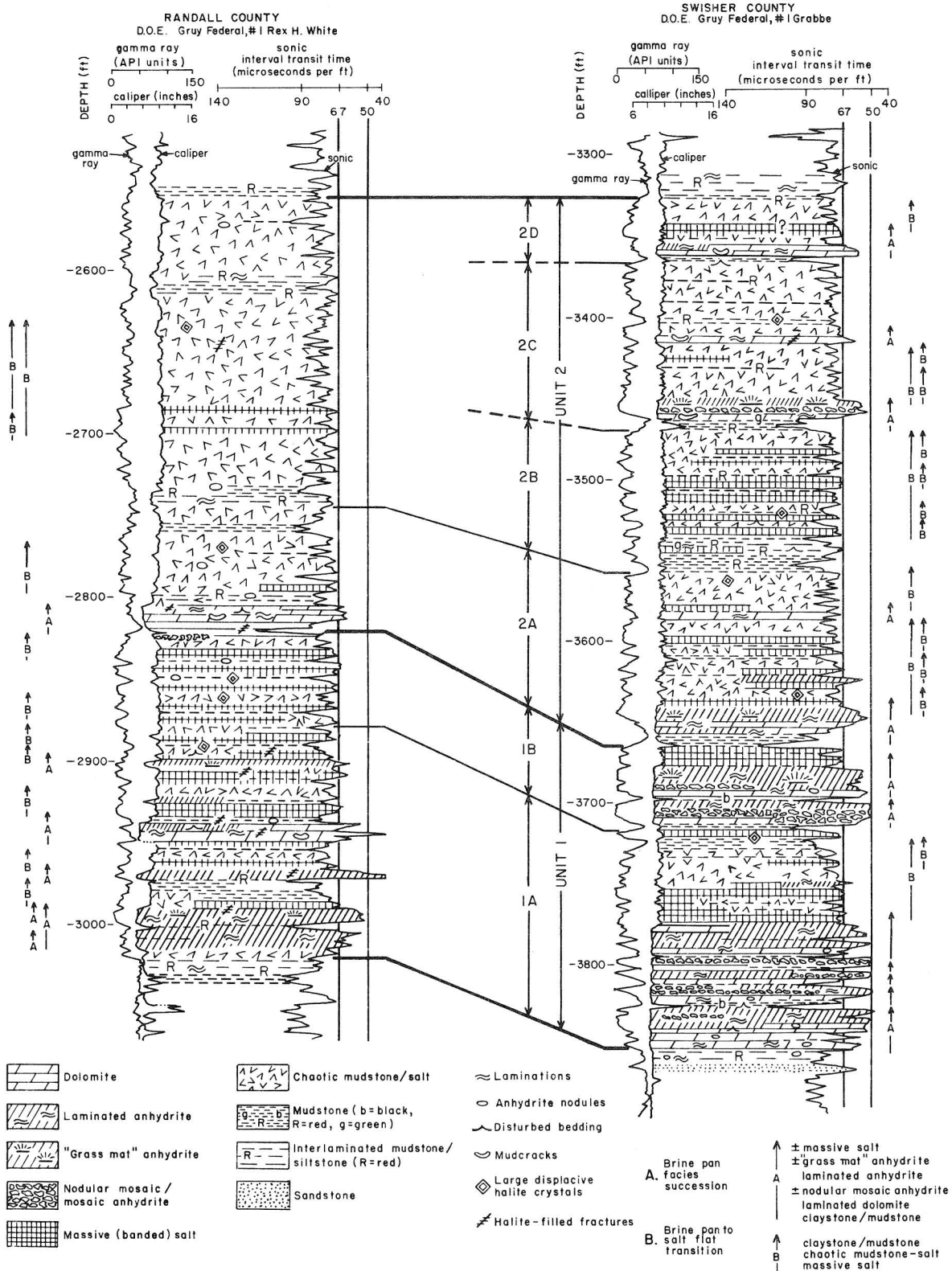
Figure 19.    Core descriptions of the upper Clear Fork Formation correlated with geophysical well log patterns, Randall and Swisher Counties test wells.    Note a progressive upward gradation from massive salt to chaotic mudstone-salt within each well and from south to north between the wells.    Succession of facies is regressive and basin wide in occurrence, allowing prediction of regional variations in salt quality and purity.
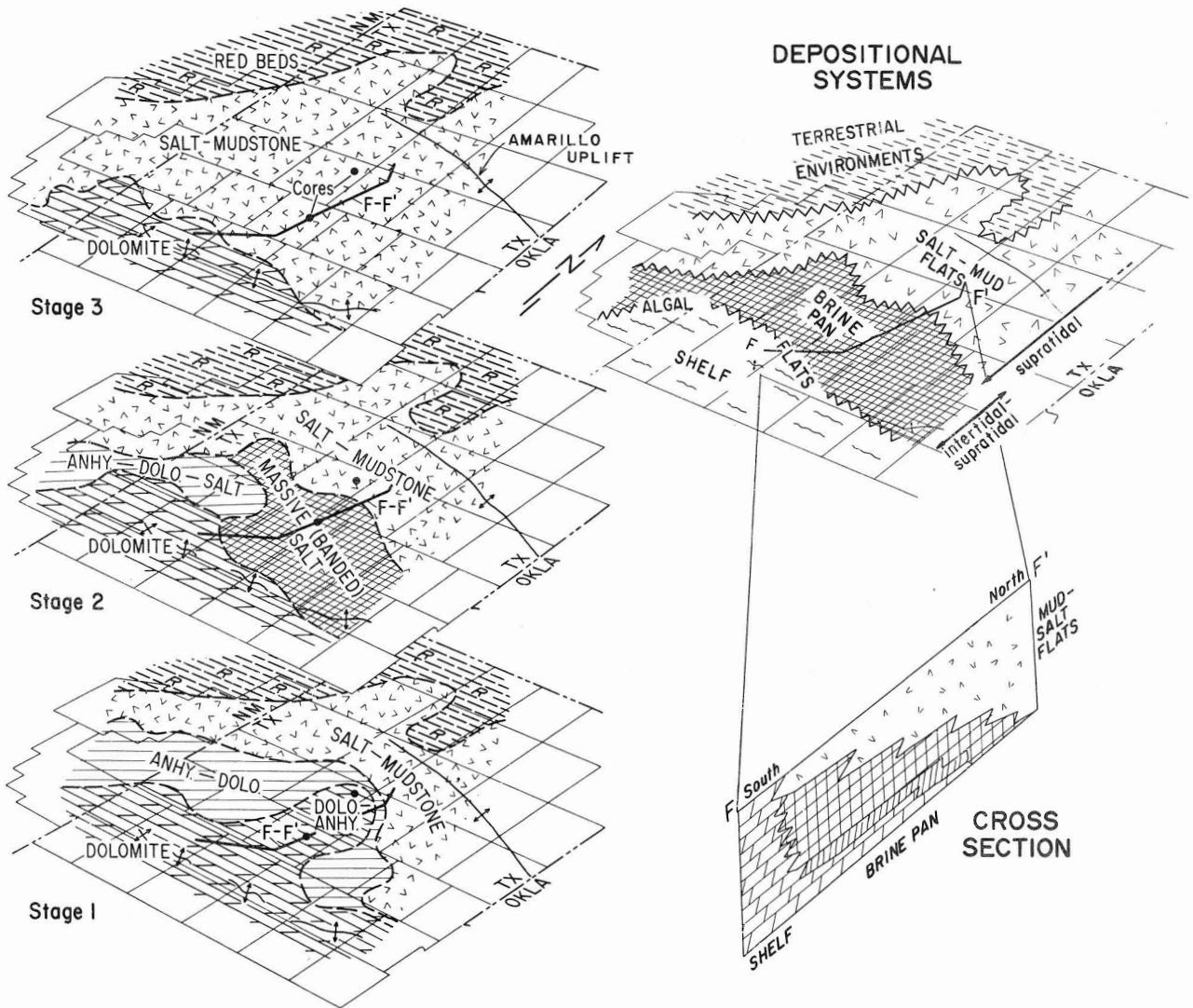
Figure 20. Maps of lithofacies distribution in upper Clear Fork unit 2A. Unit is in the middle part of the upper Clear Fork Formation (fig. 19). In central Palo Duro Basin, there was successive deposition of (1) dolomite and anhydrite in sabkha environments, (2) massive salt in brine pans, and (3) chaotic mudstone-salt in evaporitic mudflat environments. This consistent pattern of shifting facies typifies the upper Clear Fork and Glorieta sequence.

# SAN ANDRES SALT STRATIGRAPHY AND SALT PURITY

*Mark W. Presley*

*The San Andres Formation in the Palo Duro Basin contains thick, relatively pure salt beds. Salt beds occur at depths between 300 and 900 m (1,000 and 3,000 ft) over large areas. Understanding San Andres depositional systems permits prediction of regional variations in salt quality.*

The San Andres Formation in the Palo Duro Basin contains salt interbedded with anhydrite and dolomite (fig. 21). In the Dalhart and Anadarko Basins, salt is limited in areal extent owing to modern and ancient salt dissolution. The lower San Andres contains relatively pure salt beds (low clay/mudstone content), which alternate cyclically with dolomite and anhydrite. Thickest net salt in the lower San Andres Formation is in the northern Palo Duro Basin (fig. 22). The upper San Andres also contains relatively pure salt beds, but these are interbedded predominantly with anhydrite. Thickest net salt in upper San Andres rocks is in the central Palo Duro Basin (fig. 23).

Subsurface dissolution of San Andres salt has occurred at depths of 500 to 1,100 ft (150 to 330 m). Salt beds occur from these shallow depths to as deep as 4,000 ft (1,200 m) (figs. 24 and 25).

In San Andres time, relatively open-marine shelf environments (burrowed and fossiliferous carbonates) graded landward (to the north) into algal flats and carbonate sabkhas (laminated dolomite with nodular anhydrite), which in turn graded into hypersaline intertidal to supratidal brine pans (massive salt, laminated anhydrite) (fig. 6).

Lowermost San Andres evaporites and carbonates intertongue to the northwest with sandstones deposited predominantly in eolian environments landward of brine pans (see section entitled "Permeable Sheet Sandstones of the Glorieta Formation Inter-tongue with Salt-Bearing Rocks in the Northwestern Texas Panhandle") and also intertongue to the east with red beds deposited in mud-rich tidal flats and fluvial-deltaic environments (fig. 26). San Andres facies in the central Palo Duro are remarkably sand- and mud-free relative to other formations, suggesting that there was little movement of clastic sediment from basin margins into brine pans and basin center environments, possibly owing to relatively low-energy circulation of brine pan waters. Later in San Andres time, brine pans spread landward across these terrestrial facies, as well as seaward (to the south) into the northern and central Midland Basin

(fig. 6). The seaward migration of these evaporite environments followed a gradual seaward advance of carbonate inner shelf and sabkha sedimentation.

Application of facies concepts for predicting lateral and vertical changes in salt quality and purity on a regional scale and locally in the vicinity of a potential repository is considered vital in area and site characterization for nuclear waste isolation.
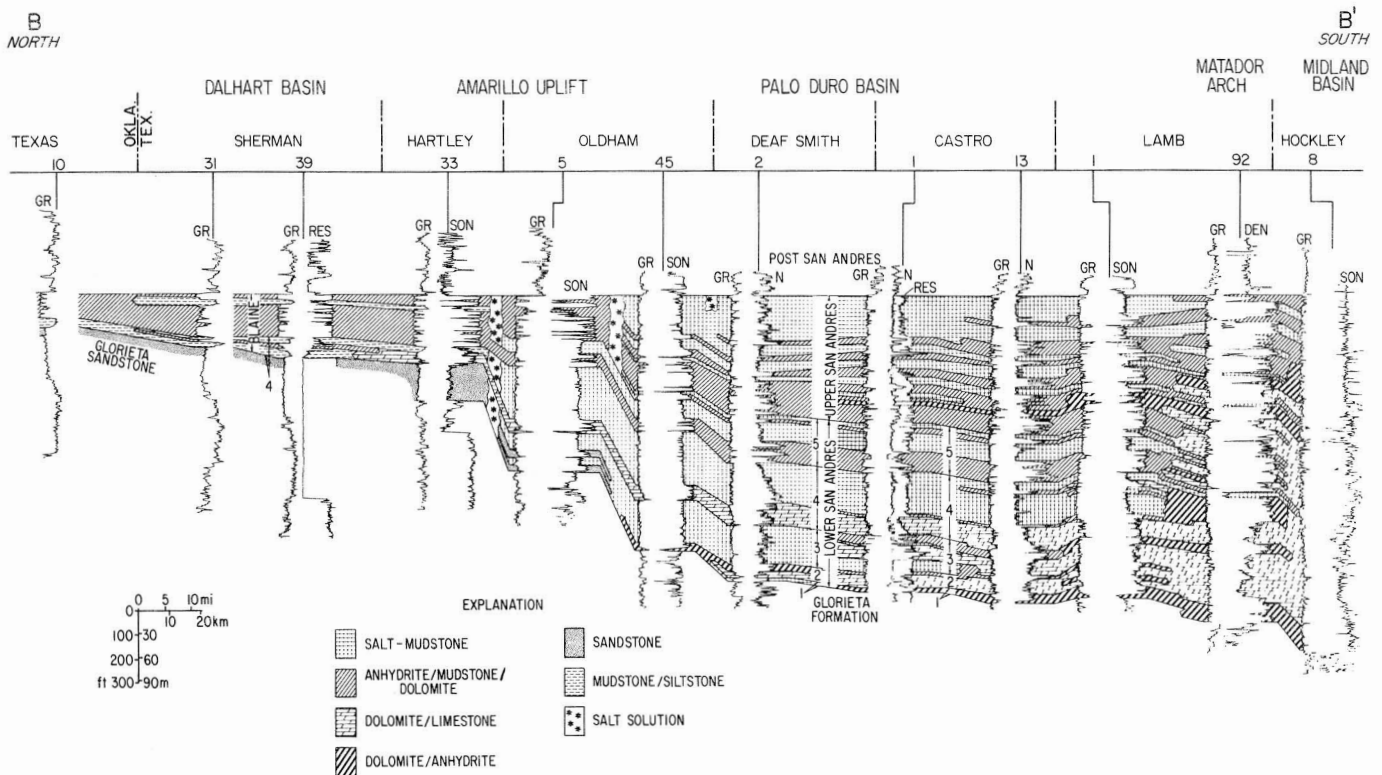
Figure 21. Regional north-south cross section B-B' of the San Andres Formation showing interpretation of lithic composition. Location shown in figure 22.
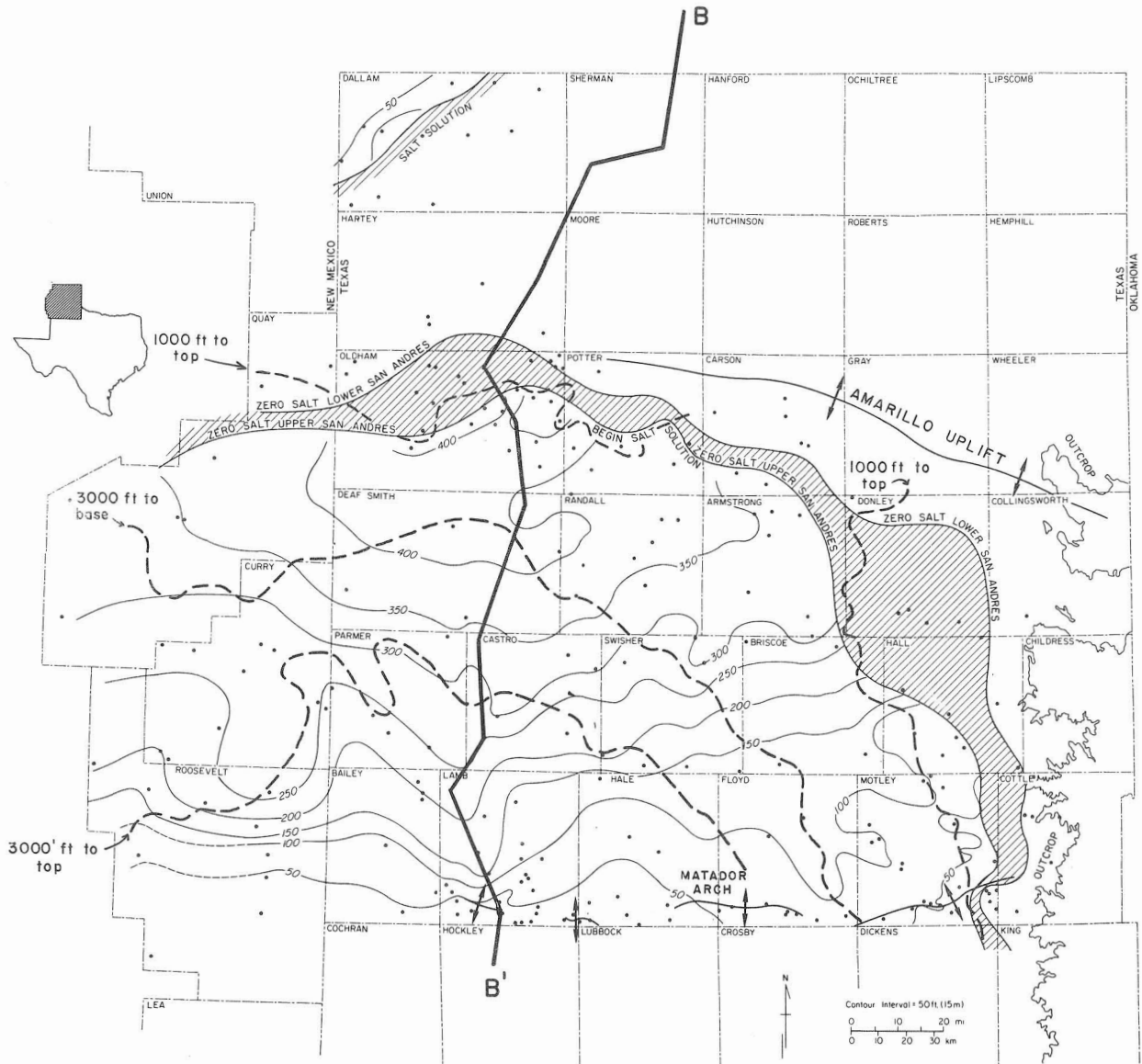
Figure 22. Net salt map, lower part of the San Andres Formation. Patterned region is the zone of subsurface dissolution of salt by ground-water processes. Depths of 1,000 and 3,000 ft (305 and 914 m) to top and base of formation are shown.
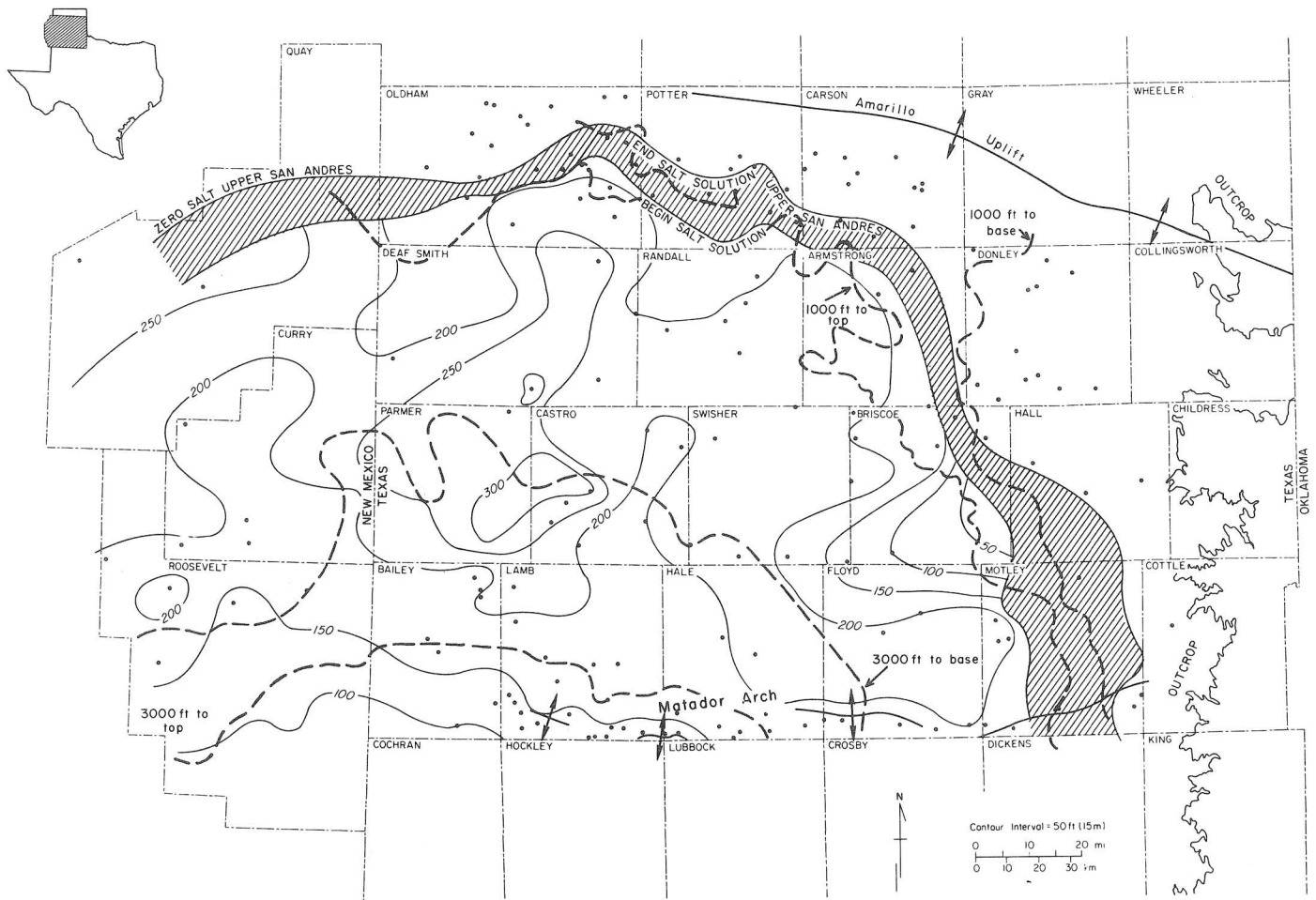
Figure 23. Net salt map, upper part of the San Andres Formation. Patterned region is the zone of subsurface dissolution of salt by ground-water processes. Depths of 1,000 and 3,000 ft (305 and 914 m) to top and base of formation are shown.
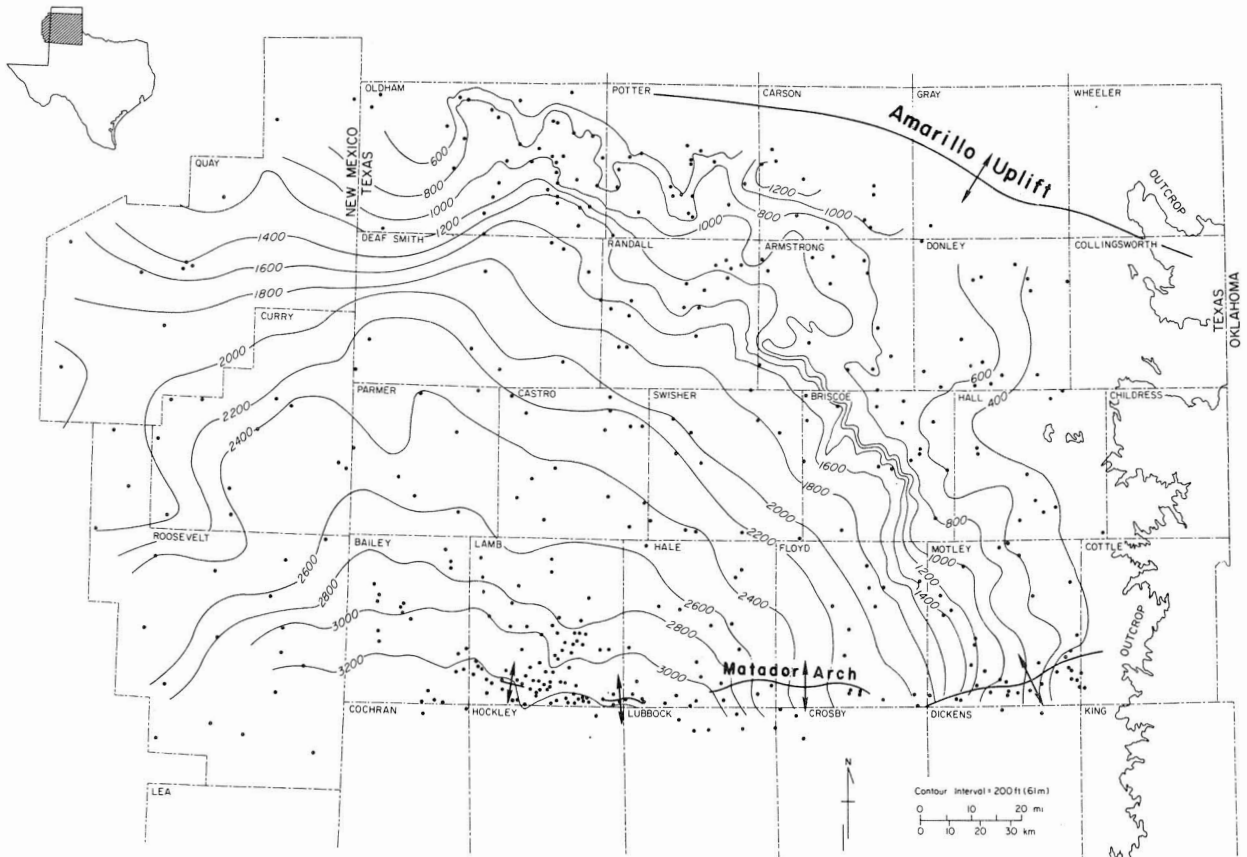
Figure 24. Depth to the top of the San Andres Formation.

38
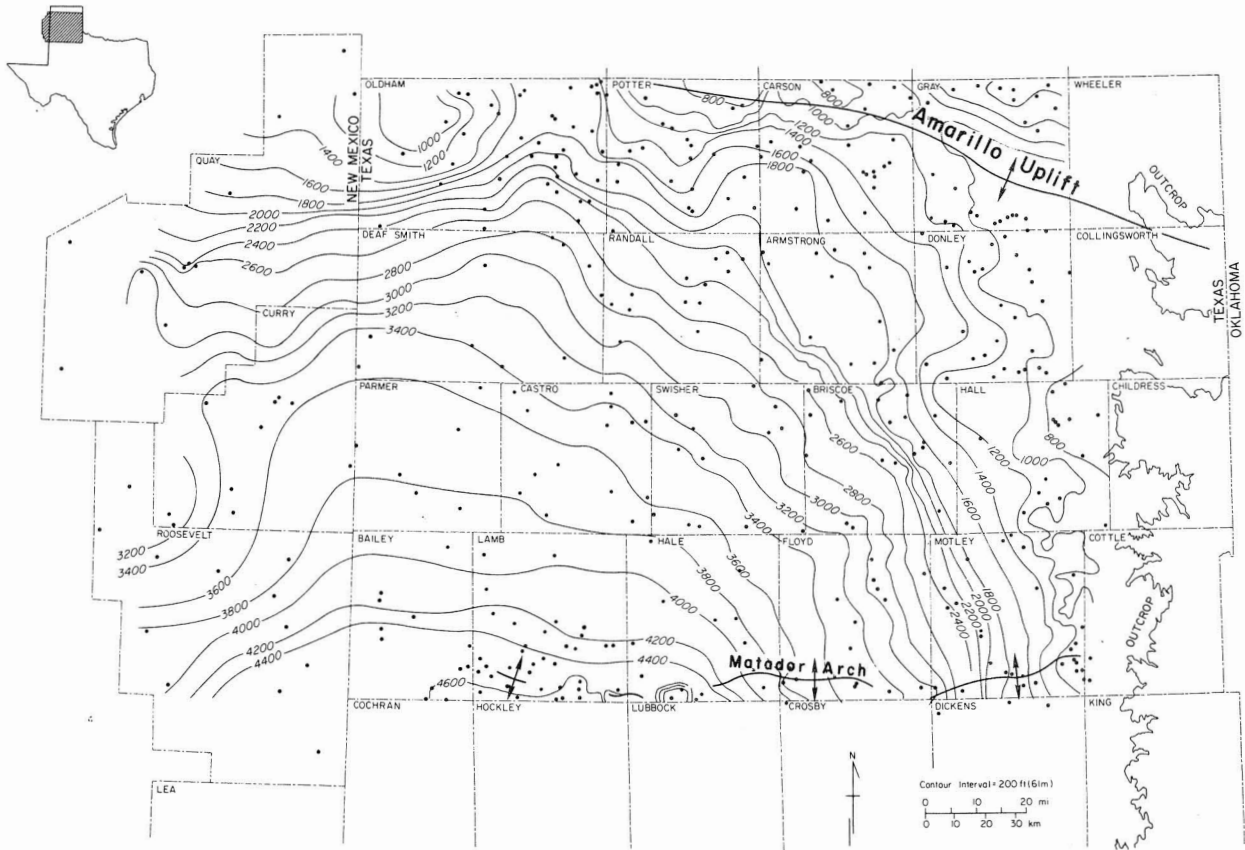
Figure 25. Depth to the base of the San Andres Formation.
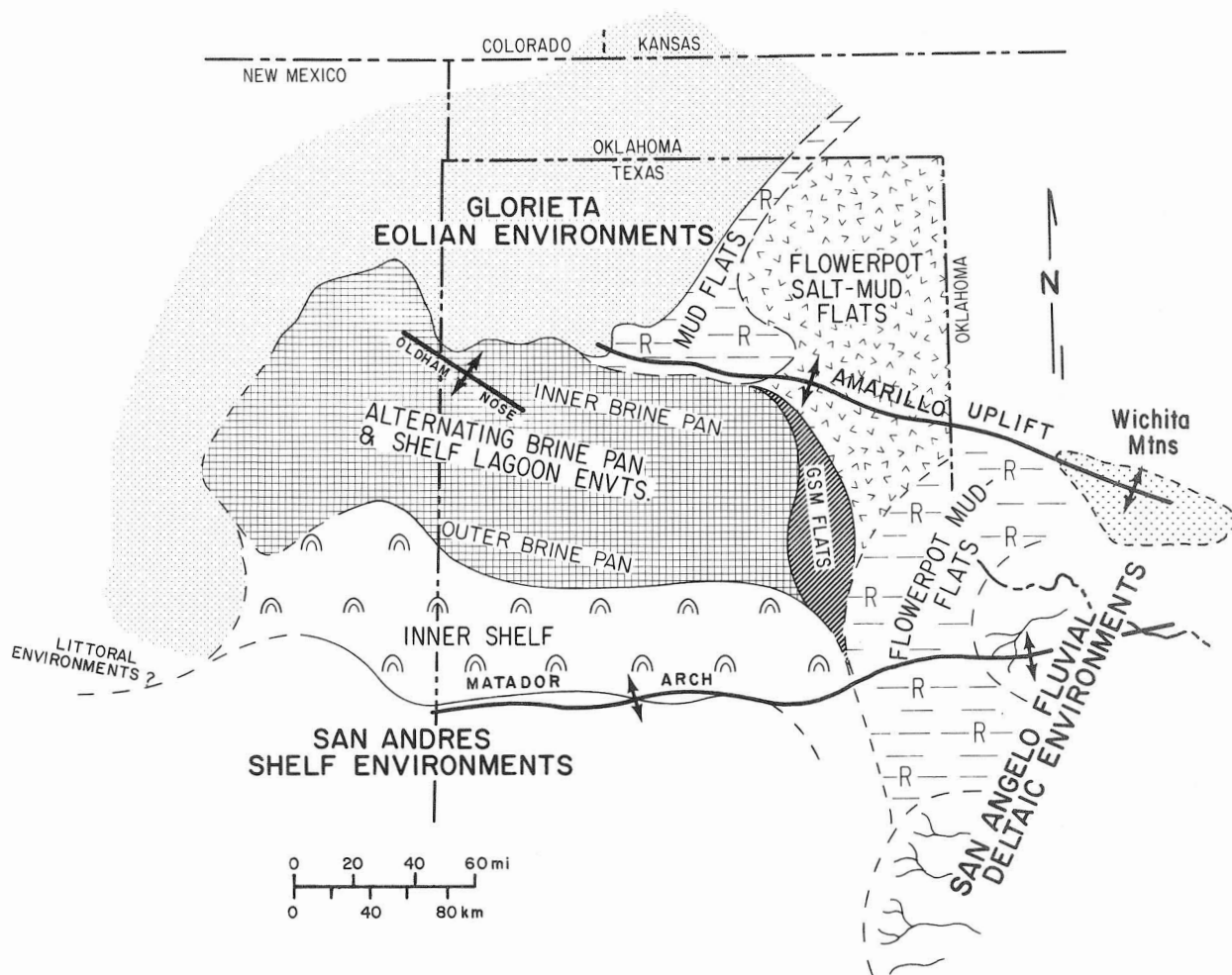
Figure 26. Paleogeography during early San Andres time, showing environments during deposition of San Andres cycles 1, 2, and 3 (see figs. 21 and 6).

## SALADO-TANSILL SALT STUDIES TO DETERMINE ORIGINAL EXTENT OF YOUNGEST PERMIAN SALT AND SALADO POTASH DEPOSITS

*Kathy A. McGillis and Mark W. Presley*

*Salado-Tansill salt and Alibates carbonates record the last incursion of marine brine into the Texas Panhandle in Late Permian time. Salado-Tansill salt was once present over large parts of the Palo Duro and Dalhart Basins but has since been removed by subsurface salt dissolution. Preliminary evaluations suggest that potash occurrences in Salado rocks in the Delaware Basin do not extend northward into the Palo Duro and Dalhart Basins.*

Salado-Tansill and Alibates strata are the youngest Permian evaporite and carbonate beds in the Texas Panhandle. They were deposited in the final stages of a shoreline regression that began in the Early Permian, and the deposits record the last incursions of Permian seas into the area. These units were studied (1) to characterize the geometry of the Late Permian evaporite basin in the Texas Panhandle, (2) to determine effects of salt dissolution on these rocks, and (3) to provide a framework for study of possible potash resources in Salado rocks in this area.

The Salado-Tansill Formation is composed of salt and red beds (fig. 27) which record final deposition in the updip parts of a Late Permian salt basin that extended northeastward from the Delaware Basin. Salado-Tansill salts, which originally extended throughout most of the Palo Duro Basin, were deposited with interbedded terrigenous mudstones and siltstones on strike-oriented (northwest-southeast), supratidal salt-mudflats. Massive, relatively mud-free (pure) salt precipitated in brine ponds scattered across the supratidal flat. Chaotic mudstone-salt mixtures resulted from syndepositional salt precipitation in mudflat sediments and from clastic influxes into brine ponds. Ancient salt dissolution events have removed Salado-Tansill salt from the northern Palo Duro Basin, and salt is currently being dissolved in the eastern part of the Palo Duro Basin (fig. 28).

Alibates strata record an initial transgression, which may have begun as early as mid-Salado-Tansill time with the deposition of an extensive dolomite bed throughout the Palo Duro and Dalhart Basins (fig. 29). Subsequent regression of the Alibates Sea resulted in the deposition of thick evaporites (predominantly gypsum) in the central and southern Palo Duro Basin (fig. 29). Alibates evaporites and carbonates were deposited in subtidal to supratidal environments in a broad, shallow-water hypersaline brine basin (fig. 30). Algal mats played a major depositional role in binding aragonite muds and gypsum crystals to form laminated dolomite and laminated anhydrite-

dolomite beds. Extensive shallow ponding is indicated by the presence of "grass-mat" gypsum texture. These "grass mats" are layers of vertically arrayed dolomite pseudomorphs after gypsum. The same texture has been studied by Nurmi and Friedman (1977) and Richter-Bernburg (1973) and is considered the result of upward growth of gypsum crystals at the sediment-water interface in shallow, hypersaline waters.

Geometry of the Salado-Tansill and Alibates basins was very similar. A comparison of facies trends and the location of centers of thickening in the two units suggest the presence of a persistent Salado-Alibates basin centered in the central and southern Palo Duro Basin.

Currently, no evidence exists for significant potash resources in Salado salt in the Palo Duro Basin. High radioactivity characteristic of potash beds has not been observed on gamma ray logs of this salt unit in the area. Although studies of potash in the Texas Panhandle are continuing, it appears that major occurrences of this resource in Salado-age rocks are limited to the Delaware Basin and adjacent areas. It is not anticipated that potash will be a limiting factor in waste isolation considerations.
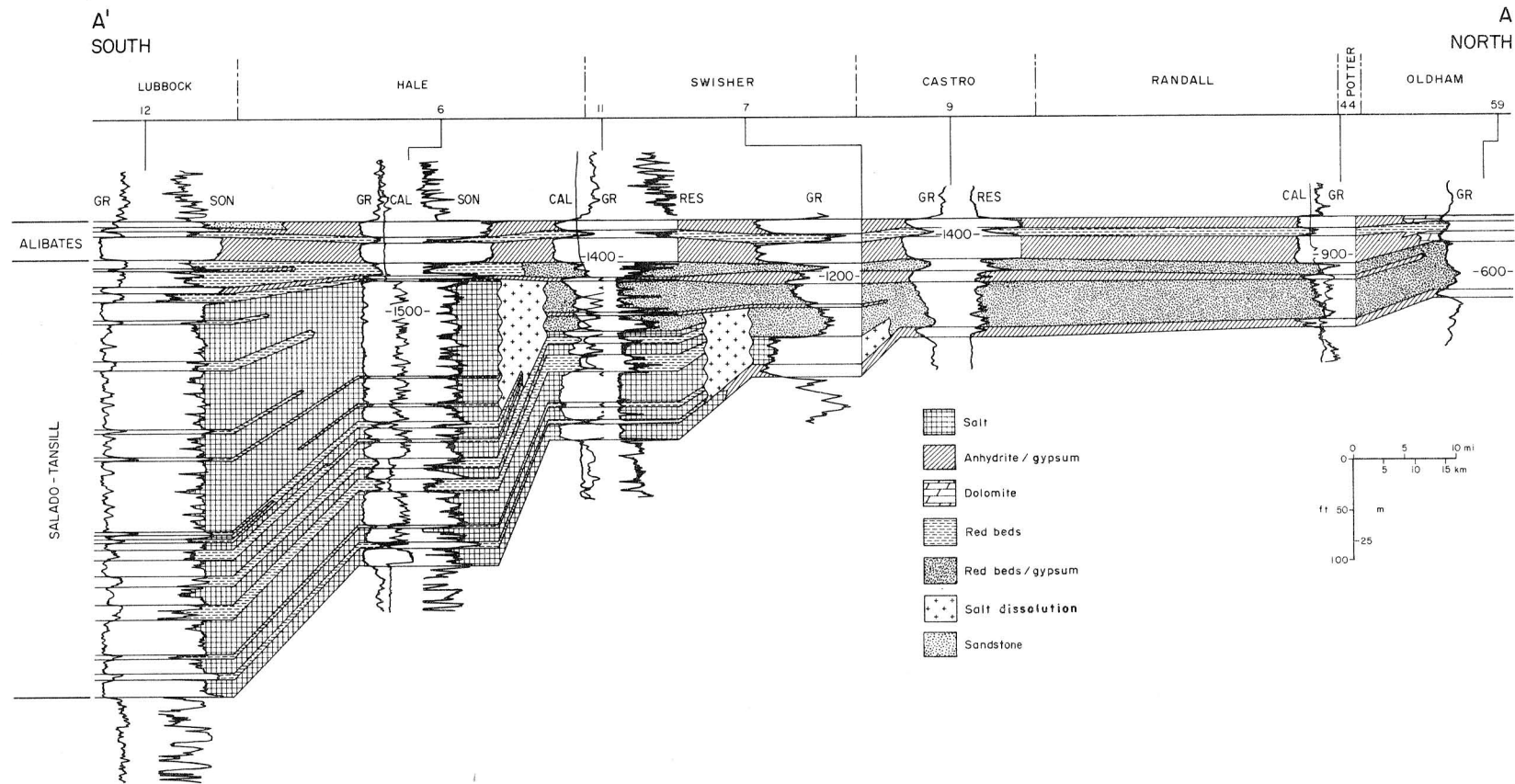
Figure 27.  North-south cross section A-A', Salado-Tansill and Alibates Formations, Palo Duro Basin.  For line of section see  figures 28 and 29.  Red beds and gypsum units are composed of collapse breccia caused by salt dissolution.
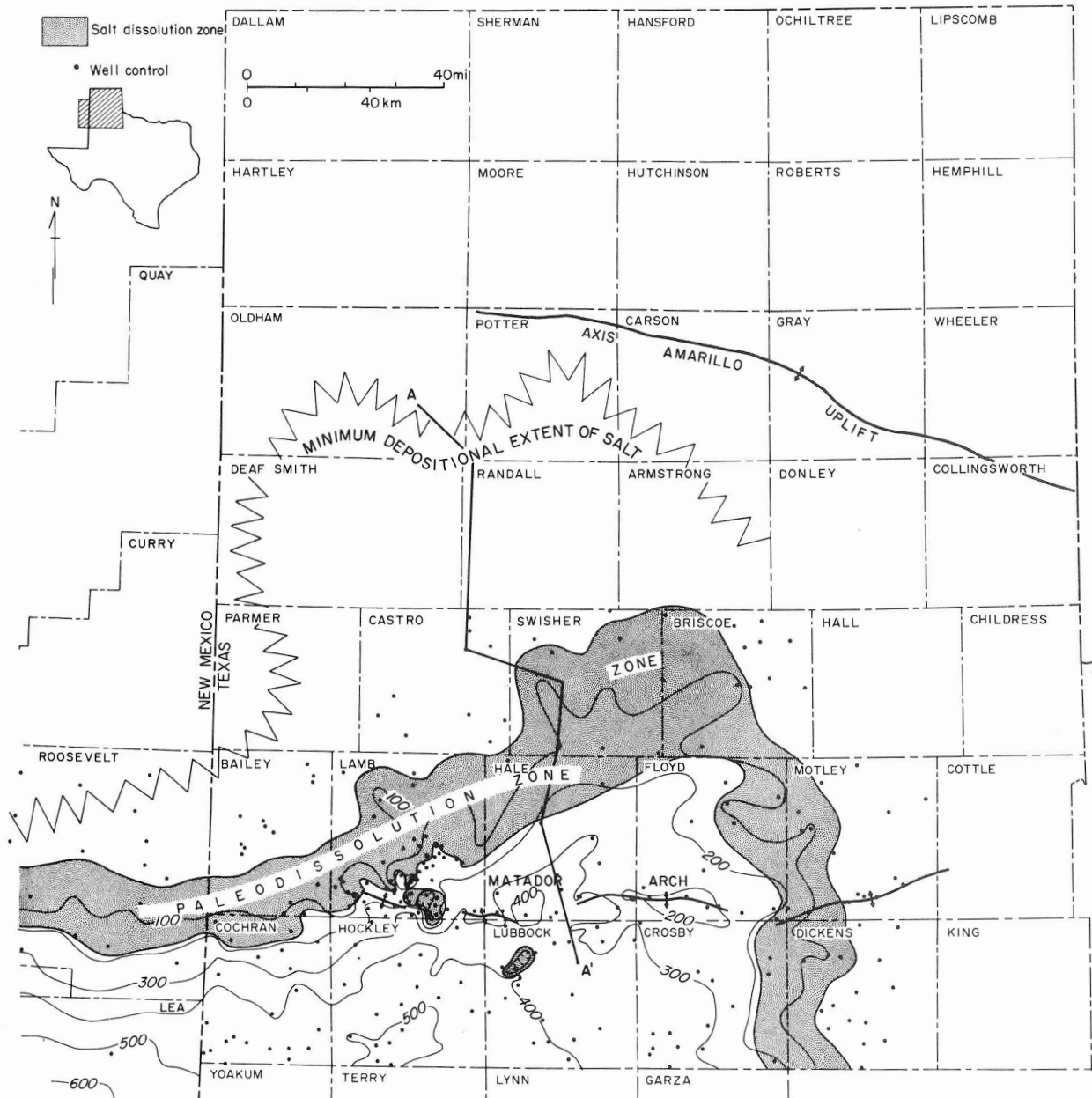
Figure 28.  Net salt, Salado-Tansill Formation.  Values determined from gamma ray logs.  Salt thickens southward and is bounded on northwest by zone of paleodissolution and on east by zone of modern dissolution.  Minimum original extent of salt shown by serrate line; dissolution-collapse breccia occurs south of line.
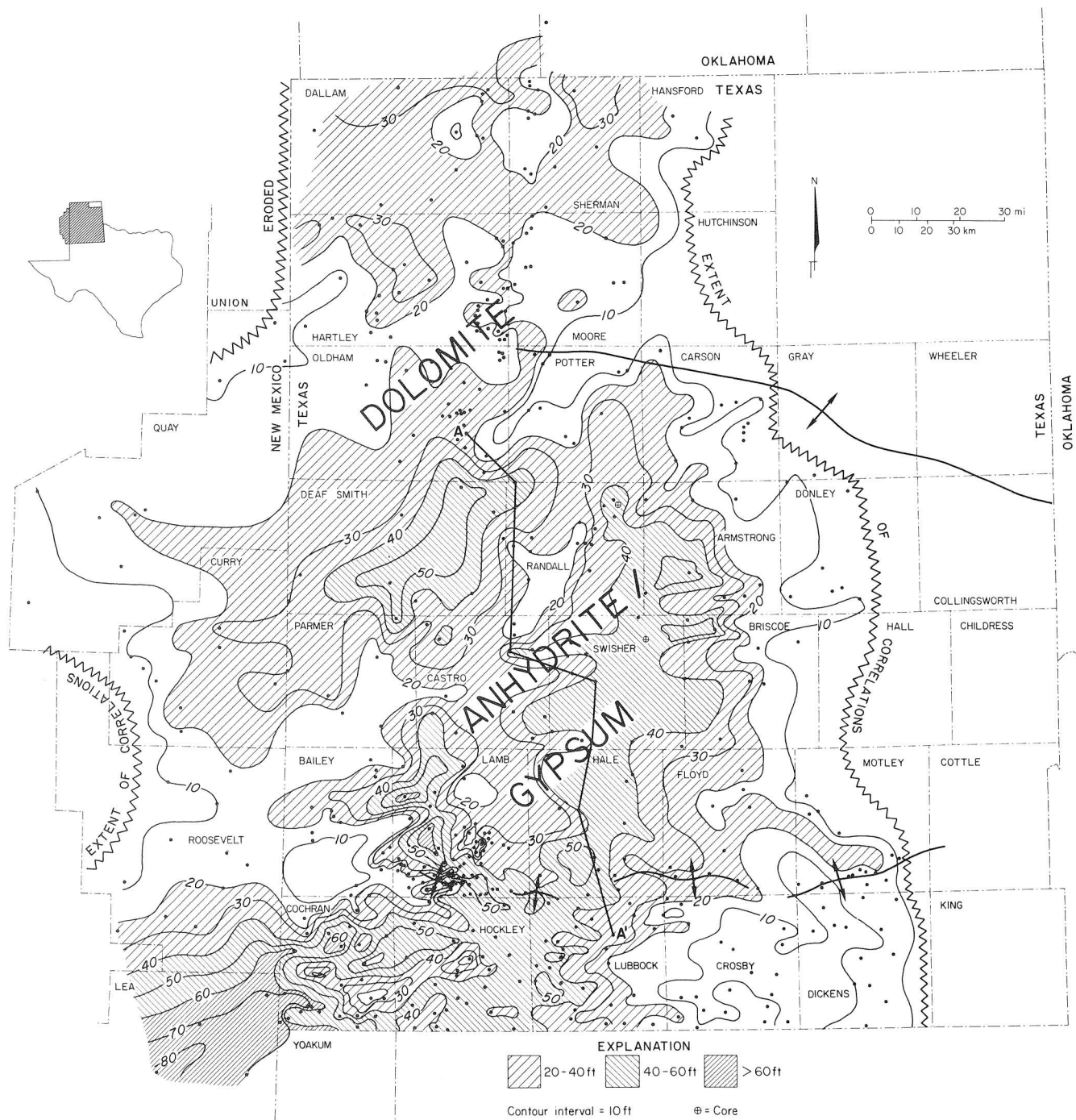
Figure 29. Isopach map, Alibates Formation. Serrate lines mark depositional and erosional boundaries of formation. Dominant lithology of Alibates as recorded on sample logs is noted.
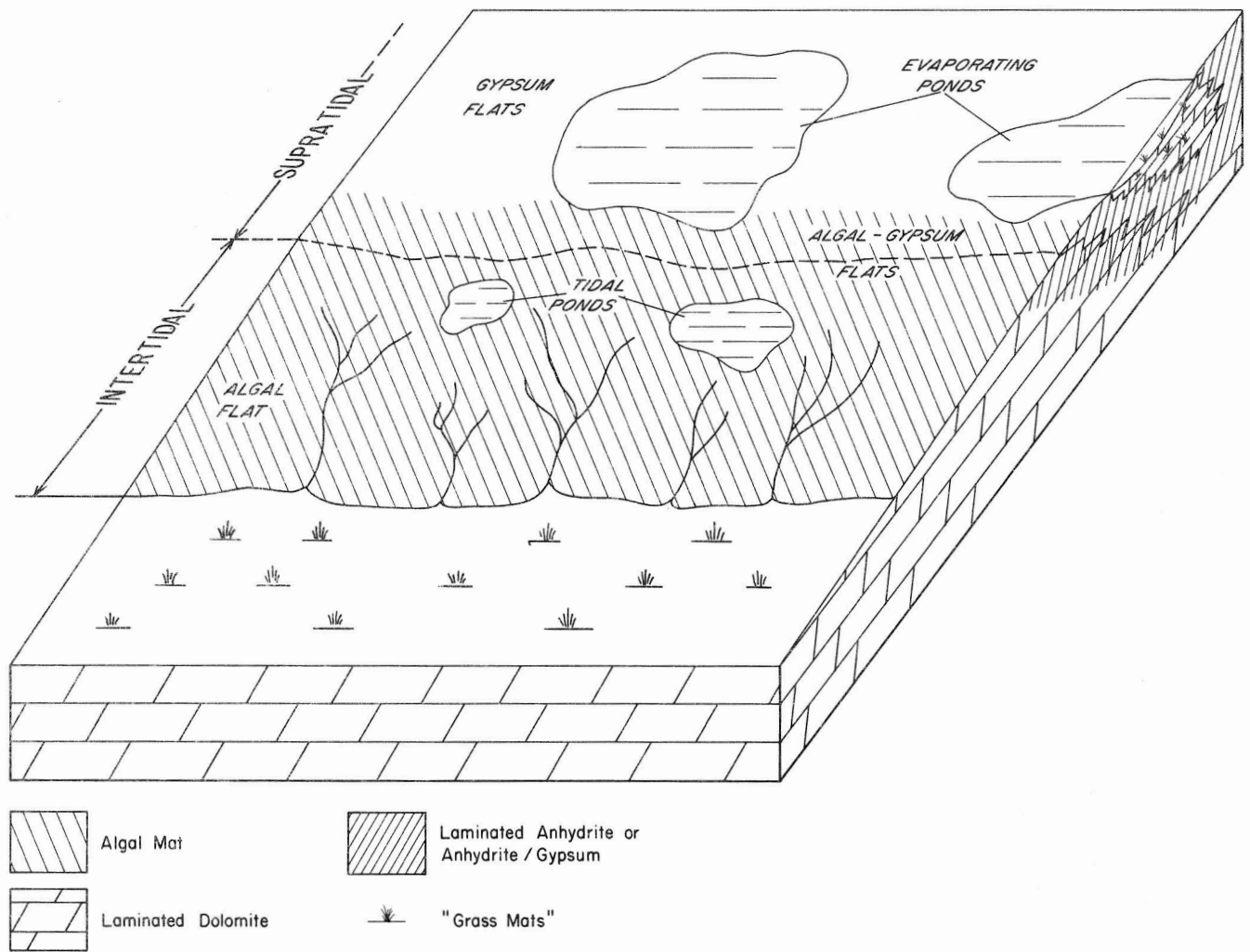
Figure 30. Depositional model of Alibates Formation.

# HYDROCARBON RESOURCE ANALYSIS OF GRANITE-WASH FACIES

*Shirley P. Dutton*

*Arkosic sand and gravel (granite wash) were deposited by alluvial fans and fan deltas adjacent to the Amarillo Uplift during Pennsylvanian and Early Permian time. These porous clastics are petroleum reservoirs in the Anadarko Basin and are valid exploration targets in the Palo Duro Basin.*

Thick wedges of granite-wash sandstone and conglomerate occur both north and south of the Amarillo Uplift, the northern boundary of the Palo Duro Basin. Strike and dip cross sections (fig. 31) constructed adjacent to the Amarillo Uplift delineate the distribution of granite wash. North of the uplift, granite-wash deposits as thick as 1,500 m (5,000 ft) occur near the main bounding fault. At 55 to 65 km (35 to 40 mi) from the uplift, the total thickness is reduced to 30 m (100 ft). Maximum granite-wash thickness in the Palo Duro Basin, south of the uplift, is about 400 m (1,200 ft). Granite-wash deposits extend farther into the Palo Duro Basin on the south side of the uplift than into the Anadarko Basin to the north. Total granite wash is 30 m (100 ft) thick near the southern margin of the Palo Duro Basin, some 130 to 140 km (80 to 85 mi) south of the uplift.

Granite-wash clastics are important hydrocarbon-producing reservoirs on the Amarillo Uplift and in the Anadarko Basin, and they are exploration targets in the Palo Duro Basin. The Mobeetie Field in northwest Wheeler County (fig. 31) produces oil and gas primarily from Missourian-age (mid-Pennsylvanian) granite wash and interbedded carbonates (Sahl, 1970). The field is located only 16 km (10 mi) north of the Amarillo Uplift, at the northern limit of late Missourian granite-wash sedimentation. Carbonate deposition was punctuated by three periods of clastic influx from prograding fan deltas.

Isopach maps of the lowest carbonate unit, L1 (fig. 32), and the overlying clastic unit, S1 (fig. 33), illustrate the depositional style. A series of elongate algal mounds developed along strike in the L1 unit and separated the open shelf from a restricted lagoonal environment. Production from this unit is mainly from algae-foraminifer wackestones and packstones along the algal-mound trend. Carbonate deposition ended with the progradation of the S1 clastic unit. Braided channels breached low areas along the algal-mound trend and deposited fan-delta sediments basinward of the underlying carbonates (fig. 33). Hydrocarbon production from the S1 unit is from distributary-braided-channel and medial fan-delta deposits.

Alternating clastic and carbonate deposition, similar to that in the Mobeetie Field, also occurred in the Palo Duro Basin. Porous facies are considered potential hydrocarbon reservoirs. Further studies of the oil and gas potential of granite-wash facies in the Palo Duro and Dalhart Basins will be required to outline areas of future exploration. Such studies are necessary to ensure the future integrity of possible nuclear waste isolation sites.
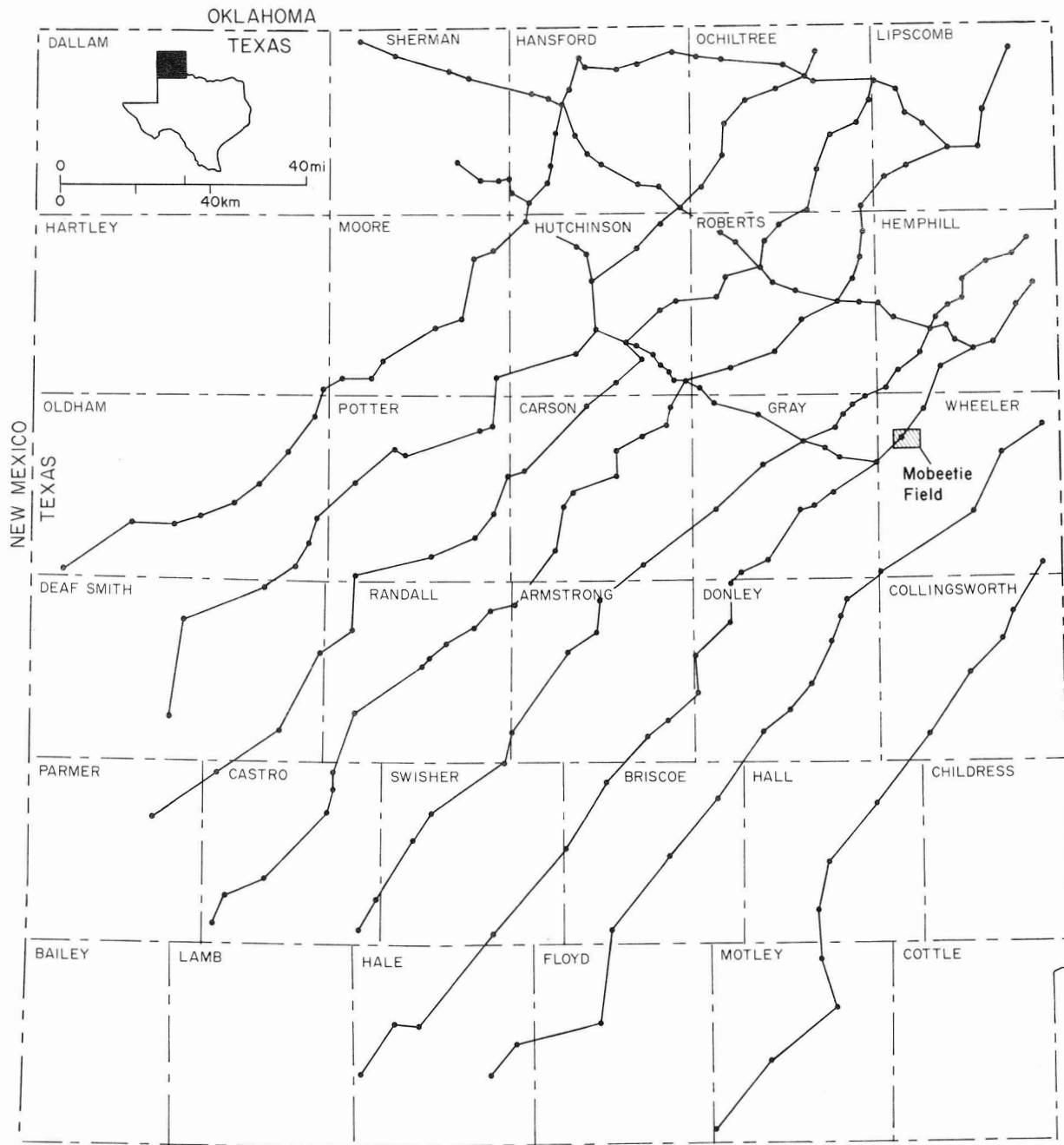
Figure 31. Index map of study area showing locations of cross sections.
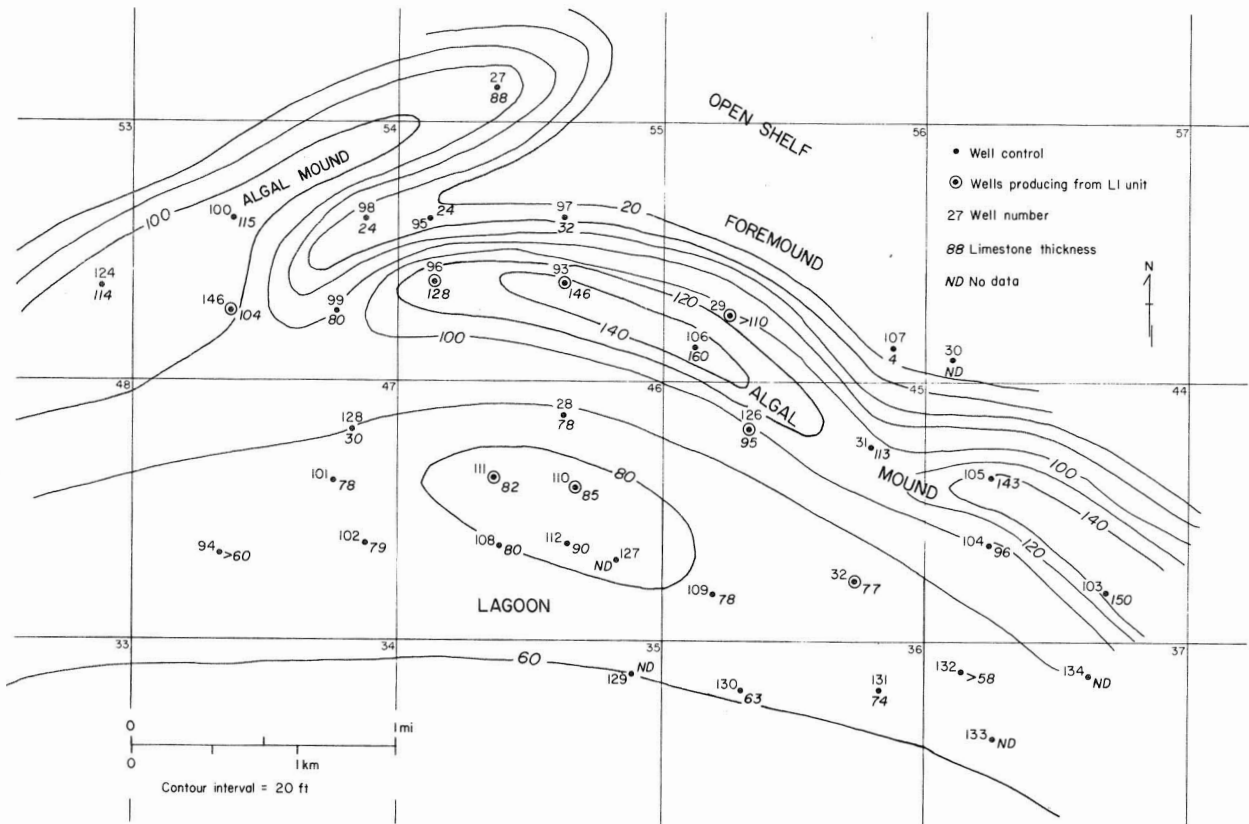
Figure 32. Isopach map of L1 carbonate unit, Mobeetie Field, showing location of producing wells.
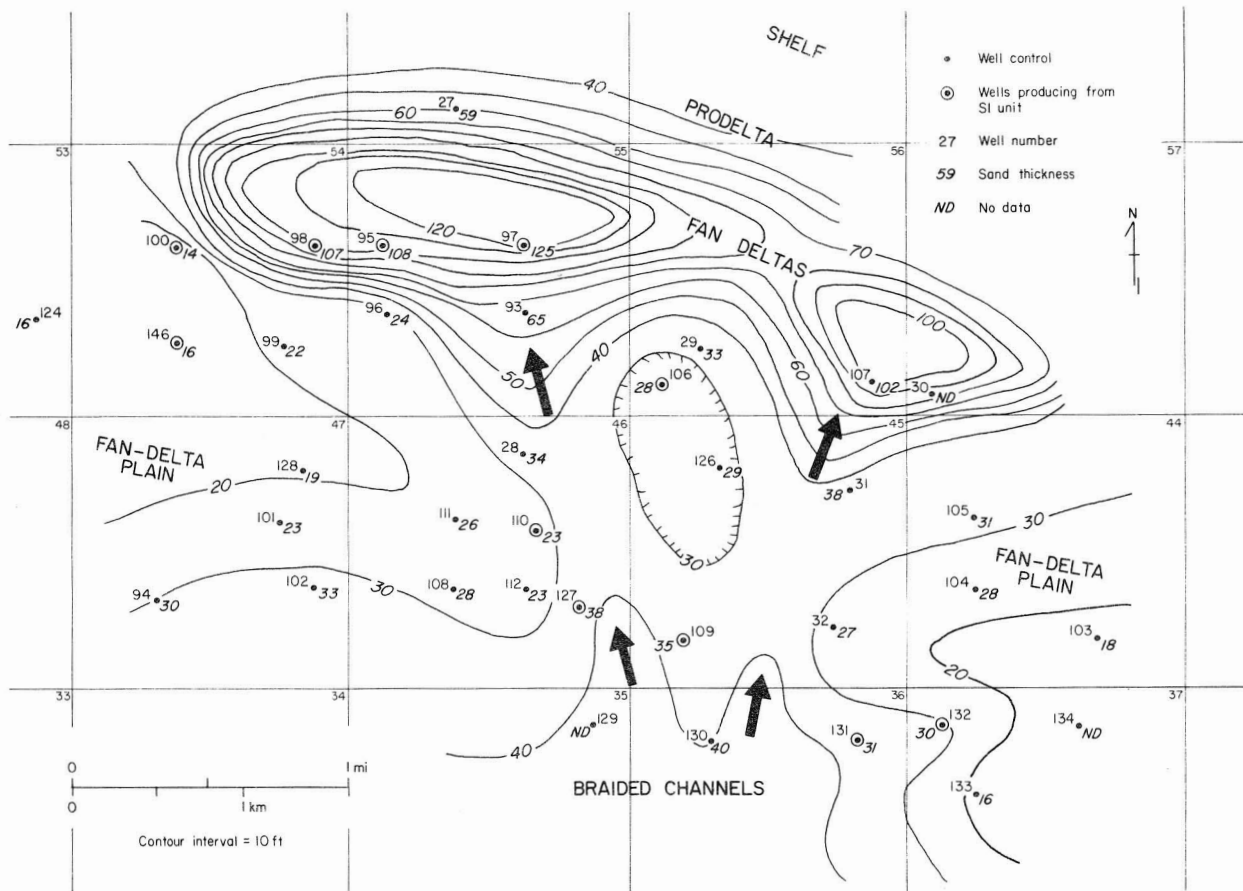
Figure 33. Isopach map of S1 clastic unit, Mobeetie Field, showing location of producing wells.

# GENESIS AND EMPLACEMENT OF SAN ANDRES OIL IN THE NORTHERN SHELF OF THE MIDLAND BASIN, TEXAS

*Paul J. Ramondetta*

*Prolific San Andres oil deposits of the Northern Shelf originated in the northern Midland Basin. This oil was expelled upward from Wolfcampian basinal facies through vertical fractures along the Abo Reef trend into the broad overlying San Andres reservoirs. Potential migration routes from the Abo Reef trend into the Palo Duro Basin are blocked by a regional porosity pinch-out just north of the Matador Arch.*

Wolfcampian basinal shales and dark argillaceous limestone of the northern Midland Basin (fig. 34) are considered likely source rocks for the large reserves of oil contained within porous San Andres shelf carbonates west and northwest of the basin. Adequate source-rock potential for Leonardian and Wolfcampian basinal clastics has been demonstrated by Houde (1979) and Dutton (1980). In contrast, San Andres and Clear Fork shelf carbonates have been shown to have poor source-rock potential, despite their prolific oil production (Ramondetta, this volume; Dutton, 1980). Hence, hydrocarbon potential in San Andres and Clear Fork shelf carbonates of the Palo Duro Basin depends on the existence of migration routes connecting these potential reservoirs with the deeper and possibly distant source rocks.

Large volumes of oil were expulsed vertically into overlying shelf carbonates along the Abo Reef trend (fig. 34). This reef trend coincides with a narrow belt of several shelf-margin buttresses. The relationship between these shelf margins and the overlying San Andres oil production is shown in figure 34.

Because of the highly compactible nature of the basinal clastics relative to the stable carbonate platform, this belt of shelf edges and the adjacent basinal areas were zones of intense differential compaction and fracturing. Fractures reported in core are parallel to the Abo Reef trend (Chuber and Pusey, 1967). In addition, surface lineaments (fig. 34), as mapped and interpreted by Finley and Gustavson (in press), are parallel and orthogonal to the reef trend. Such fracturing is probably due to the draping of brittle carbonate units over zones of differential compaction, resulting in routes for vertical oil expulsion.

Wichita-Albany and San Andres oils from the Wasson field along the Abo Reef trend were found to be compositionally similar. This is evidenced by correlation index profiles (fig. 35), liquid and gas chromatography, and the H/C ratio of the asphaltic component. A major difference, however, is the aromatic anomaly in San Andres oil,

which has been attributed to the effects of biodegradation in the sulfate-rich reservoirs of the Northern Shelf (Jones and Smith, 1965). This degradation causes an enrichment in sulfur that increases with decreasing depth (fig. 36).

San Andres oil is remarkably uniform in composition over the entire Northern Shelf, attesting to its common basinal source. The uniformity of composition is again demonstrated by liquid and gas chromatography, H/C ratio, and various other distillate analyses carried out by the Bartlesville Energy Technology Center (BETC) (fig. 37).

The trapping mechanisms in the Northern Shelf are a combination of structural and facies control. Favorable hydrocarbon reservoir conditions exist in San Andres strata that were draped and subsequently fractured over subjacent shelf-margin buttresses (Chuber and Pusey, 1967). The underlying shelf margins composed of massive carbonates had a bathymetric effect on the San Andres depositional environment and caused development of carbonate banks that separated the deeper shelf in the southeast from a broad, shallow saline shelf to the northwest. The present structure reflects, to some extent, the depositional topography. Oil production is generally concentrated along the structurally high banks that separate the shallow-water, updip facies from the deep-water, downdip strata.

A thick porous zone exists in the lower San Andres along the underlying Abo Reef trend; this zone grades shelfward into discrete porous layers (fig. 38), which reflect cyclic sedimentation in the shallow-shelf and sabkha environments (Presley, 1979c). These porous carbonates tend to thin and lose their porosity in a northward updip direction near the Matador Arch partly because of replacement of the carbonates by secondary anhydrite (Dunlap, 1967). Abundant "salt-filled porosity" within the Palo Duro Basin further diminishes the chances of continued northward migration. This progressive decrease in porosity occurs in the younger intervals first, which reflects the progradation of evaporitic conditions to the south (fig. 38). This regional, dip-oriented porosity pinch-out is another trapping mechanism and has resulted in the vast Levelland-Slaughter-Cato trend of Texas and New Mexico (fig. 34).

Therefore, because of the lack of hydrocarbon source-rock potential for San Andres strata and the blockage of migration routes into those units by anhydrite and salt within most of the Palo Duro Basin, the petroleum resource potential is poor in the San Andres of the Palo Duro Basin.
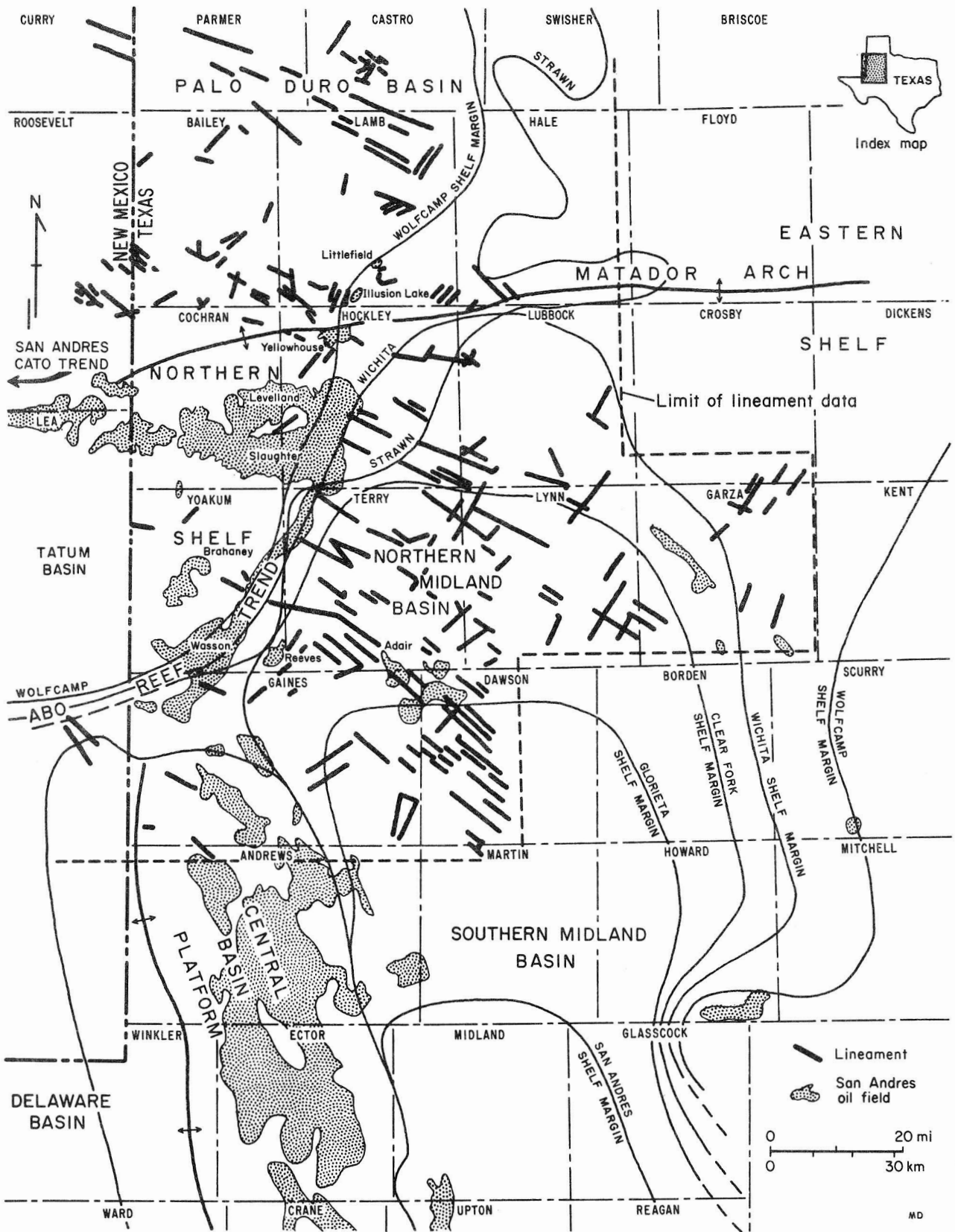
Figure 34. Map of the study area, showing San Andres oil production, shelf margins, and surface lineaments. Surface lineaments are from Finley and Gustavson (in press); shelf-margin positions from J. H. Nicholson (personal communication, 1980).

54
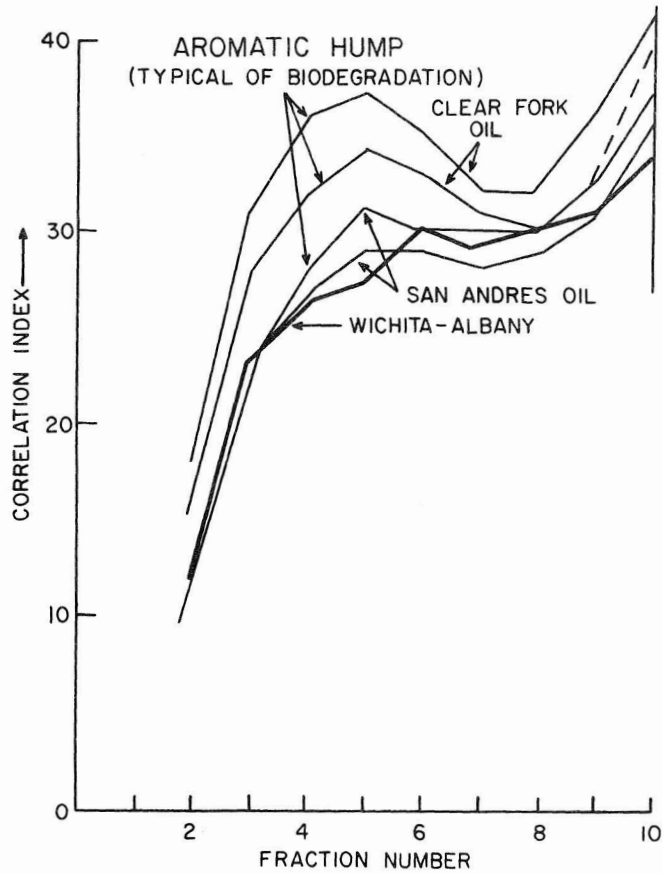
Figure 35. Correlation index profiles for San Andres and Wolfcamp oils from the multipay Wasson Field, Yoakum County, Texas.
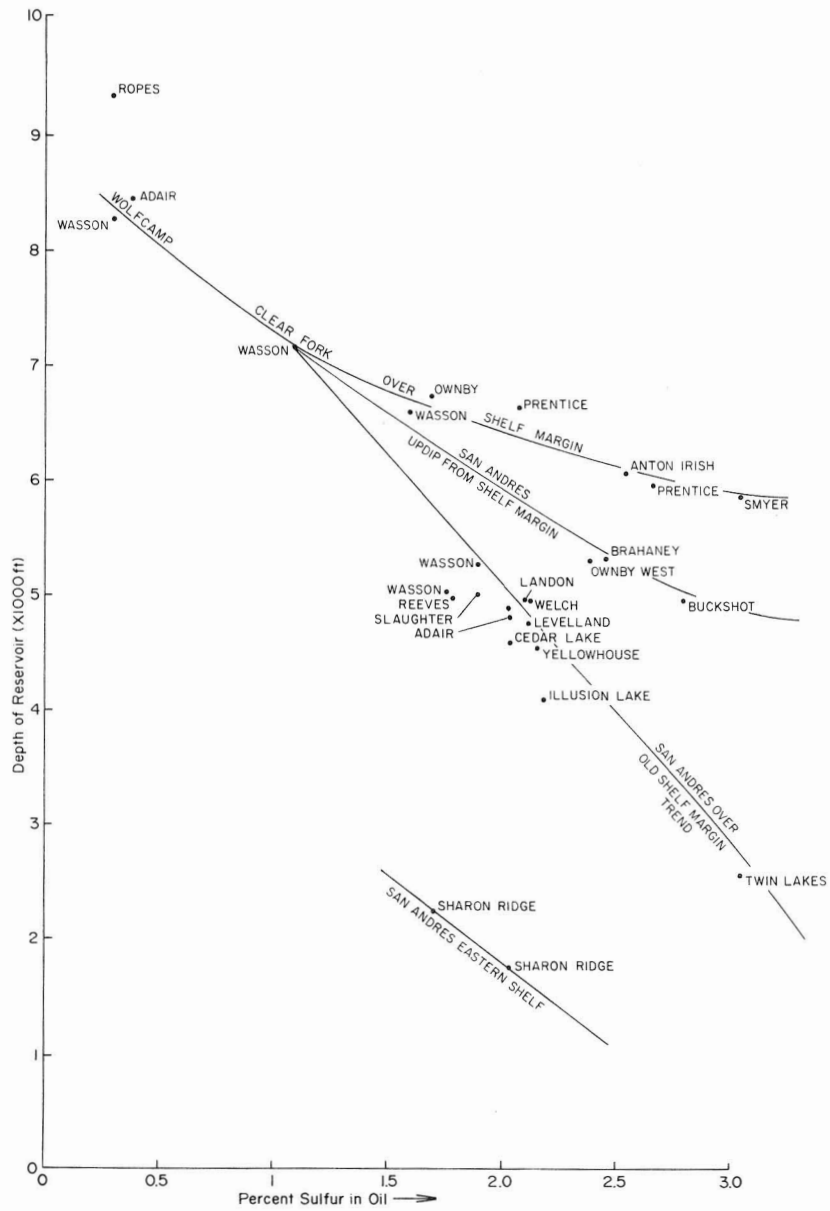
Figure 36. Graph showing percent sulfur versus depth for various oils in the study area.
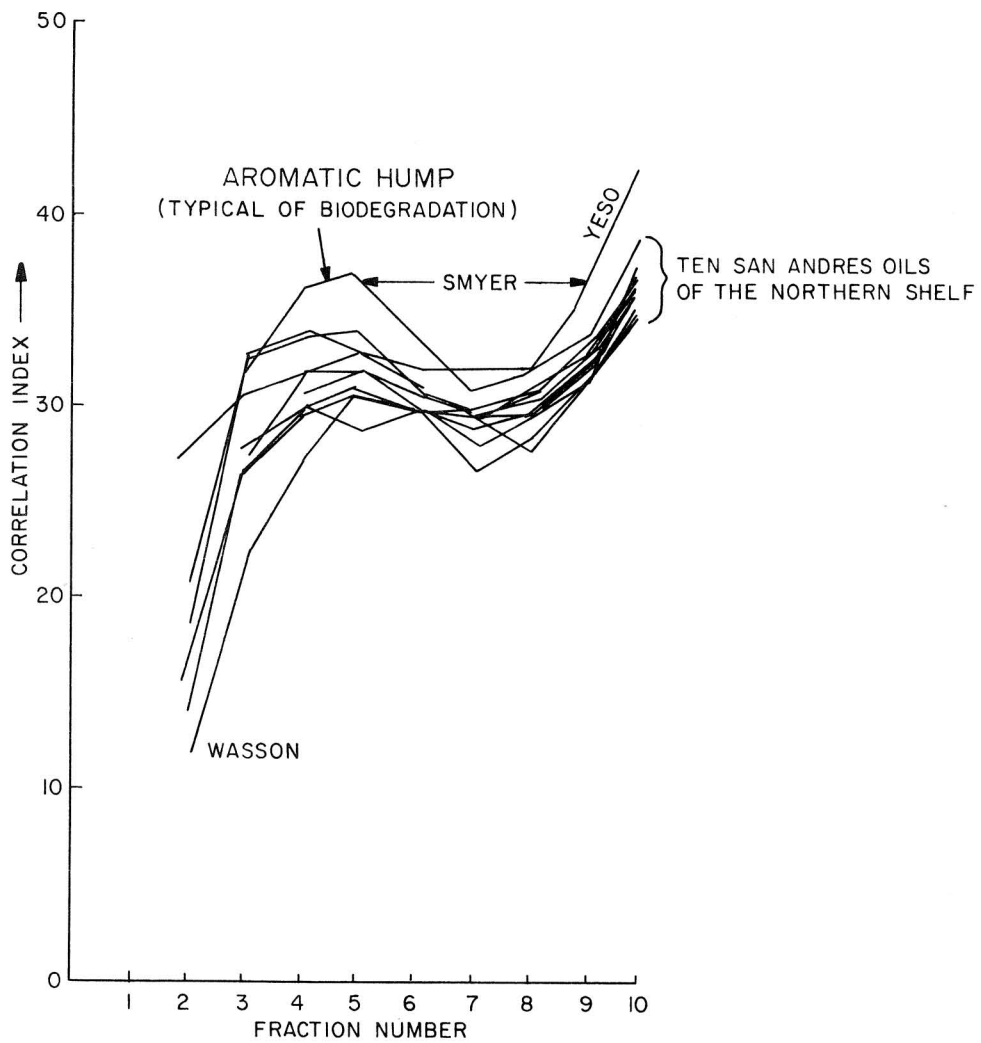
Figure 37. Correlation index profiles for 1 Yeso oil and 10 San Andres oils from the Northern Shelf.
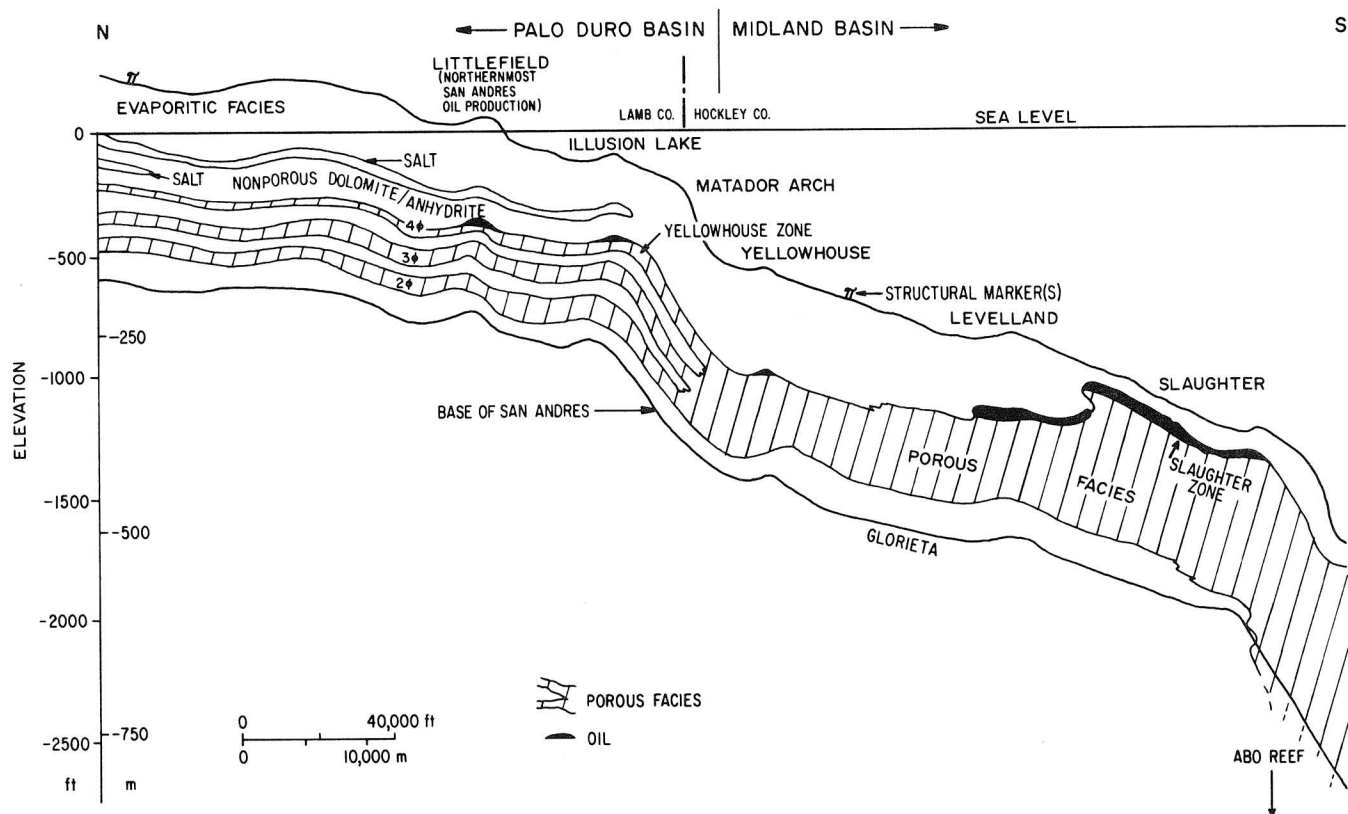
Figure 38. Cross section across the Northern Shelf, lower San Andres Formation, showing porosity relationships.

# HYDROCARBON POTENTIAL OF SAN ANDRES CARBONATES IN THE PALO DURO BASIN--STRATIGRAPHIC AND FACIES ANALYSIS

*Mark W. Presley and Paul J. Ramondetta*

*San Andres salt beds intertongue with carbonates, which are hydrocarbon reservoirs along the southern margin of the Palo Duro Basin. Current production is from inner-shelf depositional systems. Continuing studies in the Palo Duro Basin are designed to evaluate the petroleum potential to the north of current production.*

To consider San Andres salt beds in the Palo Duro Basin for burial of nuclear waste, it must be shown that no potential hydrocarbon reserves are in salt-associated strata. Along the southern margin of the Palo Duro Basin, oil and gas are produced from San Andres carbonates (fig. 39). These producing carbonates intertongue updip (to the north) over a few tens of miles with salt beds that are now being evaluated for isolation of nuclear wastes. Currently, these updip areas, particularly parts of the southwestern Palo Duro Basin, are active exploration frontiers for oil and gas.

In producing areas of the southwestern Palo Duro Basin, the San Andres Formation contains interbedded carbonates, anhydrite, and salt (figs. 40 and 41; table 1). Production is from porous carbonates, where traps are formed against updip porosity and permeability pinch-outs and beneath nonporous carbonates and evaporites on local structural highs. As observed in core, porous carbonates tend to be highly bioturbated biomicrites deposited in subtidal environments. Fabric porosity is commonly molds of bioclastic debris. Fracture porosity is also important in controlling production. Nonporous carbonates observed in core are typically algal-laminated micrites containing nodular anhydrite and deposited in intertidal to supratidal environments.

San Andres facies accumulated in a range of coastal evaporite and shallow-marine shelf depositional environments (figs. 40 and 41). To the north, deposition of salt and anhydrite was in hypersaline brine pan systems. To the south, carbonates were deposited in shallow-marine shelf environments and in algal flats and sabkhas separating shelf and brine pan systems. In general, these environments migrated to the south through time. San Andres production is mostly from inner-shelf depositional systems. The inner-shelf environment was an area where carbonate banks and/or sabkha platforms cyclically prograded into shelf environments.

Important considerations for continuing analysis of the hydrocarbon potential of San Andres carbonates in the Palo Duro Basin include (1) extent of porous shelf facies, (2) types of porosity and the occurrence of salt plugging in these rocks, (3) regional structural relationships, (4) maturity of organics within San Andres carbonates, and (5) possible migration routes of hydrocarbons.
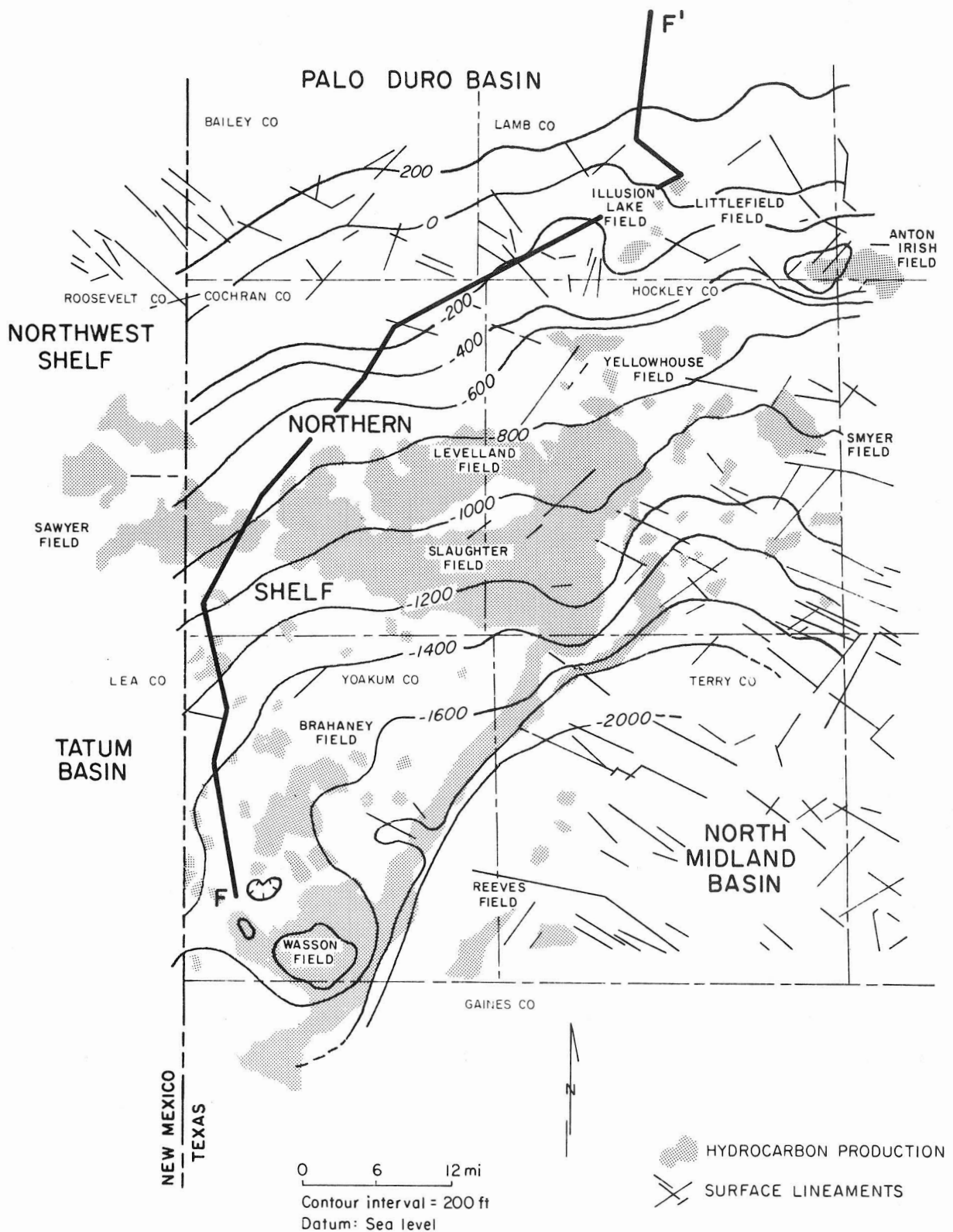
Figure 39. Structure map on π marker in the southwestern Palo Duro Basin and adjacent areas. The π marker is a regional marker bed (correlative high-radioactive peak, fig. 40) in the middle part of the San Andres. Some major oil fields are named. Surface lineaments from Finley and Gustavson (in press).

60
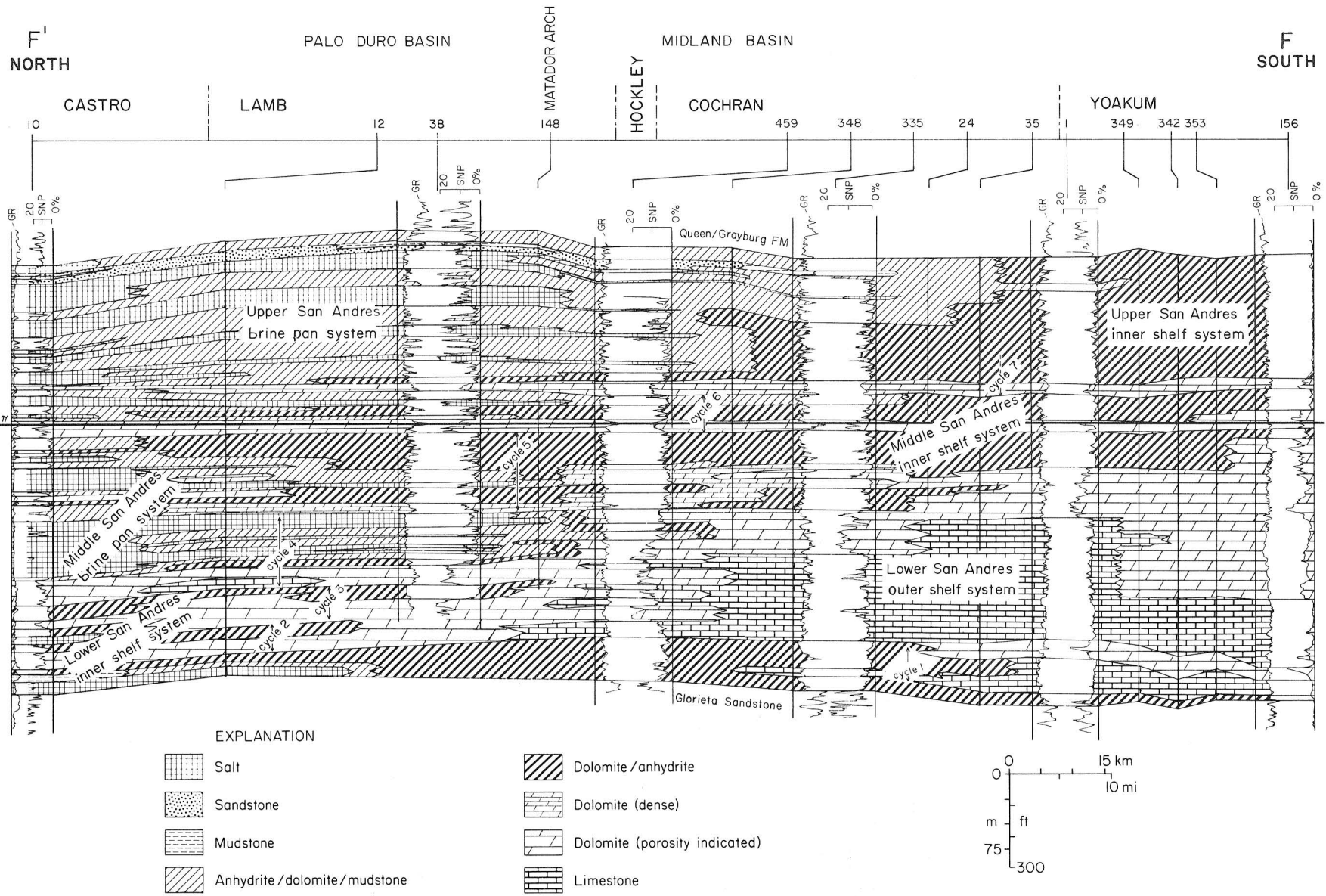
Figure 40. North-south cross section F-F' (location in fig. 39), San Andres Formation, in areas of present production, showing generalized lithic interpretations and inferred depositional systems.
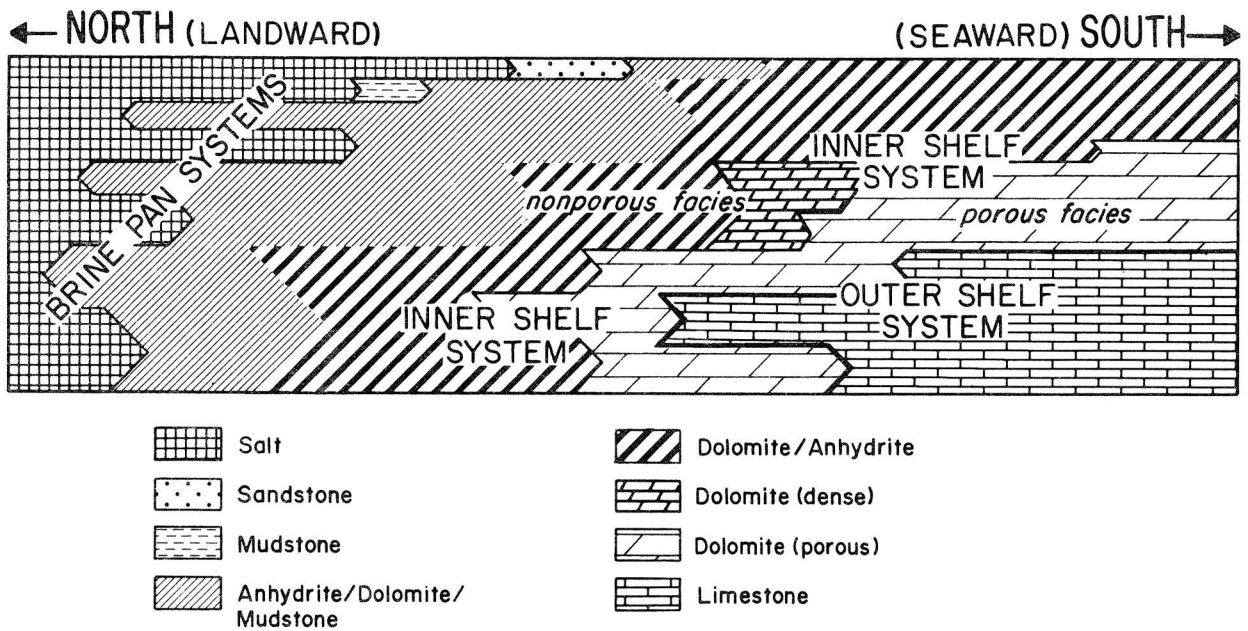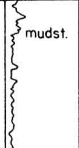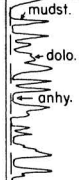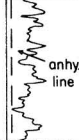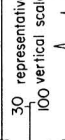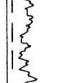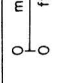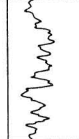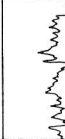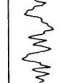
Figure 41. Diagrammatic cross section, San Andres rocks in producing areas, illustrating distribution of facies and depositional systems. This section simplifies relationships in figure 40.

Table 1. Criteria for San Andres facies interpretation using geophysical logs. Criteria are empirically derived from synthesis of well log data in Texas Panhandle.

| WELL LOG FACIES | DEPOSITIONAL SYSTEM OCCURRENCE | WELL LOG CHARACTERISTICS * | | | |
|---|---|---|---|---|---|
| | | GAMMA RAY $\quad$ API units $\quad$ 0 — 150 | SONIC VELOCITY (borehole comp.) $\quad$ microseconds (ms) $\quad$ 90 ft — 40 | NEUTRON POROSITY (sidewall) $\quad$ 30 Ø % 0 | BULK DENSITY (BD) g/cm³ $\quad$ 2.0 — 3.0 |
| SALT | Brine pan system | Low radioactivity higher with increasing clay/mudstone $\quad$ mudst. | $\Delta t \cong 67$ ms; $\Delta t$ increases with increasing clay/mudstone | Ø Commonly off scale (greater than 30%) owing to enlarged borehole from solution of salt beds; where no borehole enlargement, $\varnothing \cong 0$ | BD commonly off scale (less than 2.0 g/cm³) owing to enlarged borehole from solution of salt beds; where no borehole enlargement, $BD \cong 2.1$ g/cm³ |
| MUDSTONE | Brine pan system | Relatively high radioactivity typically as sharp peaks associated with evaporites | $\Delta t$ commonly greater than 80 ms | Ø commonly 10-20% | BD commonly 2.35 - 2.50 g/cm³ |
| ANHYDRITE with DOLOMITE and/or MUDSTONE | Brine pan system | Alternating high to low radioactivity owing to interbedded mudstone, anhydrite, and dolomite, producing "rake-tooth" pattern $\quad$ mudst. $\quad$ dolo. $\quad$ anhy. | $\Delta t \cong 50$ ms for bedded anhydrite; $\Delta t$ varies 50-70 ms for dolomite; higher for mudstone beds | $\varnothing \cong 0$ for bedded anhydrite; $\varnothing$ varies 0-20% for anhydrite – dolomite – mudstone mixture | BD generally 2.95-3.0 g/cm³ for bedded anhydrite; BD varies 2.55-3.0 g/cm³ for anhydrite – dolomite – mudstone mixtures |
| DOLOMITE with ANHYDRITE | Brine pan and inner shelf systems | Relatively medium radioactivity, lower values reflect increasing anhydrite $\quad$ anhy. line | $\Delta t$ generally varies 50-55 ms | Ø generally 0-5% | BD generally varies 2.75-3.0 g/cm³ |
| "DENSE" DOLOMITE | Inner shelf system | Relatively medium radioactivity | $\Delta t$ generally <50 ms, commonly 45 ms | Ø generally varies 0-8% | BD generally varies 2.75-2.9 g/cm³ |
| "POROUS" DOLOMITE (± LIMESTONE) | Inner shelf and outer shelf systems | Relatively medium to high radioactivity | $\Delta t$ generally varies 55-65 ms | Ø generally varies 5-20% | BD generally less than 2.75 g/cm³ ranging as low as 2.4 g/cm³ |
| LIMESTONE | Outer shelf system | Relatively medium to high radioactivity | $\Delta t$ generally varies 55-65 ms | Ø generally varies 2-7% | BD approximately 2.45 g/cm³ |

(LANDWARD ← → SEAWARD indicated on depositional system column)

(Neutron porosity column center: 30 representative vertical scale 100; m. ft; 0 — 0)

* Log scales are provided as reference guides only. The reader should be aware that many factors in addition to lithology, such as borehole diameter, type and density of drilling mud, and type and position of measuring tool, can affect absolute log values.

63

# GEOCHEMISTRY AND THERMAL MATURITY OF POTENTIAL HYDROCARBON SOURCE ROCKS, PALO DURO BASIN

*Shirley P. Dutton*

*Thermal maturity of some Pennsylvanian and Wolfcampian (Lower Permian) shales in the Palo Duro Basin is sufficient to suggest that these rocks may have generated hydrocarbons. Younger sediments in the Palo Duro Basin are thermally immature.*

Geochemical analyses of samples from seven wells in northern and central Midland Basin were made to compare source-rock quality and thermal maturity with that of shales from the Palo Duro Basin. Total organic carbon (TOC) contents of shales in the Midland Basin (fig. 42), a major hydrocarbon-producing area, are generally greater than those of shales in the Palo Duro Basin. TOC values as high as 4.4 percent are found for northern Midland Basin Pennsylvanian and Wolfcampian basinal shales; this compares with 2.4 percent for basinal shales of the Palo Duro Basin. Samples from the Leonardian-age Spraberry Formation from the central Midland Basin have TOC values as high as 5.0 percent and average TOC values between 1.1 and 2.8 percent.

Kerogen color, which indicates thermal maturity, is generally yellow in Pennsylvanian and Permian shales from the northern Midland Basin. The type of kerogen in the Midland Basin is similar in lipid content to kerogen from the Palo Duro Basin. If kerogen color (quantified as Thermal Alteration Index, or TAI) of Midland Basin samples is plotted against kerogen type (Organic Matter Index, or OMI) (fig. 43), both Pennsylvanian and Permian samples fall in the immature zone. Spraberry core samples from the central Midland Basin contain yellow to yellow-orange kerogen, which is relatively lipid rich. A cross plot of the TAI and OMI values for kerogen from the Spraberry falls in the transition zone between maturity and immaturity (fig. 43). Palo Duro Basin Pennsylvanian and Wolfcampian samples also fall in this transition zone (fig. 43). The fine-grained sediments in the Spraberry are probably the source beds for hydrocarbons produced from Spraberry reservoir rocks (Houde, 1979). Therefore, because potential source rocks of Pennsylvanian and Wolfcampian age in the Palo Duro Basin have reached a similar level of thermal maturity, they may also have generated hydrocarbons.

Younger sediments in the Palo Duro Basin were analyzed from the DOE-Gruy Federal core in Randall County. Total organic carbon was measured in samples from the Wichita, Red Cave, lower Clear Fork, and San Andres intervals of Leonardian and

Guadalupian age (table 2). High values of organic carbon, up to 5.38 percent, are present in some of these evaporite units. However, kerogen color is generally pale yellow to yellow, which indicates that these sediments never reached temperatures high enough to generate hydrocarbons.

Thermal maturity tests indicate that hydrocarbons could have been generated in the Palo Duro Basin. Therefore, because the basin may contain hydrocarbon resources, it will most likely be the site of future exploration and drilling activity. Since drilling could threaten the integrity of a nuclear waste repository, any repository site should be located away from potential hydrocarbon reservoir facies.
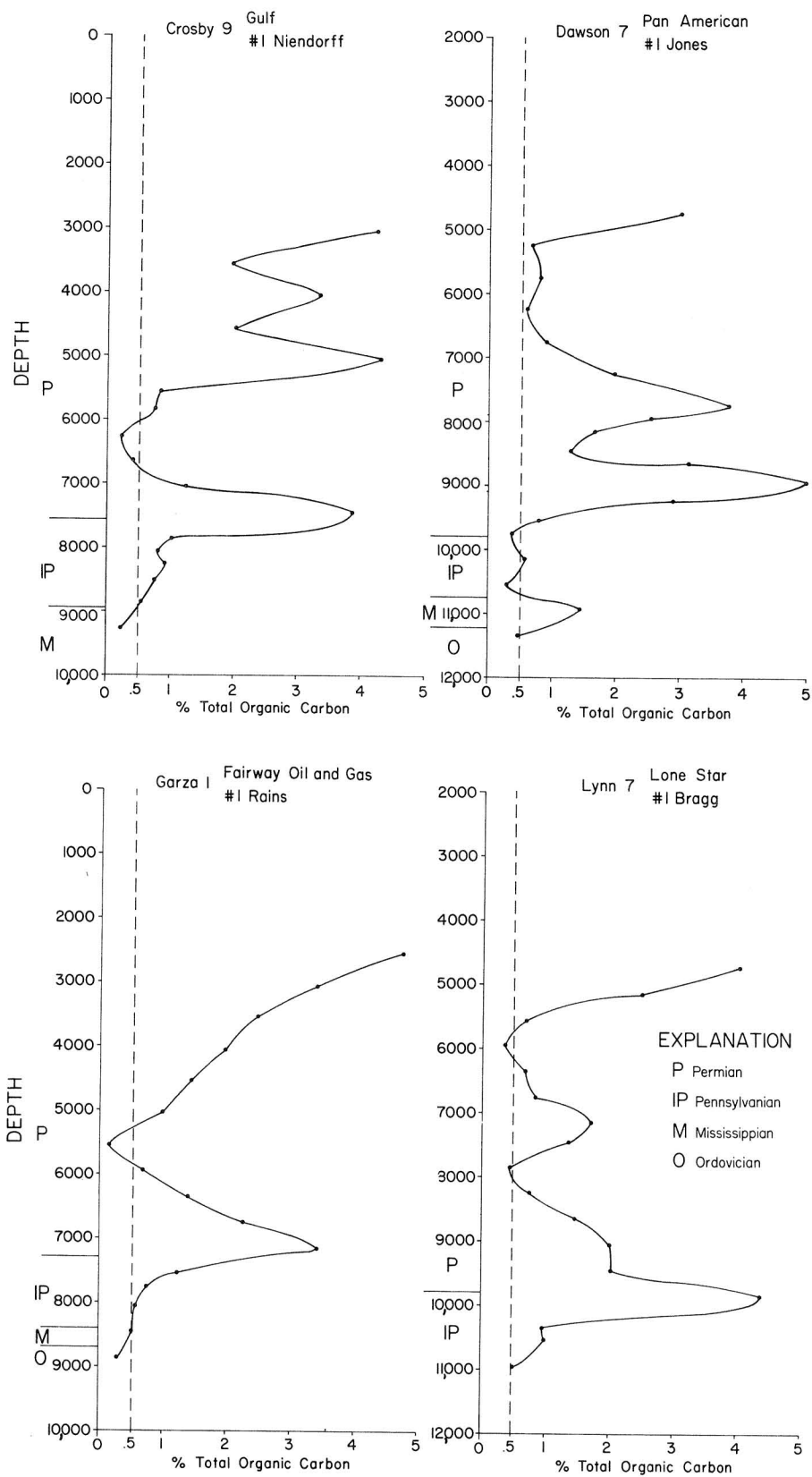
Figure 42. Plot of total organic carbon (TOC) versus depth for wells in the northern Midland Basin.
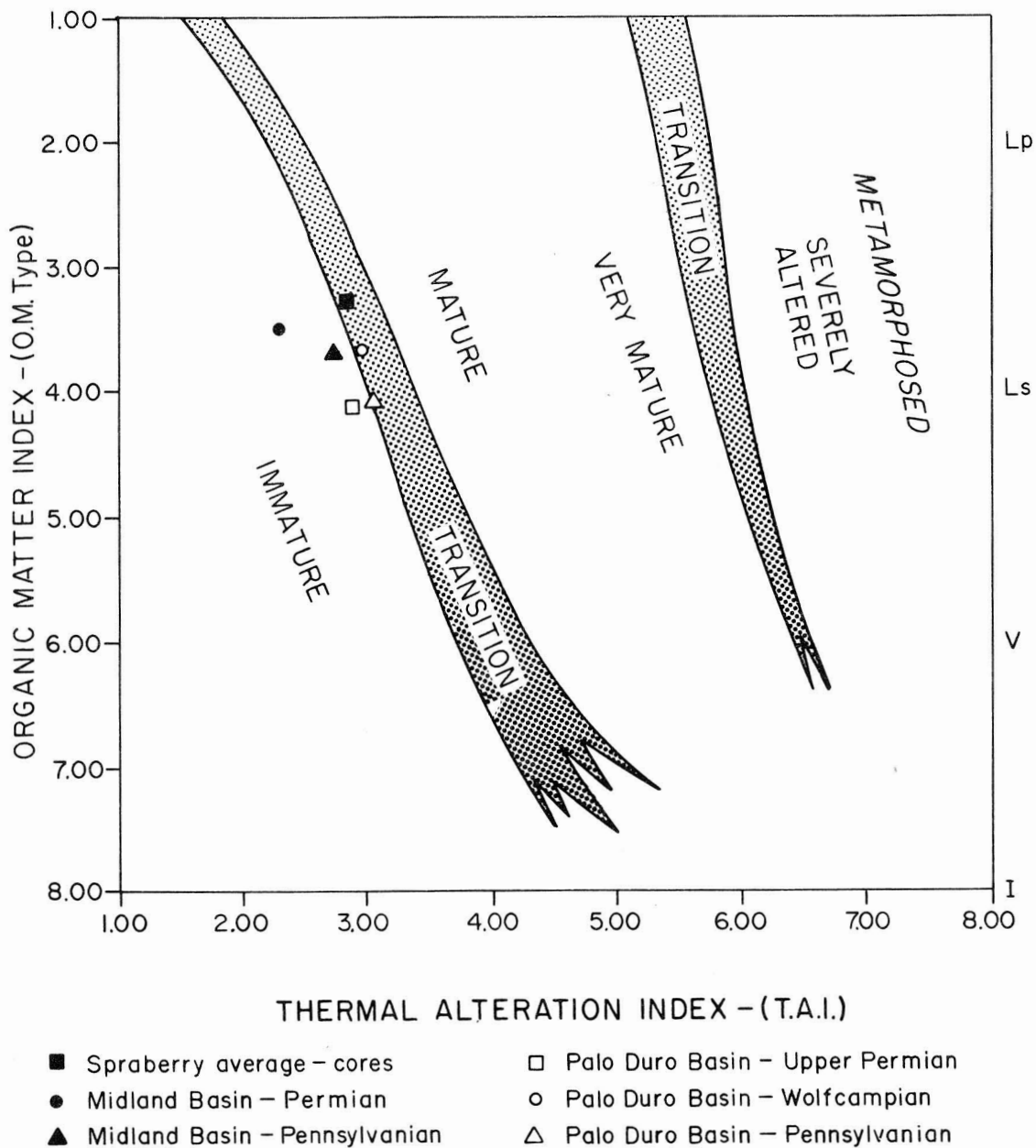
Figure 43. Thermal maturity of Midland and Palo Duro Basin samples based on kerogen color (thermal alteration index) and kerogen type (organic matter index) (from Schwab, 1977).

## Table 2. Total organic carbon content of DOE-Gruy Federal core in Randall County.

| | Depth | Lithology | Percent TOC |
|---|---|---|---|
| **San Andres** | 1427 | Banded salt | 0.074 |
| | 1948 | Banded salt | 0.040 |
| | 1960 | Anhydrite | 1.208 |
| | 1970 | Dolomite | 0.012 |
| | 1988 | Dolomite | 0.018 |
| | 2000 | Dolomite | 1.864 |
| | 2014 | Dolomite | 0.238 |
| | 2021 | Dolomite, salt | 0.014 |
| | 2023 | Dolomite | 0.088 |
| | 2028 | Shale, dolomite | 0.100 |
| | 2031 | Shale - Cycle 3 | 0.164 |
| | 2095 | Dolomite - Cycle 2 | 0.264 |
| | 2172 | Dolomite | 1.280 |
| | 2180 | Dolomite | 1.146 |
| | 2184 | Dolomite | 1.412 |
| | 2190 | Dolomite, shale | 1.202 |
| | 2200 | Dolomite, shale | 1.010 |
| | 2201 | Dolomite, shale - Cycle 1 | 0.864 |
| **Lower Clear Fork** | 3235 | Anhydrite | 0.240 |
| | 3244 | Banded salt | 0.798 |
| | 3288 | Banded salt | 0.574 |
| | 3339 | Dolomite, shale, salt | 2.140 |
| | 3376 | Banded salt | 0.024 |
| | 3384 | Anhydrite | 0.010 |
| | 3401 | Laminated dolomite | 0.100 |
| | 3432 | Nodular anhydrite and matrix | 5.380 |
| | 3451 | Laminated dolomite | 0.374 |
| | 3456 | Black shale | 1.216 |
| | 3527 | Dolomite | 0.456 |
| | 3560 | Dolomite | 1.640 |
| | 3582 | Black shale | 4.226 |
| | 3612 | Dolomite | 0.576 |
| | 3655 | Anhydrite | 4.864 |
| **Red Cave** | 3675 | Red shale | 0.012 |
| | 3715 | Dolomite, shale | 0.014 |
| | 3793 | Dark anhydrite | 0.040 |
| | 3815 | Dark anhydrite | 1.020 |
| | 3840 | Dolomite | 0.444 |
| | 3879 | Black shale | 0.012 |
| | 3887 | Red shale | 0.010 |
| | 3932 | Green shale, anhydrite | 0.018 |
| **Wichita** | 3946 | Dolomite | 0.180 |

# HYDROCARBON SOURCE POTENTIAL OF SAN ANDRES AND CLEAR FORK SHELF CARBONATES, MIDLAND AND PALO DURO BASINS, TEXAS

*Paul J. Ramondetta*

*The necessary ingredients for petroleum generation are present in the San Andres and Clear Fork carbonates of the Northern Shelf, Midland and Palo Duro Basins. Formation temperatures, however, were insufficient to have sustained significant generation of hydrocarbons from the in situ kerogen. This precludes the possibility of in situ generation of oil in San Andres and Clear Fork strata of the Palo Duro Basin.*

Ninety-eight samples of San Andres and Clear Fork shelf carbonates from 17 locations in the Palo Duro and Midland Basins were analyzed for total organic carbon (TOC), kerogen type (OMI), kerogen color (TAI), and vitrinite reflectance ($R_o$) (table 3) (Dutton, 1980). These parameters are necessary to assess hydrocarbon source-rock potential of sediments (Tissot and Welte, 1978). Permian salt deposits in the Palo Duro Basin are under study as possible host rocks for the isolation of nuclear waste. The salt deposits are interbedded with dolomites from which oil is currently being produced in the southern Palo Duro Basin.

This investigation is part of a larger study to assess the future of possible hydrocarbon exploration in the Palo Duro Basin. To determine whether hydrocarbons are trapped in the dolomites north of the present production, it is necessary to assess their source-rock potential. The possibility of in situ generation of oil could preclude the use of the area as a nuclear waste repository, because a repository in an area of potential hydrocarbon resources could be breached by future hydrocarbon exploration. Oil could migrate into these units, however, even if the rocks lack adequate source-rock potential. Sample locations are shown in figure 44.

Total organic carbon values in samples are commonly above the 0.4 percent necessary to consider carbonate rock as a potential oil source (Tissot and Welte, 1978, p. 431). These values are facies dependent and, hence, are highly variable even within short distances. Dark argillaceous facies can be up to 10 times richer in TOC than are proximal carbonates.

Visual inspection of the kerogen from these strata indicates an abundance of membranous plant debris of possible terrigenous origin and somewhat smaller amounts of amorphous sapropel and algal debris of probable marine origin. Samples from the south in Dawson, Lynn, and Garza Counties, however, exhibit a dominance of amorphous sapropel and algal debris, perhaps reflecting a deeper water origin. Amorphous sapropel and algal debris are better suited to generation of oil than are membranous plant debris. Consequently, kerogen quality is higher to the south.

$R_o$ and TAI are important for determining the degree of geothermal diagenesis of organic material. Kerogen color ranges from pale yellow to yellow orange in San Andres and Clear Fork strata in the southern part of the Northern Shelf. $R_o$ averages 0.38 in the south compared with 0.44 in the north. Although kerogen quality is lower to the north, the organic diagenesis is more advanced though not sufficient to have generated significant amounts of hydrocarbons. Figure 45 compares geothermal diagenetic criteria with respect to hydrocarbon-generating ability. San Andres and Clear Fork shelf carbonates lie in the immature zone.

Organic matter from seven samples of San Andres dolomite (Yellowhouse zone) from seven locations in the Palo Duro Basin (five from Lamb County, one from Randall County, and one from Swisher County) was analyzed by gas and liquid chromatography. It has been demonstrated that such analyses can be used to assess the petroleum source potential for a given set of rocks and to relate such potential source rocks to actual petroleum that is suspected of having originated there (Tissot and Welte, 1978). Results of these analyses are summarized in table 3. Figure 46 is the gas chromatograph of San Andres saturated hydrocarbons extracted from the Yellowhouse zone, DOE Swisher County core. It indicates a lack of maturity and does not correlate with the gas chromatograph of Illusion Lake oil, which is produced from the same stratigraphic interval in southern Lamb County. The indigenous organic liquids, however, may be responsible for some of the oil staining and petroliferous odors reported from San Andres carbonates.

The following conditions indicate immaturity for San Andres and Clear Fork carbonates of the Northern Shelf: (1) low $R_o$ and TAI values (fig. 45); (2) highly asphaltic and naphthenic nature of the rock extract; (3) predominance of branched and cyclic paraffins, especially the steranes and terpanes (fig. 46); (4) compositional mismatch between the rock extract and the crude oil produced from the same stratigraphic unit in southern Lamb County; (5) odd carbon number preference for the normal alkanes (fig. 46); and (6) lack of a light-end dominance among the various hydrocarbons (fig. 46).

In situ generation of significant amounts of petroleum is, therefore, not possible in San Andres and Clear Fork shelf carbonates. The prolific oil deposits that do occur in these units in the Midland Basin migrated from a deeper, hotter source. Examination of possible migration routes into potential reservoir units in the Palo Duro Basin will be necessary to forecast the long-range hydrocarbon potential of Clear Fork and San Andres rocks in the Palo Duro Basin.
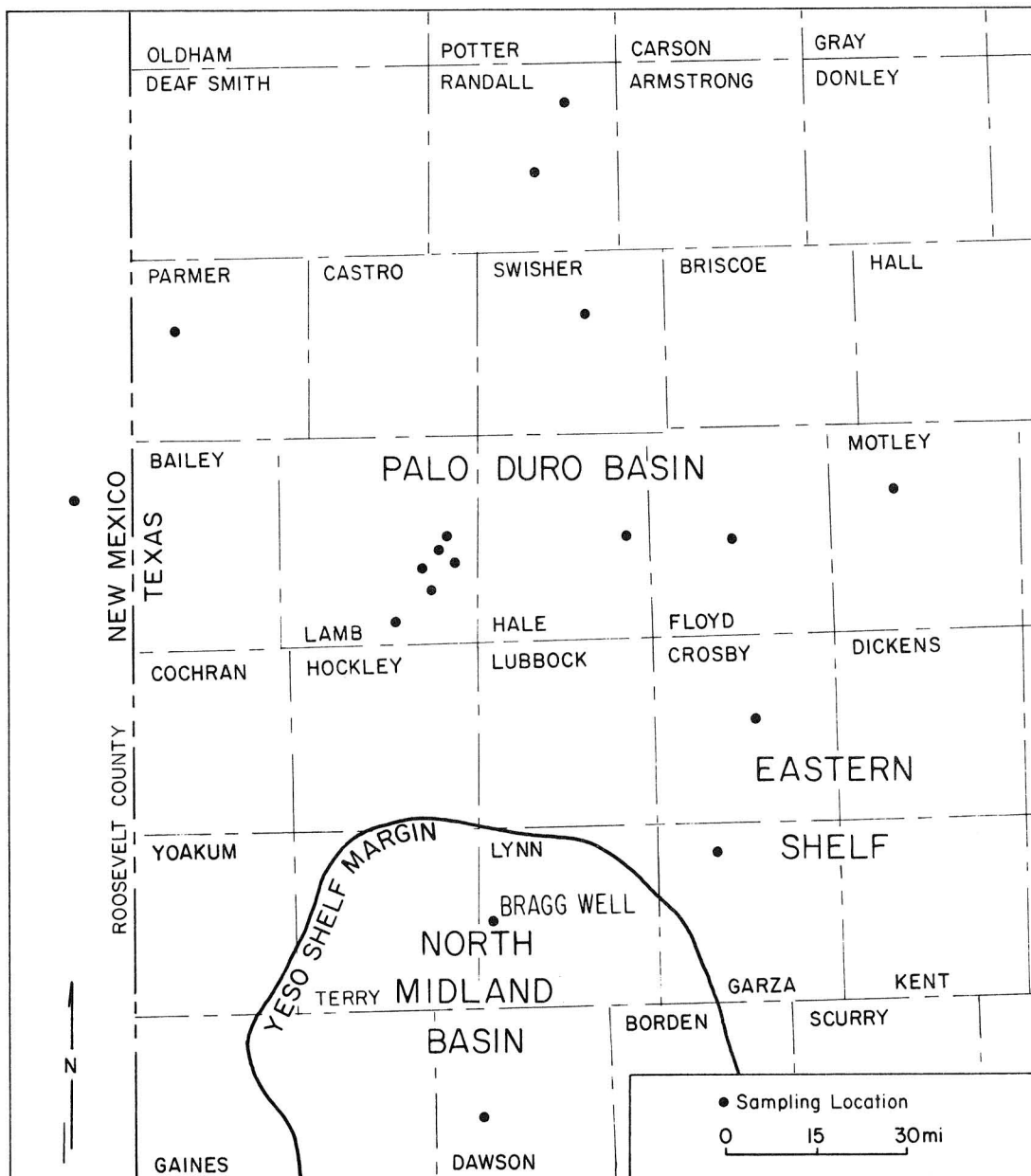
Figure 44. Map of study area showing sampling locations for TOC, OMI, TAI, and $R_o$ analyses. Most samples from Dutton (1980).
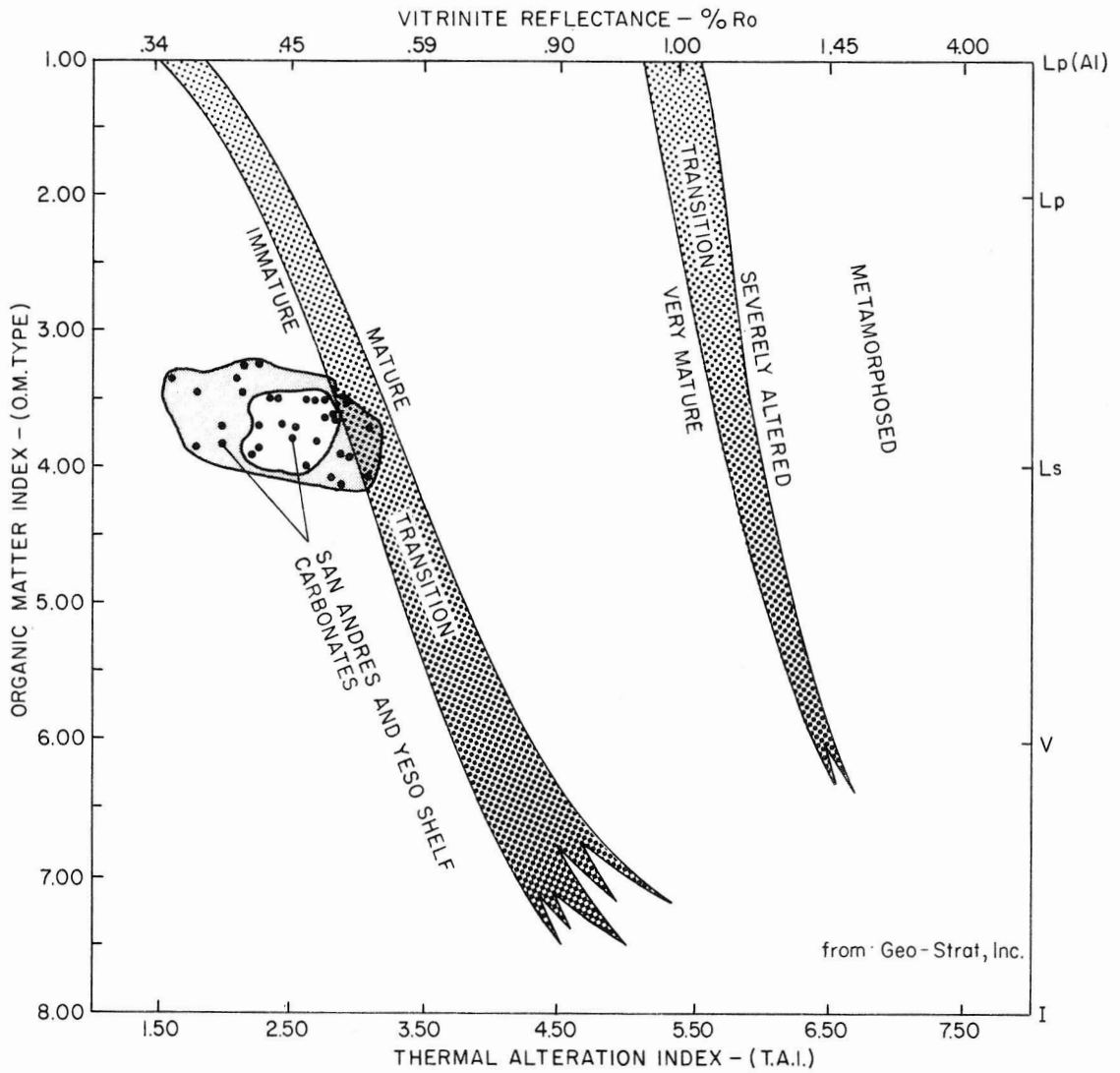
Figure 45. Cross plot showing comparison of geothermal diagenetic criteria.
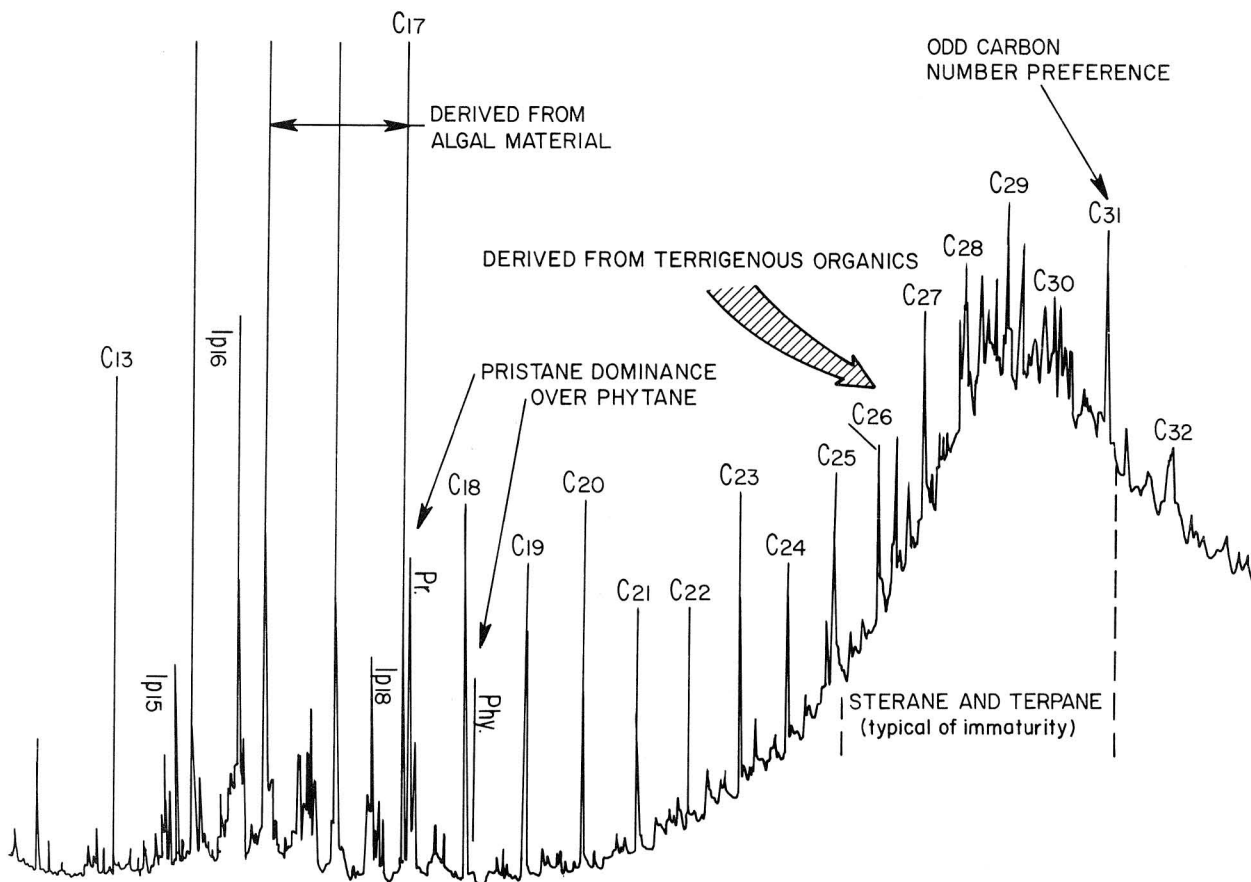
Figure 46. Gas chromatograph of the organic extract (saturates) from the Yellow-house dolomite (San Andres), DOE Swisher County core.

73

Table 3. Geochemical analysis of San Andres and Clear Fork shelf carbonates.

| County | Operator | Well | Depth (ft) | TOC % | OMI | TAI | Ro % | EOM ppm | HC ppm | HC/ EOM % | EOM/ TOC % | HC/TOC % |
|--------|----------|------|-----------|-------|-----|-----|------|---------|--------|-----------|------------|----------|
| Randall | DOE-Gruy | Rex White #1 | 1960-2030 | 0.28 | 3.70 | 2.54 | 0.39 | 494 | 191 | 39 | 18 | 6.8 |
| Swisher | DOE-Gruy | Grabbe #1 | 2693-2996 | 0.26 | 3.78 | 2.43 | 0.42 | 262 | 81 | 31 | 10 | 3.1 |
| Lamb | Shell | McCary #1 | 3892-3926 | 0.33 | 3.79 | 2.70 | 0.45 | 435 | 181 | 42 | 13 | 5.4 |
| Lamb | Atlantic Oil | Ryan #1 | 3824-3872 | 0.57 | 3.49 | 2.74 | 0.45 | 726 | 134 | 18 | 13 | 2.3 |
| Lamb | Felmont | Gray #1 | 3865-3894 | 0.43 | 3.61 | 2.72 | 0.47 | 443 | 72 | 16 | 10 | 1.6 |
| Lamb | Humble | Fowler #1 | 4075-4096 | 0.63 | --- | --- | --- | 836 | 272 | 33 | 13 | 4.3 |
| Lamb | Argonaut Energy (Crown) | Baumgart #1 | 4071-4094 | 0.87 | 3.50 | 2.67 | 0.44 | 1410 | 370 | 26 | 16 | 4.2 |
| Lamb | Stanolind | Hopping #1 | 3840-3920 | 0.5 | 4.08 | 2.80 | --- | --- | --- | --- | --- | --- |
| Hale | Amerada | Dollar et al. | 2600-5480 | 1.7 | 3.52 | 2.89 | 0.43 | --- | --- | --- | --- | --- |
| Randall | Slessman et al. | Nance #1 | 3620-4570 | 1.4 | 4.12 | 2.87 | --- | --- | --- | --- | --- | --- |
| Motley | West Central Drilling | Ross #1 | 1380-5680 | 3.1 | 3.91 | 2.93 | 0.41 | --- | --- | --- | --- | --- |
| Parmer | Stanolind | Jarrell #1 | 3300-5240 | 1.3 | 4.08 | 3.04 | --- | --- | --- | --- | --- | --- |
| Floyd | Sinclair | Massie #1 | 2210-5990 | 3.1 | 3.96 | 2.98 | 0.46 | --- | --- | --- | --- | --- |
| Roosevelt | Stevens Oil | O'Brien #1 | 2650-2835 | 2.0 | 3.65 | 3.14 | --- | --- | --- | --- | --- | --- |
| Crosby | Gulf | Niendorff #1 | 3010-6690 | 2.0 | 3.85 | 2.25 | 0.37 | --- | --- | --- | --- | --- |
| Lynn | Lone Star | Bragg #1 | 4710-6810 | 1.5 | 3.46 | 2.12 | 0.37 | --- | --- | --- | --- | --- |
| Dawson | Pan American | Jones #1 | 4710-6790 | 1.2 | 3.24 | 2.12 | 0.42 | --- | --- | --- | --- | --- |
| Garza | Fairway Oil & Gas | Rains #1 | 2510-5990 | 2.0 | 3.36 | 2.10 | 0.35 | --- | --- | --- | --- | --- |

ABBREVIATIONS:

TOC = total organic carbon

OMI = organic matter index

TAI = thermal alteration index

Ro  = vitrinite reflectance

EOM = extracted $C_{15+}$ organic matter

HC  = $C_{15+}$ hydrocarbons

# BROMIDE GEOCHEMISTRY OF PERMIAN HALITE IN THE RANDALL COUNTY CORE

*C. Robertson Handford*

*Bromide concentrations in halite were measured to determine paleosalinities and extent of diagenesis. It is important to determine whether halite in a potential repository is primary or whether it has undergone diagenetic alteration.*

Bromide analysis has long been a standard technique in the study of halite deposits (see review by Raup and Hite, 1978), and it was employed in this study. Determining the bromide concentration in marine halite rocks is useful for reconstructing paleosalinities at the depositional site, documenting postdepositional diagenetic changes, and exploring for potash deposits (Raup and Hite, 1978).

Bromide substitutes for chloride ions in minerals such as halite, sylvite, and carnallite during precipitation from evaporating brines (Boeke, 1908). The amount of $Br^-$ incorporated into the crystal phases of these minerals depends on the concentration of bromide in parent solutions. Investigative work (Boeke, 1908; Braitsch and Herrmann, 1963; D'Ans and Kuhn, 1940; Holser, 1966; Valyashko, 1956; and many others) has shown that as fresh seawater is evaporated, its bromide concentration increases from 65 ppm to about 500 ppm, which marks the beginning of halite precipitation. The partition coefficient of bromide in halite is such that about 75 ppm (Holser, 1966) would be expected in the initial halite crystallized from seawater. With further evaporation and halite precipitation, $Br^-$ steadily increases in both phases, reaching 2,300 ppm in the brine and 270 ppm in the crystals at the beginning of potash mineral precipitation (Valyashko, 1956). Bromide distribution in most marine halites can be understood on this basis (Holser and others, 1972).

Recrystallization (dissolution-reprecipitation) of halite in the presence of a brine of different bromide concentration than the original brine will change the bromide concentration of the new halite. Holser and others (1972) have shown that a marine halite can be recrystallized or recycled by seawater to produce a second-cycle salt with 10 ppm $Br^-$. Any subsequent number of recrystallizations will not produce less than 7 ppm $Br^-$. However, nonmarine water (normally low in dissolved chlorides) can recycle marine halite, either in place or through deposition in a closed basin or playa, to form a second-cycle salt of 3 ppm bromide (Holser and others, 1972). Examples of halite deposits that may have been deposited from or reworked by nonmarine water include the Permian Rotliegend salt (3.5 ppm $Br^-$) near Hamburg, Germany (Holser,

1979), the lower Elk Point salt (4 ppm Br⁻) of Devonian age, Alberta, Canada (Holser and others, 1972), and the Permian Flowerpot-Blaine salt (<5 ppm Br⁻), Kansas (Holdoway, 1978).

Bromide concentrations in 345 samples from the lower Clear Fork Formation (upper cycle) and the San Andres Formation (number 4 cycle) were determined by titration and plotted stratigraphically (figs. 47 and 48). In general, bromide values for the lower Clear Fork and the San Andres Formations average about 40 and 90 ppm Br⁻, respectively. Values for the San Andres Formation are well within the expected range of marine halite that has undergone little or no diagenesis. The relatively low bromide concentrations in the lower Clear Fork Formation may suggest that (1) the theoretical value of 75 ppm Br⁻ is not representative of natural conditions (Raup and Hite, 1978); (2) the ancient seas did not have the same Br⁻/Cl⁻ ratio as does present-day seawater (Wardlaw and Schwerdtner, 1966); (3) these rocks have been diagenetically altered; or (4) the lower Clear Fork halite precipitated from brines that reached saturation partly by re-solution of salt, which would most likely occur at a stage of evaporation in which salinity of the brines oscillated at about the point of saturation with respect to NaCl (Wardlaw and Schwerdtner, 1966). Petrographic examination of these rocks confirms that some diagenesis has occurred (primary chevron halite mixed with clear, secondary halite), but apparently no more than that which has affected the San Andres halite. In any event, very little of the lower Clear Fork primary halite approaches 75 ppm Br⁻, which implies that alternatives (1), (2), or (4) are the most likely explanations.

Neither bromide profile is very regular, which makes interpretations difficult, but both seem to illustrate recognizably different histories (figs. 47 and 48). The lower Clear Fork profile is marked by a mixture of both high (83 to 120 ppm Br⁻) and low values near the base of the upper cycle. These concentrations may suggest that, at this stage, the salt pan was not uniformly flooded, but consisted of a series of disconnected or isolated pans, some of which were more saline than others. Similar patterns of Br⁻ values near the base of halite beds in the Paradox Basin and in Thailand were noted by Raup and Hite (1978). They suggested that the high bromide values are due to crystallization of diagenetic halite from highly concentrated brines expelled by compaction from the underlying halite beds. This explanation may be acceptable for the lower Clear Fork Formation because the upper cycle is underlain by halite beds of the lower cycle (fig. 48). Contrary to the lower Clear Fork example, Br⁻ values in the basal part of the San Andres profile are not high; instead, they generally range between 64 and 80 ppm in the first 6 m (20 ft). Apparently, neither was the salt pan complex marked by isolated smaller pans with different salinities nor were these beds diagenetically altered by upward-migrating brines of compaction.

The profiles above the base of both the San Andres number 4 cycle and the lower Clear Fork upper cycle are also different (figs. 47 and 48). Generally decreasing Br⁻ concentrations in the lower Clear Fork may indicate a slight but continuous decrease in salinity during deposition of the upper cycle (fig. 47). Alternatively, decreasing Br⁻ values could be due to the increasing effects of diagenesis. As the salt pan was supplanted by saline and dry mudflats of the upper part of the lower Clear Fork and the lower Tubb Formations, mudflat brines, perhaps with lower Br⁻ concentrations, may have refluxed into the underlying halite beds. This implies, however, that these beds had already compacted and were themselves not releasing hypersaline brines.

Although fluctuating as much as 30 to 60 ppm throughout the entire profile, Br⁻ generally increases upward through the first 18 m (60 ft) of the San Andres number 4 cycle but does not essentially change through the remaining 50 m (160 ft) (fig. 48). Standard interpretations suggest that this reflects first, increasing salinity, and second, stabilization of salinity during deposition.

In an effort to determine whether bromide concentrations vary systematically within individual primary halite bands, several were sampled and analyzed. Each band is approximately 5 cm (2 inches) wide and composed of dark, organic-rich halite of variable thickness at the base and passes upward into relatively clear, prime halite at the top. Bromide showed an upward increase in four of the six bands tested, which is interpreted as being a record of deposition from brines that were progressively enriched with Br⁻ during evaporation. Bands that show an upward decrease in bromide may indicate that the brines were freshened slightly, perhaps by the inflow of less saline seawater. This brine could have either directly precipitated halite of lower Br⁻ concentration, or dissolved and reprecipitated preexisting halite to yield a second-cycle salt with lower Br⁻ content.

Because two fundamentally different types of halite, banded to massive halite and chaotic mudstone-halite, were recognized in the Randall core, Br⁻ concentrations in each were noted to determine whether variations existed. Lower Clear Fork samples showed no statistically significant differences; both halite lithofacies averaged between 38 and 40 ppm Br⁻. Thus, it is concluded that the brines that deposited and/or altered each lithofacies were of approximately the same salinity. It is unlikely that chaotic mudstone-halite, though deposited in remote saline mudflats, was precipitated from nonmarine continental waters. The mudflats were bathed by the same brines that filled the shallow salt pans of the inner sabkha.

The same bromide values in the halite are to be expected in salt precipitated from evaporated seawater as opposed to evaporated meteoric water. The retention of

these high bromide levels in the San Andres and the lower Clear Fork Formations and the preservation of primary salt textures show that the salts are marine in origin and that destructive processes have not been active subsequent to deposition. The salt is essentially primary, having been insulated from the effects of ground water.

Figure 47. Bromide content (ppm) for 124 halite samples in the lower Clear Fork Formation, plotted with increasing depth.

79
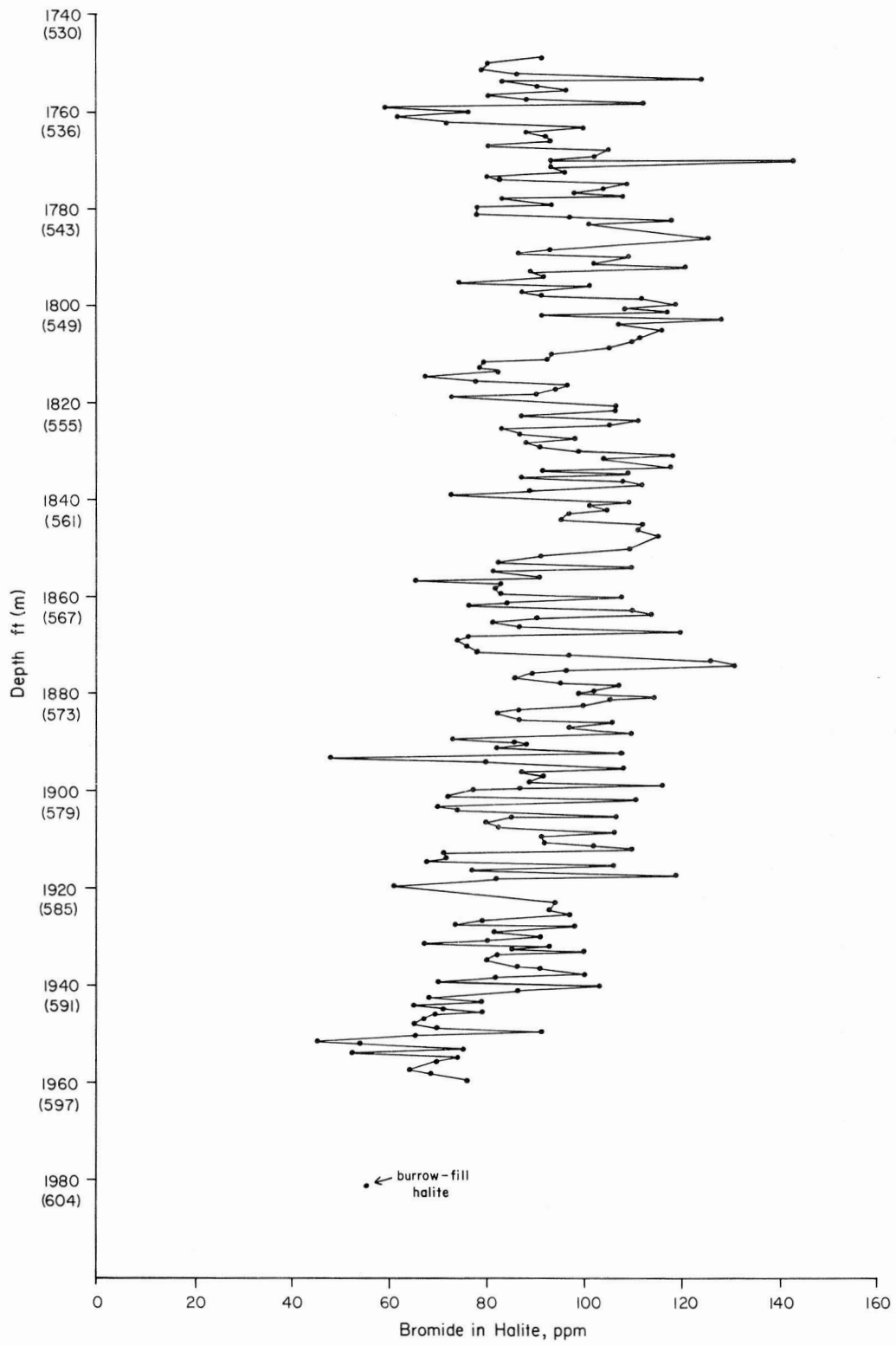
Figure 48. Bromide content (ppm) for 221 halite samples from the San Andres Formation, plotted with increasing depth.

# VERTICAL LITHOFACIES SEQUENCES WITHIN PERMIAN SALT-BEARING STRATA, RANDALL COUNTY CORE

*C. Robertson Handford*

*Simple mathematical analyses help to distinguish contrasting styles of deposition and the preferred arrangement of lithofacies in the Randall core. Such analyses may improve prediction of vertical and lateral variations of facies.*

It has long been recognized that a careful systematic analysis of conformable vertical lithofacies sequences may be used to determine the lateral juxtaposition of similar facies. This basic geologic principle is known as Walther's Law of Facies. The sequence in which facies occur may normally contribute as much paleoenvironmental information as the facies themselves (Walker, 1979). Thus, a borehole sequence through a modern prograding sabkha or delta system should display an orderly and predictable sedimentary record of the juxtaposed environments within that system. The principle may be applied, however, only to lithofacies successions without major stratigraphic breaks. As was noted by Middleton (1973), a break in a succession may represent the passage of any number of environments from which sedimentary products were later eroded.

Clearly, systematic lithofacies changes in Permian evaporite-bearing strata are expressed laterally across the Texas Panhandle by an updip (depositional) transition from dolomite to anhydrite, halite, and red beds (Handford and Fredericks, 1980; Presley, 1979e). Furthermore, these lateral relationships are practically duplicated in numerous vertical successions, which suggests that a careful application of Walther's Law of Facies may be useful in unraveling the depositional history of Permian cyclic evaporite sequences.

As a means of analyzing objectively the vertical arrangement of lithofacies, a simple mathematical method, devised by Selley (1970) and modified by Walker (1979), was employed. Facies relationship diagrams were constructed to document the preferred vertical arrangement of lithofacies in the Randall County core (fig. 49). However, some evaporite formations in each genetic facies group contain significantly greater quantities of terrigenous sediment than do others; thus, it is probable that two different styles of evaporite deposition were active. Mud-rich and mud-poor stratigraphic sequences were analyzed to determine variability in the vertical succession of lithofacies. Data used to construct each diagram are shown in tables 4 and 5. Each diagram of facies relationships shows the most commonly occurring vertical succession of lithofacies that formed in response to migration of both mud-rich and mud-poor

coastal sabkha environments. The cyclic and orderly repetition of each lithofacies and the interrelationship among them will aid in prediction of both vertical and horizontal variation of facies in areas where geophysical logs and cores are not available or in areas of potential site characterization where extensive drilling is precluded.
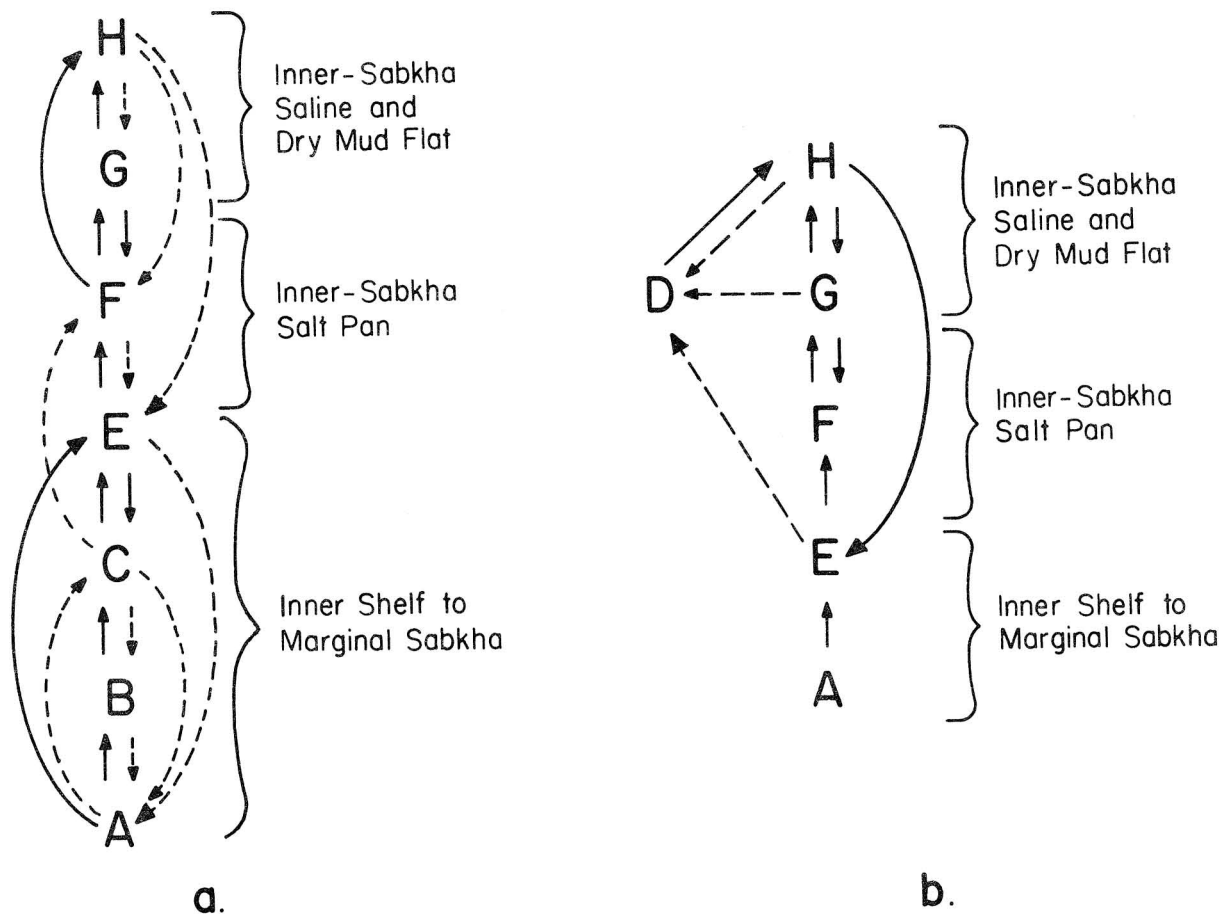
Figure 49. Facies relationship diagram for (a) mud-poor lower Clear Fork and San Andres Formations, and (b) mud-rich Tubb, upper Clear Fork, Glorieta, Queen/Grayburg, and Seven Rivers Formations. Solid arrows indicate more frequent transitions. For explanation of methods, see Selley (1970).

Table 4. Lithofacies transitions in the lower Clear Fork and San Andres Formations. For explanation of A through H see figure 49.

(a) Data array constructed from the arrangement of lithofacies of the core.

|   | H | G | F | E | C | B | A |
|---|---|---|---|---|---|---|---|
| H |    | 4  | 14 | 6  | 2  | 1  | 2 |
| G | 10 |    | 34 | 1  |    |    | 1 |
| F | 13 | 42 |    | 7  | 3  | 1  | 3 |
| E | 3  |    | 10 |    | 28 | 1  | 4 |
| C | 3  | 3  | 8  | 20 | 9  | 8  | 8 |
| B |    |    |    | 2  | 14 |    | 7 |
| A |    |    | 1  | 10 | 4  | 14 |   |

(b) Predicted data array, assuming a random lithofacies arrangement.

|   | H | G | F | E | C | B | A |
|---|---|---|---|---|---|---|---|
| H |   | 5  | 6  | 4  | 5  | 2 | 2 |
| G | 4 |    | 10 | 7  |    |   | 4 |
| F | 7 | 11 |    | 11 | 14 | 6 | 6 |
| E | 4 |    | 10 |    | 10 | 4 | 4 |
| C |   | 6  | 13 | 9  | 6  | 3 | 3 |
| B |   |    |    | 4  | 5  |   | 2 |
| A |   |    | 6  | 4  | 3  | 2 |   |

(c) Difference between (a) and (b).

|   | H | G | F | E | C | B | A |
|---|---|---|---|---|---|---|---|
| H |    | -1 | 8  | 2  | -3 | -1 |    |
| G | 6  |    | 24 | -6 |    |    | -3 |
| F | 6  | 31 |    | -4 | 11 | -5 | -3 |
| E | -1 |    |    |    | 18 | -3 |    |
| C | 3  | -3 | -5 | 11 | 3  | 5  | 5  |
| B |    |    |    | -2 | 9  |    | 5  |
| A |    |    | -5 | 6  | 1  | 12 |    |

Table 5. Lithofacies transitions in the Tubb, upper Clear Fork, Glorieta, Queen-Grayburg, and upper and lower Seven Rivers Formations. For explanation of A through H see figure 49.

(a) Data array constructed from the arrangement of lithofacies of the core.

|   | H | G | F | E | D | A |
|---|---|---|---|---|---|---|
| H |    | 45 | 5 | 10 | 3 | 1 |
| G | 51 |    | 8 | 1 | 3 | 1 |
| F | 4 | 15 |    | 1 |   |   |
| E | 5 | 4 | 5 |    | 1 |   |
| D | 6 |   | 1 |   |   |   |
| A |   | 1 |   | 2 |   |   |

(b) Predicted data array, assuming a random lithofacies arrangement.

|   | H | G | F | E | D | A |
|---|---|---|---|---|---|---|
| H |    | 23 | 6.7 | 7.8 | 2.4 | .7 |
| G | 23 |    | 6.7 | 5.7 | 2.4 | .7 |
| F | 7 | 7 |    | 1.7 |   |   |
| E | 8.1 | 8.1 | 1.8 |    | .6 |   |
| D | 2.5 |   | .7 |   |   |   |
| A |   | 1 |   | .3 |   |   |

(c) Difference between (a) and (b).

|   | H | G | F | E | D | A |
|---|---|---|---|---|---|---|
| H |    | 22 | -1.7 | 2.2 | .6 | .3 |
| G |    | 2.8 | 1.3 | -4.7 | .6 | .3 |
| F | -3 | 8 |   | -4.7 |   |   |
| E | -3.1 | -4.1 | 3.2 |   | .4 |   |
| D | 3.5 |   | .3 |   |   |   |
| A |   |   |   | 1.7 |   |   |

# OXYGEN ISOTOPES AND PARAGENESIS OF DOLOMITES FROM PERMIAN SALT-BEARING SEQUENCES, RANDALL COUNTY CORE

C. Robertson Handford and W. David Wiggins

*Oxygen isotopic analysis of dolomites from the number 4 cycle of the San Andres Formation indicates syngenetic emplacement by hypersaline waters followed by recrystallization under the influence of mixed meteoric-marine waters. There is no evidence of late-stage recrystallization or reequilibration with subsurface brines, which indicates long-term hydrologic isolation, a critical factor in nuclear waste isolation.*

Sedimentologic and petrographic evidence suggests that dolomitization of Permian carbonates in the Randall County core was syngenetic, occurring contemporaneously with deposition. Dolomitization by evaporative pumping (Hsu and Siegenthaler, 1969) or capillary processes (Shinn and others, 1965) created the fine-grained, poorly crystallized dolomite in the supratidal (marginal sabkha) zone. Dense hypersaline brines may have refluxed (Adams and Rhodes, 1960; Deffeyes and others, 1965) from the marginal sabkha downward into underlying subtidal carbonates, dolomitizing the carbonate matrix and some aragonite grains. Dissolution of aragonite grains and maturation, or recrystallization, of dolomite to form semilimpid euhedra can be attributed to mixing of fresh meteoric water and seawater, as stated by Folk and Land (1975). Petrographic evidence also suggests that all stages of dolomite diagenesis preceded compaction and halite cementation of primary and secondary pores.

As a means of testing and further evaluating the origin of dolomite (principally the lower San Andres Formation, number 4 cycle), oxygen and carbon stable isotope ratios were measured for 10 $CO_2$ gas samples collected from the dolomites. Measurement was done according to the method of McCrea (1950). Results are shown in figure 50, and they are compared to oxygen isotopic values of Recent and ancient dolomites (fig. 51) believed to represent a spectrum of diagenetic environments.

The Randall County core dolomites are enriched in $C^{13}$ relative to modern dolomites (Milliman, 1974) but fall within the normal range of values for Permian dolomites. The high $C^{13}/C^{12}$ ratios in Permian carbonates tested worldwide indicate that the Permian Period was one of global changes in seawater chemistry (Veizer and Hoefs, 1976).

Modern evaporitic dolomites from the Persian Gulf are characterized by high $O^{18}/O^{16}$ ratios (fig. 51, line 1) relative to normal marine carbonates (Milliman, 1974). However, sediments dolomitized by meteoric waters are isotopically light (fig. 51,

line 3), and dolomites formed or recrystallized in a zone of fresh-water and seawater mixing show intermediate $O^{18}/O^{16}$ ratios (fig. 51, lines 2, 4, and 5).

Number 4 cycle San Andres dolomites vary in $O^{18}$ between -0.1 and +2.8 per mil (PDB) (fig. 50). Number 4 cycle dolomites (fig. 51, line 6) are light relative to the Recent Persian Gulf (supratidal) samples but compare favorably to dolomites that have recrystallized in meteoric-marine mixing zones.

Geochemical, petrographic, and sedimentologic data confirm that the bulk of carbonate diagenesis occurred during three major phases: (1) Marginal sabkha and subtidal inner shelf carbonates were dolomitized by hypersaline water during deposition and sabkha progradation. Seepage reflux or development of a thick hypersaline wedge of ground water along the shoreline led to dolomitization of the carbonate matrix in underlying subtidal facies. (2) Islands sufficiently large to support fresh-water lenses were formed by either normal sedimentation or sea-level fluctuations. Aragonite grains were dissolved, and fine-grained, isotopically heavy matrix dolomite was recrystallized to coarser grained, semilimpid, and isotopically lighter euhedral dolomite. (3) An extensive inner-sabkha salt pan formed above the porous dolomitized carbonates, and dense brines seeped downward through these near-surface dolomites, precipitating halite in the remaining intercrystalline and moldic pores.

Each diagenetic phase was essentially synsedimentary (or "syngenetic") in timing, and no evidence suggests late-stage recrystallization or reequilibration with subsurface brines. Possibly, the chemistry and fabric of the dolomites were "locked in" owing to low permeabilities created by pervasive halite cementation. The isolation of these dolomites from subsurface brines suggests postdepositional hydrologic integrity of the sequences investigated.
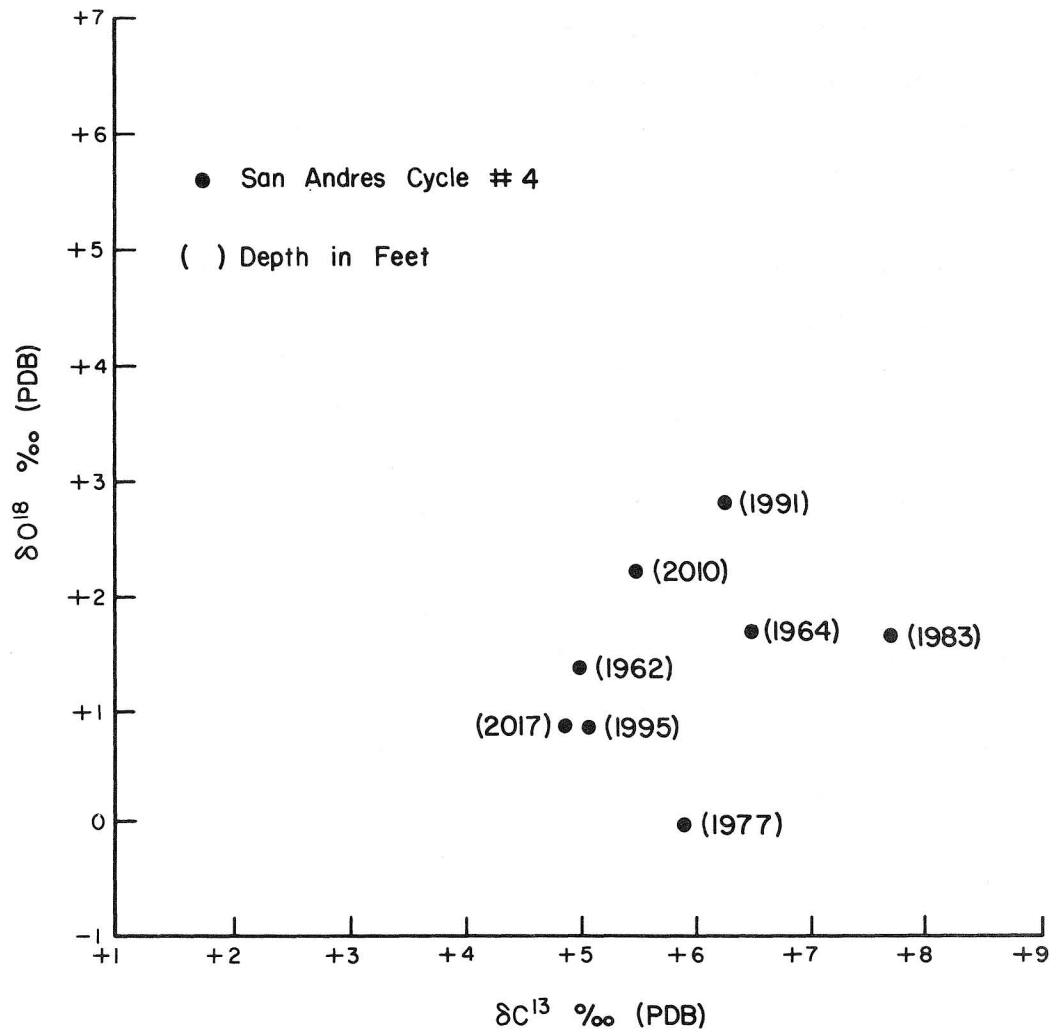
Figure 50. Stable isotope composition of nine dolomite samples from the Randall County core. Analytical accuracy is approximately ±0.2 per mil.
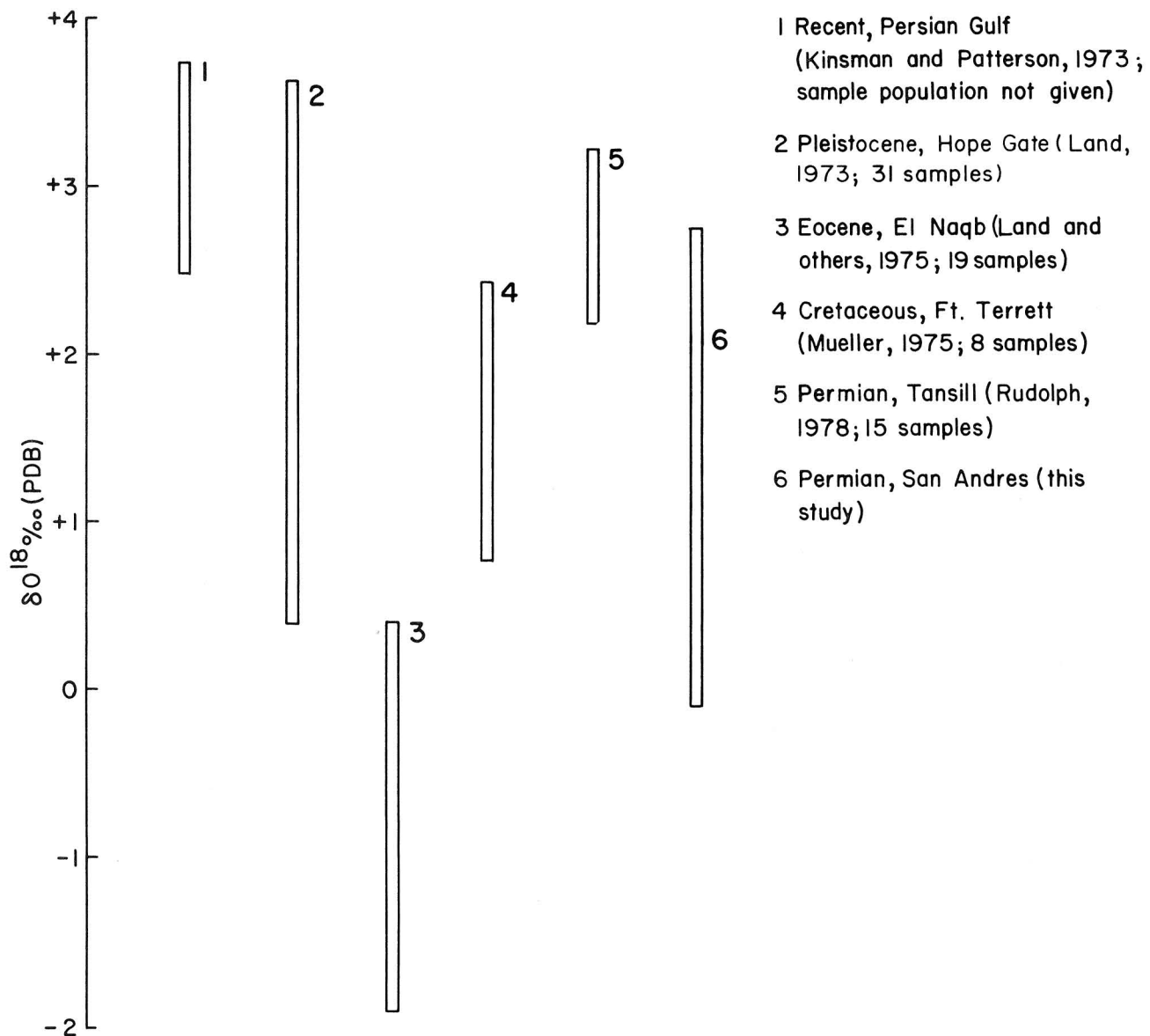
Figure 51. A comparison of oxygen isotopic compositions of selected dolomites from the literature and the San Andres cycle number 4 of the Randall County core.

# DEPOSITIONAL SEQUENCES AND ASSOCIATED SEDIMENTARY DIAGENETIC FACIES: AN ONGOING INVESTIGATION OF SALT-BEARING CORE, SWISHER COUNTY, TEXAS

J. H. McGowen

*The record of large-scale sedimentary cycles, resulting from alternating expansion and reduction in size of shallow seas, is contained in chemical (salt, anhydrite, dolomite) and terrigenous clastic (mudstone, siltstone, sandstone) deposits. Depositional environments dictated the initial sedimentary parameters and subsequently influenced diagenesis. Sedimentary and diagenetic history of salt-bearing Permian strata has influenced rock properties (salt thickness and purity, and permeability of associated rocks) requisite for a nuclear waste repository.*

Detailed petrographic, geochemical, and mineralogical studies of the Swisher County core (and cores to be taken in 1981) are being conducted primarily to characterize, in detail, the various salt-bearing lithofacies as a means of determining the suitability of these facies as nuclear waste repositories (Galloway, 1979). A second objective is to assess the mineral and energy resource potential of all stratigraphic units from ground level to a depth of 1,200 m (4,000 ft).

Four major lithofacies occur in the Permian evaporite-bearing strata contained in cores from the Randall County DOE-Gruy Federal, Rex White no. 1 well and the Swisher County DOE-Gruy Federal, D. M. Grabbe no. 1 well (pl. 1, in pocket). The lithofacies are (1) siliciclastic, (2) salt, (3) anhydrite, and (4) dolomite, which can be combined into two broad groups of sedimentary rocks: (1) terrigenous clastics and (2) chemical. Previous studies have described the lithofacies, the inferred depositional environments, and the large-scale sedimentary cycles exhibited by Permian evaporite-bearing strata: Handford (1979, 1980), McGillis (1980), and Presley (1979a, b, d, 1980a, b).

Chemical rocks were precipitated from shallow marine water, shallow hypersaline water bodies, or interstitial waters, and are represented by salt, anhydrite, and dolomite. These rocks make up 3 to 87 percent of various stratigraphic units composing the Permian section in the Swisher County core (fig. 52). The lower and upper Clear Fork, the lower and upper San Andres, and the Alibates Formations are chiefly evaporites and dolomite.

Environments of deposition of chemical rocks as reported by earlier workers are as follows: (1) salt - upper sabkha, (2) anhydrite - lower to upper sabkha, (3) dolomite - shallow subtidal, intertidal, and supratidal.

Terrigenous clastic rocks, derived chiefly from older sedimentary rocks lying beyond the depositional basin, are composed of sandstone, siltstone, mudstone, and claystone (siliciclastic facies). These rocks make up from 11 to 97 percent of the various stratigraphic units composing the Permian section of the Swisher County core (fig. 52). The Tubb, Glorieta, Queen/Grayburg, lower and upper Seven Rivers, Yates, and Dewey Lake Formations are dominated by terrigenous clastic rocks. Terrigenous clastic strata (siliciclastic facies) accumulated in mud-rich sabkhas bordering a shallow marine basin.

Large-scale sedimentary cycles are apparent from the sequences of chemical and terrigenous clastic rocks contained in the Swisher County core. Within the Swisher County area there were perhaps five episodes of major expansions of the shallow Permian seas as shown by the (1) lower Clear Fork, (2) upper Clear Fork, (3) lower and upper San Andres, (4) upper Seven Rivers, and (5) Alibates Formations. Shrinking of the Permian seas is recorded by the predominantly terrigenous clastic units: (1) Tubb, (2) Glorieta, (3) Queen/Grayburg, (4) lower Seven Rivers, (5) Yates, (6) Salado/Tansill, and (7) Dewey Lake Formations. The underlying controls of expansion and construction of Permian seas are not positively known at this time. Controlling factors could have been (1) tectonic, (2) climatic, (3) variations in terrigenous clastic input (influenced by tectonics and/or climate), or (4) opening and closing of the Permian seaway to the south.

Chemical and terrigenous clastic rocks accumulated under different physical and chemical circumstances. As a consequence of accumulating in different depositional environments, these rocks have undergone somewhat diverse burial diagenesis and remain subjected to physical and chemical alteration in the shallow subsurface, chiefly as a consequence of ground-water flow.

Currently, the Swisher County core is being subjected to petrographic, geochemical, and mineralogical studies to determine the diagenetic history (including porosity/permeability, dissolution, cementation) and the presence of potential economic mineral deposits. A product of the study will be a detailed physical, chemical, and mineralogical characterization of the Permian facies, described by those authors cited in this paper, the Triassic facies, defined by McGowen and others (1979), and the Pliocene facies, defined by Seni (1980). Each stratigraphic unit will be systematically studied in the order in which it accumulated; data are now being generated on the lower Clear Fork and the Tubb Formations.
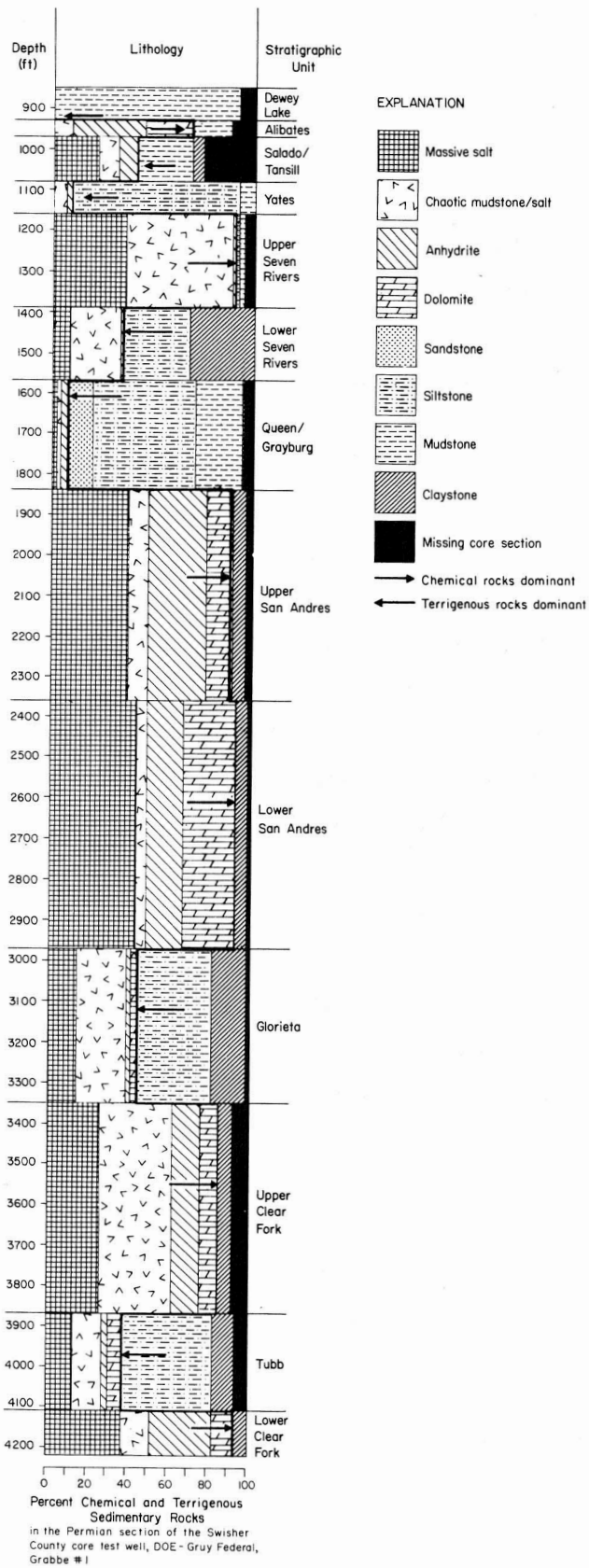
Figure 52. Swisher County core test well DOE-Gruy Federal, Grabbe no. 1: percent lithologic type per stratigraphic unit.

# REGIONAL HYDRAULICS OF BRINE AQUIFERS, PALO DURO AND DALHART BASINS, TEXAS

M. E. Bentley

*Patterns of hydraulic head derived from drill-stem-test data suggest that very slow (1.3 to 13 cm/yr) regional eastward flow occurs in brine aquifers below the salt-bearing section. Although pressures in these aquifers are "subnormal" in the Palo Duro Basin, fluids are confined, and head elevations are above repository level.*

Several water-related hazards affect the construction and long-term integrity of a repository sited in the salt-bearing section: (1) seepage of water into the repository during its active life, (2) rapid inflow of water into the repository owing to intersection of abandoned, improperly cased or plugged boreholes during construction, (3) natural dissolution of the salt layer, (4) dissolution caused by migration of fluids through future boreholes inadvertently drilled through the repository layer, and (5) transport of contaminants from a failed repository to the biosphere by natural ground-water flow. Assessment of the probabilities of such hazards requires knowledge of the local and regional hydrogeology. Though water is present in the Panhandle region in clay minerals, oxyhydroxides, and other hydrous minerals and in fluid inclusions in salt, the most mobile fluids are located above and below the evaporite section in porous and permeable aquifers.

The most important sources of water are the shallow fresh-water sands of the Ogallala Formation and the Dockum Group and the deep Paleozoic carbonate and sandstone brine (>35,000 mg/l TDS) aquifers of Wolfcampian (Lower Permian) age and older. The hydraulic properties of the Ogallala deposits are well known because of extensive development for irrigation; on the other hand, few reliable data exist on the hydrogeology of the deep brine aquifers.

The deep-basin pressure data consist of reports of 1,104 drill-stem tests (DSTs) conducted in the Palo Duro and Dalhart Basins by the petroleum industry. The relatively sparse data in these basins increase toward the basin margins, and coverage in the adjacent Anadarko and Midland Basins is relatively dense. Published pressure values are normally lower than the true formation-water pressure because insufficient test time was allowed for recovery of pressure after flow tests. More rarely, erroneously high values result from failure to relieve overpressure caused by drilling-mud invasion. Head maps constructed from these data were subjectively interpreted by manual elimination of the typically high percentage (>80 percent) of unreasonably low values. Despite these factors, the distribution of head values was considered to

show reliably general pressure conditions, principal flow directions, and magnitudes of potential gradients in the deep Palo Duro and Dalhart Basins.

Each pressure was converted to an equivalent fresh-water head (density = 62.4 lb/ft$^3$, 1,000 kg/m$^3$). No attempt was made to adjust heads to account for the density of the brines because the regional fresh-water head gradients are too large to be cancelled or reversed in direction by an unfavorable distribution of the known fluid densities (65.5 to 70.5 lb/ft$^3$, 1,050 to 1,130 kg/m$^3$) within the vertical interval provided by the structural relief of the aquifers.

The vertical uniformity of heads in the deep basin suggests that the Wolfcampian aquifer is not isolated from underlying aquifers. Aquifers may be locally connected by depositional thinning of the numerous shale aquitards that are interbedded with the carbonates and sandstones, or faults and fractures may act as conduits that allow equalization of heads. The principal flow direction in the Texas Panhandle is to the east, according to heads in Wolfcampian, Pennsylvanian (figs. 53 and 54), and underlying aquifers. An area of low (preproduction) heads in Wolfcampian rocks in the Panhandle Oil and Gas Field creates an anomaly at the Amarillo Uplift that cuts across the regional trend. Heads are significantly higher in correlative water-filled limestones and sandstones immediately adjacent to the reservoir. About 40 billion mcf of gas and 1.5 billion bbl of oil have been produced from the uplift in 60 years. The pattern of pressure decline indicates depletion-drive conditions, suggesting that the reservoir is isolated from the rest of the aquifer by faults or by a large permeability contrast. The gentle eastward tilt of oil-water and gas-water contacts may reflect the general eastward drainage of Wolfcampian brines.

The thick, low-permeability evaporite section effectively prevents local recharge or discharge of the underlying deep-basin aquifers. Petrographic examination of cores of the evaporite interval, which were obtained from DOE stratigraphic test holes in Swisher County (McGowen, this volume) and Randall County (Handford and Wiggins, this volume) showed that former pore space in potentially permeable sandstones and dolomites is occluded by halite and other cements. The few drill-stem tests conducted in these rocks in the Palo Duro Basin have produced either small amounts of water or none at all, except near the Matador Arch, where San Andres carbonate facies become more dominantly normal marine and where halite cements are less extensive (Ramondetta, this volume) (fig. 55). Some occurrences of lost circulation of drilling fluids may document the existence of isolated areas of porous dolomite. Most recharge to the deep aquifers probably takes place in updip areas to the west in New Mexico, where the evaporite beds thin and carbonate aquifers are

interbedded with and overlain by sandstones that crop out east of the uplifted Sacramento Mountains-Pedernal Hills trend (fig. 57).

Beneath the High Plains, deep-basin fluids are underpressured but artesian. The term "underpressured" is used because water levels in boreholes open to deep aquifers typically stabilize at depths greater than 1,000 ft (300 m) below the High Plains surface. The levels are, however, well above most salt beds. The potential, therefore, exists for water to flow upward through unplugged boreholes from the deep aquifers into air-filled mines in salt. On the upper hand, the large head differential between normally pressured Ogallala and underpressured Wolfcampian aquifers could allow improperly cased or plugged boreholes connecting them to conduct fresh waters downward, a situation that can result in salt dissolution around the well bore. Dissolution under similar conditions has resulted in subsidence and collapse in the Hutchinson salt basin in Kansas, though occurrences are rare compared with the number of existing boreholes. No subsidence related to drilling has been identified within the Palo Duro Basin (Gustavson and others, 1980b). This may be due to differences in the history of well-completion practices in the two regions, or to higher permeability of the deep receptor aquifer in Kansas (vuggy Ordovician Arbuckle dolomite).

East of the High Plains, the deep aquifers are not underpressured; head levels still decline steadily to the east, but the rapid decrease in topographic elevation at the Caprock Escarpment allows water levels to reach the land surface. Figure 56 illustrates the distribution of reported Wolfcampian pressures in regions that have different topographic elevations, as well as the trends of pressure with depth in each area. The abrupt decline in the elevation of the land surface (and shallow water tables) at the Caprock Escarpment does not appear to coincide with an increase in pressure gradients in deep aquifers that would signal an appreciable topographic influence on upward components of flow and discharge.

The shallow (<1,000 ft; 300 m) natural dissolution of salt has occurred typically in the structurally highest part of each salt bed (McGookey, this volume; Gustavson and others, 1980b). The permeability of the evaporite section is too low to permit significant flow from deep aquifers to shallow brine-emission areas east of the caprock, since here deep and shallow heads are about equal. The deep-basin aquifers discharge farther east, either by seepage to streams that incise their outcrops, by upward leakage to the lower parts of fresh-water aquifers, or by cross-formational flow to other formations that transmit deep ground waters farther down the general structural and topographic dip toward the Gulf of Mexico.

95

The Wolfcampian aquifer provides a long path from a repository to the biosphere, given any of these discharge points. Pore velocities calculated from mapped head gradients, an assumed average permeability of 2 millidarcys ($1.6 \times 10^{-3}$ m/day), and a reasonable range of porosity (0.5 to 5 percent) are only 1.3 to 13 cm/yr, slower than some of the possible rates of contaminant diffusion. More direct pathways may exist in erratically permeable dolomites in the evaporite section in the Palo Duro Basin. Well tests could provide field confirmation of the permeability of these dolomites at critical sites.

EXPLANATION

∘  DST in Wolfcampian

⤙✕⤚  Basement uplift and arches

⟹  Inferred direction of flow

⟋2400⟍  Equipotential contour, feet above sea level

N

0                    40mi
0          40km
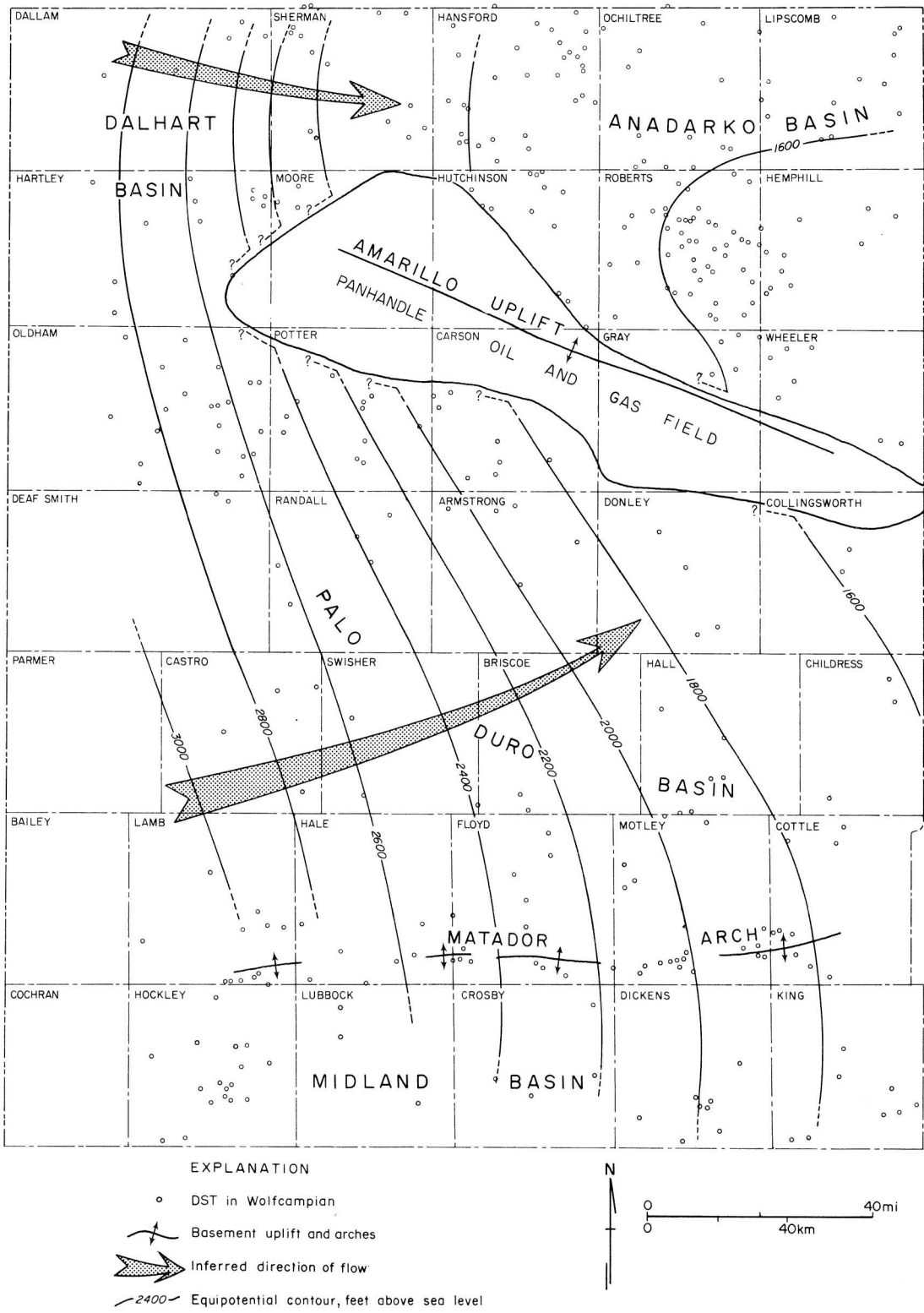
Figure 53.   Hydraulic head map, Wolfcampian aquifer, Texas Panhandle.   Head contours interpreted from fresh-water heads calculated from uncorrected shut-in pressures.   Low heads (approximately 1,000 ft) in the Panhandle Oil and Gas Field appear to cut across regional trends and may represent relative hydraulic isolation of eastward-drained porous strata.   Well locations not shown in Panhandle Field.

97
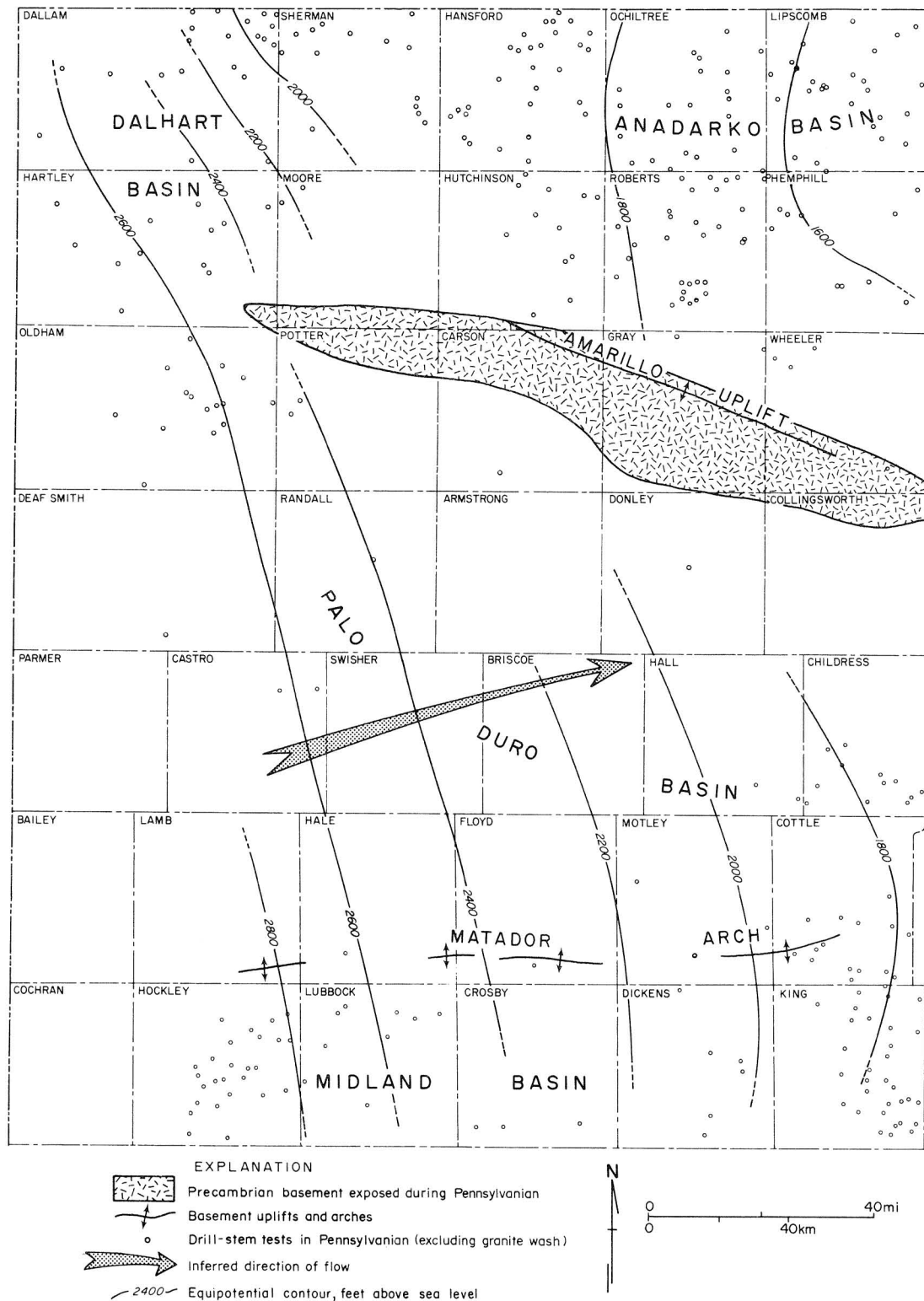
Figure 54. Hydraulic head map, Pennsylvanian aquifer (excluding granite wash), Texas Panhandle. In the Anadarko Basin, only Virgilian (Upper Pennsylvanian) strata are included since deeper fluids are affected by overpressures that are concentrated in Lower Pennsylvanian aquifers in western Oklahoma. Head contours interpreted from fresh-water heads calculated from uncorrected shut-in pressures.
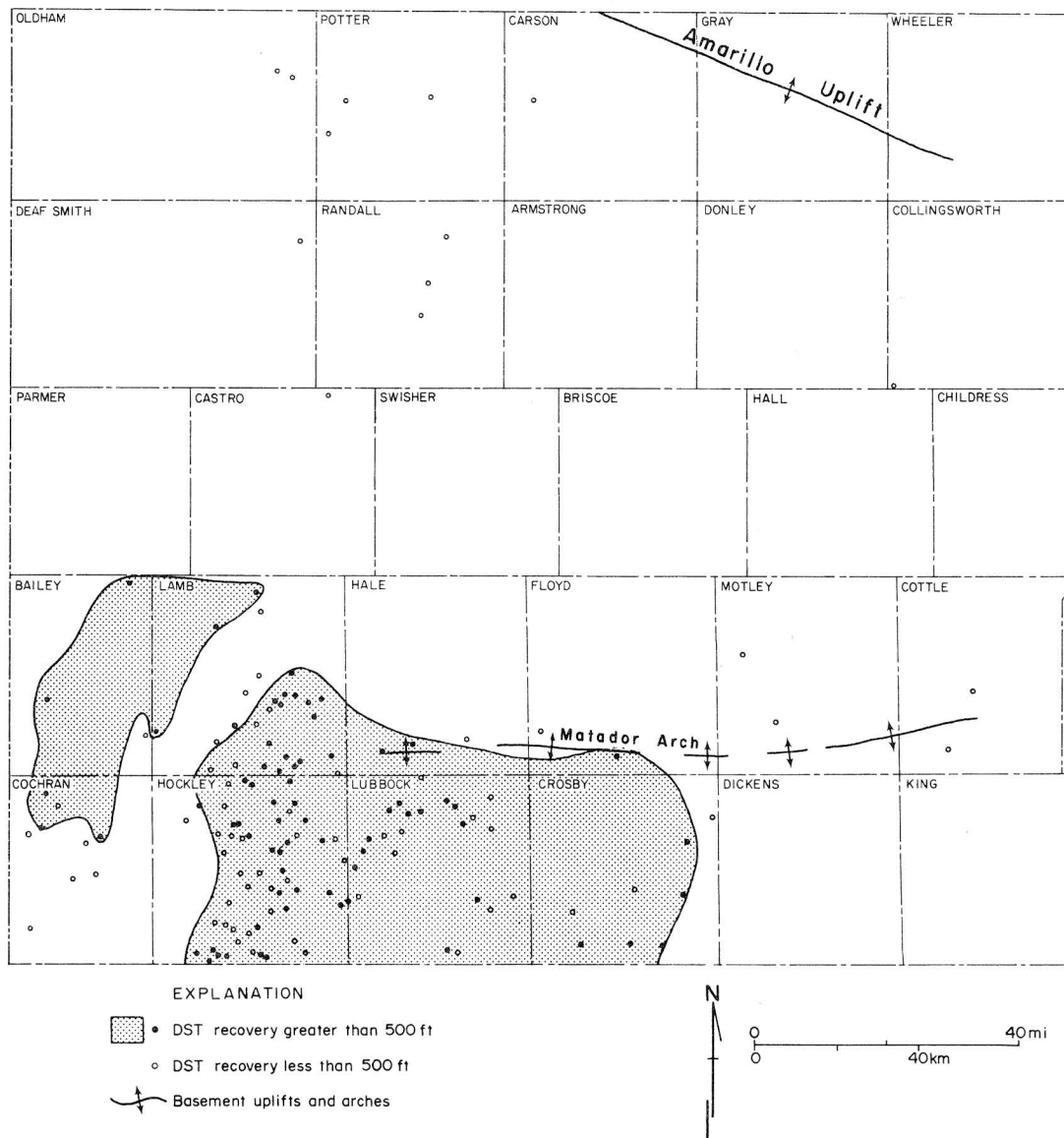
Figure 55. Locations of drill-stem tests, Middle and Upper Permian salt-bearing stratigraphic units, Palo Duro Basin. Tests that flowed 150 m (500 ft) or more of fluid into empty pipe in 30 minutes to 2 hours time are shown in shaded areas. Significant production of fluids in these rocks is limited to the southern basin margin, where San Andres coastal sabkha evaporites and red beds grade into increasingly thick sequences of porous intertidal and shelf carbonates. Underlying Permian and Pennsylvanian shelf carbonates commonly produce 300 to 900 m (1,000 to 3,000 ft) of fluid in similar tests.

99
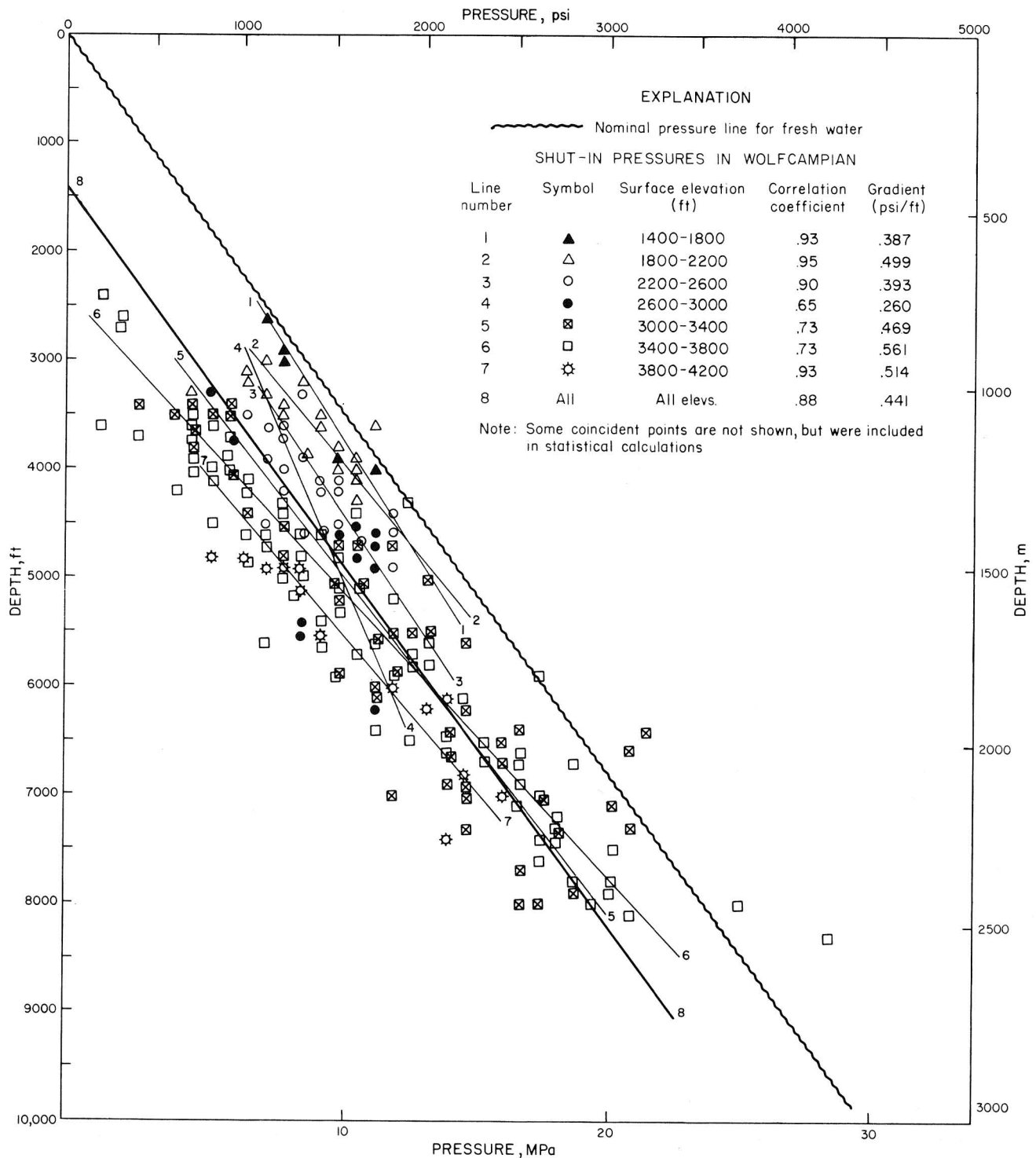
Figure 56. Reported shut-in pressure versus depth, Wolfcampian strata, Palo Duro Basin. Hydrostatic gradient of fresh water (0.433 psi/ft) approximates conditions in the shallow Ogallala aquifer, and the "normal" trend of pressure with depth. Pressures recorded in tests with higher wellhead elevations are further left of the "normal" line. Pressure versus depth gradients do not increase at shallow wellhead elevations; therefore, no apparent upward-directed component of flow is associated with the break in topography at the caprock (at about 3,000 ft above sea level).

100
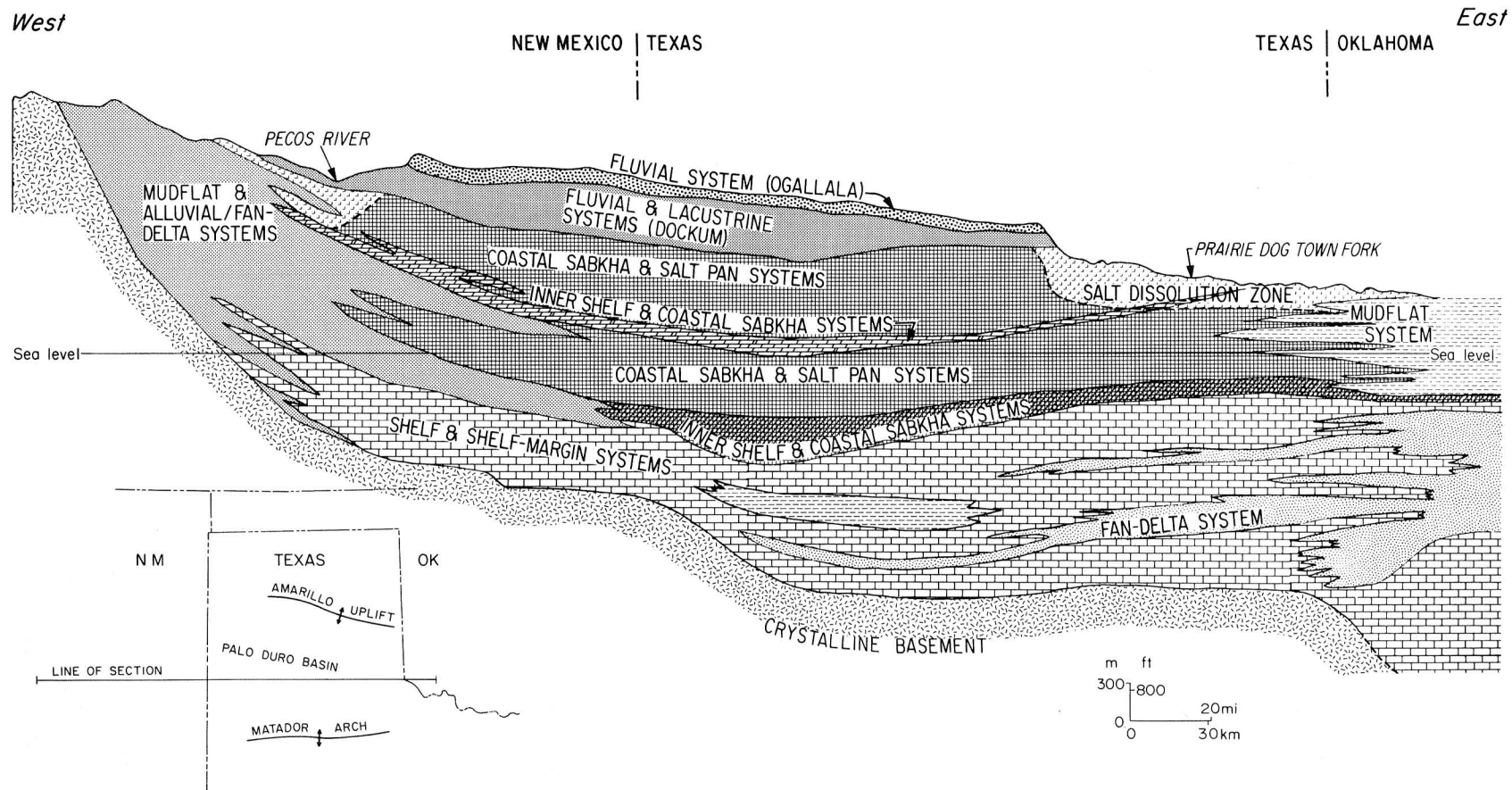
Figure 57. Regional east-west cross section illustrating spatial relationships of the major depositional systems in the Palo Duro Basin.

# REGIONAL GROUND-WATER FLOW IN THE PANHANDLE OF TEXAS: A CONCEPTUAL MODEL

R. L. Bassett, M. E. Bentley, and W. W. Simpkins

*Existing data have been assembled for construction of a preliminary model for regional ground-water flow in the Palo Duro Basin of the Texas Panhandle. An understanding of directions and magnitudes of fluid movement is necessary in evaluating the long-term safety of potential repository sites.*

A model of ground-water flow in the Panhandle of Texas describes the nature of the regional hydrologic environment that would surround any proposed nuclear waste repository site. The basinwide permeability distribution is nonhomogeneous and anisotropic: hydraulic properties are regionally applicable more to genetic depositional packages rather than to time-stratigraphic units. The east-west vertical section shown in figure 57 illustrates the extent of the major depositional units within the region.

In any ground-water regime, the flow system is defined by the potential field, the geometry or shape of the region, its boundary conditions, and the distribution of inhomogeneities within the system. In vertical cross section, the flow system is bounded by the land surface with a water table that essentially follows topography, and by basement rocks, which are assumed to be impermeable. The flow system is considered to be currently under steady-state conditions.

Shallow unconfined aquifers in this region have been used for agricultural, industrial, and domestic purposes for decades, and published information on the characteristics of these aquifers is readily available. Using these data, a head map has been constructed of the unconfined aquifers that overlie the Palo Duro Basin (fig. 58). In the Ogallala Formation, ground-water flow and surface drainage follow eastward-sloping topography. Ground water in the Permian aquifers in the Rolling Plains east of the Ogallala ranges from unconfined to locally confined and circulates deep enough to dissolve evaporites and then discharge into either the Red River or the Brazos River drainage basin. In New Mexico, the shallow ground-water flow system also encounters soluble evaporite facies, then converges toward the Pecos River.

The lithostratigraphy of the deep-basin system has been mapped in other studies (Dutton and others, 1979; Gustavson and others, 1980c). Preliminary values of permeability have been assigned to geologic units on the basis of limited analysis of drill-stem tests and lab tests performed for petroleum companies (table 6).

Preliminary values of assumed average permeability of the major regional hydrologic units are summarized in table 7. No measurements are available for sabkha deposits; the listed permeability represents a suggested generic value for shale (Geotechnical Engineers, Inc., 1978). Unfractured salt (and anhydrite) may have essentially zero permeability at depth (Geotechnical Engineers, Inc., 1978). Fractures may locally increase bulk permeabilities. The listed values were used to construct the conceptual flow lines shown in figure 59. Flow lines approximate only the east-west component of flow; actual flow in many cases is at an acute angle to the section shown. The flow pattern is based on known potential distributions; however, equipotential lines were not included because of the vertical exaggeration of the diagram.

The following are conclusions reached to date by the investigation: (1) Flow is governed primarily by the regional topography and the heterogeneous distribution of permeability associated with multiple genetic depositional units; local topographic influences do not extend below the shallow aquifers where thick evaporites are present. (2) Potential exists for downward movement through the evaporite section, which is the proposed repository host media; however, the fluid velocities even along fractures may be extremely slow. (3) Steady eastward decline of potentials in deep brine aquifers indicates that regional hydraulic continuity may exist from outcropping recharge areas to discharge areas. (4) Discharge points are difficult to discern, and the emergence of deep-basin flow is chemically and quantitatively imperceptible.

A mathematical model is being constructed to generate equipotential and flow lines for the basin. The model is constructed using known boundary conditions and permeabilities, and then it is calibrated with existing head data and used to predict the effects of stress on the system. A finite element solution technique has been chosen to reduce the number of nodal points and to reproduce more accurately the depositional geometry.

The conceptual model indicates the direction of fluid movement and the potential pathways for transport of nuclides away from a repository located in the Permian evaporites; the mathematical digital model is being constructed to quantify the fluid transport and to predict solute transport.
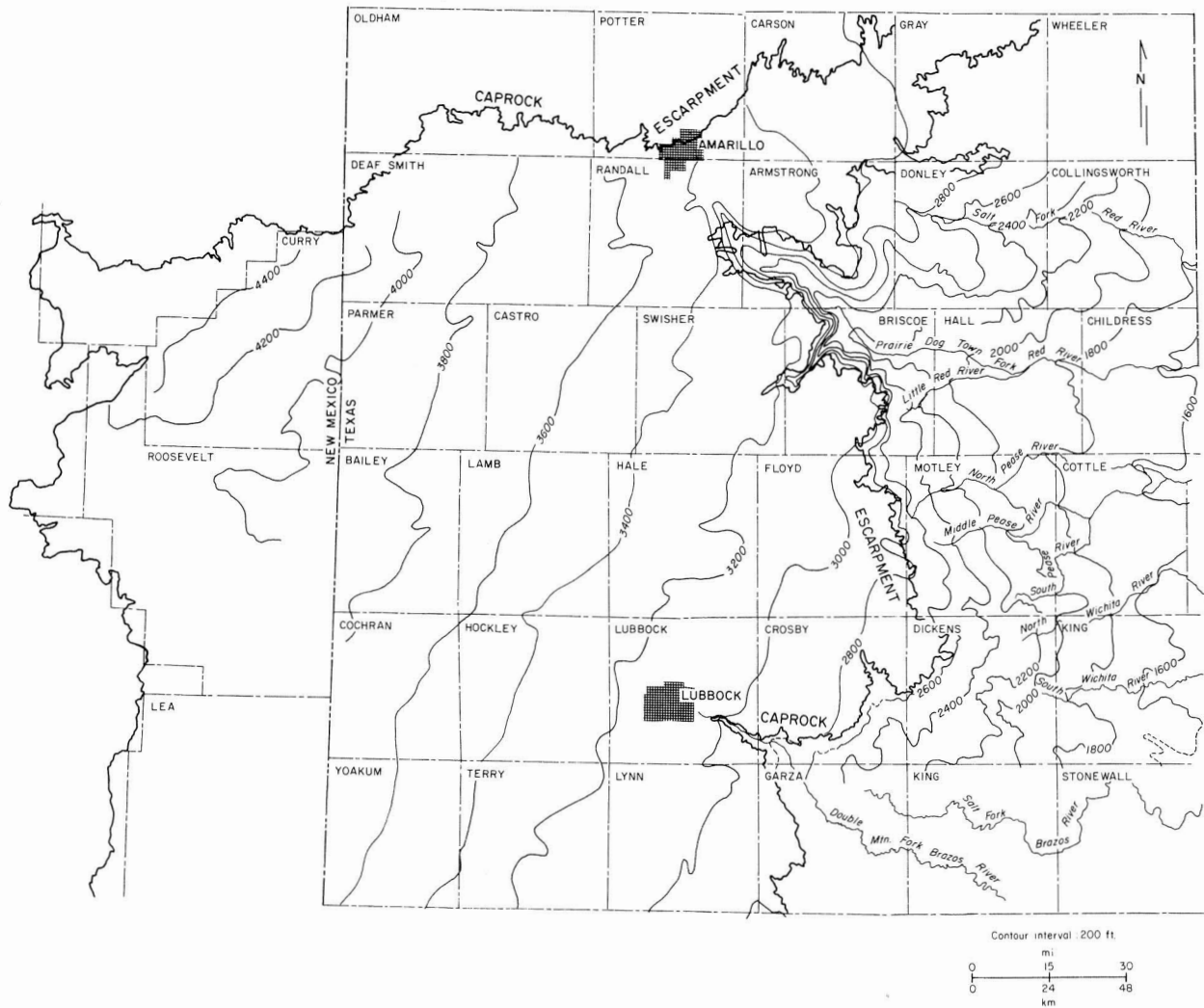
Figure 58. Head map of the unconfined aquifers that overlie the evaporite sequences in the Palo Duro Basin.

West

East

NEW MEXICO | TEXAS

TEXAS | OKLAHOMA

PECOS RIVER

$K=10^8$

$K=10^6$

$K=10^6$

$K=10^6$

SPRING DISCHARGE

PRAIRIE DOG TOWN FORK

$K=10^6$

$K=10^3$

Sea level

Sea level

$K=1$

$K=10^6$

$K=1$

$K=10^4$

NM

TEXAS

OK

AMARILLO UPLIFT

PALO DURO BASIN

LINE OF SECTION

MATADOR ARCH

CRYSTALLINE BASEMENT

m ft

300  800

0

20mi

0

30km
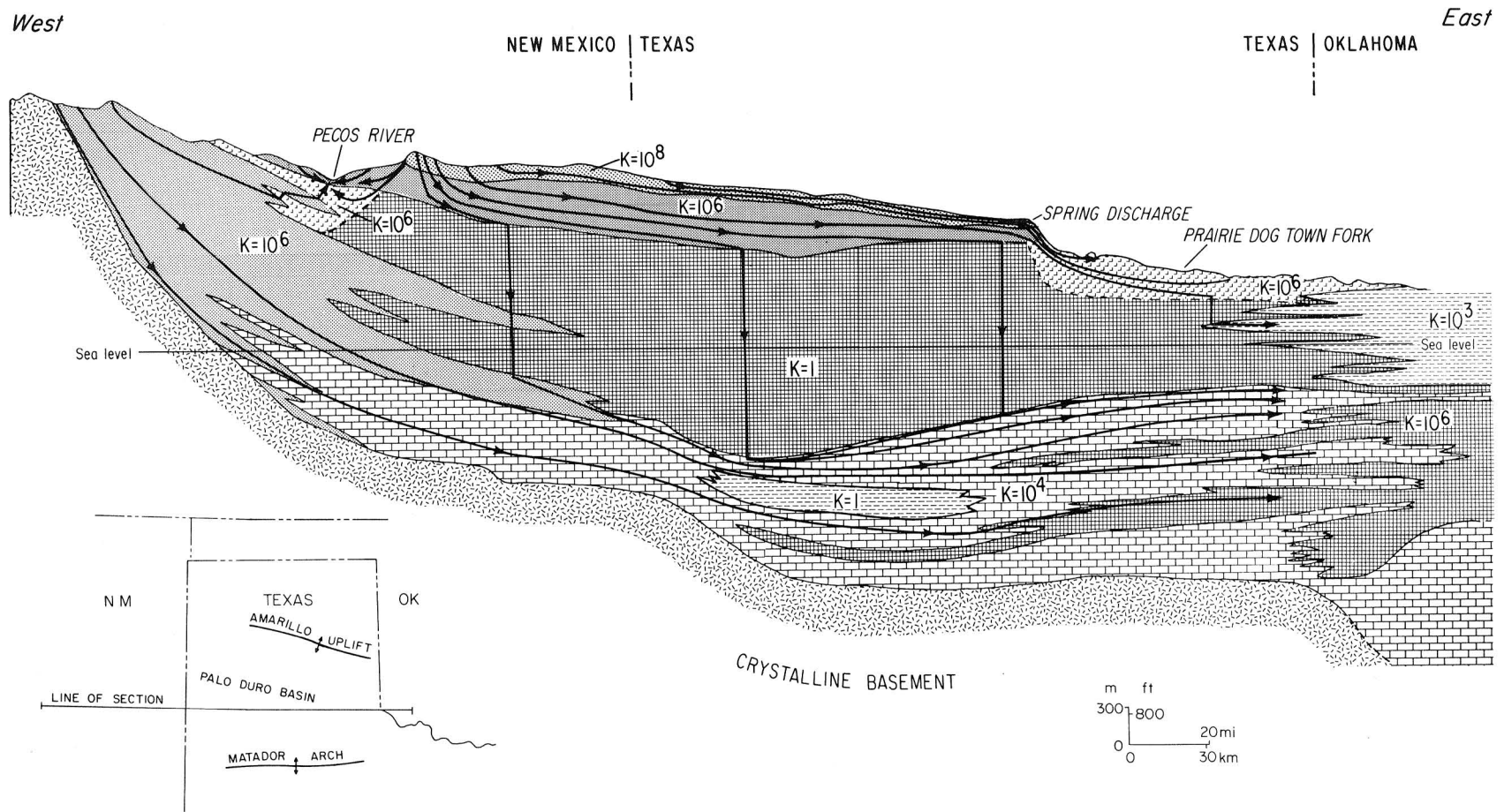
Figure 59. Conceptualized flow lines through the major hydrologic units, based on computed potentiometric surfaces and average permeabilities for genetic depositional units (see fig. 57 for unit descriptions).

Table 6. Preliminary summary of deep-basin permeability measurements.

| Age | Lithology | Location | Depth (ft) | Method | No. of Analyses | Analyst or Source | Permeability (mD) | Remarks |
|---|---|---|---|---|---|---|---|---|
| Lower Permian (Wolfcampian) | Dolomite | Oldham Co. | 5,340 | DST | 1 | TBEG | 0.9 | |
| | Dolomite | Panhandle Field | 3,000± | Various | 6 | TRC | to 25 | Reported to TRC by operators |
| Pennsylvanian | Arkosic sandstone | Panhandle Field | 3,002-3,140 | Lab test | 100 | Well operator | to 1,740 | |
| | Arkosic sandstone | Hartley Co. | 6,302 | DST | 1 | PRC | 20.0 | |
| | Limestone | Swisher Co. | 8,287 | DST | 1 | PRC | 2.0 | |
| Mississippian | Dolomite | Parmer Co. | 9,326 | DST | 1 | PRC | 1.3 | |
| Ordovician | Carbonate | Gray Co. | 4,800 | DST | 1 | PRC | 2.0 | |

Sources of Data-- TBEG: Analysis by Texas Bureau of Economic Geology
TRC: Texas Railroad Commission
PRC: Analysis by Petroleum Research Corp., Denver

Table 7. Assumed permeability values for the major hydrologic systems, Texas Panhandle region.

| Hydrologic unit | Hydraulic condition gallons/day/ft$^2$ | Relative permeabilities |
|---|---|---|
| Ogallala fluvial system[1] | 200 | $10^8$ |
| Triassic fluvial/lacustrine system[1] | 20 | $10^6$ |
| Permian (salt dissolution zone)[2] | 2 | $10^6$ |
| Permian sabkha system[3] | $2 \times 10^{-6}$ | 1 |
| Permian mudflat system[4] | .002 | $10^3$ |
| Permian/Pennsylvanian shelf carbonates[5] | .02 | $10^4$ |
| Permian/Pennsylvanian basinal system[3] | $2 \times 10^{-6}$ | 1 |
| Permian/Pennsylvanian fan-delta systems[5] | 2 | $10^6$ |

Sources of data:

1. Various reports of Texas Department of Water Resources.
2. U.S. Geological Survey open-file data.
3. See text.
4. Typical clay-silt (Freeze and Cherry, 1980).

## CLAY MINERALOGY OF THE PALO DURO BASIN EVAPORITE SEQUENCES, RANDALL COUNTY CORE

*R. L. Bassett and D. P. Palmer*

*Clay mineral assemblages within Permian evaporite sequences are dominantly chlorite vermiculite, chlorite smectite, and chlorite-swelling chlorite mixed-layer phases, as well as discrete phases of illite and chlorite. Expanding clay assemblages such as these must be identified early in the research program because of the potential effect on waste repository design.*

Clay mineral assemblages within Permian evaporites in the Palo Duro Basin have been identified by chemical analysis and X-ray diffraction. Samples are from the Randall County core (DOE-Gruy Federal, Rex White no. 1 well), which penetrates the entire evaporite section. Studies of detrital components in bedded salt are timely because the presence of clay minerals may affect engineering design criteria or safety assessment. Clays and colloids retard the transport of solutes by adsorption and ion exchange and, owing to low permeability, restrict the movement of fluids. In contrast, the presence of swelling clays may jeopardize the stability of the repository site.

Identified clay mineral assemblages were combinations of mixed-layer clays, chlorite-swelling chlorite, chlorite vermiculite, and chlorite smectite, as well as discrete phases of illite and chlorite, as discussed below. A correlation of clay mineralogy with depth and a schematic representation of clay behavior determined by X-ray diffraction are shown in figure 60.

(1) *corrensite.* Corrensite is a regularly ordered, chlorite-swelling chlorite originally defined by Lippmann (1954). Chlorite-swelling chlorite is identified by the behavior of its diffraction pattern (fig. 61). The 002 reflection expands from $14.28\text{Å}$ to $15.65\text{Å}$ with glycolation, indicating that a $28\text{Å}$ mixed-layer superlattice expands to $31\text{Å}$. Heated to $400^{\circ}\text{C}$, the clay reverts to a $14.2\text{Å}$, 002 basal spacing. Heating to $600^{\circ}\text{C}$ collapses the lattice only slightly further to the range of $13.9\text{Å}$ to $14.0\text{Å}$. Corrensite is most common in salt pan and mudflat environments and is rarely associated with marginal sabkha anhydrites.

(2) *chlorite-vermiculite.* The behavior of a large number of samples ranges between two end members, corrensite and a randomly to partially ordered swelling chlorite-vermiculite. The diffraction trace for a poorly ordered vermiculite-swelling chlorite (fig. 62) shows a $14\text{Å}$ clay expanding to $15.25\text{Å}$ with glycolation, indicating a $28\text{Å}$ mixed-layer superlattice that expands to $31\text{Å}$. Heating to $400^{\circ}\text{C}$ collapses the mixed layer to a $14\text{Å}$, 002 basal spacing. When heated to $600^{\circ}\text{C}$, the poorly ordered

clay collapses to a basal spacing ranging from 10.8$\overset{o}{A}$ to 12.1$\overset{o}{A}$. This response results from the collapse of vermiculite layers to 10$\overset{o}{A}$ and chlorite-vermiculite layers to 12$\overset{o}{A}$, and suggests that this sample is high in vermiculite interlayers. Samples rich in hydroxide chlorite interlayers would collapse to 12$\overset{o}{A}$ from 13.5$\overset{o}{A}$. Chlorite-vermiculite is associated with clay layers in upper sabkha bedded halite, in chaotic mudstone-halite, and in marginal sabkha anhydrites.

(3) *chlorite-smectite.* Half of the samples studied contain a chlorite-smectite and illite clay mineral assemblage. The upper 240 m (800 ft) of core have a more expansive chlorite-smectite, which is a reflection of a change in source material.

The smectite (probably saponite) containing minor amounts of poorly crystallized chlorite-hydroxyl interlayers expands from 12.7$\overset{o}{A}$ to 16.9$\overset{o}{A}$ when glycolated with ethylene glycol. It reverts to 12.3$\overset{o}{A}$ after heating to 400$^{o}$C and collapses to 10$\overset{o}{A}$ at 600$^{o}$C (fig. 63). The presence of partial hydroxide interlayers probably prevented complete collapse to 10$\overset{o}{A}$ at lower temperatures.

Chlorite-smectite samples below 240 m (800 ft) are uniformly chlorite rich. They have a 002 reflection at 14.0$\overset{o}{A}$ to 14.4$\overset{o}{A}$ (representing a 28$\overset{o}{A}$ superlattice), which expands to 15$\overset{o}{A}$ to 16$\overset{o}{A}$ with glycolation and collapses to 12$\overset{o}{A}$ to 13$\overset{o}{A}$ at 600$^{o}$C (fig. 64). Incomplete collapse is due to more abundant and well-crystallized hydroxide interlayers. Chlorite-smectite is abundant in saline mudflat chaotic mudstone-halite and salt-pan-bedded halite and less common in dry mudflat red beds and marginal sabkha anhydrites.

(4) *chlorite.* Discrete chlorite occurs in minor amounts in most clay samples but is more common in a mixed-layer assemblage. The diffraction trace in figure 65 represents a chlorite and illite assemblage. The chlorite basal spacing has moderate to strong even-order 00$\ell$ peaks and weak to moderate odd-order 00$\ell$ reflections. The diffraction pattern was moderately influenced by iron in the octahedral layer, but not enough to classify the chlorite as Fe-rich. The 060 peak at 1.54$\overset{o}{A}$ gave a $b_o$ parameter of 9.24$\overset{o}{A}$, corresponding to 0.8 $Fe^{2+}$ in a unit octahedral layer (Shirozu, 1958). The 14.24$\overset{o}{A}$ basal spacing yields a c-dimension, suggesting 1.1 $Al^{3+}$ in a unit tetrahedral layer (Brindley, 1961). This sample has an Fe/Al ratio diagnostic of clinochlore (Hey, 1954).

All chlorite samples were similarly examined and found to be generally Mg rich, with low to moderate iron (0.27 to 0.97 $Fe^{2+}$) substitution in octahedral sites, and moderate aluminum (0.8 to 1.72 $Al^{3+}$) substitution in the tetrahedral layer (fig. 66). These results define a continuum between penninite and an Fe-rich grochauite. The presence of magnesium chlorites is consistent with the associated magnesium-rich minerals already identified.

109

(5) *illite.* Well-crystallized dioctahedral illite is ubiquitous throughout the core. Illite is represented on each diffraction trace by its $10.0\mathring{A}$ to $5.0\mathring{A}$ to $3.3\mathring{A}$ basal spacing sequence. This sequence showed no change with glycolation or heating. The 060 reflection at $1.50\mathring{A}$ confirmed that the illite is dioctahedral (Grim, 1968). The percentage of illite in the total clay fraction increases noticeably with depth.

The mineral suites within the evaporite deposits reflect the reactive nature of the hypersaline brines. Many detrital clay phases become unstable in the brine environment and diagenetically alter to magnesium-rich, mixed-layer clays. The suspected location of the selected samples in the sabkha environment is illustrated in figure 67. In most cases and certainly in the Palo Duro Basin, the combination of depositional environment and source lithology contributes to the formation of the clay mineral assemblages within the evaporite sequences.

The effects of expanding clays in potential host rock should be evaluated early enough in the waste isolation studies to ensure proper design of repository facilities. Permian evaporite sequences sampled from the Randall County core definitely contain expanding clays. The lateral persistence of these clay assemblages will be investigated as additional core material becomes available.
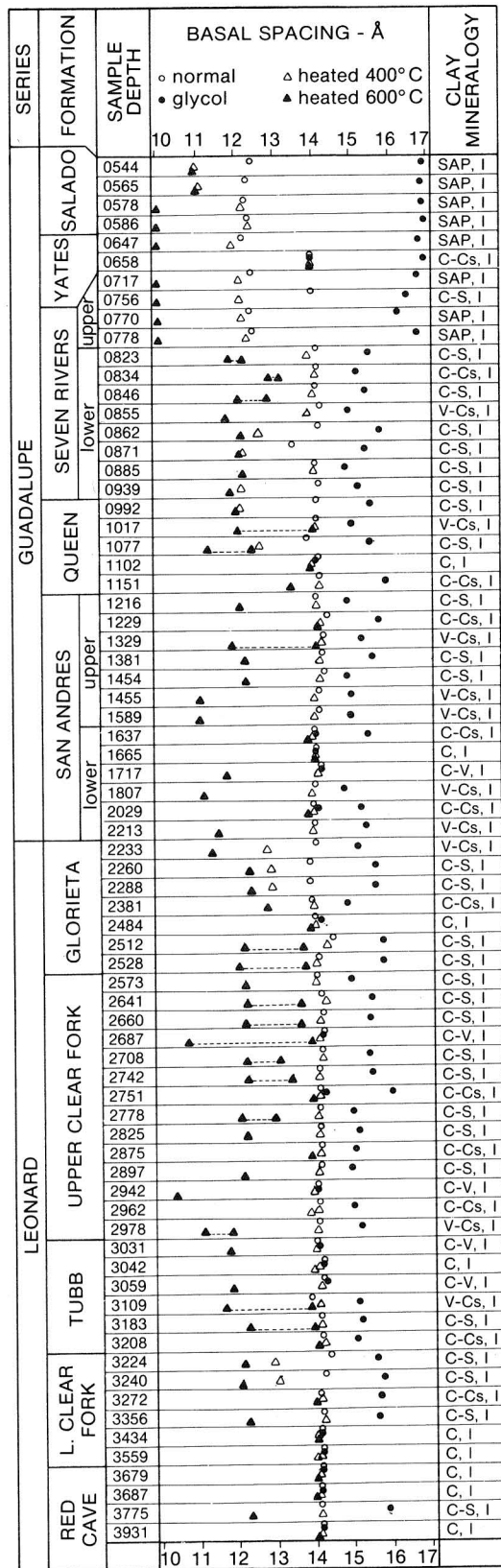
Figure 60. Depth profile of expanding and collapsing nature of clay minerals in Randall County core. Clay minerals illustrated are saponite (SAP), illite (I), corrensite (C-C$_s$), vermiculite chlorite mixed-layer (V-C$_s$), and chlorite smectite mixed-layer (C-S).

111
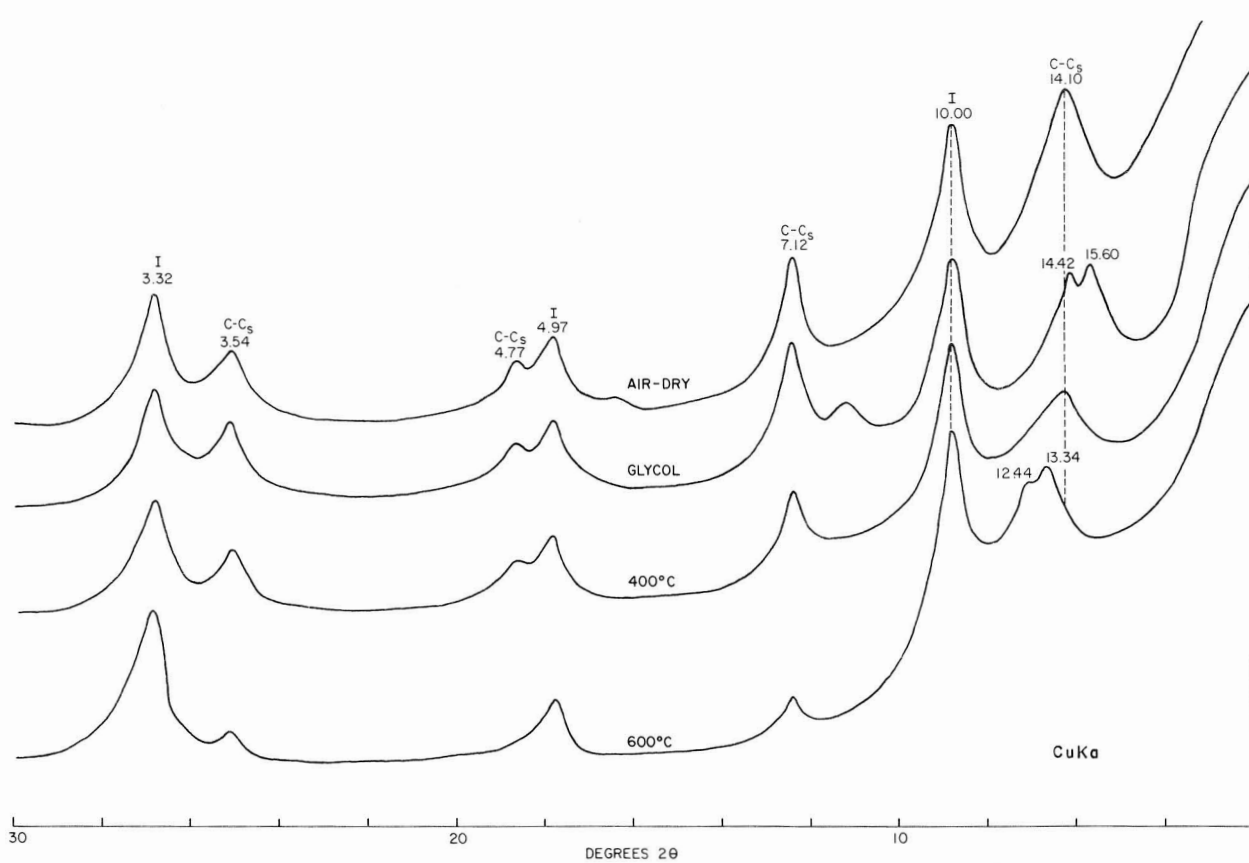
Figure 61. Typical X-ray diffractometer traces illustrating the slight expanding nature, having no noticeable collapse, of the chlorite-swelling chlorite (C-C$_s$), or corrensite, found in numerous locations in the Permian evaporite sequences. Samples were collected from the Randall County core (DOE-Gruy Federal, Rex White no. 1). Illite (I) is also present in the <2 μ clay fraction; the sample is from a depth of 982 m (3,272 ft).

112
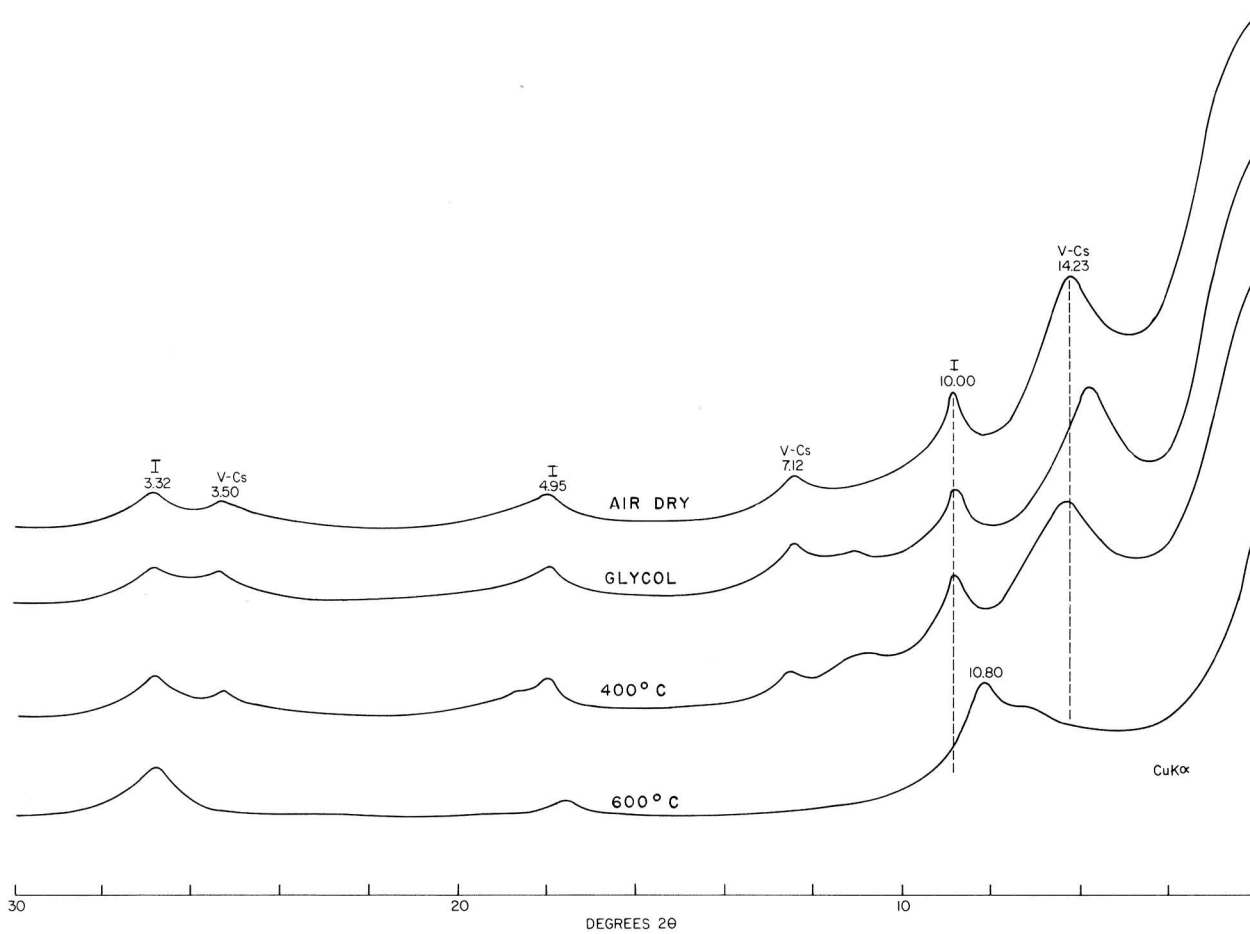
Figure 62. Typical X-ray diffractometer traces illustrating the expanding and collapsing nature of vermiculite-swelling chlorite (V-C$_s$) mixed-layer clays found at a number of depths throughout the Permian evaporite sequence. Samples were collected from the Randall County core (DOE-Gruy Federal, Rex White no. 1). Illite (I) is also present in the <2 μ fraction; this sample is from a depth of 437 m (1,455 ft).
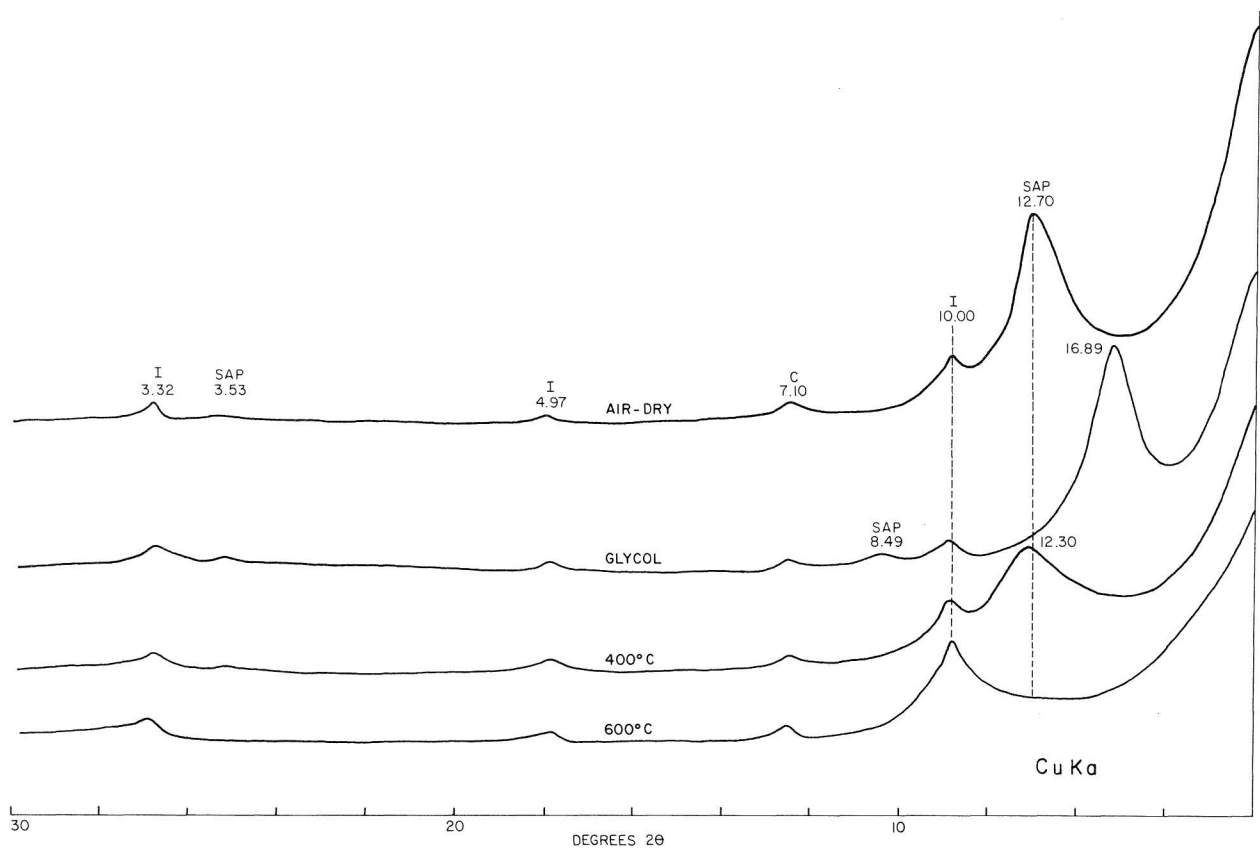
Figure 63.    Typical X-ray diffractometer traces illustrating the expanding and collapsing nature of saponite (SAP) clays found in the upper Seven Rivers, Yates, and Salado Formations of late Guadalupian age.  Samples were collected from the Randall County core (DOE-Gruy Federal, Rex White no. 1).  Illite (I) is also present in the <2 μ clay fraction; sample is from a depth of 233 m (778 ft).

114
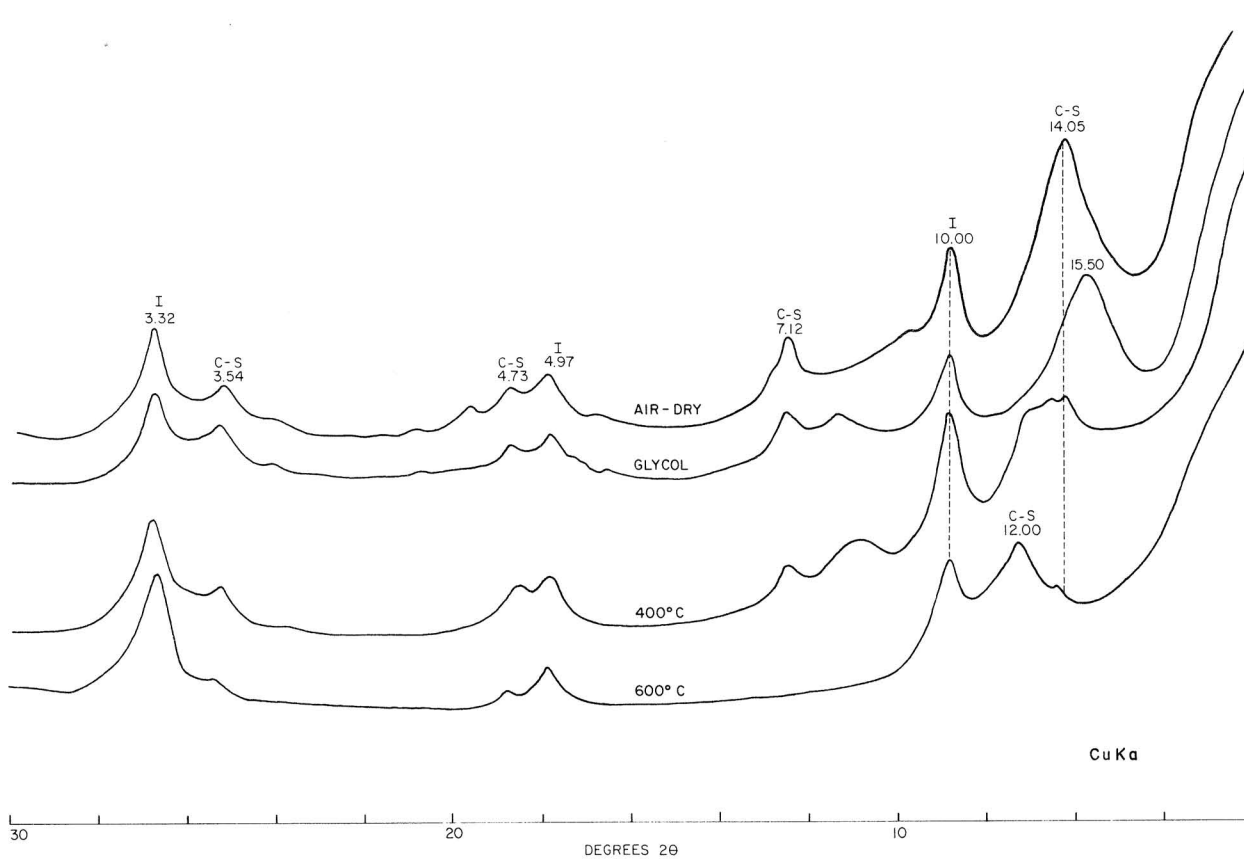
Figure 64.    Typical X-ray diffractometer traces illustrating the expanding and collapsing nature of chlorite smectite mixed-layer clays found at depth below 240 m (800 ft) in the Permian evaporite sequence.  Samples were collected from the Randall County core (DOE-Gruy Federal, Rex White no. 1).  Illite (I) is also present in the <2 μ fraction; sample is from a depth of 414 m (1,381 ft).
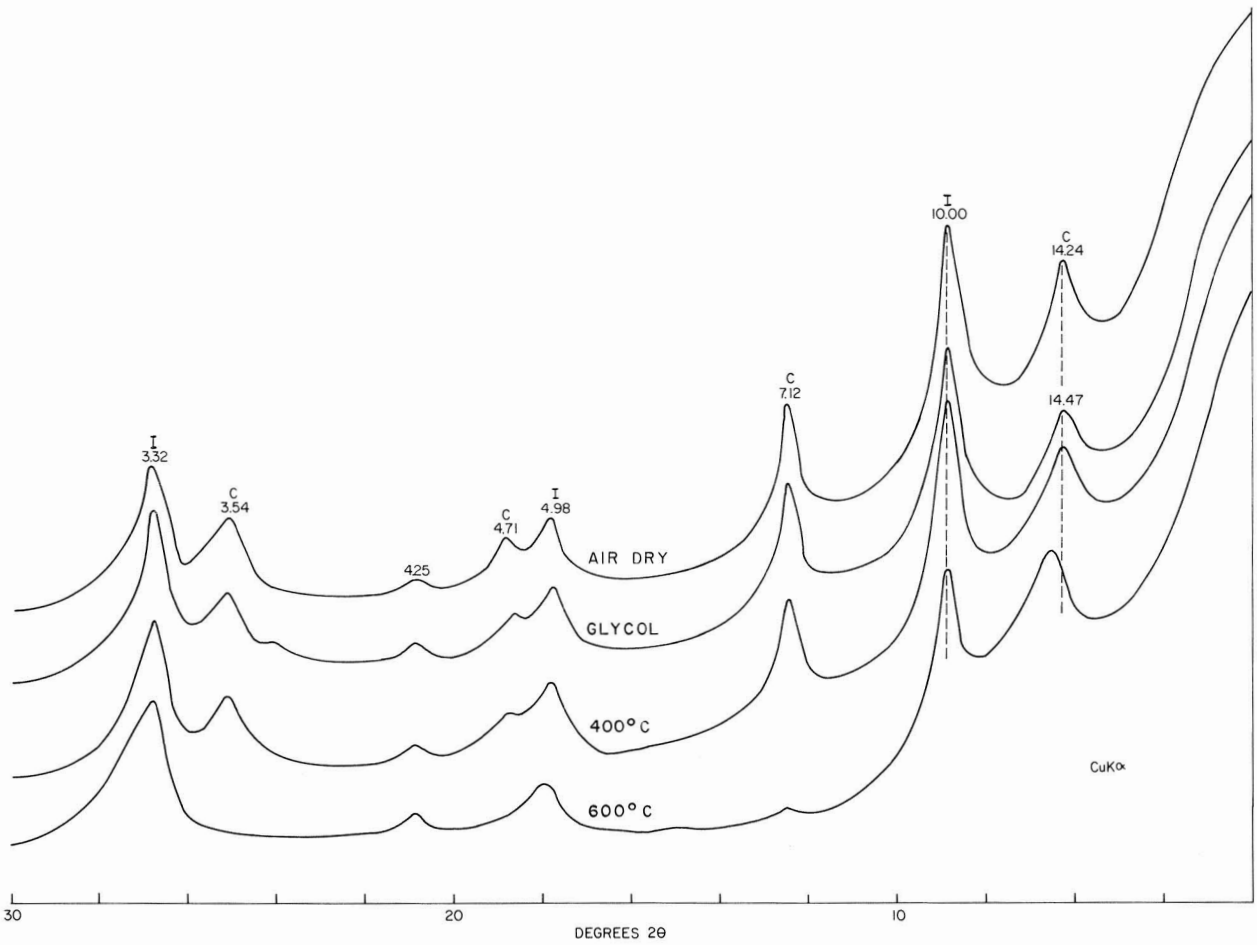
Figure 65. Typical X-ray diffractometer traces illustrating the nonexpanding or collapsing nature of discrete chlorite and illite clays found at many depths throughout the Permian evaporite sequence. Samples were collected from the Randall County core (DOE-Gruy Federal, Rex White no. 1). Sample is from a depth of 745 m (2,484 ft).
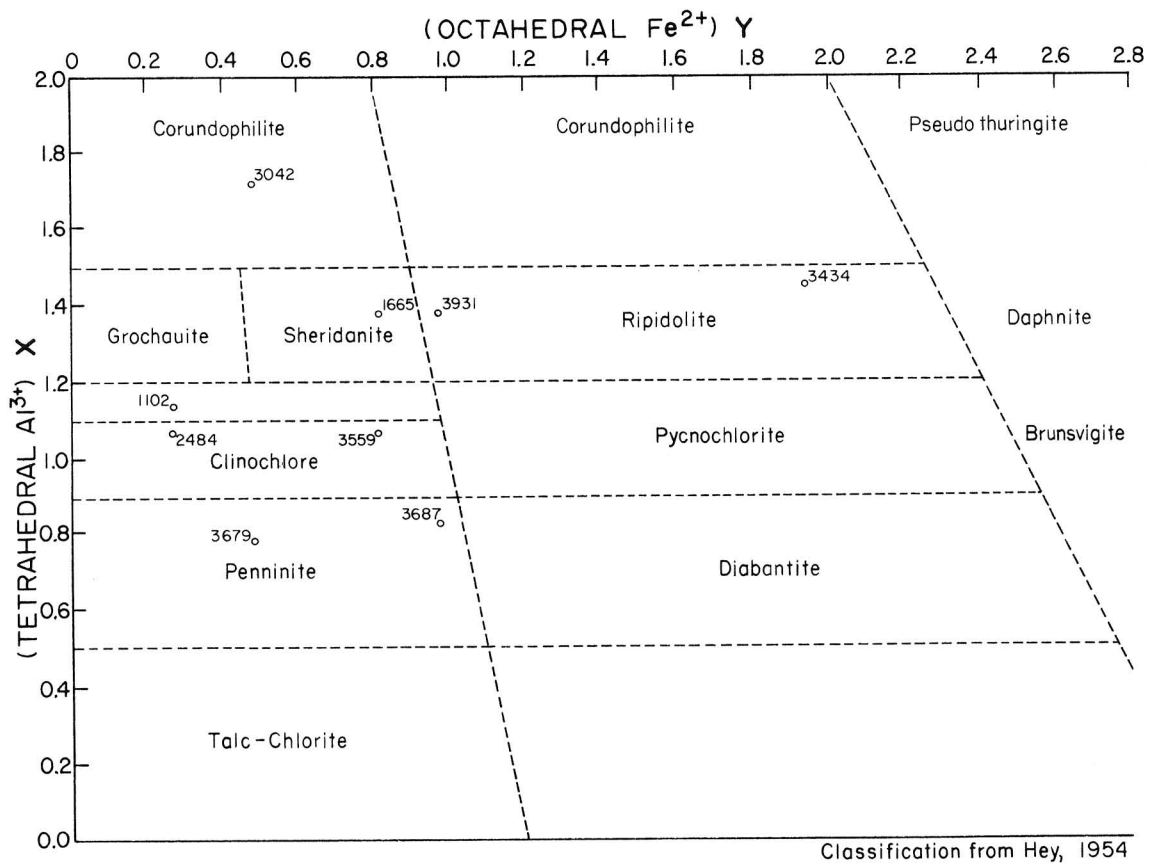
Figure 66. Classification of chlorites on the basis of iron and aluminum content, after Hey (1954). Samples collected from the Palo Duro Basin have been located in this scheme on the basis of X-ray diffraction analysis.

117

| DEPOSITIONAL ENVIRONMENT / CLAY MINERALOGY | INNER SABKHA | | | MARGINAL SABKHA | NUMBER OF SAMPLES |
| --- | --- | --- | --- | --- | --- |
| | DRY MUDFLAT | SALINE MUDFLAT | SALT PAN | | |
| SAPONITE | | | | | 9 |
| CHLORITE-SMECTITE | | | | | 28 |
| CHLORITE-VERMICULITE | | | | | 15 |
| CHLORITE - SWELLING CHLORITE | | | | | 12 |
| CHLORITE | | | | | 8 |
| NUMBER OF SAMPLES | 16 | 30 | 15 | 11 | 72 |
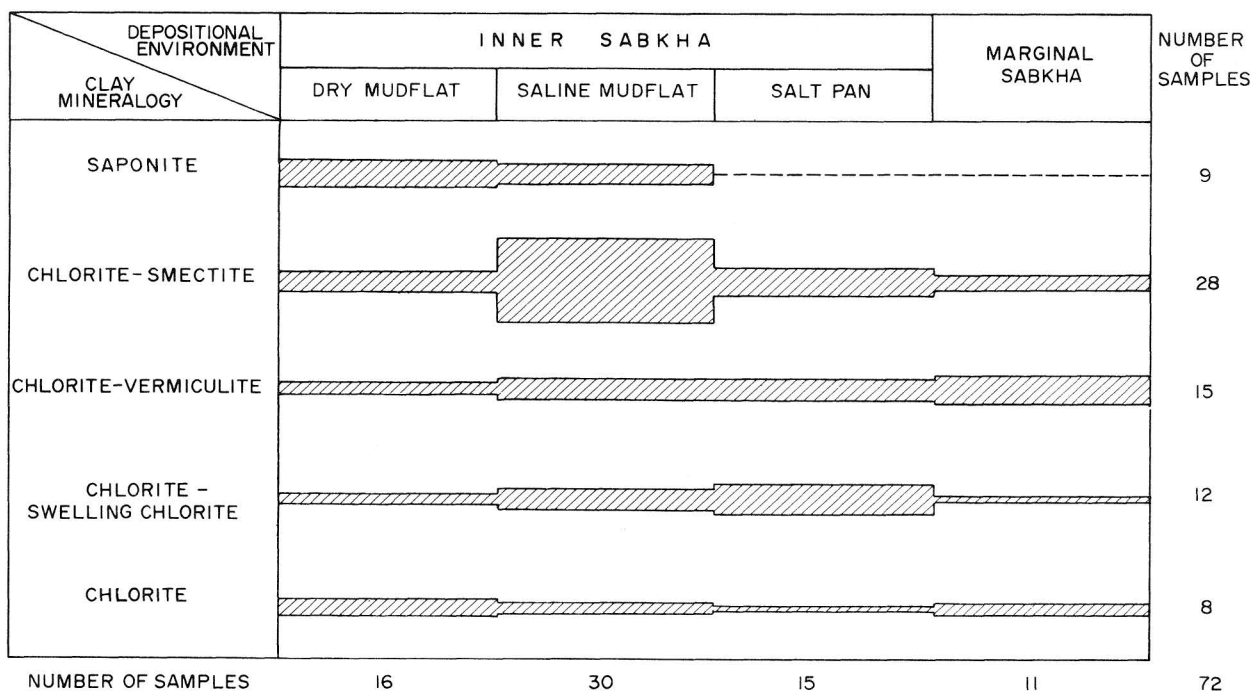
Figure 67. Relative abundance of clay minerals in each subenvironment of the sabkha depositional system, on the basis of analyses of 72 samples from Randall County core.

118

# WATER CONTENT IN PALO DURO SALT, RANDALL AND SWISHER COUNTY CORES

R. L. Bassett and E. Roedder[1]

*Preliminary values of water content in Palo Duro salt have been obtained by two analytical methods. Free water ranges from 0.15 to 2.16 weight percent. Water trapped in evaporite minerals affects their structural properties and may become mobile when placed in a thermal gradient. Inconsistencies in published values reflect a misunderstanding of the exact nature of water in salt.*

The in situ water content of bedded salt and the exact nature of its occurrence are important in several aspects of the design and operation of nuclear waste storage facilities within the salt. The presence of water, particularly at elevated temperatures, lowers the physical strength of salt and greatly increases the corrosion rate of most of the suggested common waste-canister materials. Thus, determinations of the water contents of salt samples are needed early in the site evaluation and selection process.

Determinations have been made by a variety of physical and chemical methods. However, most determinations of water in salt are not truly comparable and reflect serious or systematic errors, generally on the low side. These problems arise from a combination of the multiple sources of water in the samples and the sampling, sample preparation, and analytical techniques used.

The *total* water present in a given small sample can be determined by various existing chemical methods. Such determinations may be highly precise and may yield accurate results but are subject to two major shortcomings: (1) their validity is seriously limited by the difficulty in obtaining a truly representative sample and by the changes in this sample during sample preparation; and (2) even if the sampling and analysis are both correct, an analysis for total water alone may not be very useful. Water may be present in salt in a variety of forms, and each form may behave differently: (1) as *hydrous minerals* (clays, hydrated salts, etc.), (2) as *intergranular pore fillings*, and (3) as *intragranular fluid inclusions*.

The amount of water present in hydrous minerals can be calculated fairly accurately from mineralogical data. The result can sometimes be verified by thermogravimetric analysis (TGA) or differential thermal analysis (DTA) on the bulk

---

[1]U.S. Geological Survey, Reston, Virginia.

sample, but water from both opened and unopened fluid inclusions in the sample can make this verification ambiguous.

*Intergranular water* includes water in pores having a wide range of sizes, from microinclusions on grain boundaries to brine pockets having volumes of many cubic meters; its distribution is extremely erratic. Microinclusions on grain boundaries are still present when cores are pulled from the core barrel, but their rapid loss is plainly indicated by the white efflorescences that commonly form, outlining grain boundaries, on core that has been exposed to air. The resultant water loss is small, however, compared with that from the larger pores ( $\sim$1 cm, 0.4 inch) that are evident as cavities on some core surfaces.

*Intragranular water* in fluid inclusions presents a similar sampling problem, in that a few large inclusions can be equal in volume to millions of small ones. Furthermore, the distribution of such inclusions is extremely erratic, even in adjacent 1-cm (0.4-inch) thick slabs cut perpendicular to bedding surfaces. Simple heating has been used to determine intragranular water. The heating of larger samples for weight loss (or recovery of evolved water) may help to minimize this sampling problem, but it will generally give low values for several reasons. For example, some fluid inclusions in salt decrepitate at low temperatures. If, however, the heating rate is sufficiently low, the inclusions may stay sealed and simply cause the host salt to expand by plastic deformation without release of the water, even if the salt contains 1 percent inclusion water and is heated to $250^{\circ}$C.

Several analyses were carried out to determine water content in salt samples taken from the Randall County core (DOE-Gruy Federal, Rex White no. 1 well) and the Swisher County core (DOE-Gruy Federal, D. M. Grabbe no. 1 well). The samples were analyzed at two laboratories selected by the Office of Nuclear Waste Isolation: the Oak Ridge National Lab (ORNL) and a U.S. Geological Survey (USGS) lab operated by R. J. Hite. These data were intended as preliminary and are presented here to illustrate the difficulties encountered (table 8). The Bureau of Economic Geology is currently investigating the analytical schemes required to measure accurately the water content in salt; results will be available in FY81.

The water mass determined with the Karl-Fischer method is that which is adsorbed on mineral surfaces or trapped as molecular water within the crystal. Water lost in heating includes much of the molecular water but also includes waters of hydration and hydroxyl water within the structure of associated clay minerals and oxy-hydroxides. The problem is compounded if the heating ceases below the melting point of salt and leaves trapped molecular water in fluid inclusions which was not released under those conditions.

In six of the eight samples analyzed by ORNL, the water content measured by heating was substantially greater than that determined by titration. This certainly reflects the contribution from structural water in associated minerals. Because of the extremely small sample size (1 to 2 g) used by ORNL, the values from the heating (150°C) and the values from the titration are similar in several cases. A larger sample of coarser material would have contained more of the larger inclusions, which were preselected against, in the crushing process. These larger inclusions would have been virtually unaffected by this low-temperature heating and thus not measured by weight-loss methods, probably resulting in a larger error.

Comparison between the two values obtained by Karl-Fischer titration is also difficult, primarily because the samples (1 to 2 g for ORNL and >1 kg for USGS) greatly differ in weight and are from different parts of the core section. In three out of six cases, the larger samples contain nearly twice the percent of free water measured for the small samples. In the upper San Andres sample (Swisher core) and the upper Seven Rivers sample (Randall core), the values are similar, and in the upper Clear Fork sample the difference is anomalous. A variable percentage of insoluble material makes comparison between samples difficult.

The investigation currently underway will include optical evaluation of water content to correct for the effect of insoluble phases as well as provide an independent estimate of free water in fluid inclusions. The results will then be directly compared to Karl-Fischer and heat-treatment analytical schemes.

An accurate quantification of moisture content in salt is required to (1) evaluate properly the structural properties of salt and (2) design thermal and permeability environments around the waste that protect it from invasion by brines derived from fluid inclusions.

Table 8. Preliminary values of water content as weight percent in samples of bedded salt from Palo Duro Basin core material. Analyses were performed by Oak Ridge National Lab staff (ORNL) and by R. J. Hite of the U.S. Geological Survey (USGS).

| Formation | Sample depth (ft) | KF[a] (USGS) | Insolubles[b] (USGS) | KF[c] (ORNL) | Insolubles[b] (ORNL) | 150°C[d] (ORNL) | 650°C[e] (ORNL) |
|---|---|---|---|---|---|---|---|
| Randall County | | | | | | | |
| U. Seven Rivers | 741 | 1.822 | 60.0 | 2.16 | 11.37 | 2.27 | 3.56 |
| U. San Andres | 1,400 | 0.513 | 3.2 | 0.28 | 0.93 | 0.12 | 0.48 |
| L. San Andres | 1,847 | 0.265 | 2.0 | 0.15 | 0.51 | 0.30 | 0.76 |
| L. San Andres | 2,143 | -- | -- | 0.39 | 3.24 | 0.09 | 0.55 |
| U. Clear Fork | 2,603 | 1.229 | 34.0 | 1.23 | 32.66 | 1.03 | 3.33 |
| Swisher County | | | | | | | |
| U. Seven Rivers | 1,265 | -- | -- | 1.76 | 9.82 | 1.62 | 6.07 |
| U. San Andres | 1,955 | 0.322 | 5.6 | 0.43 | 1.61 | 0.10 | 0.18 |
| L. San Andres | 2,525 | 0.625 | 4.5 | 0.34 | 1.67 | 0.13 | 0.32 |

a. Karl-Fischer titration on >1 kg of intact core material (average of duplicate analyses).
b. Water-insoluble material in the sample as weight percent.
c. Karl-Fischer titration on 1 to 2 g of crushed material (average of duplicate analyses).
d. Heating of 1 g of material for 1 hour at 150°C.
e. Heating of 1 g of material for 1 hour at 650°C (average of duplicate analyses).

122

# AQ/SALT: A MATHEMATICAL MODEL FOR COMPUTING THE REACTION POTENTIAL OF BRINES

*R. L. Bassett and J. A. Griffin*

*Brines that are present or that may be introduced into basins being considered as sites for nuclear waste disposal may be reactive, and this reaction potential must be evaluated. Geochemical models previously available were intended for fluids with low to intermediate ionic strengths. A digital computer model has been written that computes the activities of ions in brines up to saturation with the common evaporite minerals.*

A digital computer model called AQ/SALT has been written to evaluate the potential of a given saline fluid to react with minerals typically found in evaporite sequences. One of the most critical technical concerns in the program to dispose of nuclear waste safely is the problem of protecting the waste from ground-water intrusion. Reactive fluids may produce a breach in the containment material and subsequently transport the nuclides back into the biosphere.

Potentially reactive fluids are present in the Palo Duro Basin in a variety of locations: (1) shallow ground-water systems overlying the evaporites, (2) fluids circulating more deeply around the basin margins, where bedded salt is dissolving, (3) deep-basin brines with regional throughput, particularly in permeable carbonates below the evaporite sequence, and (4) water trapped in the evaporite minerals as intergranular water or intragranular fluid inclusions. Except for the shallow aquifer systems, all these fluids have brine compositions (>35,000 ppm, Winslow and Kister, 1956) that range upward to compositions saturated with halite (>350,000 ppm).

The current version of AQ/SALT will compute the thermodynamic reaction state of a fluid on the basis of its chemical composition. The model will then determine whether a given set of mineral assemblages is unstable and most likely to dissolve in the brine, or whether the solution has the appropriate composition to precipitate mineral phases as it moves through the system. This kind of evaluation is particularly instructive when unraveling diagenetic changes, mixing two or more fluids, or predicting effects along a flow path, such as engineered barriers in waste isolation planning.

During the last decade, a comprehensive theory of interionic potentials of concentrated electrolyte solutions was developed based primarily on semiempirical modifications to the classical Debye-Hückel equation (Pitzer, 1977; Harvie and Weare, 1980). To compute the thermodynamic activity $(a_i)$ of the individual ions, an activity

coefficient ($\gamma_i$) is computed, then multiplied by the initial concentration of each ion in molal units ($m_i$):

$$a_i = \gamma_i m_i \tag{1}$$

The form of the activity coefficient expression is similar to equation (2) with some rearrangement and modification for the effects of mixed and unsymmetrical electrolytes, as well as for computational ease (Pitzer, 1977; Harvie and Weare, 1980):

$$\ln\gamma_{\pm} = -z^2 A_{\phi}[I^{1/2}/(1+bI^{1/2}) + (2/b) \ln (1+bI^{1/2})]$$
$$+ m\{2\beta^{(0)}_{MX} + (2\beta^{(1)}_{MX}/\alpha^2 I)[1-$$
$$(1+\alpha I^{1/2} - \alpha^2 I/2) \exp(-\alpha I^{1/2})]\} + m^2(3C^{\phi}_{MX}/2) \tag{2}$$

$$z = \text{ionic charge}$$
$$A_{\phi} = \text{Debye-Hückel coefficient}$$
$$I = \text{ionic strength}$$
$$b, \beta^{(j)}, \alpha, C^{\phi} = \text{second and third virial coefficients}$$

The ionic activity coefficients are computed for each species, followed by the individual activities according to equations (1) and (2). Subsequently, the activity products ($K_{ap}$) for minerals of interest are computed, then compared with the thermodynamic equilibrium constant ($K_{eq}$) to determine potential reactants, products, and their stability fields.

Previously, one of the most difficult factors affecting the computation of equilibria between brines and hydrous minerals was the determination of the activity of water. As ionic strength increases, much of the unbound water in solution is incorporated into the ionic hydration sheaths. This effectively reduces the activity of free water. In AQ/SALT, the activity of water may be computed from an equation presented by Wood (1975) and is given as equation (3):

$$\ln a_{H_2O} = -0.018 \left[ \sum_i \frac{\nu_i y_i\{I-2.303|z_+ z_-|A\sqrt{I}\}}{3} \sigma(\mathring{a}B\sqrt{I}) + 2.303\frac{\nu_+\nu_-}{\nu} \bar{B}_i I^2 \right] \tag{3}$$

where the function $\sigma(x)$ is defined as

$$\sigma(x) = \left\{(1+x) - 2\ln(1+x) -\frac{1}{(1+x)}\right\} \frac{3}{x^3}$$

In the program, equation (3) is modified according to suggestions made by Bodine and Jones (1980) to facilitate the computation. Water activity may also be computed with an equation presented by Harvie and Weare (1980), which is an option in AQ/SALT.

124

The flow diagram for AQ/SALT is shown in figure 68 and additional discussion is given in the model documentation (Bassett and others, 1980; Bassett and Griffin, in preparation).

Calibration of the model was accomplished by checking the computations against solubility data. A comparison of simulated values and solubility data from published sources for the systems of greatest utility in the Palo Duro Basin is shown in figures 69 and 70.

Preliminary calculations made using available data from the salt dissolution zones and from analyses of oil field brines below the evaporite section illustrate the saturation state of the fluids. Comparison can be made to fresher ground waters in the region and to average composition of seawater (fig. 71). Numerous additional data sets will be available next fiscal year, and a thorough evaluation will be made at that time.

A model such as AQ/SALT may be used to determine potential for dissolution or precipitation of static fluids of known composition or may be used in conjunction with hydrologic data to decipher the flow path, to interpret diagenetic changes, or to predict failure scenarios of nuclear waste storage facilities.

FLOW DIAGRAM FOR AQ/SALT

SUBROUTINE NAMES

| Box | Subroutine Names |
|-----|------------------|
| READ LIBRARIES | RTABLE, RTHETA RPSI, RMINRL RSZDEV, RHARND |
| READ INPUT DATA | RSAMPL |
| COMPUTE EQUATION PARAMETERS | CONV, CCONST, COMPB, CPHI COMPF |
| COMPUTE THE ACTIVITIES & ACT. COEFFICIENTS | CGAMMA |
| PARTITION SALTS | CSALT |
| COMPUTE DEVIATION | CBBAR |
| COMPUTE WATER ACTIVITY | CAH2O |
| COMPUTE MINERAL REACTION POTENTIAL / PRINT MINERAL SATURATION STATES | CSINDX |

Decision: $^oH_2O$ PROVIDED

STOP

PRINT INPUT AND COMPUTED DATA

Figure 68. The computational flow scheme and identification of the subroutines for AQ/SALT.
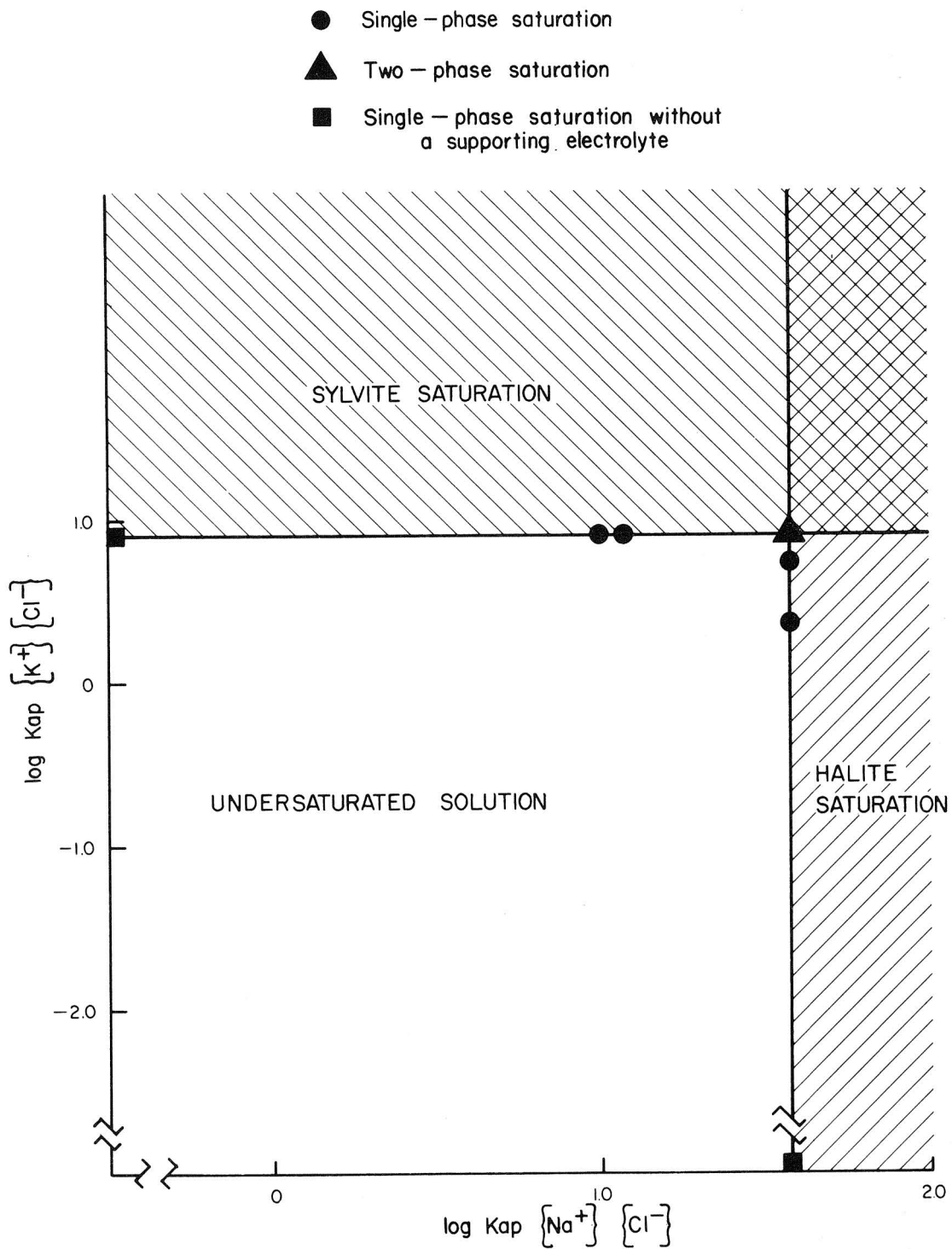
Figure 69. Phase diagram for the KCl-NaCl system, using solubility data from Linke (1958) for the calibration.
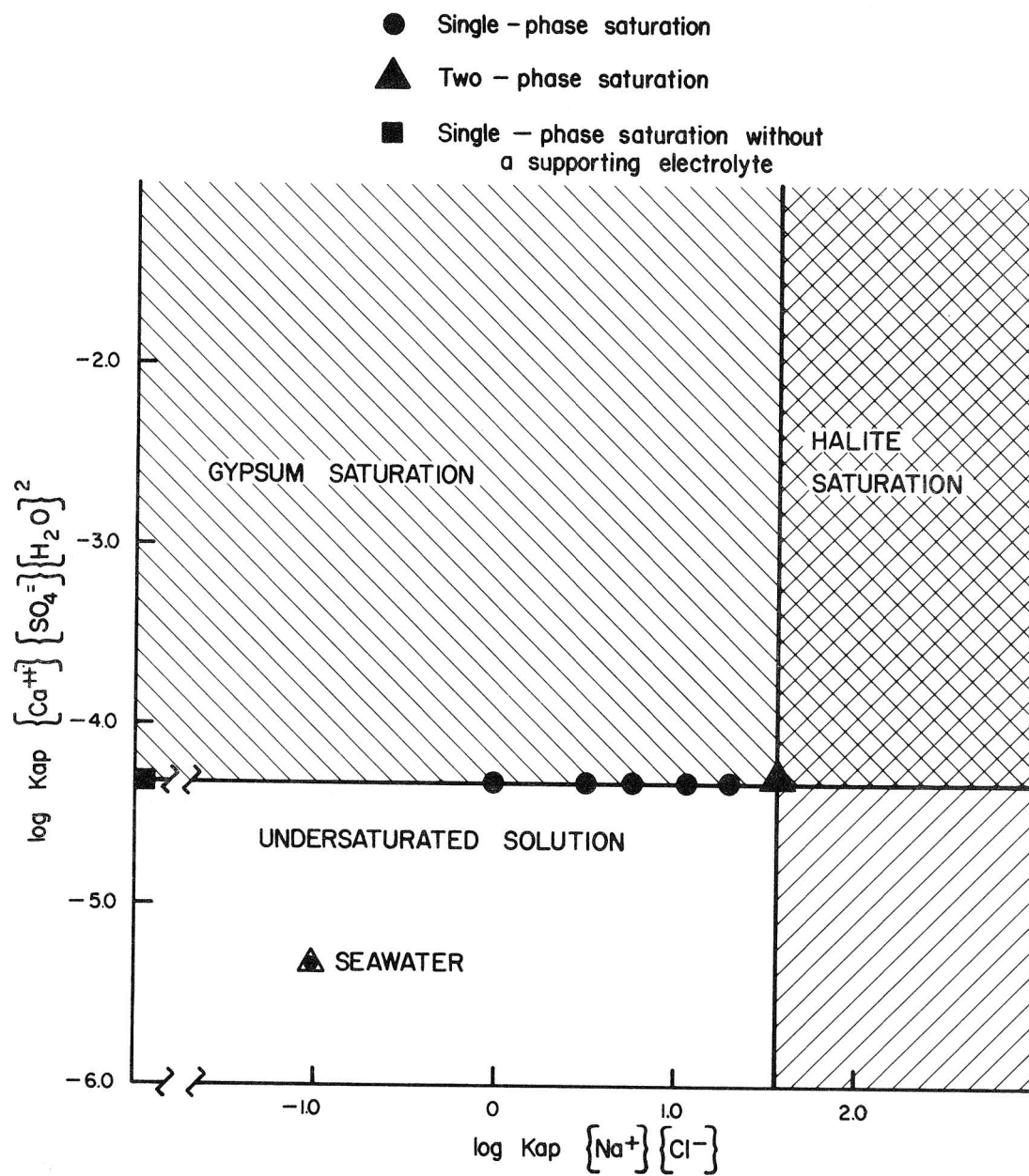
127

Figure 70. Phase diagram for the NaCl-CaSO$_4$ system, using solubility data from Linke (1958) for the calibration.
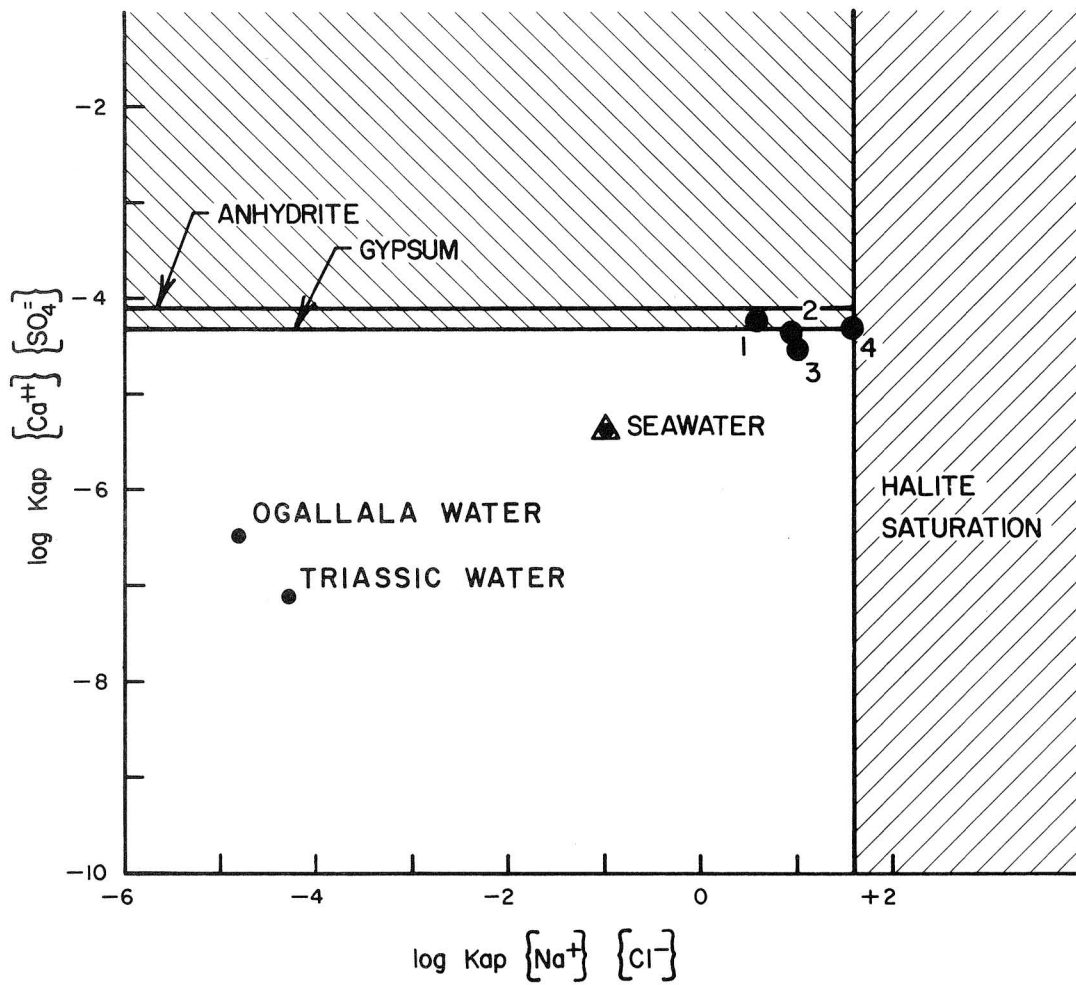
Figure 71. Phase diagram for brines and fresh waters illustrating the saturation state with respect to halite and gypsum.

# SALT DISSOLUTION AND COLLAPSE ALONG THE MARGIN OF THE SOUTHERN HIGH PLAINS

*T. C. Gustavson, A. D. Hoadley, and W. W. Simpkins*

*A wide zone of subsurface salt dissolution borders Permian bedded salts in eastern New Mexico and the Texas Panhandle. The zone of salt dissolution occurs beneath the Pecos River and the Canadian River valleys on the west and north and beneath the Rolling Plains on the east.*

Bedded Permian salts that occur beneath the Texas Panhandle and in eastern New Mexico are truncated at their western, northern, and eastern margins by dissolution. The zones along which truncation has occurred have been mapped in Texas (Dutton and others, 1979; Gustavson and others, 1980b). Construction of additional cross sections has resulted in identification of the limits of subsurface salt units in eastern New Mexico (fig. 72). Grouped on a regional basis, the zones of truncation or dissolution of each salt-bearing unit mark a zone of active salt dissolution.

Salt dissolution zones are identified by (1) abrupt loss of salt sequences between relatively close-spaced wells and abrupt thinning of stratigraphic sequences away from salt-bearing strata, suggesting dissolution rather than facies change, (2) maps of regional facies distribution showing that zones of abrupt salt thinning truncate facies tracts, and indicating that thinning is due to dissolution rather than facies change, and (3) examination of cored intervals through the Seven Rivers and Salado Formations (DOE-Gruy Federal no. 1 Grabbe and no. 1 White wells), revealing that dissolution of the upper parts of these salt beds has occurred. Several feet of red-brown mud overlie the uppermost salt beds penetrated by these wells. The muds are probably an insoluble residue.

Salt dissolution is an active process as indicated by the high solute loads of the Pecos and Canadian Rivers and the streams that drain the eastern part of the Texas Panhandle. Salt seeps, springs, and pans occur along some stream valleys, and areas of high brine discharge occur where streams cross outcrops of the major salt-bearing formations. Furthermore, historical examples of collapses that formed sinkholes, broad undrained depressions, and open fractures have been noted throughout the salt dissolution zone.

*The land surface that overlies the zone of active dissolution of bedded Permian salt in the Texas Panhandle and in eastern New Mexico is undergoing rapid karstification and collapse.*

The geologic structure of eastern Briscoe and Hall Counties is illustrated in a structure cross section that reflects the southwesterly regional dip of strata toward the axis of the Palo Duro Basin (fig. 73). Salt dissolution has occurred to depths of approximately 195 to 275 m (600 to 900 ft). Strata that lie below or to the west of the zone of salt dissolution dip gently to the southwest. Strata that have undergone collapse as a result of salt dissolution no longer conform to the regional structural pattern. Locally, salt dissolution and collapse have reversed regional dip. In western Hall County approximately 80 m (260 ft) of salt are in the lower San Andres Formation in the Lewis Ranch no. 1 well (fig. 73), but east of the well all this salt is missing. No lower San Andres salt remains in the Jonah Creek no. 1 well. The original stratigraphic thickness of the salt-bearing strata has been reduced to approximately 34 m (110 ft); the strata consist of insoluble sandstones and mudstones that were originally interbedded with the salt. This indicates that the surface in the vicinity of the Jonah Creek no. 1 well has probably collapsed approximately 46 m (150 ft).

Active salt dissolution is evidenced by the high solute loads in area streams and the formation of collapse or karst features. The annual average solute load (1969 to 1974) for the Prairie Dog Town Fork of the Red River was $1.0335 \times 10^{6}$ tons dissolved solids, including $4.235 \times 10^{5}$ tons chloride and $1.558 \times 10^{5}$ tons sulfate.

Karst features including sinkholes, shallow undrained depressions, and surface fractures have recently developed within Hall and Briscoe Counties. To determine how fast and where karstification is taking place, the karst features of Hall and eastern Briscoe Counties have been mapped, using low-level aerial photographs taken in several different years, and catalogued.

Over 200 sinkholes were noted, which ranged in size from approximately 1 m (40 inches) wide and 1 m (40 inches) deep to 100 m (330 ft) wide and 30 m (100 ft) deep (fig. 74). Characteristically, these features are circular to oval in plan view and have nearly vertical sides when newly formed. In older sinkholes, the sides are generally degraded; this is especially true if the sinks are water filled. Within a small test area in eastern Hall County, 36 new sinkholes formed between 1940 and 1972 (fig. 75).

Over 200 undrained depressions were also noted in the study area (fig. 74). These features are broad, shallow depressions, which are normally oblong in plan view and can be nearly as long as 3.5 km (2 mi) and as deep as 10 to 15 m (30 to 45 ft). They

differ from sinkholes in that they are substantially larger and are not bounded by sharp inward-facing fault scarps. Two new undrained depressions formed in the test area between 1950 and 1964 (fig. 75). The features are approximately 0.75 km (0.5 mi) long and 0.5 km (0.3 mi) wide. Several of the elongate depressions show preferential alignments in northwestern, northern, and northeastern directions, which are similar to observed fracture alignments and to drainage lineaments in this region (Dutton and others, 1979). Eleven surface fractures were detected in Hall County (fig. 74); all were less than 30 cm (12 inches) wide, and only 4 cm (1.5 inches) of vertical offset was observed across one highway fracture. All fractures were oriented N. 30°E. to N. 60°E.

Areas of active karstification and collapse have been noted throughout the Texas Panhandle and eastern New Mexico region (fig. 76) by the writers and by the staff members of the Texas Department of Highways and Public Transportation, the New Mexico State Highway Department, and the U.S. Department of Agriculture Soil Conservation Service and Agriculture Stabilization and Conservation Service. The geographic extent of the region that is undergoing active collapse conforms to the salt dissolution zones delineated by Dutton and others (1979) (fig. 72).

The major drawback to the use of salt as a medium for the disposal of high-level nuclear waste is the high solubility of salt. The safe storage of nuclear waste in salt requires that the integrity of the repository not be breached by dissolution, which requires examination of evidence of salt dissolution in the Palo Duro Basin. The preliminary conclusion of this research is that a zone of active salt dissolution and surface collapse exists along the western, northern, and eastern margins of the Palo Duro Basin, but that salt dissolution is not currently active beneath most of the Southern High Plains or the central part of the Palo Duro Basin.
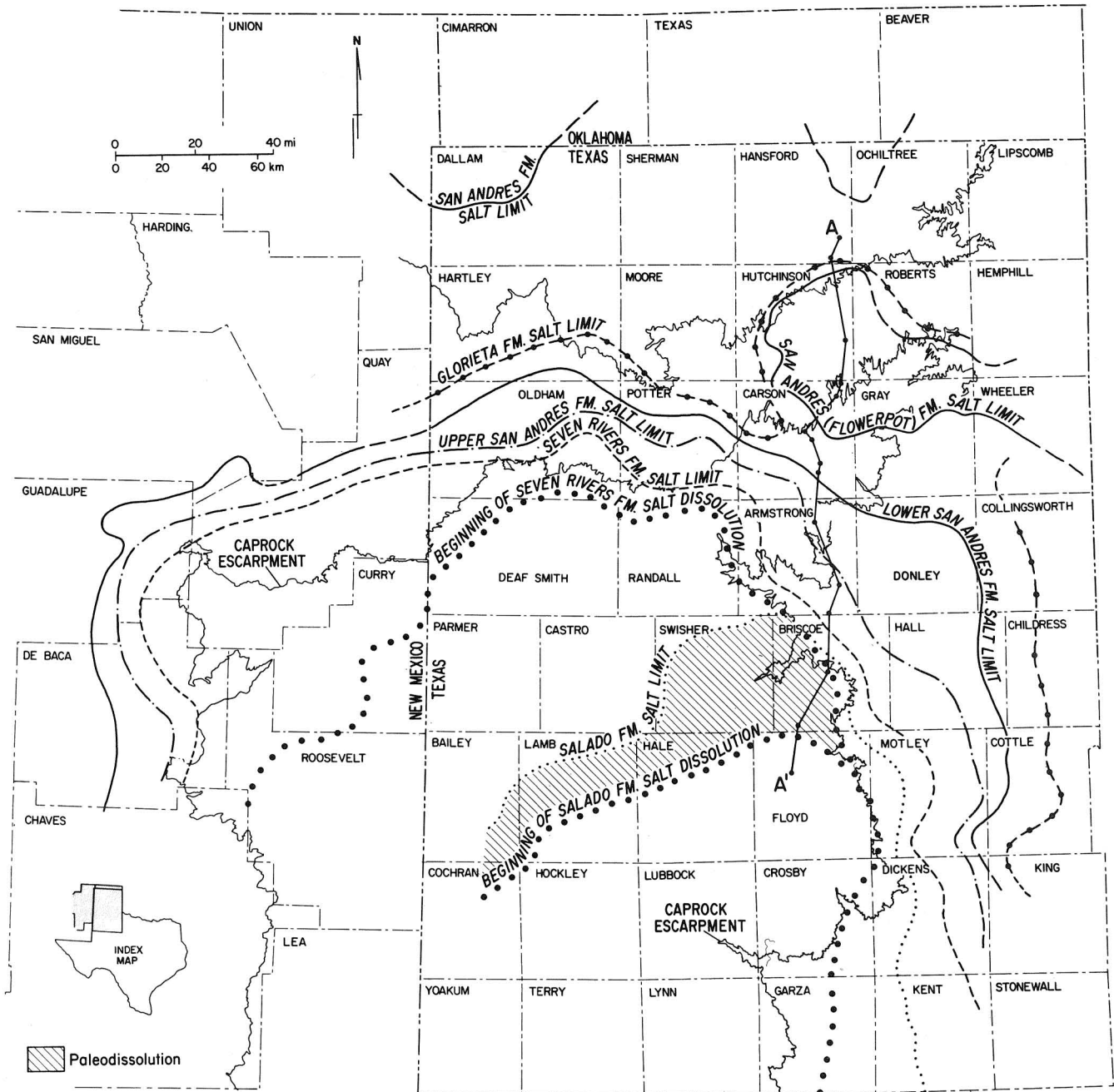
Figure 72. Salt dissolution zones, Texas Panhandle and eastern New Mexico. Except for the Seven Rivers and Salado Formations, where both the beginning of salt dissolution and the limit of salt are shown, the limit of salt for the younger formation marks the approximate beginning of salt dissolution for the next older formation (from Dutton and others, 1979).
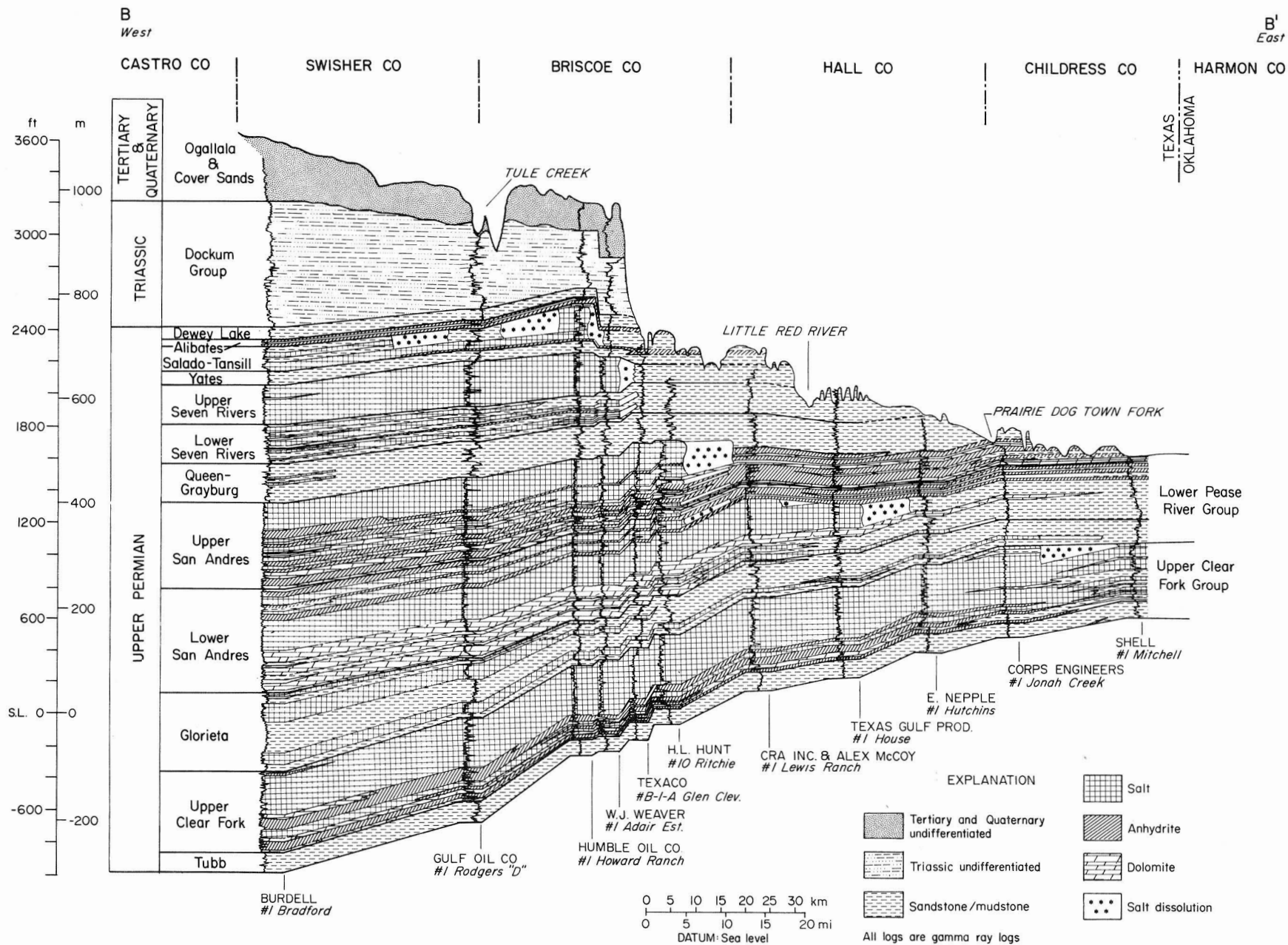
Figure 73. Structural and stratigraphic cross section B-B', eastern margin of the Palo Duro Basin. See figure 74 for location. Note the off-stepping development of salt dissolution zones in stratigraphically older units. Dip reversals are apparent as a result of collapse.
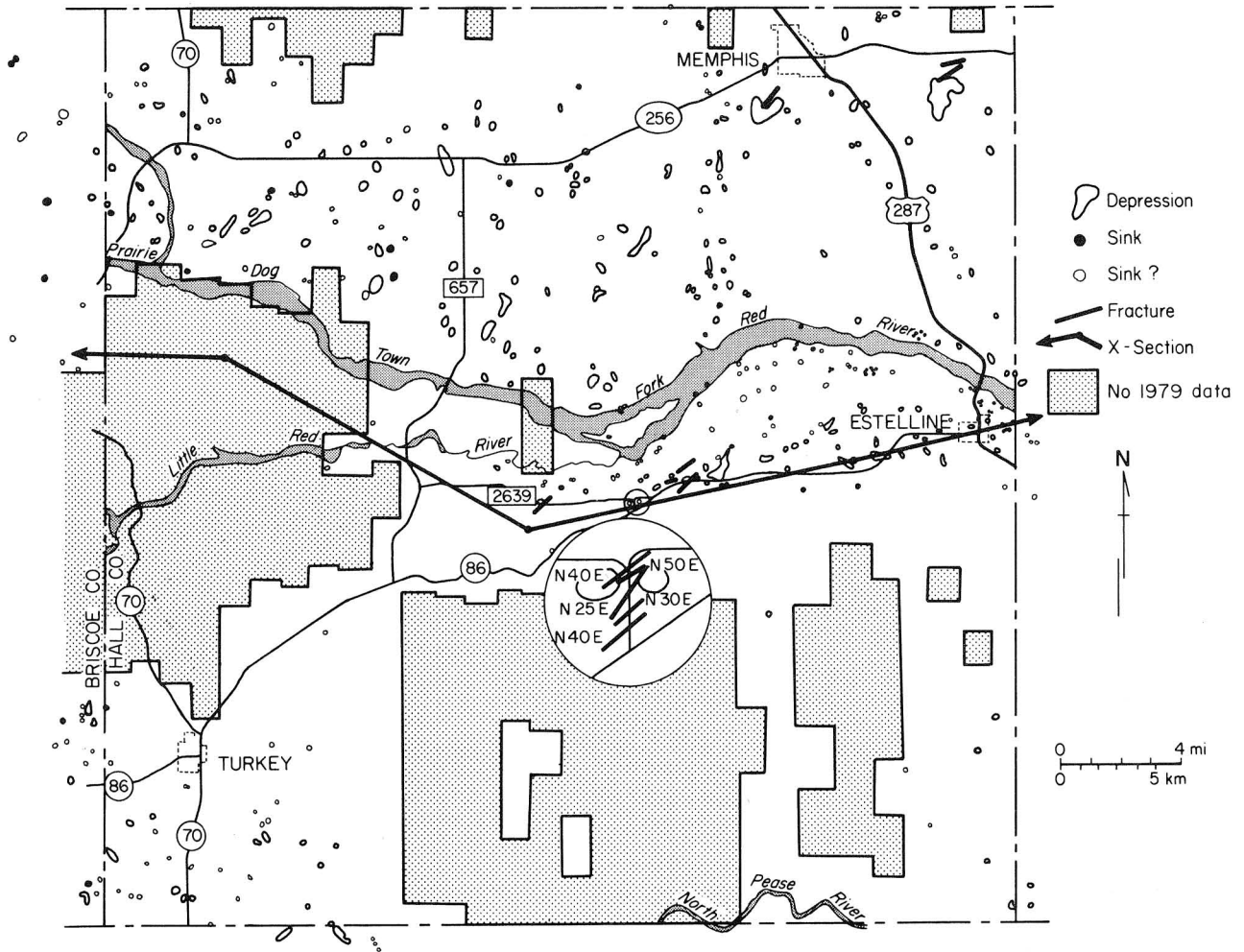
Figure 74. Map of sinkholes, undrained depressions, and open fractures in Hall and eastern Briscoe Counties.
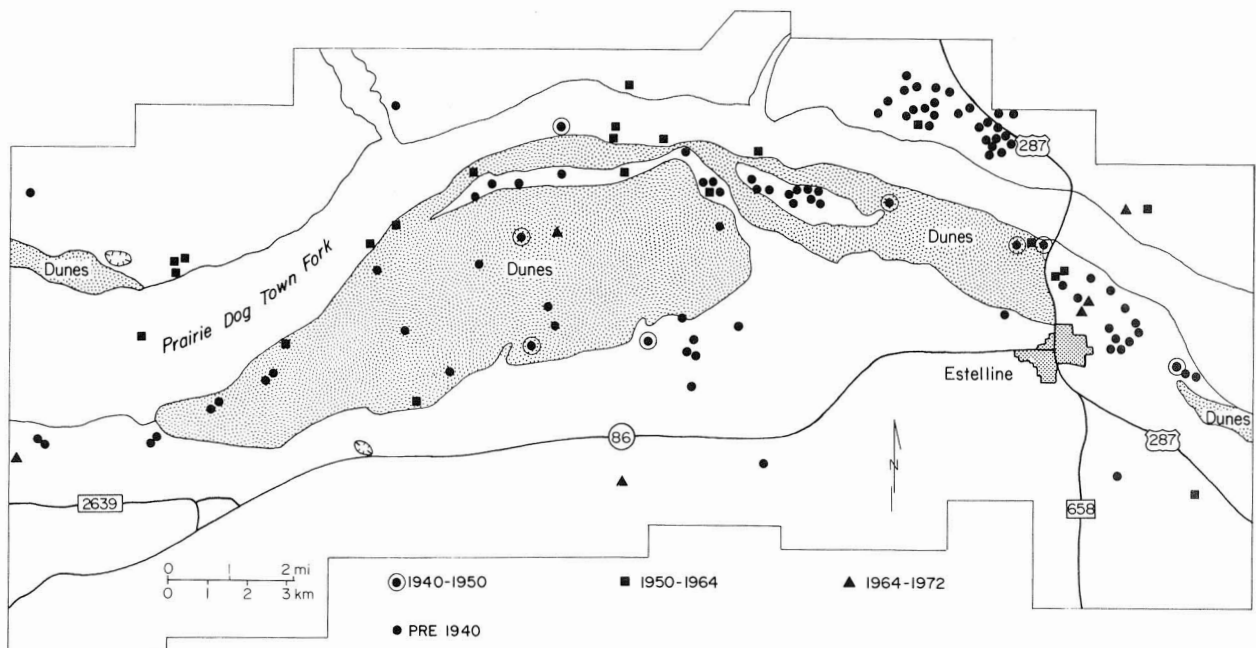
Figure 75. Thirty-six sinkholes and two collapse depressions developed between 1940 and 1972 in this 256-km² (128-mi²) test area along the Prairie Dog Town Fork in eastern Hall County.
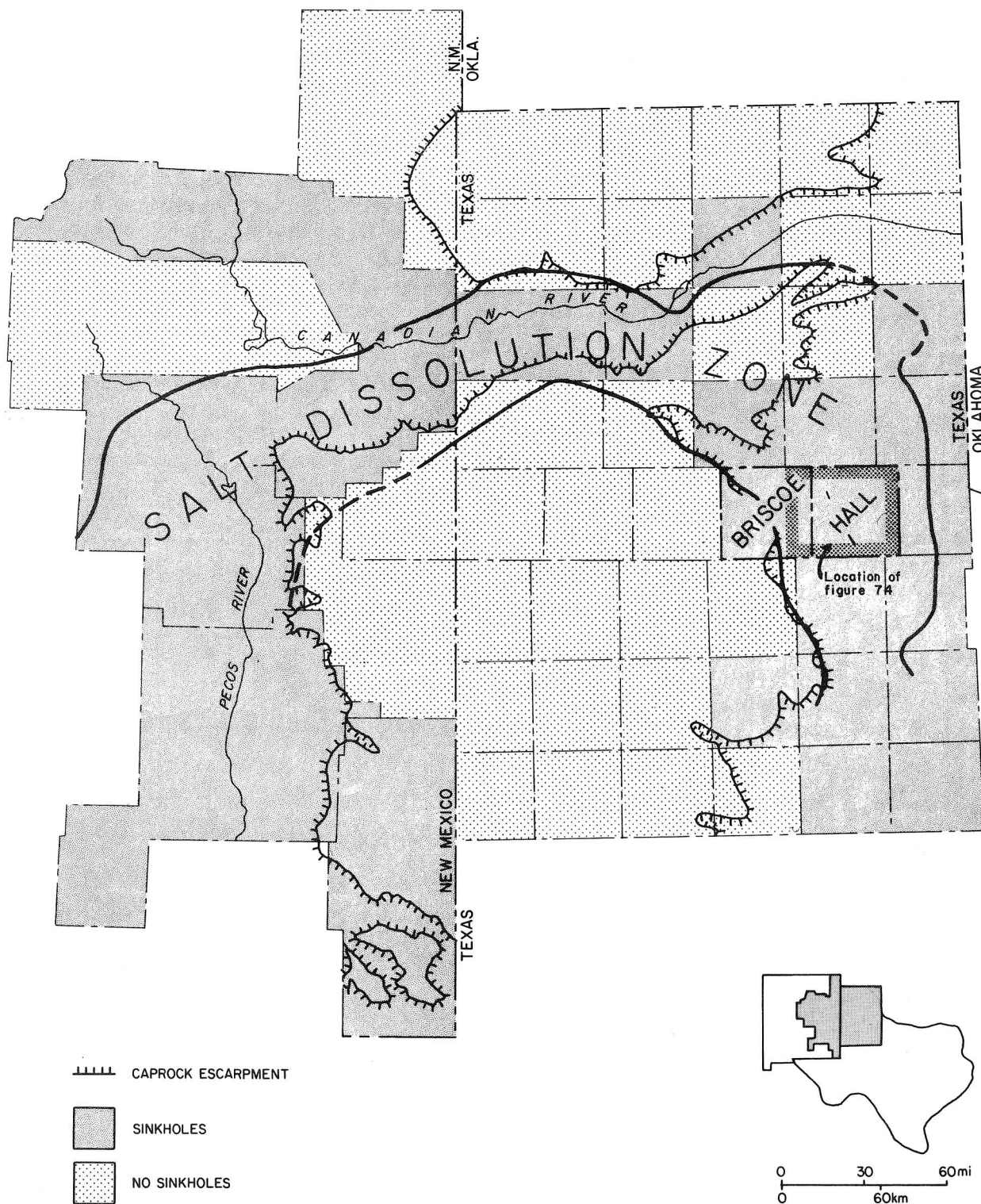
Figure 76. Eastern New Mexico and Texas counties where recent sinkholes occurred completely or partly within the zone of salt dissolution, an indication that dissolution and collapse is active throughout much of this region.

137

# A 10-YEAR STORM: ITS EFFECTS AND RELATIONSHIP TO AGE-DATED ALLUVIAL STRATIGRAPHY, RANDALL COUNTY, TEXAS PANHANDLE

R. J. Finley

*A 10-year-return-period storm caused significant slope erosion and upstream headcut migration in a 640-m (2,100-ft)-long canyon cut into the Ogallala Formation. Alluvial sequences containing radiocarbon-dated bone suggest a minimum average rate of downcutting of 1.95 mm (0.077 inch) per year over 1,070 years. This rate is higher than the rate obtained in the Little Red River Basin and indicates that stream incision is a hazard to any waste repository.*

On May 26, 1978, a thunderstorm over the Buffalo Lake monitoring locality in Randall County, Texas, resulted in 71 mm (2.8 inches) of rainfall over 3.2 hours. The return period of a storm of this magnitude is approximately 10 years, and the maximum rainfall intensity over a 30-minute period was 64 mm per hour (2.5 inches per hour). Some effects of this storm, including the extent of slope erosion, have been previously reported (Finley, 1979), but the specific changes in headcuts within alluvial fill on the canyon floor (fig. 77) have not been reported. Also, 41 percent of mostly pebble-sized clasts were moved from their original position on painted rock lines placed on the eroded slopes of the Ogallala Formation (table 9).

Review of these effects plus regional climatic data shows that surface flow processes of sheetwash and rillwash, aided by rainsplash erosion from raindrop impact, are dominant slope erosion mechanisms in the Texas Panhandle (Finley and Gustavson, 1980). Processes of erosion and deposition are operative and affect differently each of the major component areas of the drainage basin (fig. 78). On the High Plains surface, above the rim and head of the canyon, concentration of overland flow resulted in erosion of the margins of the Pleistocene silt deposit by sheetwash and rillwash. On the slopes of the Ogallala Formation, sheetwash, rillwash, and gullying were active, removing sand and gravel and concentrating these sediments in fans at the base of the canyon slopes. These sediments were incorporated into irregular bars of mostly cobble to pebble gravel and sand with some boulders that developed during high-energy flow conditions on the canyon floor. Although scour and headcut migration dominated the upper reaches of the canyon, the middle and downstream reaches were primarily depositional (fig. 78). Beyond the confines of the canyon walls, little gravel was transported, and a deposit of fine sand up to 25 cm (10 inches) thick, 70 m (230 ft) wide, and over 100 m (330 ft) long was formed at the junction of the study canyon thalweg and Tierra Blanca Creek.

138

Although the alluvial stratigraphy is poorly exposed in the drainage basin that was studied, an adjacent canyon revealed a sequence of irregular beds of caliche gravel, mixed sand, and gravel and fine sand. One vertical section along the incised thalweg of this canyon contains *Bison* spp. bone (identified by E. Lundelius, personal communication, 1979) in a sequence dominated by gravelly sand (fig. 79). The bone was dated by The University of Texas Radiocarbon Laboratory (Tx-3759) (S. Valastro, personal communication, 1980) at $990 \pm 80$ years B.P. If the present incised thalweg along which this deposit is exposed developed entirely since the bones were deposited, then the average minimum rate of downcutting has been 1.95 mm per year, assuming the maximum age of 1,070 years for the bones. This is one longer term estimate of downcutting under the present climatic regime for the Buffalo Lake area. We know, however, from the effects of the May 26, 1978, storm that short-term rates of geomorphic change may show great temporal variation, and that erosion, deposition, and stream incision are most active in discrete steps related to periods of intense rainfall characteristic of the Panhandle region.

These results show that minor tributaries of streams flowing across the High Plains surface, such as Tierra Blanca Creek, are eroding as actively as those along the eastern Caprock Escarpment. Not only retreat of major escarpments but also local stream incision will have to be considered in repository siting.

DEPOSITION

≥0.8 m

0.8 to 0.4 m

0.4 to 0.0 m

SCOUR

0.0 to -0.4 m

-0.4 to -0.8 m

-0.8 to -1.2 m

-1.2 to -1.6 m

≥1.6 < 2.2 m

Original headcut scarp

Post-storm headcut scarp

| 0 | 1 | 2 | 3 | 4 | 5 | 6 m |
|---|---|---|---|---|---|-----|
| 0 | | 5 | | 10 | | 15 | 20 ft |
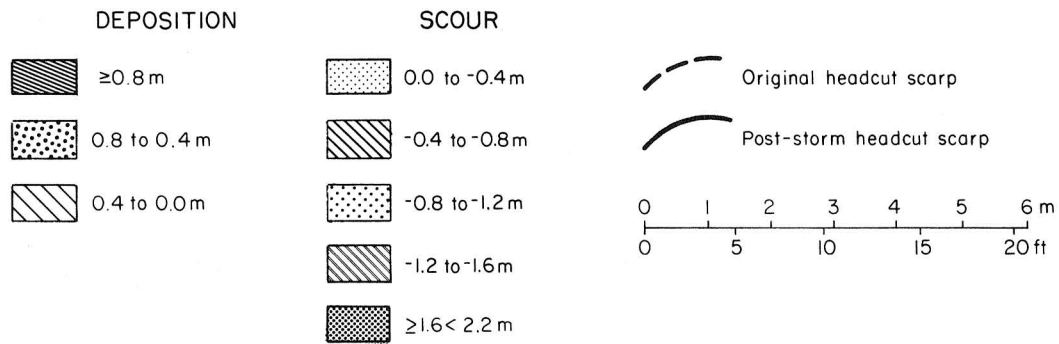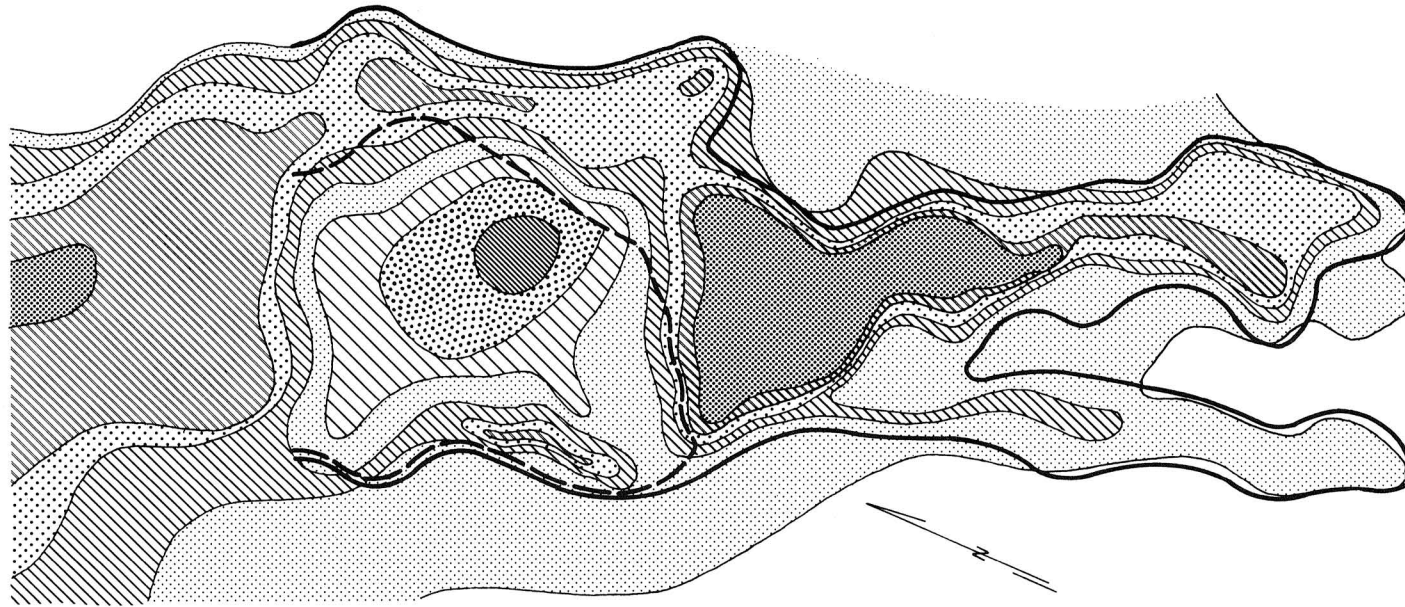
Figure 77. Net change map for a headcut within the alluvial fill of the main study canyon at the Buffalo Lake monitoring locality, February 3 to June 3, 1978.
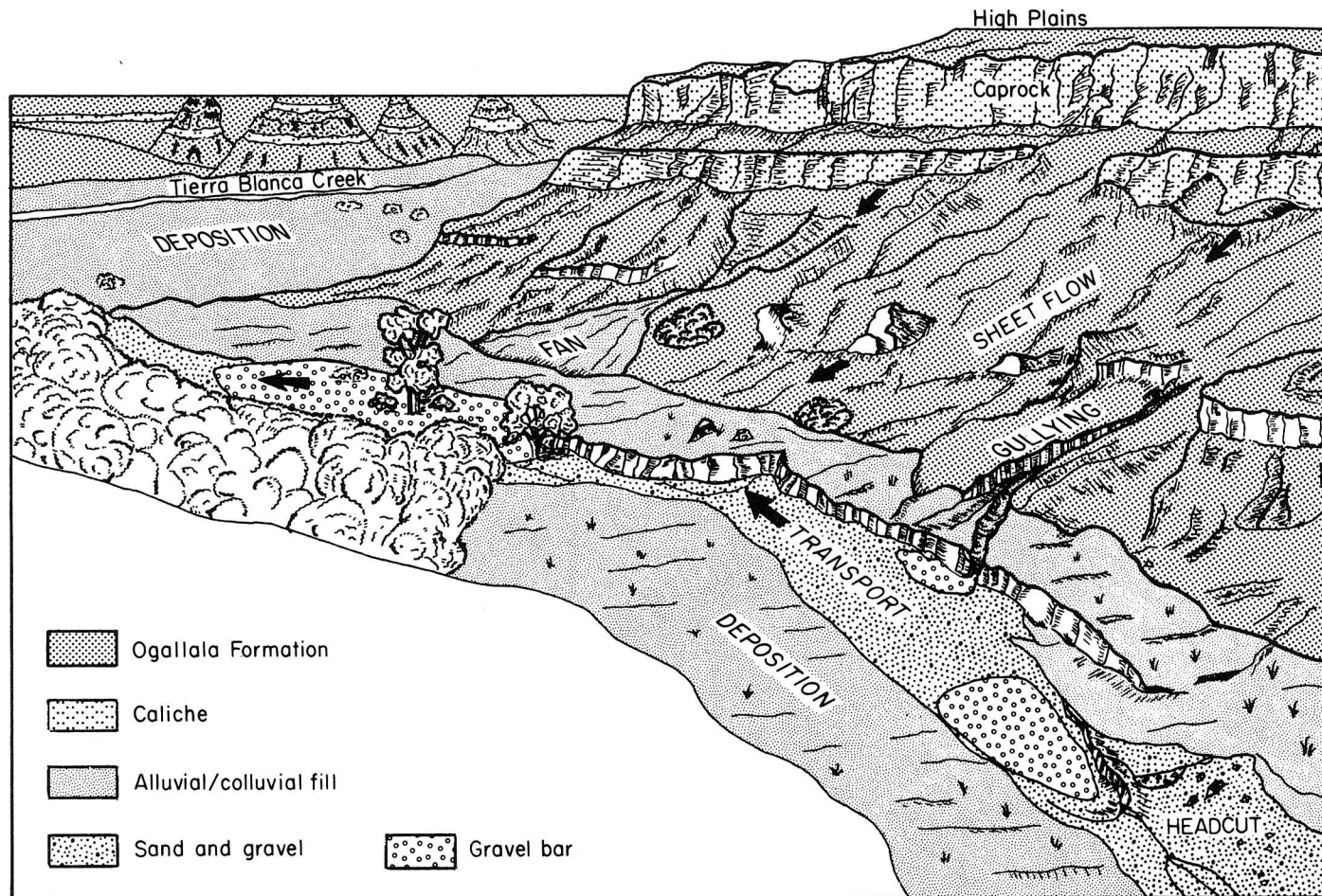
Figure 78. Summary of processes operating on the sedimentary rocks and alluvial sediments exposed in short tributaries of Tierra Blanca Creek in the Buffalo Lake area, Randall County, Texas.

# SECTION A



Modern soil profile.

Cobble to pebble sandy gravel; It. brown fine sand; clasts to 11cm.

Lt. brown fine gravelly sand.

Pebble gravel and fine sand.

Lt. brown fine gravelly sand; irregular thin beds and laminae of coarse sand; scattered pebble gravel; bones.

Lt. brown, fine to coarse gravelly sand.

Lt. brown fine sand.

Lt. brown fine gravelly sand.

Lt. brown fine gravelly sand.

Lt. brown to grayish brown, fine to very coarse gravelly sand.

Gravel mostly <2cm in long axis.

Colluvium.

Figure 79. Alluvial stratigraphy in the adjacent canyon southwest of the canyon being studied at the Buffalo Lake erosion monitoring locality.

142

Table 9. Painted rock line data for the main study canyon at the Buffalo Lake
erosion monitoring locality, March 14, 1978, to June 3, 1978.

|  | Locality | | |
| --- | --- | --- | --- |
|  | 1 | 2 | 3 |
| Slope | $31^{o}$ | $27^{o}$ | $19^{o}$ |
| Vegetative cover, percent | 17 | 10 | 15 |
| March count, number of clasts | 75 | 100 | 150 |
| June count, number of clasts | 40 | 56 | 101 |
| Percent moved | 47 | 44 | 33 |
| Number of clasts recovered | 10 | 10 | 23 |
| Distance downslope of recovered clasts: | | | |
| average | 0.79 m | 1.41 m | 0.63 m |
| maximum | 3.86 m | 5.29 m | 3.42 m |
| minimum | 0.10 m | 0.06 m | 0.07 m |

# SLOPE PROCESS MONITORING AND DATA ANALYSIS, TEXAS PANHANDLE

*R. J. Finley and R. C. Howard*

*Data from erosion process monitoring localities are being analyzed via computer processing and standard statistical programs. Preliminary results show the correlation of increased erosion with steeper, less vegetated slopes, and further data will yield erosion rates characteristic of the present climatic regime.*

Field investigations have shown continuous surface denudation for most erosion pins and net deposition for only a few pins, generally those in lower slope classes. All data illustrate a trend toward greater erosion on steeper slopes where vegetation generally is less dense and where movement of surficial material affects the ability of vegetation to stabilize the surface. Data from the south side of John Haynes Ridge in Caprock Canyons State Park suggest increasing vegetative cover with decreasing slope angle. This pin field is set in relatively thin soils and has an average vegetative cover of 7.8 percent (varying from 0 to 32 percent), indicating that vegetative cover is sparse on slopes ranging from $3^{\circ}$ to $44^{\circ}$ and averaging $21^{\circ}$.

This same trend toward an upper limit of vegetative cover applies to data distributions taken across multiple monitoring localities. Pins registering the highest two classes of net erosion are generally found on slopes of $20^{\circ}$ or greater and 10 percent or less vegetative cover. Individual pins may deviate from this trend, depending on their location relative to preferred paths of sheetwash and rillwash. Consequently, 470 erosion pins have been deployed across a variety of surface materials, slope angles, and vegetative cover densities to obtain a large sampling of slope conditions.

Young (1972) reports that the relationship between surface-wash erosion and slope angle varies in different investigations from a linear to a quadratic form. Data from 142 erosion pins at 4 monitoring localities show increasing erosion with increasing slope angle (fig. 80) according to the following equation:

$$E = 0.05A + 0.69$$

where E is erosion as the ordinate, and A is slope angle on the abscissa. This linear relationship is shown by the dashed line in figure 80. These data show a wide scatter and a low correlation coefficient ($r = 0.24$) since (1) only short periods of monitoring are represented, (2) relatively few pins are included, and (3) variables such as substrate type and slope exposure are not considered in the analysis. The linear relationship between erosion and slope angle is statistically significant at the 95-percent level,

indicating that the variables are correlated; further data collection and analysis should refine the relationship. Similarly, the relationship between slope erosion and vegetative cover (fig. 81) is poorly defined by these preliminary data; however, a tendency toward greater erosion on less vegetated slopes is evident.

Monitoring of slope erosion yields both a short-term estimate of erosion rates and an understanding of erosion mechanisms and their relationships to the present climatic regime. Active retreat of slopes must be considered in siting any potential repository within the Texas Panhandle region.
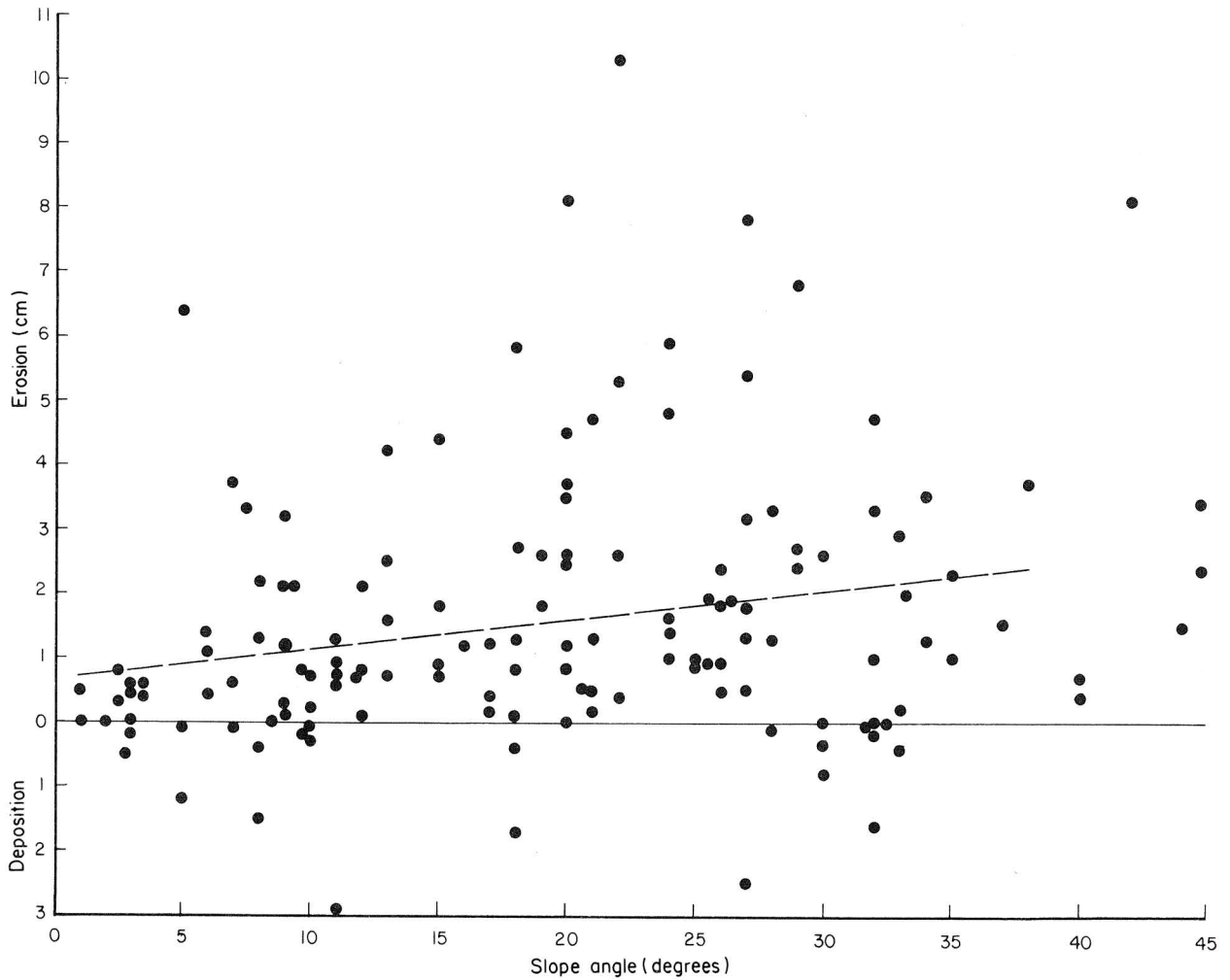
Figure 80. Net erosion and deposition versus slope angle measured using erosion pins at four monitoring localities for the periods (1) December 12, 1978, to August 8, 1979, at Caprock Canyons State Park, (2) June 26, 1978, to August 24, 1979, at Palo Duro Canyon State Park, (3) June 6, 1978, to May 1, 1979, at Muleshoe National Wildlife Refuge, and (4) February 3, 1978, to December 11, 1978, at Buffalo Lake National Wildlife Refuge. Dashed line computed by linear regression.

Figure 81. Net erosion and deposition versus vegetative cover measured using erosion pins for the same sites and time periods as listed in figure 80.

147

# SEDIMENTOLOGY AND BASIN MORPHOMETRY OF THE LITTLE RED RIVER BASIN: INSIGHTS INTO RETREAT OF THE EASTERN CAPROCK ESCARPMENT, TEXAS PANHANDLE

*R. J. Finley and R. W. Baumgardner, Jr.*

*The Little Red River Basin, estimated to have developed over 380,000 years, contains approximately 30 percent of the original rock mass present over the basin area. The eastern Caprock Escarpment has retreated approximately 40 km (25 mi) in this time period. Present erosional processes are active and include slope erosion of 1.4 cm (0.55 inches) in 8 months and export of more than 340,000 metric tons (375,000 tons) of suspended sediment in the 1979 water year.*

The Little Red River, a tributary of the Prairie Dog Town Fork of the Red River, is an intermittent stream heading along the eastern Caprock Escarpment of the Southern High Plains. The river basin has a gaged area of 360 km$^2$ (139 mi$^2$), a maximum relief of 390 m (1,248 ft), and a relief ratio of 0.011. The Ogallala Formation and the Dockum Group crop out at the head of the basin. Poorly consolidated Upper Permian shales, siltstones, and sandstone covered with thin soils and sparse vegetation occupy most of the basin (fig. 82).

Rates of development and denudation of the Little Red River Basin were estimated using hypsometric analysis, a method that relates the distribution of mass with elevation within the basin (fig. 83). As erosion removes mass from the basin, the hypsometric integral decreases. For the Little Red River Basin, the present hypsometric integral is 0.30, meaning that 30 percent of the original material remains. The original rock mass was about 190 km$^3$ (46 mi$^3$), and more than 133 km$^3$ (32 mi$^3$) of rock have been removed. On the average, the ground surface in the Little Red River Basin has been lowered 270 m (886 ft) since the basin began to form.

An estimate of the age of the basin is based on the location of the eastern edge of the Ogallala Formation and on the rate of its retreat to its present location at the Caprock Escarpment. An estimate of its average rate of retreat of 110 mm per year (4.3 inches per year) is derived from the 3-million-year-old age of the formation and a total retreat of 320 km (200 mi) (Gustavson and others, 1980a). On this basis, the 40-km (25-mi) -long basin is 380,000 years old, and the denudation rate for removal of the 270 m (886 ft) of material has been 0.47 mm per year (0.019 inches per year), when allowing for 90 m (300 ft) of vertical collapse owing to subsurface salt dissolution.

Geomorphic studies within the Little Red River Basin have centered on present and past erosional processes, especially at the head of the basin in Caprock Canyons State Park. Field investigations have shown continuous surface denudation for most

erosion pins and net deposition for few pins, generally those in lower slope classes (table 10). These data show that slope erosion measuring 1.7 cm (0.67 inch) can be related to rainfall that is limited to just the early part of the seasonal precipitation cycle. That period included at least one high-intensity storm of not more than a 5-year return period.

Much of the slope-derived sediment is exported from the basin as suspended-sediment load. Sporadic, intense rainfall within the upper Little Red River Basin produces stream flow with an estimated velocity as high as 3.1 m per sec (10.2 ft per sec). This estimate is based on surveys of trash lines and channel geometry and on use of the Manning equation for a point in Caprock Canyons State Park. Such flows move a significant amount of bed load as well as suspended load, including gravel clasts up to 13.5 cm (5.3 inches) in long axis.

Suspended-sediment load for the 1979 water year, measured near the mouth of the Little Red River Basin, showed export of 340,644.5 metric tons (375,496.3 tons) of sediment. Assuming specific weights of 801 to 1,161 kgs per m$^3$ (50 to 72.5 lbs per ft$^3$), this sediment weight is equivalent to a basin-wide denudation rate of 1.18 to 0.81 mm (0.046 to 0.032 inches) per year.

In addition to these studies, the sedimentology of representative meander bends is being analyzed as an indication of flow competence and processes of terrace development. The distribution of as many as five levels of terraces along the Little Red River has been mapped to determine which are age-equivalent and therefore useful in the construction of paleo-stream profiles. Radiocarbon dating of organic materials (paleosoils and organic-rich pond deposits) in alluvial sequences will be used to provide further data on rates of fluvial downcutting within the Little Red River Basin.

The geomorphic processes active within the Little Red River Basin are operating along much of the eastern Caprock Escarpment. On a geologic time scale, these processes are reducing the extent of the Southern High Plains and hence reducing the rock mass over any potential repository site beneath the High Plains. The Little Red River Basin is similar to many other basins along the Caprock Escarpment; therefore, results of this study can be extended to other areas. Where differences in lithology and local relief indicate that geomorphic processes or rates may vary, two additional drainage basins have been selected for similar detailed study.
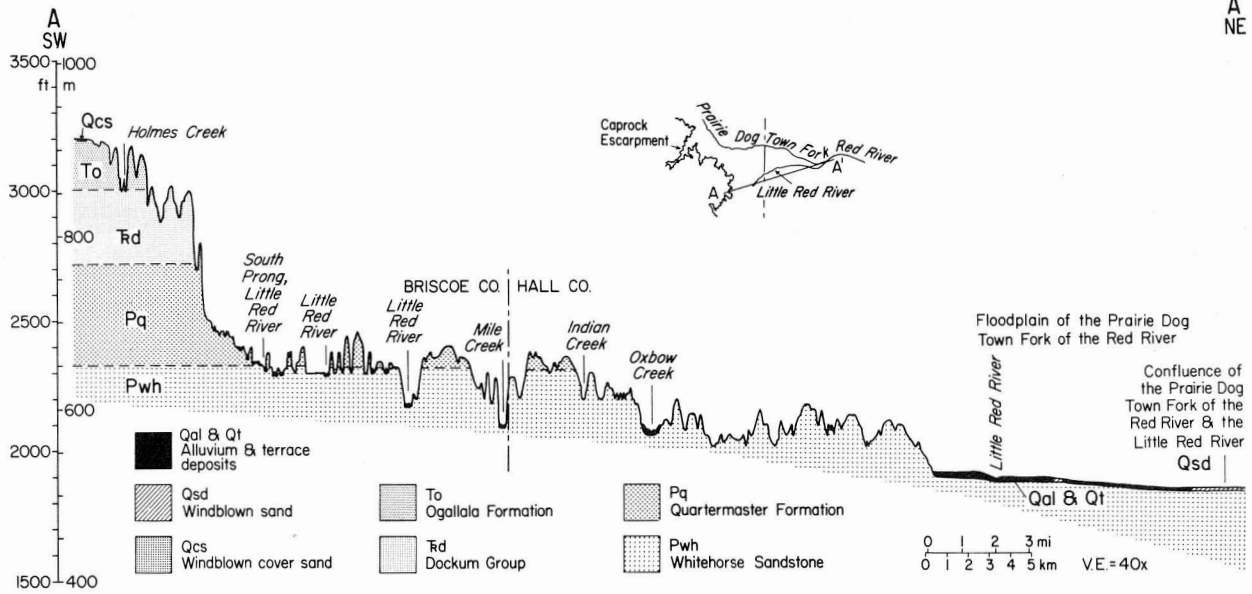
**Figure 82.** Topographic cross section of the Little Red River Basin from the Caprock Escarpment to the junction of the Little Red River and Prairie Dog Town Fork of the Red River. Geologic units are generalized.
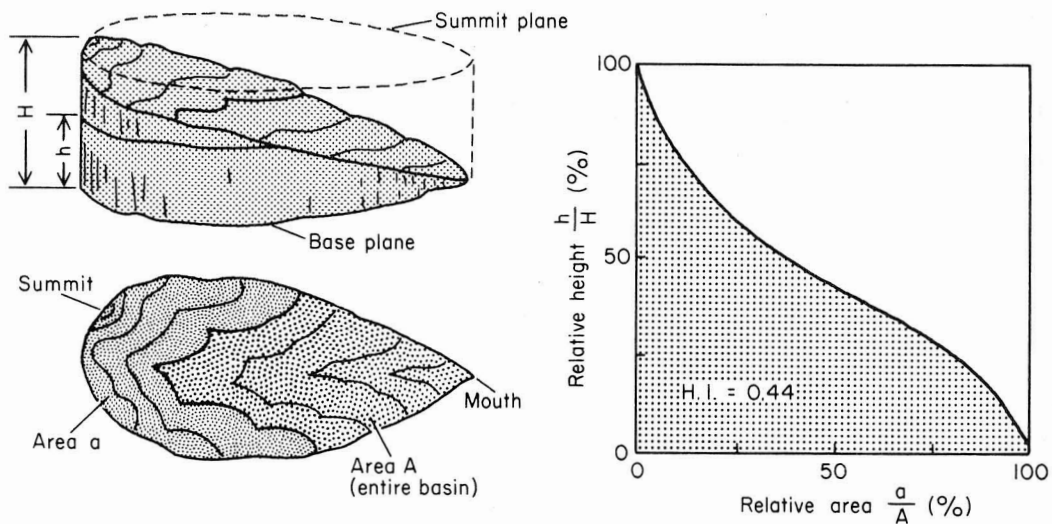


**Figure 83.** Derivation of the hypsometric integral for a theoretical basin that has undergone erosion. The three-dimensional geometric solid defined by the drainage divides of the basin, a horizontal plane at the highest elevation in the basin and one at the lowest elevation, has a hypsometric integral of 1.0, signifying that 100 percent of the original mass of the basin is still in place. In this figure, 44 percent of the original mass remains (after Strahler, 1957).

150

Table 10. Erosion pin measurements, Caprock Canyons State Park, Briscoe County, Texas, net change from December 16, 1978, to April 11, 1979.

| Slope class | Number of pins in class | Net erosion, cm* | | |
| --- | --- | --- | --- | --- |
| | | Average | Maximum | Minimum |
| $0°-9°$ | 8 | 0.46 | 1.1 | 0 |
| $10°-19°$ | 12 | 0.75 | 1.6 | 0 |
| $20°-29°$ | 15 | 0.74 | 1.8 | 0.2 |
| $30°-39°$ | 3 | 1.17 | 1.8 | 0.3 |
| $40°-49°$ | 1 | 1.0 | 1.0 | 1.0 |
| | | Net deposition, cm* | | |
| $0°-9°$ | 1 | 0.2 | 0.2 | 0.2 |
| $10°-19°$ | 1 | 0.6 | 0.6 | 0.6 |
| $20°-29°$ | 1 | 1.7 | 1.7 | 1.7 |
| $30°-39°$ | 1 | 1.7 | 1.7 | 1.7 |
| $40°-49°$ | 2 | 0.3 | 0.5 | 0.1 |

*1 cm = 0.39 inch

# SALT DISSOLUTION AND THE FORMATION OF THE WINK SINK, WINKLER COUNTY, TEXAS

R. W. Baumgardner, Jr., A. D. Hoadley, and T. C. Gustavson

*Preliminary results suggest that the Wink Sink may have begun as a dissolution chamber 610 m (2,000 ft) below the surface. As the chamber migrated upward, the brine it contained was significantly diluted by water in aquifers above the salt. This process could pose a threat to repository integrity.*

The study of the Wink Sink, Winkler County, Texas, was designed to gather information about a process that is a potential threat to repository integrity. Ground water circulating at depths greater than 610 m (2,000 ft) may have produced a dissolution chamber that migrated upward until it breached the surface. The sinkhole, which formed June 3, 1980, is about 110 m (360 ft) wide and 33 m (110 ft) deep at its deepest point.

Salt dissolution has been occurring in the Delaware Basin since Permian time (Adams, 1944). During the Quaternary, dissolution at depth was manifested at the surface as sinkholes, large closed depressions, and disrupted stream courses (Nicholson and Clebsch, 1961; Bachman, 1976). Dissolution now is occurring in two regional zones: (1) along a dissolution front that is advancing from west to east across the basin and is currently located west of the Pecos River, and (2) parallel to the inner margin of the Capitan Reef on the northeast side of the Delaware Basin (fig. 84) (Maley and Huffington, 1953).

The Wink Sink is in the second zone; Anderson and Kirkland (1980) modeled the formation of this zone. According to these authors, water unsaturated with respect to salt under artesian pressure moves upward from the Capitan Reef aquifer into salt-bearing strata. Salt is dissolved, and the resulting brine drains downward owing to its higher density relative to the density of fresher water in the underlying reef. A continuous circulation of water removes large volumes of salt and forms dissolution chambers, which can become sinkholes if successive roof failures cause the chamber to migrate upward to the ground surface.

Gamma ray logs from wells in the vicinity of the Wink sinkhole show a dissolution zone in the Salado Formation at a depth of 425 to 610 m (1,400 to 2,000 ft) (fig. 85). If the chamber formed in this interval, it was probably continually filled with brine ($\geq$30,000 mg/l TDS), which was displaced upward as roof material collapsed into the chamber. Water samples taken from the sinkhole two days after it formed contained only 2,077 mg/l chloride and 5,984 mg/l TDS. Apparently, the water within

the chamber was significantly diluted as it moved upward through strata containing less saline water. The volume of the sinkhole is about 159,500 m$^3$ (208,000 yd$^3$); thus the volume of water that was probably transported upward into the overlying strata was about 42 x 10$^6$ gallons.

The formation of this sinkhole clearly illustrates one potential problem associated with salt repositories. Dissolution of salt occurs in complex hydrologic circumstances, and a thorough understanding of the hydrology of dissolution zones is essential for the selection of a safe repository.
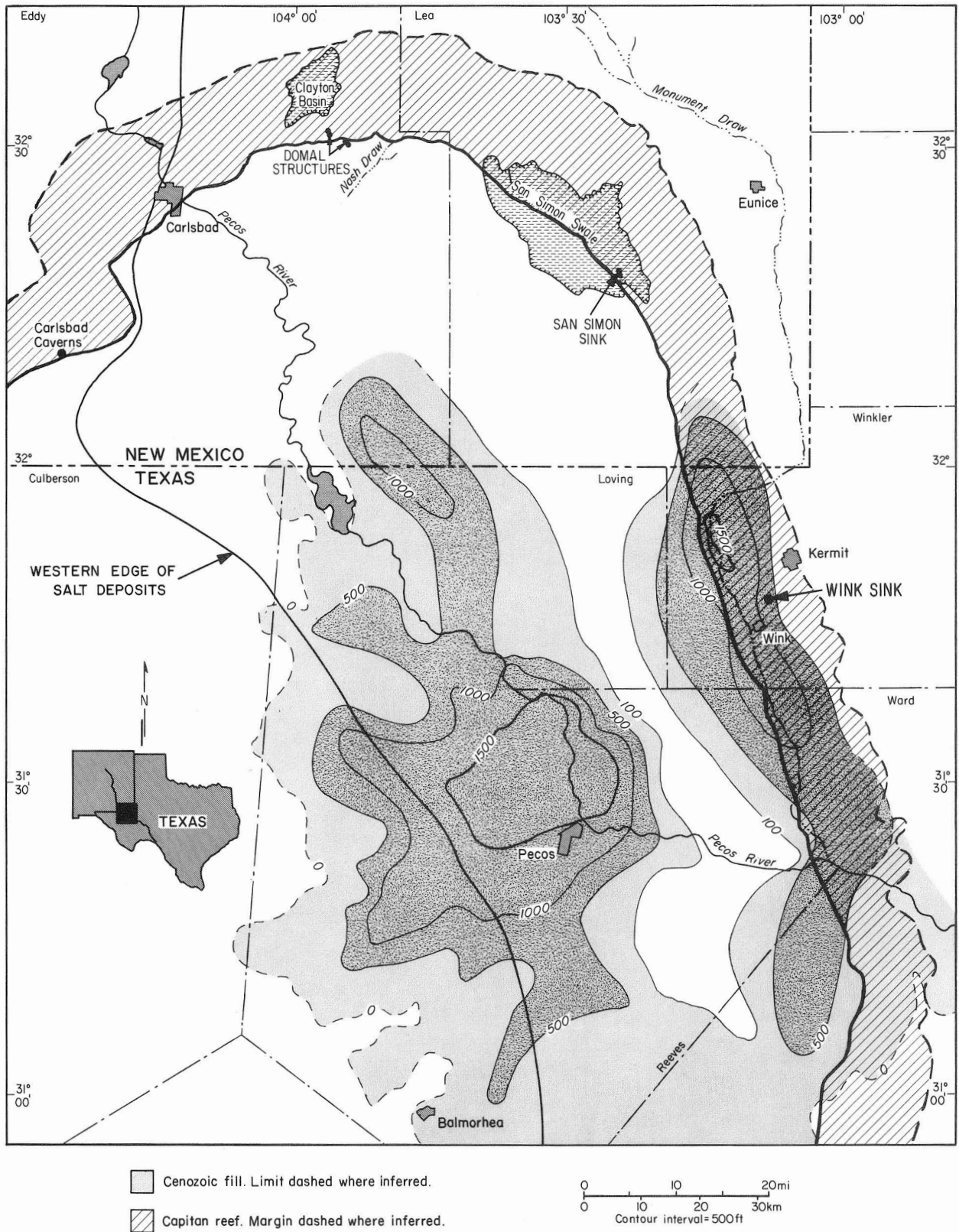
Figure 84. Map of the Delaware Basin showing the solution-collapse features and the extent of bedded salts. Adapted from Bachman, 1976; Cooper, 1962; Hiss, 1975; Maley and Huffington, 1953; and Vine, 1960.
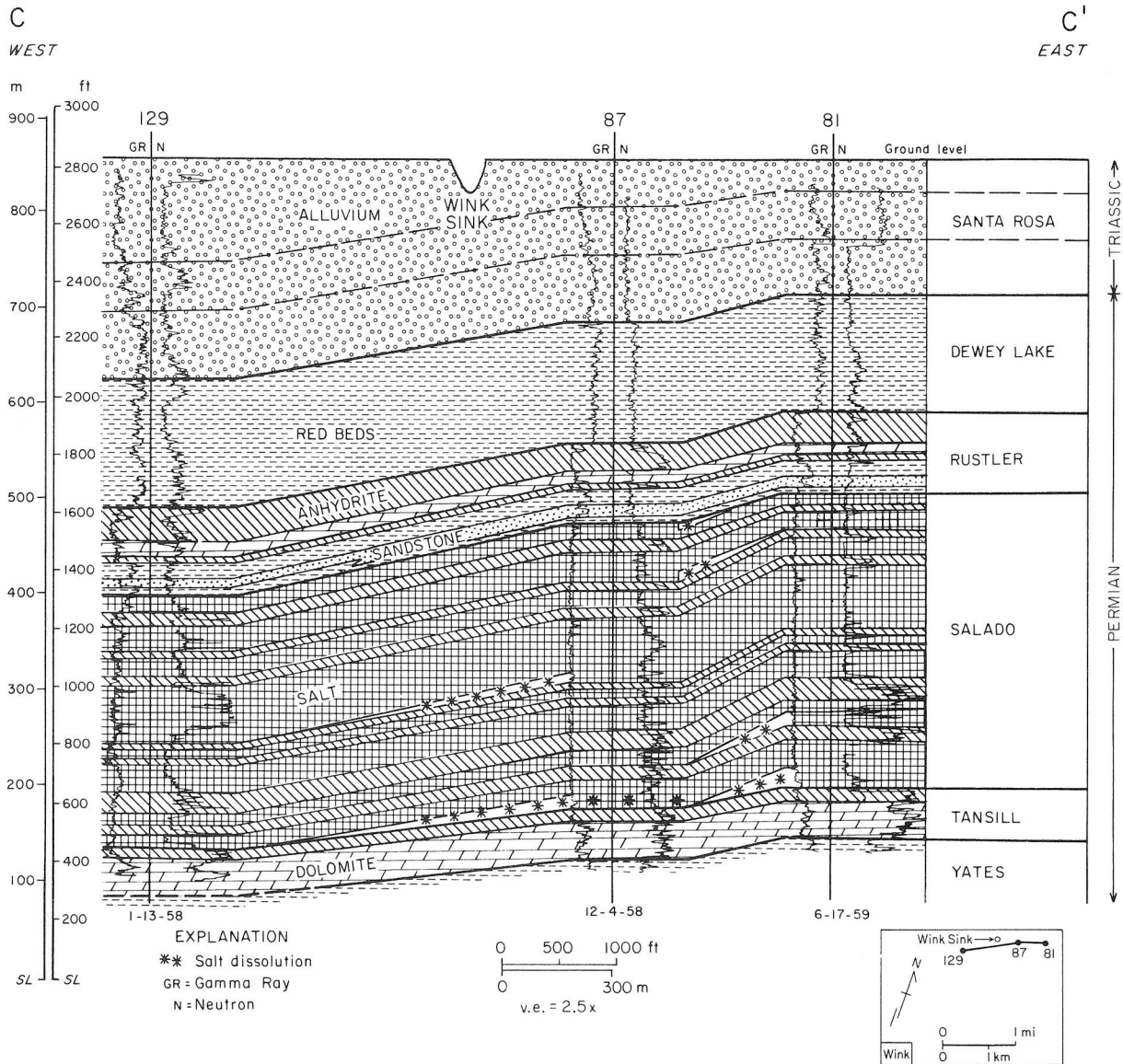
154

Figure 85. Cross section through the Salado Formation in the vicinity of the Wink Sink. Salt dissolution is documented on gamma ray logs as a thinning of the salt-bearing section between two distinct formations: the Rustler and the Tansill.

155

# APPLICATION OF GLORIETA-FLOWERPOT FACIES ANALYSES TO MAP AND DISTINGUISH BETWEEN SALT DISSOLUTION AND FACIES TRANSITIONS, WESTERN AMARILLO UPLIFT AND ADJACENT AREAS

D. A. McGookey

*Detailed stratigraphic correlations of Glorieta and Flowerpot strata across the western Amarillo Uplift and the Anadarko Basin demonstrate that both salt dissolution and lateral facies changes explain the absence of salt in some areas.*

When determining the original extent and thickness of Permian evaporites, it is difficult to distinguish between areas where salt was removed by salt dissolution and areas where salt was not deposited because of lateral changes in depositional environments. In the central part of the Texas Panhandle (fig. 86), during Glorieta and Flowerpot time, terrestrial eolian environments graded southeast into sabkha evaporite and mudflat environments. Cenozoic salt dissolution erased the post-Clear Fork record of salt deposition in many areas north of the Canadian River. In the study area, however, salt of the Glorieta and Flowerpot Formations has not been dissolved.

The shallowest salts, which are the structurally highest salt strata, are generally the first to be dissolved. After the salt has been removed, it is difficult to determine the volume of original salt because facies changes may also account for the absence of salt, especially over structurally high areas. Therefore, the distribution of environments of deposition must be identified to distinguish between areas where salt was not deposited and areas where it has been dissolved.

Near the Amarillo Uplift a succession of Upper Permian facies grades upward from (1) Glorieta sandstone and mudstone deposited on eolian flats and mudflats (figs. 87, 88) to (2) Flowerpot salt deposited in brine pans (fig. 89) and to (3) Blaine dolomite that marks the updip limit of lower Blaine carbonate deposition (fig. 90). In Late Permian, the Amarillo Uplift was probably a subtle topographic feature surrounded by basinal sediments that were subsiding more rapidly. The uplift controlled various facies boundaries during Late Permian time. Eolian sands of the Glorieta Formation were transgressed by Flowerpot sabkha sediments, and salt was deposited in both the subsiding Anadarko and the Palo Duro Basins. Over the Amarillo Uplift, these depositional environments received less salt precipitation than did surrounding basins. In post-Permian time, subsidence of the Anadarko and Palo Duro Basins continued, so that salts deposited over the Amarillo Uplift remained structurally higher than surrounding basinal salts (figs. 91, 92, table 11).

In the study area, salt dissolution occurs over the structurally high Amarillo Uplift and beneath the Canadian River and White Deer Creek. Evidence of salt dissolution is demonstrated by collapse of overlying Blaine Anhydrite into dissolution troughs. Salt dissolution and collapse zones are labeled on cross sections A-A' and B-B' (figs. 91 and 92). An hourglass-shaped dissolution front occurs under the Canadian River (fig. 89). A collapse feature can be observed near the Amarillo Uplift west of Carson County well no. 42, depicted on cross section A-A' (fig. 91), where the salt has been removed over the Amarillo Uplift beneath the Canadian River. This documents that salt dissolution has been and is occurring beneath current surface drainage that has eroded to within 120 to 260 m (400 to 800 ft) of the salt (Johnson, 1976). Note that 150 m (500 ft) of Tertiary Ogallala sediments have been eroded beneath the Canadian River and above the salt dissolution zone (figs. 86, 89). The shallowest salts of Flowerpot age lying over the Amarillo Uplift are completely missing (fig. 89). In the westernmost part of the Anadarko Basin, Flowerpot salt is structurally lower and deeper than the salt that was dissolved. Dissolution is currently occurring at the top of the Flowerpot salt beneath the Canadian River valley, where the salt is at a shallow depth beneath surface drainage.

In this facies analysis, evidence indicates that salt dissolution is and has been occurring under the Canadian River and other drainage areas. Changes in facies and older dissolution of updip salts are reasons that Glorieta-Flowerpot salt beds do not drape the Amarillo Uplift. In studies of similar salt dissolution areas, both depositional pinch-out and subsequent dissolution should be evaluated to determine the original volume of salt deposited before estimating the rates and amount of salt dissolution.
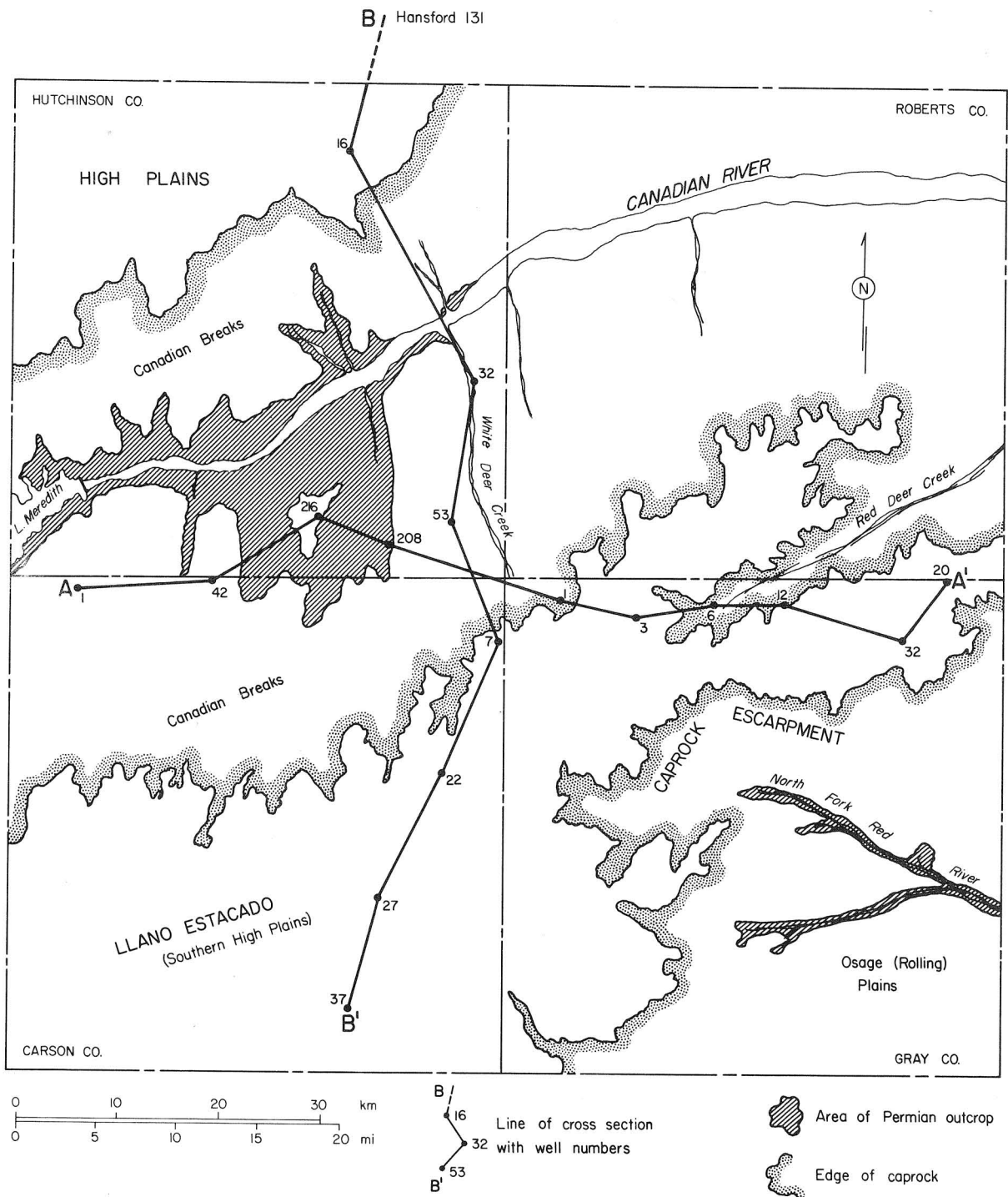
Figure 86. Surface geologic and geomorphic features of the study area. The Canadian River has eroded a wide valley across the High Plains in Hutchinson and Roberts Counties. The Caprock Escarpment marks the boundary between the High Plains and the Osage (Rolling) Plains. Along the Canadian River in Hutchinson County, the Ogallala Formation has been breached.
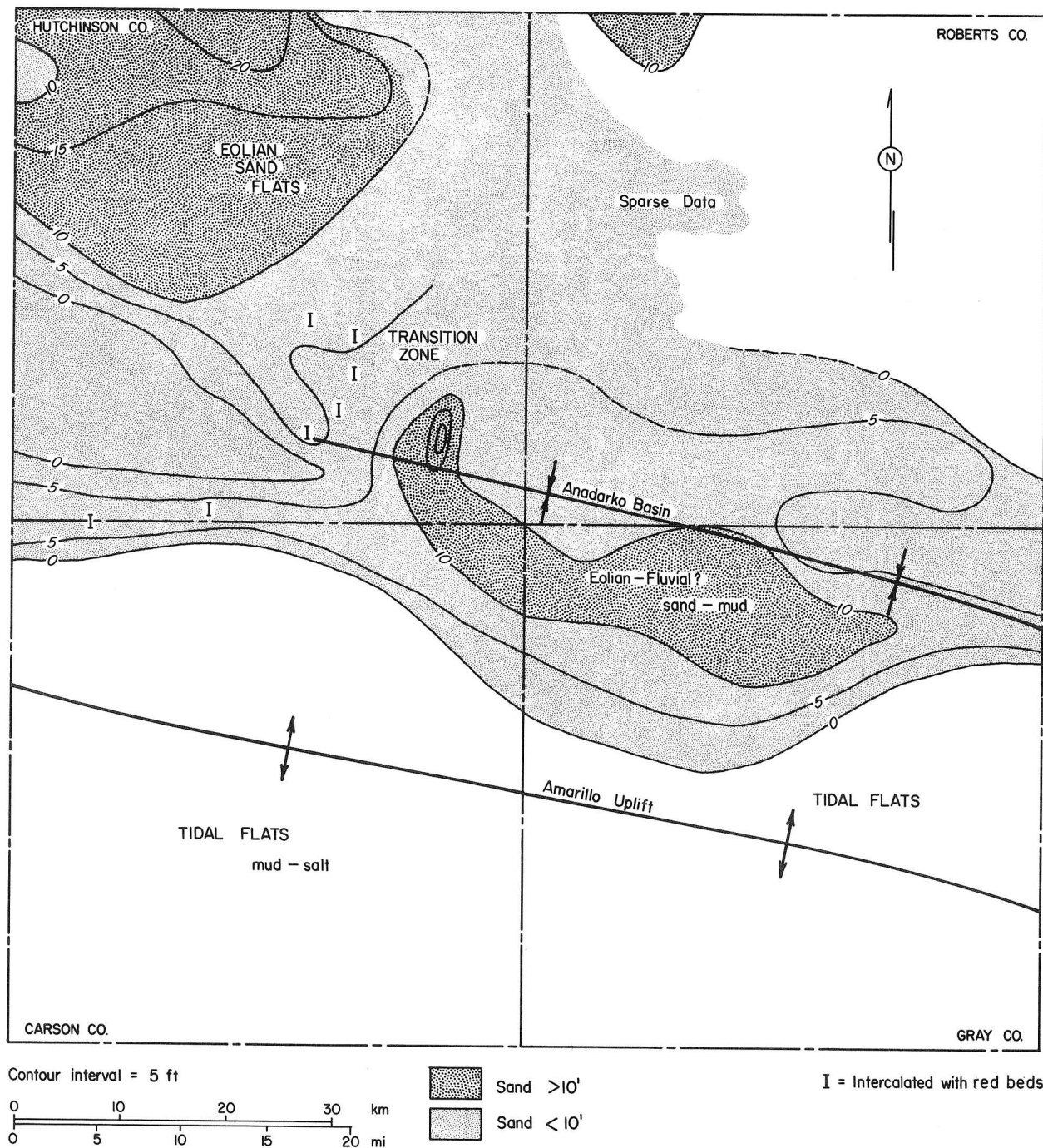
158

Figure 87. Isopach map of lower Glorieta sandstone bed (see figs. 91 and 92). During early Glorieta time, sand dispersal was preferentially into the subsiding and low-lying areas of the Anadarko Basin. Pinch-out of the sand against the Amarillo Uplift indicates that at that time the uplift was a subtle topographic high that blocked sand-bearing wind or rivers from the Palo Duro Basin. (Use of informal terms "upper and lower Glorieta sandstone" differs from Presley's use, this volume.) Basement structures shown on all isopach maps from Nicholson (1960).
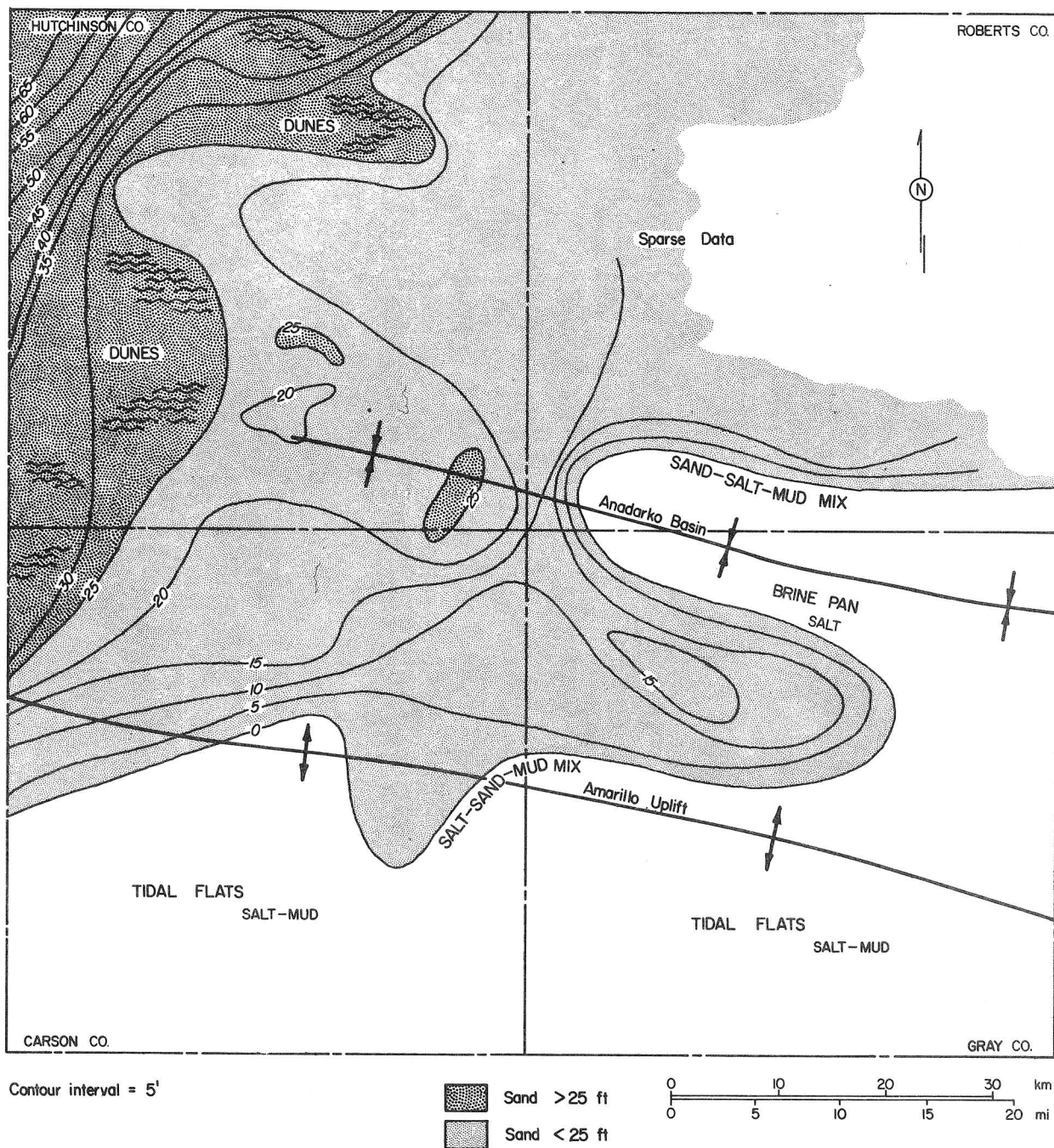
Figure 88. Isopach map of upper Glorieta sandstone bed. By late Glorieta time, the pattern of sand dispersion had changed. Up to 20 m (65 ft) of eolian sands (Presley, this volume) accumulated in the northwest corner of the study area. The Amarillo Uplift, upon which arkosic tidal-flat sands were altered to mud, remained topographically higher. In latest Glorieta time, a brine pan developed in the subsiding Anadarko Basin.
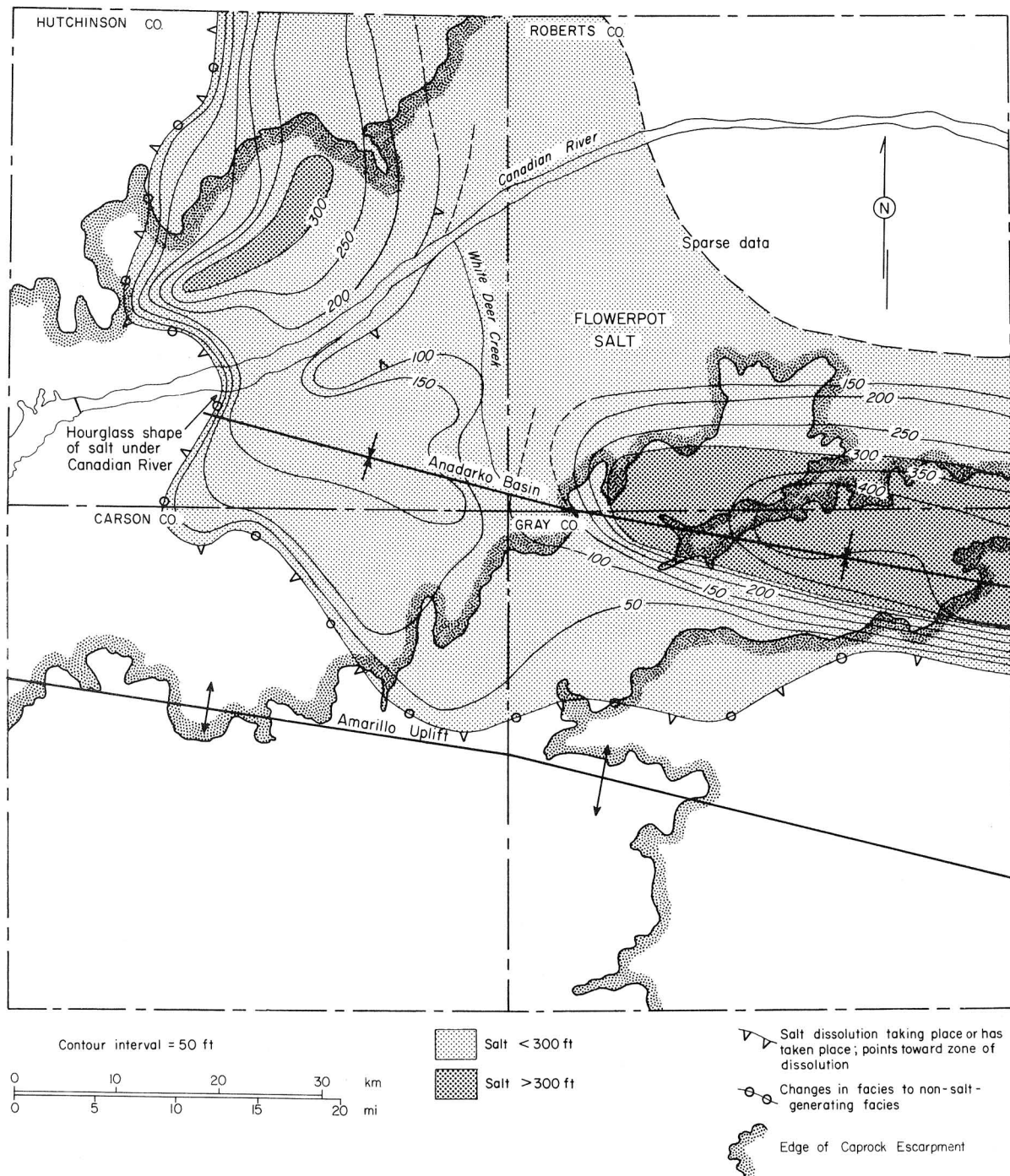
Figure 89. Isopach map of the Flowerpot salt. In the most rapidly subsiding parts of the Anadarko Basin, up to 135 m (450 ft) of salt precipitated during deposition of the Flowerpot. Superimposed Caprock Escarpment outlines breaches in the High Plains surface.
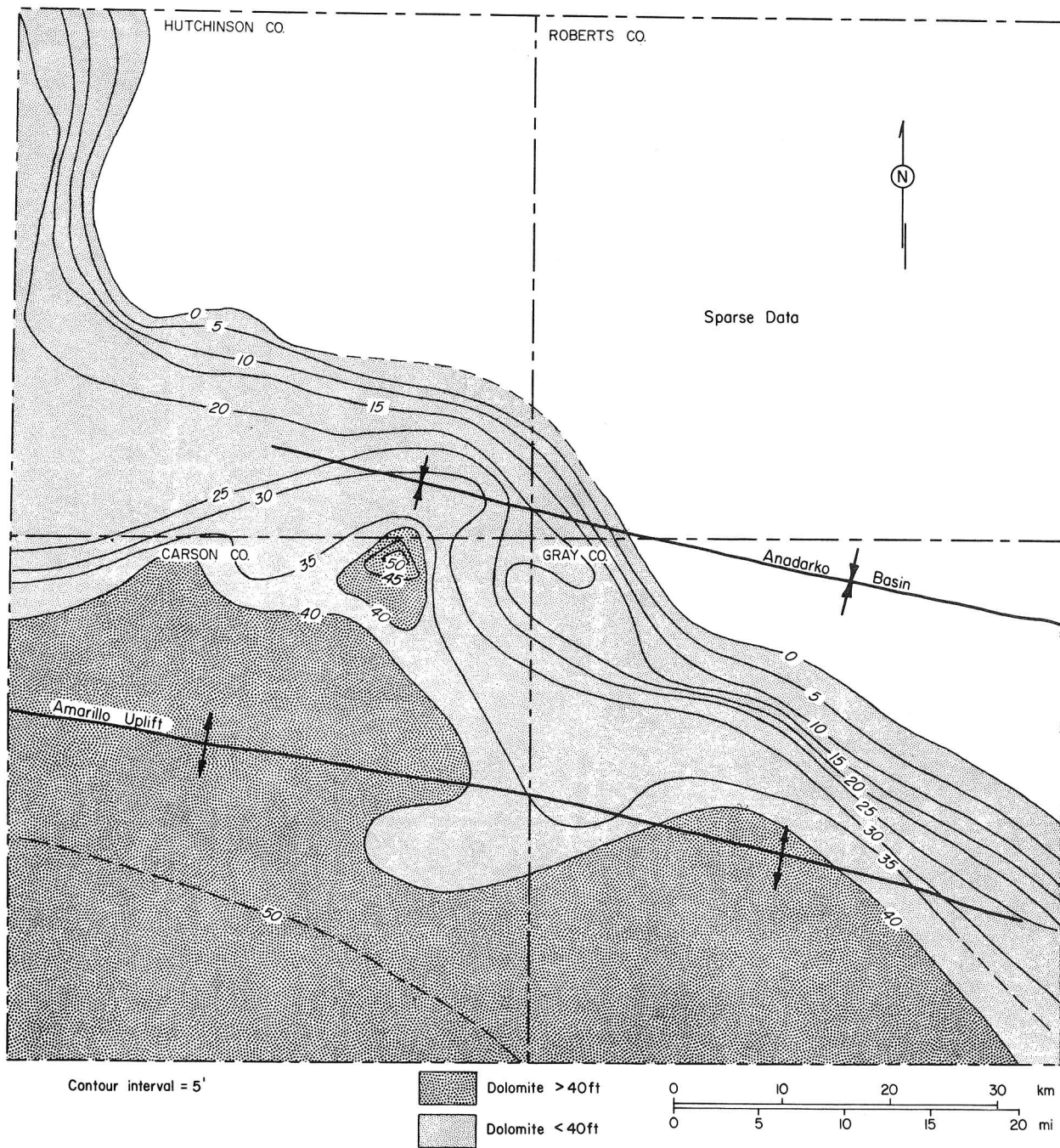
Figure 90. Isopach map of Blaine dolomite bed. During deposition of the Flowerpot, the brine pan environment spread across the mudflats and covered most of the study area. An isopach map of early Blaine dolomite suggests that shelf carbonates were bordering the central parts of the Anadarko Basin.
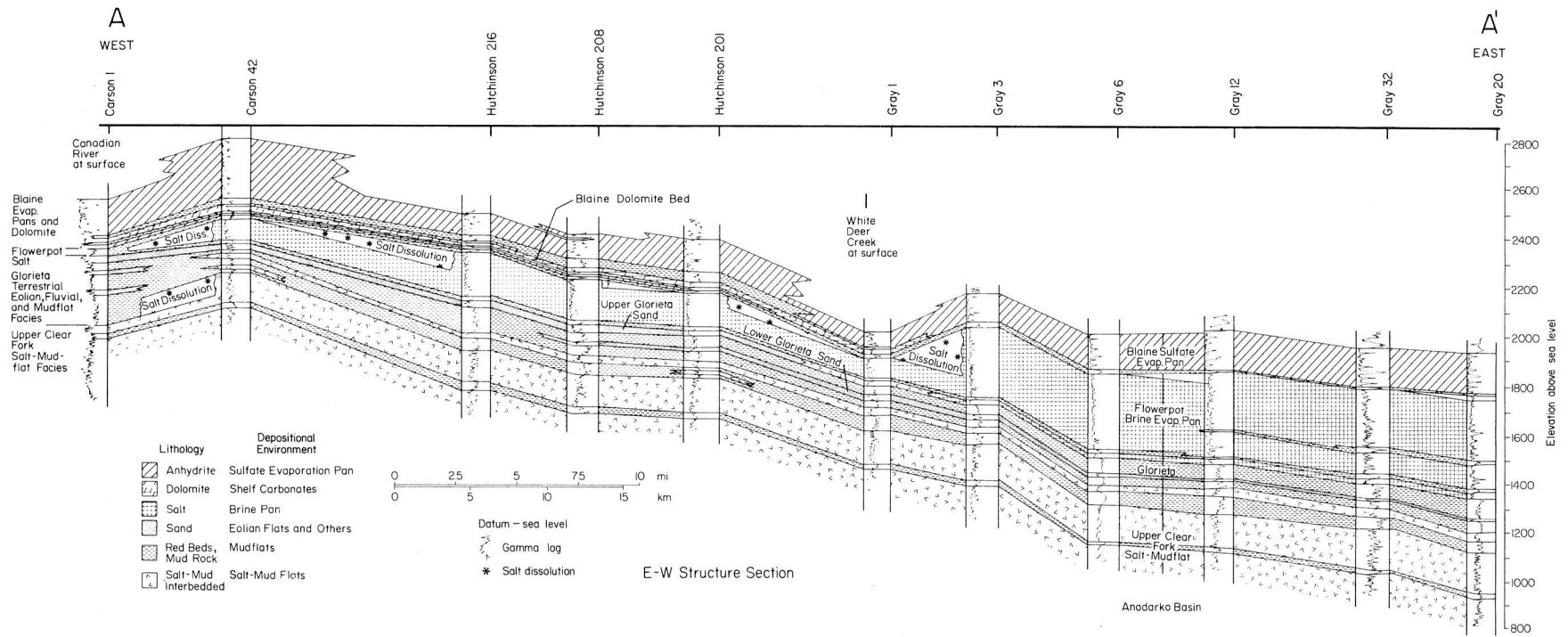
Figure 91. East-west structure section of Glorieta, Flowerpot, and Blaine strata in the study area. See figure 86 for line of section.
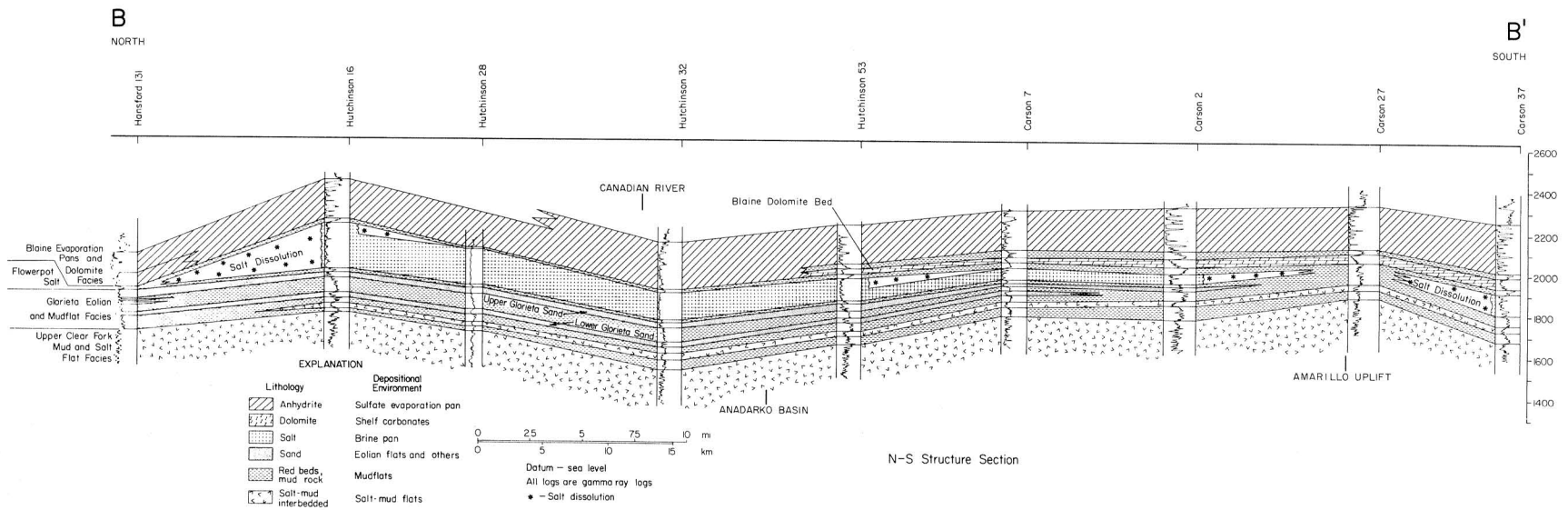
163

Figure 92. North-south structure section of Glorieta, Flowerpot, and Blaine strata in the study area. See figure 86 for line of section.

164

## Table 11. Logs used in cross sections.

| County | BEG number | Operator | Well name |
|---|---|---|---|
| Carson | 1 | Hendington | D-1 Sanford |
| Carson | 7 | Skelly | #262 Schafer |
| Carson | 22 | Consolidated ETA | #1 Biggs A |
| Carson | 27 | L. B. Newman | #9 Meaker |
| Carson | 37 | J. M. Huber | # 1 Newton |
| Carson | 42 | Gulf Oil | S. B. Burnett #64 |
| Gray | 1 | E. B. Clark Drilling Co. | #1 D. J. Barnett |
| Gray | 3 | Gulf Oil | #1 Graham |
| Gray | 6 | Cabot Corp. | #1 Hobart-Fatheree |
| Gray | 12 | Underwood | #1 Jackson |
| Gray | 20 | Standard of Texas | #1 A. R. Bell |
| Gray | 32 | Phillips | #1-B Troy |
| Hansford | 131 | Southern Calif. Pet. Co. | #1 Yanda |
| Hutchinson | 16 | Anadarko Production | #B-1 Kirk |
| Hutchinson | 28 | Claro Inc. | #1 M. A. T. Petroleum |
| Hutchinson | 32 | Gulf Oil | #1 Duncan |
| Hutchinson | 53 | Ploy H. King | #1 T. J. Price |
| Hutchinson | 201 | Texaco Inc. | L. E. Cooper #1 |
| Hutchinson | 208 | The Texas Co. | J. W. Moore #15 |
| Hutchinson | 216 | Phillips | Cockerell Ranch #103 |

# ACKNOWLEDGMENTS

# REFERENCES

Adams, J. E., 1944, Upper Permian Ochoa Series of Delaware Basin, West Texas and southeastern New Mexico: American Association of Petroleum Geologists Bulletin, v. 28, p. 1596-1625.

Adams, J. E., and Rhodes, M. L., 1960, Dolomitization by seepage refluxion: American Association of Petroleum Geologists Bulletin, v. 53, p. 2314-2323.

Anderson, R. Y., and Kirkland, D. W., 1980, Dissolution of salt deposits by brine density flow: Geology, v. 8, p. 66-69.

Babcock, E. A., 1973, Regional jointing in southern Alberta: Canadian Journal of Earth Science, v. 10, p. 1769-1781.

Bachman, G. O., 1976, Cenozoic deposits of southeastern New Mexico and an outline of the history of evaporite dissolution: Journal of Research of the U.S. Geological Survey, v. 4, no. 2, p. 135-149.

Bassett, R. L., Bentley, M. E., Duncan, J. R., and Griffin, J. A., 1980, Predicting the reaction state of brines in proposed regions of nuclear waste isolation, in Scientific basis for nuclear waste management: Boston, Materials Research Society, p. 25-32.

Bassett, R. L., and Griffin, J. A., in preparation, AQ/SALT: a computer program for brines: The University of Texas at Austin, Bureau of Economic Geology.

Bodine, M. W., and Jones, B. F., 1980, Unpublished progress report: on file with R. L. Bassett, The University of Texas at Austin, Bureau of Economic Geology.

Boeke, H. E., 1908, Über das Kristallisationsschema der chloride, bromide, iodide von natrium, kalium und magnesium, sowie über das vorkemmen des broms und das fehlen von jod in den Kalisalzlagerstatten: Zeitschrift für Kristallographie und Mineralogie, v. 45, p. 346-391.

Braitsch, O., and Herrmann, A. G., 1963, Zur geochemie des broms in Salinaren sedimenten. Teili: Experimentelle bestemund der Br$^-$ verteilung in verdscheiden en naturlichen salzsystemen: Geochimica et Cosmochimica Acta, v. 27, p. 361-391.

Brindley, G. W., 1961, Chlorite minerals, in Brown, G., ed., The x-ray identification and crystal structures of clay minerals: London, The Mineralogical Society, p. 242-296.

Chuber, S., and Pusey, W. C., 1967, San Andres facies and their relationship to diagenesis, porosity and permeability in the Reeves Field, Yoakum County, Texas: West Texas Geologic Society Symposium on Cyclic Sedimentation, October 20, 1967.

Coffman, J. L., and Von Hake, C. A., eds., 1973, Earthquake history of the U.S.: Environmental Data Service, National Oceanic and Atmospheric Administration, U.S. Department of Commerce, Publication 41-1, 208 p.

Cook, A. C., and Johnson, K. R., 1970, Early joint formation in sediments: Geology, v. 107, p. 361-368.

Cooper, J. B., 1962, Ground water in Cenozoic fill in collapse structures, southeastern Eddy County, New Mexico: U.S. Geological Survey Professional Paper 450-E, p. 152-153.

D'Ans, J., and Kuhn, R., 1940, Über den bromgehalt von Salzgesteinen der Kalisalz-lager stätten: Kalisalzlager, v. 34, p. 42-83.

Deffeyes, K. S., Lucia, F. J., and Weyl, P. K., 1965, Dolomitization of Recent and Plio-Pleistocene sediments by marine waters on Bonaire, Netherlands Antilles, in Dolomitization and limestone diagenesis: Society of Economic Paleontologists and Mineralogists Special Publication 13, p. 71-88.

Dunlap, W. H., 1967, San Andres oil exploration in the Cato-Slaughter trend of southeastern New Mexico, in The oil and gas fields of southeastern New Mexico, 1966 supplement--a symposium: Roswell, New Mexico, Roswell Geological Society, p. 21-24.

Dutton, S. P., 1980, Petroleum source rock potential and thermal maturity, Palo Duro Basin, Texas: The University of Texas at Austin, Bureau of Economic Geology Geological Circular 80-10, 48 p.

Dutton, S. P., Finley, R. J., Galloway, W. E., Gustavson, T. C., Handford, C. R., and Presley, M. W., 1979, Geology and geohydrology of the Palo Duro Basin, Texas Panhandle, a report on the progress of nuclear waste isolation feasibility studies (1978): The University of Texas at Austin, Bureau of Economic Geology Geological Circular 79-1, 99 p.

Finley, R. J., 1979, Runoff characteristics and a flood in the Texas Panhandle, in Dutton, S. P., and others, Geology and geohydrology of the Palo Duro Basin, Texas Panhandle: The University of Texas at Austin, Bureau of Economic Geology Geological Circular 79-1, p. 69-74.

Finley, R. J., and Gustavson, T. C., 1980, Climatic controls on erosion in the Rolling Plains and along the Caprock Escarpment of the Texas Panhandle: The University of Texas at Austin, Bureau of Economic Geology Geological Circular 80-11, 50 p.

_____ in press, Landsat lineament analysis of the Texas Panhandle: The University of Texas at Austin, Bureau of Economic Geology Geological Circular.

Folk, R. L., 1978, Angularity and silica coatings of Simpson Desert sand grains, Northern Territory, Australia: Journal of Sedimentary Petrology, v. 48, no. 2, p. 611-624.

Folk, R. L., and Land, L. S., 1975, Mg/Ca ratio and salinity: two controls over crystallization of dolomite: American Association of Petroleum Geologists Bulletin, v. 59, p. 60-68.

Freeze, R. A., and Cherry, J. A., 1980, Groundwater: Englewood Cliffs, N.J., Prentice Hall, 604 p.

Galloway, W. E., 1979, Basic objectives of basin analysis--genetic description of the salt-bearing interval and associated strata, in Dutton, S. P., and others, Geology and geohydrology of the Palo Duro Basin, Texas Panhandle: The University of Texas at Austin, Bureau of Economic Geology Geological Circular 79-1, p. 3-5.

Geotechnical Engineers, Inc., 1978, Final report on uncertainties in the detection, measurement, and analysis of selected features pertinent to deep geologic repositories: submitted to University of California, Lawrence Livermore Laboratory, Project 77393, purchase order no. 901603, 96 p.

Gilbert, G. K., 1882, Post-glacial joints: American Journal of Science, third series, v. 23, p. 25-27.

Grim, R. E., 1968, Clay mineralogy: New York, McGraw-Hill, 596 p.

Gustavson, T. C., Finley, R. J., and Baumgardner, R. W., Jr., 1980a, Preliminary rates of slope retreat and salt dissolution along the eastern Caprock Escarpment of the Southern High Plains and in the Canadian River valley, in Gustavson, T. C., and others, Geology and geohydrology of the Palo Duro Basin, Texas Panhandle: The University of Texas at Austin, Bureau of Economic Geology Geological Circular 80-7, p. 76-79.

Gustavson, T. C., Finley, R. J., and McGillis, K. A., 1980b, Regional dissolution of Permian salt in the Anadarko, Dalhart, and Palo Duro Basins of the Texas Panhandle: The University of Texas at Austin, Bureau of Economic Geology Report of Investigations No. 106, 40 p.

Gustavson, T. C., Presley, M. W., Handford, C. R., Finley, R. J., Dutton, S. P., Baumgardner, R. W., Jr., McGillis, K. A., and Simpkins, W. W., 1980c, Geology and geohydrology of the Palo Duro Basin, Texas Panhandle: The University of Texas at Austin, Bureau of Economic Geology Geological Circular 80-7, 99 p.

Ham, W. E., Dennison, R. E., and Merritt, C. A., 1964, Basement rocks and structural evolution of southern Oklahoma: Oklahoma Geological Survey Bulletin 95, 302 p.

Handford, C. R., 1979, Resources, in Dutton, S. P., and others, Geology and geohydrology of the Palo Duro Basin, Texas Panhandle: The University of Texas at Austin, Bureau of Economic Geology Geological Circular 79-1, p. 59-62.

_____ 1980, Lithofacies and depositional environments of evaporite-bearing strata based on Randall and Swisher County cores, in Gustavson, T. C., and others, Geology and geohydrology of the Palo Duro Basin, Texas Panhandle: The University of Texas at Austin, Bureau of Economic Geology Geological Circular 80-7, p. 5-7.

Handford, C. R., and Fredericks, P. E., 1980, Facies patterns and depositional history of a Permian sabkha complex: Red Cave Formation, Texas Panhandle: The University of Texas at Austin, Bureau of Economic Geology Geological Circular 80-9, 38 p.

Harlton, B. H., 1963, Frontal Wichita fault system of southwestern Oklahoma: American Association of Petroleum Geologists Bulletin, v. 47, p. 1552-1580.

Harvie, C. E., and Weare, J. H., 1980, The prediction of mineral solubilities in natural waters: Geochimica et Cosmochimica Acta, v. 44, p. 981-997.

Hey, M. H., 1954, New review of the chlorites: Mineralogical Magazine, v. 30, p. 277-292.

Hiss, W. L., 1975, Thickness of the Permian Guadalupian Capitan aquifer, southeast New Mexico and West Texas: New Mexico Bureau of Mines and Mineral Resources, Resource Map 5.

Hodgson, R. A., 1965, Genetic and geometric relations between structures in basement and overlying sedimentary rocks, with examples from Colorado Plateau and Wyoming: American Association of Petroleum Geologists Bulletin, v. 49, p. 935-949.

Holdoway, K. A., 1978, Deposition of evaporites and red beds of the Nippewalla Group, Permian, western Kansas: Kansas Geological Survey Bulletin 215, 43 p.

Holser, W. T., 1966, Diagenetic polyhalite in Recent salt from Baja California: American Mineralogist, v. 51, p. 99-109.

_____ 1979, Rotliegend evaporites, Lower Permian of northwest Europe, geochemical confirmation of the non-marine origin: Erdol und Kohle-Erdgas-Petrochemie vereinigt mit Brennstoff-Chemie, Bd. 32, Heft 4, p. 159-162.

Holser, W. T., Wardlaw, N. C., and Watson, D. W., 1972, Bromide in salt rocks: extraordinarily low content in the Lower Elk Point salt, Canada, in Geology of saline deposits, Hanover Symposium proceedings, 1968: Earth Sciences, v. 7, p. '69-75.

Houde, R. F., 1979, Sedimentology, diagenesis, and source bed geochemistry of the Spraberry Sandstone, subsurface Midland Basin, West Texas: The University of Texas at Dallas, Master's thesis, 168 p.

Hsu, K. J., and Siegenthaler, C., 1969, Preliminary experiments on hydrodynamic movement induced by evaporation and their bearing on the dolomite problem: Sedimentology, v. 12, p. 11-25.

Johnson, K. S., 1976, Evaluation of Permian salt deposits in the Texas Panhandle and western Oklahoma for underground storage of radioactive wastes: Oak Ridge, Tennessee, Oak Ridge National Laboratories, Report to Union Carbide Corporation.

Jones, T. S., and Smith, H. M., 1965, Relationships of oil composition and stratigraphy in the Permian Basin of West Texas and New Mexico: American Association of Petroleum Geologists Memoir 4, p. 101-224.

Kinsman, D. J. J., and Patterson, R. J., 1973, Dolomitization process in sabkha environment (abs.): American Association of Petroleum Geologists Bulletin, v. 57, p. 788-789.

Krinsley, D. H., and Doornkamp, J. C., 1973, Atlas of quartz sand surface textures: Cambridge, England, Cambridge University Press, 91 p.

Land, L. S., 1973, Holocene meteoric dolomitization of Pleistocene limestones, North Jamaica: Sedimentology, v. 20, p. 411-424.

Land, L. S., Salem, M. R. I., and Morrow, D. W., 1975, Paleohydrology of ancient dolomites: geochemical evidence: American Association of Petroleum Geologists Bulletin, v. 59, p. 1602-1625.

Linke, W. F., 1958, Solubilities: New York, D. Van Nostrand Co., Inc., v. 1, 1487 p.

Lippmann, F., 1954, Über einen keuperton von zaiserweiher bei maulbron: Heidelberg-Beitrag Mineralogisch Petrographie, v. 4, no. 1-2, p. 130-134.

Magara, K., in preparation, Burial history, petroleum generation, and migration in Midland Basin: The University of Texas at Austin, Bureau of Economic Geology.

Maley, V. C., and Huffington, R. M., 1953, Cenozoic fill and evaporite solution in the Delaware Basin, Texas and New Mexico: Geological Society of America Bulletin, v. 64, p. 539-546.

McCrea, J. M., 1950, On the isotopic chemistry of carbonates and a paleotemperature scale: Journal of Chemical Physics, v. 18, p. 849-857.

McGillis, K. A., 1980, Mapping of facies by well log interpretation, in Gustavson, T. C., and others, Geology and geohydrology of the Palo Duro Basin, Texas Panhandle: The University of Texas at Austin, Bureau of Economic Geology Geological Circular 80-7, p. 8-11.

McGowen, J. H., Granata, G. E., and Seni, S. J., 1979, Depositional framework of the lower Dockum Group (Triassic), Texas Panhandle: The University of Texas at Austin, Bureau of Economic Geology Report of Investigations No. 97, 60 p.

Middleton, G. V., 1973, Johannes Walther's law of the correlation of facies: Geological Society of America Bulletin, v. 84, p. 979-988.

Milliman, J. D., 1974, Marine carbonates: New York, Springer-Verlag, 375 p.

Milner, Sam, 1978, Genesis, provenance and petrography of the Glorieta Sandstone of eastern New Mexico: New Mexico Bureau of Mines and Mineral Resources Circular 165, 25 p.

Mueller, H. W., 1975, Centrifugal progradation of carbonate banks: a model for deposition and early diagenesis, Fort Terrett Formation, Edwards Group, Lower Cretaceous, Central Texas: The University of Texas at Austin, Ph.D. dissertation, 300 p.

Nicholson, Alexander, and Clebsch, Alfred, 1961, Geology and ground-water conditions in southern Lea County, New Mexico: New Mexico Bureau of Mines and Mineral Resources, Ground-Water Report 6, 123 p.

Nicholson, J. H., 1960, Geology of the Texas Panhandle, in Aspects of the geology of Texas, a symposium: University of Texas, Austin, Bureau of Economic Geology Publication No. 6017, p. 51-64.

Nurmi, R. D., and Friedman, G. M., 1977, Sedimentology and depositional environments of basin center evaporites, Lower Salina Group (Upper Silurian), Michigan Basin, in Fisher, J. H., ed., Reefs and evaporites--concepts and depositional

models: American Association of Petroleum Geologists Studies in Geology 5, p. 23-52.

Pitzer, K. S., 1977, Electrolyte theory--improvements since Debye and Hückel: Accounts of Chemical Research, v. 19, p. 371-377.

Presley, M. W., 1979a, Data, in Dutton, S. P., and others, Geology and geohydrology of the Palo Duro Basin, Texas Panhandle: The University of Texas at Austin, Bureau of Economic Geology Geological Circular 79-1, p. 6-9.

_____ 1979b, Salt deposits, in Dutton, S. P., and others, Geology and geohydrology of the Palo Duro Basin, Texas Panhandle: The University of Texas at Austin, Bureau of Economic Geology Geological Circular 79-1, p. 50-57.

_____ 1979c, San Andres facies patterns, Palo Duro and Dalhart Basins, Texas: American Association of Petroleum Geologists Bulletin, v. 63, p. 1427- 1428.

_____ 1979d, Upper Permian evaporites and red beds, in Dutton, S. P., and others, Geology and geohydrology of the Palo Duro Basin, Texas Panhandle: The University of Texas at Austin, Bureau of Economic Geology Geological Circular 79-1, p. 39-49.

_____ 1979e, Upper Permian evaporites and red beds of the Palo Duro Basin, Texas--facies patterns through time (abs.): American Association of Petroleum Geologists Bulletin, v. 63, p. 511-512.

_____ 1980a, Salt depositional systems--an example from the Tubb Formation, in Gustavson, T. C., and others, Geology and geohydrology of the Palo Duro Basin, Texas Panhandle: The University of Texas at Austin, Bureau of Economic Geology Geological Circular 80-7, p. 24-32.

_____ 1980b, Upper Permian salt-bearing stratigraphic units, in Gustavson, T. C., and others, Geology and geohydrology of the Palo Duro Basin, Texas Panhandle: The University of Texas at Austin, Bureau of Economic Geology Geological Circular 80-7, p. 12-23.

Ramondetta, P. J., 1980, Source potential of San Andres and Yeso shelf carbonates: The University of Texas at Austin, Bureau of Economic Geology, annual contract report to U.S. Department of Energy.

Raup, O. B., and Hite, R. J., 1978, Bromine distribution in marine halite rocks, in Marine evaporites: Society of Economic Paleontologists and Mineralogists Short Course No. 4, Oklahoma City, p. 105-123.

Richter-Bernburg, Gerhard, 1973, Facies and paleogeography of the Messinian evaporites in Sicily, in Drooger, C. W., ed., Messinian events in the Mediterranean: Amsterdam, North-Holland Publishing Company, p. 124-141.

Rudolph, K., 1978, Diagenesis of back-reef carbonate rocks: an example from Capitan Complex: The University of Texas at Austin, Master's thesis, 159 p.

Sahl, H. L., 1970, Mobeetie Field, Wheeler County, Texas: Oklahoma City Geological Society, Shale Shaker, v. 20, p. 108-115.

Schwab, K. W., 1977, Source rock evaluation (visual kerogen): Houston, Texas, Geo-Strat, Inc., commercial brochure.

Selley, R. C., 1970, Studies of sequence in sediments using a simple mathematical device: Geological Society of London, Quarterly Journal, v. 125, p. 557-581.

Seni, S. J., 1980, Sand-body geometry and depositional systems, Ogallala Formation, Texas: The University of Texas at Austin, Bureau of Economic Geology Report of Investigations No. 105, 36 p.

Shinn, E. A., Ginsburg, R. N., and Lloyd, R. M., 1965, Recent supratidal dolomite from Andros Island, Bahamas, in Dolomitization and limestone diagenesis: Society of Economic Paleontologists and Mineralogists Special Publication 13, p. 89-111.

Shirozu, H., 1958, X-ray patterns and cell dimensions of chlorites: Mineralogical Journal, v. 2, p. 209-223.

Smith, G. E., 1974, Depositional systems, San Angelo Formation (Permian), north Texas: facies control of red-bed mineralization: The University of Texas at Austin, Bureau of Economic Geology Report of Investigations No. 80, 73 p.

Strahler, A. N., 1957, Quantitative analysis of watershed geomorphology: EOS, v. 38, no. 6, p. 913-920.

Tissot, B. P., and Welte, D. H., 1978, Petroleum formation and occurrence: New York, Springer-Verlag, 538 p.

Valyashko, M. G., 1956, Geochemistry of bromine in the processes of salt deposition and the use of the bromine content as a genetic and prospecting criterion: Geochemistry, v. 6, p. 570-589.

Veizer, J., and Hoefs, J., 1976, The nature of $O^{18}/O^{16}$ and $C^{13}/C^{12}$ secular trends in carbonate rocks: Geochimica et Cosmochimica Acta, v. 40, p. 1387-1395.

Vine, J. D., 1960, Recent domal structures in southeastern New Mexico: American Association of Petroleum Geologists Bulletin, v. 44, p. 1903-1911.

Walker, R. G., 1979, Facies and facies models 1, general introduction, in Facies models: Geoscience Canada Reprint Series 1, p. 1-7.

Wardlaw, N. C., and Schwerdtner, W. M., 1966, Halite-anhydrite seasonal layers in the Middle Devonian Prairie evaporite formation, Saskatchewan, Canada: Geological Society of America Bulletin, v. 77, p. 331-342.

Winslow, A. G., and Kister, L. R., 1956, Saline-water resources of Texas: U.S. Geological Survey Water-Supply Paper 1365, 105 p.

Wood, J. R., 1975, Thermodynamics of brine-salt equilibria--the systems $NaCl$-$KCl$-$MgCl_2$-$CaCl_2$-$H_2O$ and $NaCl$-$MgSO_4$-$H_2O$ at $25^{\circ}C$: Geochimica et Cosmochimica Acta, v. 39, p. 1147-1163.

Young, A., 1972, Slopes: New York, Longman Group Limited, 288 p.